UNIVERSITY OF CALIFORNIA SAN DIEGO

The role of DNA Polymerase Alpha-Primase in controlling telomere length homeostasis

A dissertation submitted in partial satisfaction of the requirements for the degree

Doctor of Philosophy

in

Biology

by

Marion A. Meunier

Committee in charge:

Professor Victoria “Vicki” Lundblad, Chair
Professor Arshad Desai
Professor James Kadonaga
Professor Jan Karlseder
Professor Huilin Zhou

2021

The Dissertation of Marion A. Meunier is approved, and is acceptable in quality and form for publication on microfilm and electronically.

University of California San Diego

2021

DEDICATION

Cette dissertation est dédiée à ma famille. Merci d'avoir toujours été patients lorsque je posais 1000 questions sur tout et n'importe quoi étant enfant. Merci de nous avoir offert le kit du parfait scientifique, de nous avoir envoyé au centre aéré pour explorer des tas de cailloux l'été, de nous avoir trainé dans la nature les dimanches et de toutes ces choses que vous avez faites qui ont fait de moi ce que je suis aujourd'hui. Par-dessus tout, merci de m'avoir toujours aidée et supportée dans mes choix, même si cela implique de vivre sur des continents opposés.

TABLE OF CONTENTS

LIST OF FIGURES

LIST OF TABLES

ACKNOWLEDGMENTS

My first and biggest thank you goes to my advisor Vicki. She gave me a chance from across the world over an email and supported both my professional and personal projects all throughout my past 7 years in the laboratory. Thank you for your trust and availability, sense of humor and constant positivity.

Thank you to my committee members Arshad Desai, Jan Karlseder, Jim Kadonaga and Huilin Zhou for always being flexible with your busy schedules to discuss my project.

Finally, I would like to thank present (Abigail Gillespie, Corinne Moeller, Cynthia Reyes and Austin Kang) and past members of the laboratory or the floor of MCBL for always being available to help or answer a question, even at odd hours on a weekend.

Data from chapters 2 through 6 are currently in preparation to be published (Meunier and Lundblad, in preparation). The dissertation author was the primary researcher and author of this material.

VITA

EDUCATION

2016-2021

University of California San Diego, La Jolla, CA, USA

Ph.D in Biology

2013-2014

University Pierre and Marie Curie, Paris, FRANCE

MS in Molecular and Cellular Biology, specialized in Genetics

2009-2012

University of Nantes, Nantes, FRANCE

BS in Science, Technology and Health, specialized in Biology - Biochemistry

RESEARCH

2014-2021

Salk Institute for Biological Studies, La Jolla, CA, USA

DNA Replication and Telomere length regulation in *S. cerevisiae*

Professor Victoria "Vicki" Lundblad, Ph.D

ABSTRACT OF THE DISSERTATION

The role of DNA Polymerase Alpha-Primase in controlling telomere length homeostasis

by

Marion A. Meunier
Doctor of Philosophy in Biology

University of California San Diego, 2021
Professor Vicki Lundblad, Chair

As cells prepare to divide, their genetic information needs to be duplicated. In order to do so, many proteins work together into the replisome that faces many hurdles and difficult-to-replicate areas. Among which, the antisense nature of the lagging strand itself results in the end-replication problem, a gradual erosion of the extremities of eukaryotic linear chromosomes each cell cycle. Extreme shortening of telomeres, the ends of chromosomes, can trigger DNA recombination, chromosome fusion and overall increase the chance of deleterious damage that potentially threatens viability. DNA polymerase alpha-primase is the main complex responsible for antisense lagging strand replication. It has been argued to closely interact with t-RPA (telomeric Replication Protein A), a telomere-specific DNA binding complex. This heterotrimer, made out of Cdc13, Stn1 and Ten1 and also known as the CST complex, is known to be an essential player to recruit the enzyme telomerase. Telomerase is able to generate *de novo* telomeric sequences to maintain the ends of chromosomes over cell cycles.

This dissertation is the result of my focus on Pol12, non-catalytic subunit of polymerase alpha. This protein, although essential, has had very little insights about its function. By applying a genetic screening assay adapted in our laboratory, we uncovered several clusters of residues on the surface of the protein in *Saccharomyces cerevisiae*. These clusters have distinct DNA replication and telomere homeostasis-related phenotypes. Most notably, a subset of these mutants is synthetically lethal when combined with a t-RPA defect. Those same mutations show a decreased level of interaction between Pol12 and its hypothesized interacting t-RPA subunit, Stn1. It is expected that this loss of interaction impairs the post-replicative C-strand fill-in process of telomeres after elongation of the G-strand by telomerase, leaving unprocessed, single-stranded DNA exposed, triggering damage checkpoint and cell death. This study further confirmed how the two complexes seem to work closely, both genetically and physically.

CHAPTER 1:
Introduction

DNA Replication and the discovery of CDC proteins

As living organisms develop and grow, their cells divide. Every actively dividing cell follows a cycle alternating between Interphase, broken down into G1, S and G2 phases, and Mitosis during which a mother cell physically divides into two theoretically identical daughter cells. In most species, cells spend the vast majority of their time in Interphase to prepare for Mitosis. Its main goal is to ensure complete and accurate replication of the genetic information happening during S phase. This step is critical for integrity and viability of the daughter cells and is therefore highly regulated by multiple factors, pathways and checkpoints.

An original screening searching for mutants that resulted in impaired cell cycle progression identified factors subsequently labeled as CDC (Cell Division Cycle) genes in Yeast (*Hartwell et al. 1970*). As the list of those factors expanded, they were shown to play various roles in replication-related processes (*Hartwell et al., 1973*). Some of them, such as Cdc2, Cdc9 or Cdc17, are essential for lagging strand Replication (*Johnston & Nasmyth 1978, Carson and Hartwell, 1985*). Others, like Cdc13, indirectly maintain genome integrity by protecting the DNA from degradation (*Garvik et al. 1995*). Mutants of all the CDC proteins listed above result in cell stalling at the same stage of mitosis, arguing for a common shared essential role. Without regulation by Cdc13, cells show a senescence phenotype, which equates to a permanently stalled cell cycle state resulting from an extreme, unresolved shortening of telomeres, the ends of DNA (*Lendvay et al. 1996*). This erosion process naturally happens in dividing cells as a result of a natural replication-related problem.

The end-replication problem: implications at telomeres and counter mechanisms

Eukaryotic genomes are made out of linear chromosomes. The Replication machinery, also called replisome or replication fork, travels unidirectionally in a 5' to 3' direction. Because of the antiparallel nature of the double stranded DNA, the 5' to 3'-oriented leading strand is able to be replicated continuously as the fork travels, whereas the opposite 3' to 5' strand has to be copied discontinuously (*Watson & Crick 1953*). Extra hurdles and an overall slower replication rate resulting from the antisense orientation earned the latter its "lagging" strand status (*Morris et al. 1975*). DNA polymerase alpha-primase, also called pol-prim or primosome in Humans, participates in both early leading strand and lagging strand replication. Its primase subunits synthesize evenly spaced small ~10 ribonucleotides RNA primers that are elongated by polymerase alpha with ~20 to 30 deoxyribonucleotides. Because of its lack of proofreading activity, polymerase alpha-primase is then replaced by other polymerases of the same B family to ensure accurate DNA replication of both strands. Polymerase epsilon and delta have been identified as likely candidates taking over polymerase alpha-primase on the leading and lagging strand, respectively. Polymerase delta continues the extension process started by polymerase alpha on the lagging strand into ~200 nucleotides long Okazaki fragments (*Okazaki et al. 1968*). The resulting DNA-RNA hybrid is then processed through removal of the RNA primers, filling and ligation of the gaps into one continuous replicated strand. Yet, when reaching the extremity of each chromosome, the machinery is physically unable to bind to fill the most outer RNA primer. Once removed, it leaves a few nucleotides' gap on the 5' ends of all replicated lagging strands that, if left untouched, will be inherited by one of the daughter cells (*Olovnikov et al. 1973*). Repeated every round of cell cycle, this end-replication problem results in a slow and steady erosion of the ends of chromosomes.

In order to protect the genetic information, those ends are made out of non-coding, highly repetitive sequences called telomeres. To counter the end-replication problem, telomerase can be recruited to the telomeres. Acting as a reverse transcriptase, it adds G-rich telomeric repeats on the 3' end of the leading strand, using its own RNA as a template *(Greider & Blackburn 1985)*. This allows polymerase alpha-primase to add additional RNA primers to be filled with complementary C-rich repeats in the opposite strand (*Zhao et al. 2009*). Whether the C-strand fill-in process happens within the fork or as its own post-replication process is unclear.

DNA polymerase-alpha primase: description and function of the complex

The DNA polymerase alpha-primase complex is made out of 4 subunits, all essential throughout Evolution. In budding yeast *Saccharomyces cerevisiae*, our model organism, its primase function is carried out by the Pri1 and Pri2 subunits. Pri1 bears the active DNA binding site necessary for RNA primer synthesis and is ATP-dependent (*Scherzinger et al. 1977, Lucchini et al. 1987*). Pri1 is therefore categorized as a specialized DNA-dependent RNA Polymerase. It directly interacts with the C-terminal side of Pri2 through its own N-terminal domain (*Nakayama et al. 1984*). Although Pri2 is less characterized, it has several hypothesized functions that renders it indispensable. It contains an iron-sulfur (Fe-S) cluster that plays an essential role for both loading of the entire complex onto DNA as well as catalysis of primase activity (*Klinge et al. 2007*, *Liu and Huang 2015*). It is also thought to be the linker between primase and polymerase and maintain the whole complex integrity (*Longhese et al. 1993*).

Pol1 is the biggest subunit of the complex and carries out the DNA polymerase activity. It was initially discovered as Cdc17 through the *cdc-* screen (*Carson & Hartwell 1985*). Polymerases are highly conserved, both throughout evolution (*Bernad et al. 1987, Pizzagalli et*

al. 1988) but also between the different types found within the same species (*Kawasaki et al. 2001*). There are as many as 6 polymerases described in *Saccharomyces cerevisiae*, with data arguing for some degree of redundancy and strong structural similarities between them (*Matsumoto et al. 1990*). All of Pol1's known functions gather in the C-terminal half of the protein, with a Zinc finger/DNA binding active site for primer extension and a protein binding domain thought to interact with primase and/or its B subunit Pol12 (*Halling et al., 1977, Grossi et al., 2004*). The N-terminal domain of the protein is necessary for its interaction with Cdc13, a subunit of the t-RPA complex (*Sun et al., 2011*).

The sequence and structure similarities of polymerases throughout species has been a useful tool to characterize Pol12, fourth subunit of polymerase alpha-primase (*Foiani 1994*). It contains a catalytically inactive phosphodiesterase (PDE) domain that is highly specific to DNA polymerases (*Aravind & Koonin 1988*). Pol12 is thought to play a tether role by binding factors that stimulate the complex's activity (*Collins et al. 1993*). More recently, a crystal structure of polymerase alpha argued it helped Pol1 bind to DNA (*Suwa et al. 2015*). In addition to the PDE domain, Pol12 contains an oligonucleotide/oligosaccharide (OB)-fold. OB-folds are primarily found in single-stranded DNA binding proteins, such as the Replication Protein A (RPA) complex or its telomere specific homolog t-RPA (*Flynn & Zou, 2010*). They traditionally allow for binding to DNA or RNA but protein interactions, though OB-folds contact have also been demonstrated. In particular, Pol12 and Stn1, a subunit of t-RPA, have been shown to directly interact through their respective OB-fold (*Grossi et al., 2004*). This observation puts Pol12 at the interface of DNA Replication and telomere homeostasis although this essential protein has no true known function.

Polymerase alpha-Primase and the discovery of t-RPA, a telomere-dedicated complex

The main subunit of the t-RPA complex, Cdc13, was discovered through the *CDC* screen looking at mutants disrupting the normal cell cycle progression (*Weinert & Hartwell 1988*). The temperature sensitivity (TS) phenotype of the *cdc13-1* allele allowed for the discovery of one of its interacting partners Stn1, named after its ability to suppress the TS phenotype when overexpressed (*Grandin et al., 1997*). Through a similar approach, Ten1 was characterized as a suppressor of the TS allele *stn1-13* when overexpressed (*Grandin et al. 2001*). In parallel to the discovery of its t-RPA interacting partners, the role of Cdc13 at telomeres was characterized by the observation that some Cdc13 mutants mimicked alleles inactivating telomerase subunits (*Lendvay et al. 1996*). This result was later explained by showing that Cdc13 is necessary to recruit telomerase at telomeres through its Est1 subunit (*Evans and Lundblad 1999*). Similarly, Cdc13 was shown to also directly interact with the N-terminal region of Pol1 (*Qi and Zakian 2000; Sun et al. 2011*).

Yet, independently of the *CDC* alleles screen, mammalian equivalents of Cdc13 and Stn1 were originally characterized as accessory stimulatory factors of polymerase alpha-primase (*Goulian et al. 1990*), for both its primase and polymerase activities (*Goulian and Heard 1990*). All this data argues for a very close interaction between DNA Polymerase-Alpha Primase and t-RPA. The insights of this interaction, in particular through Pol12, have yet to be investigated and constitute the main object of focus of this thesis.

CHAPTER 2:
Discovery of previously uncharacterized Pol12 surface residues using the Overexpression Dominant Negative assay

Abstract

In order to understand the function(s) of a protein, scientists have historically been introducing mutations in various ways, with the goal of generating studiable phenotypes arising from disrupted pathways. Relying on a combination of protein sequence conservation over Evolution and available crystal structures, we generated a library of single residue charge-swap substitutions of the suspected Pol12 surface in overexpression plasmids. Using the *in vivo* competition nature of peptides, flooding the cells with mutated alleles creates an ODN (Overexpression Dominant Negative) growth phenotype specifically with surface separation-of-function alleles. The ODN assay highlighted 3 distinct clusters of amino acids. Each of them flanks with various levels of overlap with the published interface with its polymerase partner Pol1. Surfaces 1 and 2 showed an ODN phenotype in a Pol1 temperature sensitive (TS) strain whereas surfaces 1 and 3 had a growth defect in a Cdc13 TS strain. This observation argues that the assay may have uncovered at least two Pol12 interfaces performing distinct functions. Furthermore, this assay highlighted several putative phosphorylation sites and could even have the ability to distinguish protein surfaces interacting with DNA compared to binding partners.

Introduction: A walkthrough of historically used mutagenesis methods and their drawbacks

Because of its lack of enzymatic activity, Pol12 was the last subunit of the DNA polymerase alpha-primase complex to be characterized and cloned in order to be mutated (*Foiani et al. 1994*). One of the only methods available at the time to disrupt gene expression included plasmidic insertions or deletions using restriction enzymes to create *in vitro* mutations. The goal was to generate temperature sensitive alleles that allow for easy observation of phenotypes at permissive VS non-permissive temperatures and determine the function(s) of the protein that are disrupted. Indeed, that category of often buried mutations results in a protein with a loss of function that increases with the temperature. At permissive temperature, the protein is considered like Wild-Type (WT). At non-permissive temperature, it is unable to perform its functions.

Yet, such a method has notable drawbacks. Insertions and deletions can create a frame shift if not as multiples of three nucleotides, codon-forming units. This would result in a moderate to complete disruption of the targeted protein production, depending on its severity and position in the reading frame. In-frame insertions of two codons, as described by Foiani and colleagues, also aren't ideal. Indeed, relying on sequence-specific restriction enzymes doesn't guarantee an homogenous repartition of insertions throughout the reading frame. More generally, both insertions and deletions, even targeted, can result in unstable proteins even at permissive temperatures. It is now understood that heat-sensitive mutations result in a defect in peptide folding that increases alongside the temperature. Furthermore, it was shown to also possibly exhibit a phenotype even at permissive temperature, rendering phenotype comparison tricky or impossible *(Paschini et al. 2012)*. Although proving useful to find out the general function of Pol12 in DNA Replication and telomere maintenance, it didn't allow for a detailed structural insight.

Random mutagenesis is arguably one of the more broadly used tools to generate *in vivo* mutations. Use of chemicals such as Ethyl Methanesulfonate (EMS) or UltraViolet (UV) lights modify DNA base bonds and trigger DNA repair pathways. EMS creates single Thymine to Cytosine substitutions whereas UVs damage DNA in various ways that, when repaired, can give rise to both single and double base-pair substitutions *(Roberts and Warwick 1957; Rupert 1961)*. Therefore, EMS only affects one codon at a time, while UVs could potentially alter up to two codons. Whether those substitutions are silent (encodes for the same amino acid), missense (encodes for a different amino acid) or nonsense (encodes for a STOP codon) is random. Furthermore, the entire genome is hit indiscriminately beyond the targeted gene, and each cell accumulates potentially thousands of substitutions when mutagenized that could create additional phenotypes.

Zou and Rothstein utilized EMS to generate and study the very first *S. cerevisiae* Pol12 conditional mutants in the context of Holliday Junction formation (*Zou and Rothstein 1997*). To ensure that the TS phenotype wasn't the result of other mutations outside of their gene of interest, they backcrossed the strain by forcing it into meiosis. Meiosis segregates the genome in order to form spores, randomly separating theoretically half of the EMS-generated mutations every round. Zou and Rothstein backcrossed their *pol12-100* TS strain for 11 generations, a lengthy process that still didn't fully guarantee that no other mutations may also contribute to the observed defects. They also confirmed Pol12 being the main causal gene by rescuing the TS phenotype with complementation using a plasmid expressing unmutated Pol12.

Although some additional reverse genetic methods, such as the "pop-in pop-out", allowed for targeted and specific mutagenesis before the recent rise of CRISPR technologies, the lack of availability of many sequences prohibited such techniques (*Boeke et al. 1987*). Furthermore, they

are also time-consuming protocols and do not allow to test a high number of mutants. Finally, alleles that result in inviability, either because of overall instability or a disrupted essential function, cannot be distinguished or pursued through that method.

The Overexpression Dominant Negative assay: principle

Described by Ira Herskowitz, the Overexpression Dominant Negative (ODN) assay takes advantage of natural protein competition properties to uncover mutations of interest (*Herskowitz 1987*). A 2-micron (2µ) plasmid allows for overexpression of the mutated protein at a high copy number (~200) per cell (*Futcher 1988*). By transforming a plasmid that results in an overexpression of the allele, its product physically outcompetes the endogenous Wild-Type (WT) protein by saturating ligands, resulting in a potential growth defect deemed "ODN phenotype". The key advantage of this approach is that any mutation that destabilizes the folding of the protein will not give a phenotype as it does not have the ability to compete with the endogenous WT version.

The ODN assay allows to test mutations *in vivo* without the hassle of integrating them onto the genome. Transforming a plasmid is much easier, faster and cheaper than integrating one, as it doesn't require sequencing confirmation of the presence of the mutation but the sole use of a growth selection marker. Therefore, one can take advantage of this method to scale up screens and generate whole libraries of plasmids containing various mutations to be tested. This assay was successfully used in our laboratory for over a dozen proteins with a single occurrence where overexpression of the protein resulted in lethality and did not allow for such an approach.

Choosing the right residues to mutate in Pol12

Looking at sequence conservation throughout Evolution is the easiest way to identify key amino acids. Indeed, what is unnecessary to fitness and/or survival of an organism is expected to change or disappear over generations. Furthermore, it has been shown that highly conserved residues are more likely to be a part of a catalytic or allosteric site (*Yang et al. 2012*). In the case of Pol12, early eukaryotes' share a lot of homology, whereas the mammalian equivalent POLA2 is shorter and less conserved compared to ancestor species (*Suwa et al. 2015*). Aligning Yeast and Human sequences therefore showed to be a challenging process and was only successfully achieved for the C-terminal half of the peptide. The variations of homology at the amino acid level add up to the observation that the Yeast Pol12 sequence contains several sections absent in Humans'. Yet, although small parts of the protein were found to be disposable or redundant, most of the Pol12 sequence is conserved up to Humans, highlighting its importance. For this study, we gathered sequences throughout 12 species of Plant and Fungi to compare to our model organism *S. cerevisiae* (**Figure 2.1**).

Thanks to the progress in crystallography, the structure of budding yeast Pol12 in complex with Pol1 was unraveled by Klinge and colleagues (*Klinge et al. 2009*). Having the structure of the protein available in addition to the sequence allows to pinpoint key surface residues with increased accuracy. In this publication, they highlighted eight amino acids in both Pol1 and Pol12 that are hypothesized to be important for their interface. Yet, there is no further literature investigating those residues, or any targeted mutations in Pol12 to this day.

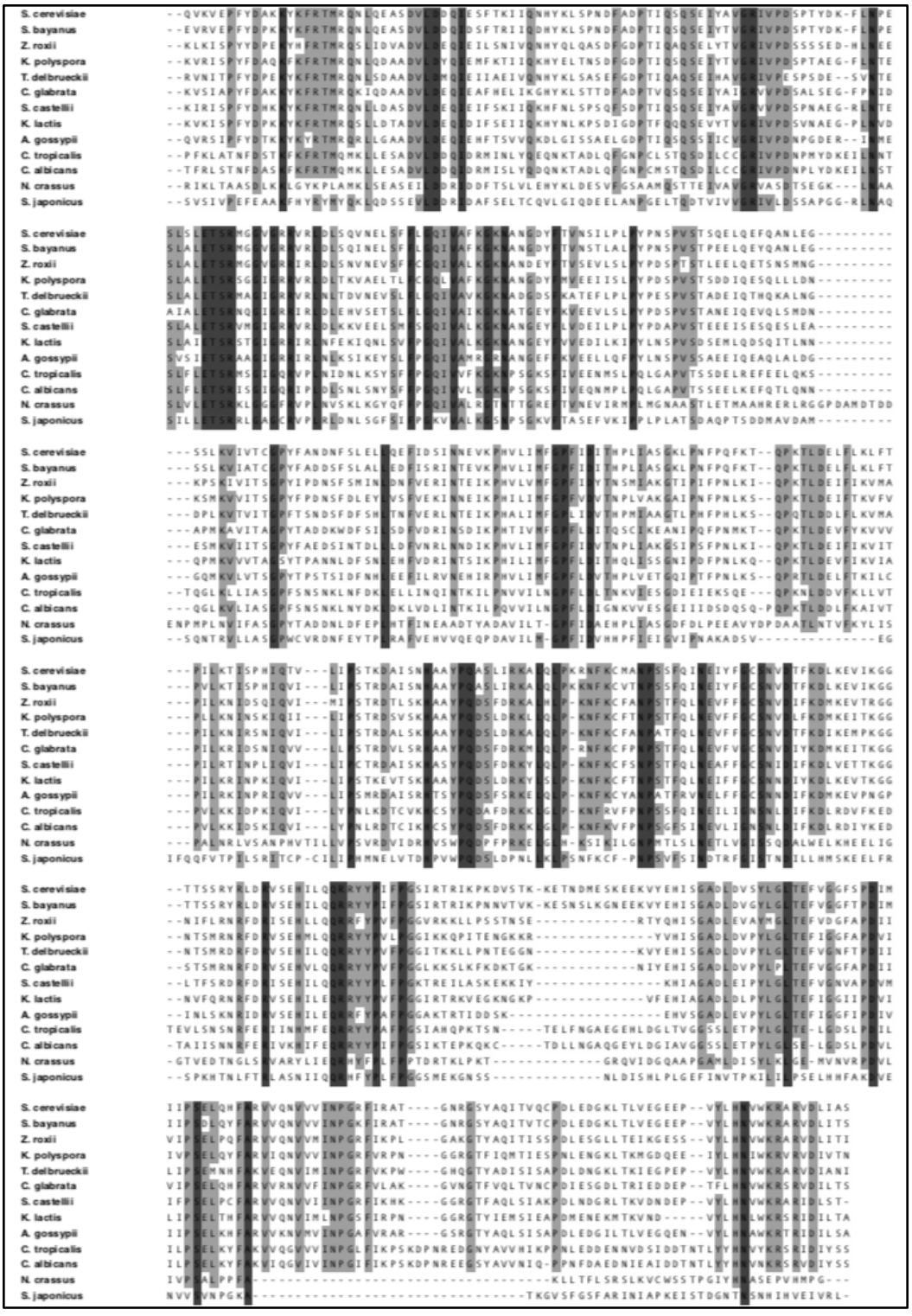

Figure 2.1: Pol12 sequence alignment and conservation throughout 13 yeasts species

Highly Conserved and strictly conserved residues are highlighted in light grey and dark grey, respectively. Amino acids missing for a particular species compared to S. cerevisiae are indicated with a dash. Alignment was done using Macvector.

Although informative, crystal structures often only provide a limited view of the protein and have notable caveats. Klinge and colleagues used a Pol12 template without the first 246 residues. That makes up for over a third of the 705 amino acid-protein sequence and is based on the assumption that this region was overall less conserved. This strategy maximizes chances of success as the smaller the peptide, the easier it is to crystallize. Yet, this region contains many important and conserved residues, including a nuclear localization motif as well as at least one suspected phosphorylation site (*Farrow et al. 2005; Holt et al. 2009*). Furthermore, the folding of the protein lacking part of its sequence may vary from its *in vivo* conformation. The crystal is also lacking a 26 amino acid stretch between position 580 and 606, located right next to its interface with Pol1. Yet, a closer look at the alignment between *S. cerevisiae* Pol12 and its Human equivalent POLA2 provided by Sawa and colleagues shows that this section is completely gone in the latest. Adjacent to this missing section, they acknowledged the low stability of amino acids 306 through 310. Typically, areas that do not crystallize are either naturally disordered or highly moving parts of the protein. We indeed usually witness the first and last few amino acids of a protein sequence being excluded from its structure as being located at its extremities. Studies of the nature of structurally missing amino acids show that they're more likely to be a part of solvent interacting areas (*Djinovic-Carugo and Carugo 2015*). Therefore, a missing portion might be the indication of an important structure, as it could also be the consequence of experimental drawbacks.

As crystal formation happens *in vitro* and under extreme physiological conditions of pH, temperature and salts, their conformation might not faithfully reflect that of the *in vivo* protein. It is therefore worth considering that the crystallization conditions may also force interactions that wouldn't occur naturally. To illustrate this, this structure shows Pol12 as a dimer, interacting

with itself around amino acids 330 to 350. There is no further evidence of such dimerization, and the nature of the replisome itself argues it may be an artifact. It is possible that this part of the protein is in fact responsible for binding to a partner but defaults to itself in its absence. As a more general thought, some proteins might be unstable or adopt a different conformation when not in contact with their interacting partner(s).

For these reasons, and similarly to sequences, looking at several protein crystals might help highlighting structural similarities and surfaces. To this day, there are only three other existing structures, all of Pol12 Human equivalent POLA2. Two of them characterize the interaction of the N-terminal region of the first ~75 amino acids of the protein with the viral SV40 antigen, one of its first discovered binding partners (*Huang et al. 2010; Zhou et al. 2012*). The third and most recent published structure shows the entire polymerase Alpha-Primase complex or Primosome (*Baranovskiy et al. 2016*). While also lacking some of the N-terminal region, POLA2 started to crystallize at the equivalent of residue 186 of Pol12. All of those additional studies point out the last downside of relying too strongly on crystal structure. The entire complex is indeed very flexible, depending on which step of replication it is at. Crystal structures only provide a snapshot of the protein that doesn't necessarily reflect its conformations and surfaces at all times.

Charge swap as the preferred strategy to identify surface residues

In addition to conservation and possible crystal structures, looking at the nature of the amino acid side chain helps select relevant candidates. The surface of proteins tends to be hydrophobic to allow for cohesion in the nucleoplasm as well as binding to ligands (*Young et al. 1994*). Charged residues, both acidic and basic, are also more likely to be involved in protein-

protein interactions with a residue of the opposite charge, like magnets. Positively charged amino acids are expected to be overly present at protein-DNA interfaces as the DNA molecule is negatively charged (*Kumar and Govil 1984*). An important residue may vary throughout species but its homologs will conserve its overall nature in order to maintain its function.

Historically, reverse Genetics screens were performed by mutating residues of interest into alanine (*Cunningham 1989*). Alanine was chosen due to its simplicity; it is both non-reactive and one of the smallest amino acids. Therefore, it was expected to abolish possible interactions while limiting disruption of the protein folding. Yet, the nature of the ODN assay allows us to mutate without worries about denaturation, as such alleles will not give a phenotype. Therefore, the most efficient approach to disrupt a surface residue is to mutate it into a residue of the opposite charge. To illustrate this idea, a past member of our laboratory disrupted the interaction between t-RPA subunits Stn1 and Ten1 by changing a positively charged aspartic acid on the latter into a negatively charged tyrosine (*Paschini et al. 2010*). They then restored it by reverse mutagenizing the interacting Stn1 leucine, a negatively charged hydrophobic residue, into an aspartic acid to show the specificity of the interaction between the two residues.

Using this same strategy, another past member of our laboratory used the ODN assay to screen telomerase subunit Est3 (*Lubin et al. 2013*). At the time, as no structure of the protein was available, they relied solely on conservation and charge data. Yet, they successfully identified multiple residues, all of which showed to be located on the surface of the protein once the crystal was solved (*Rao et al. 2014*). This work highlights the strength and versatility of the assay, which can be accomplished even in the absence of an existing structure of the protein of interest in a variety of proteins.

Using sensitized strains to identify separation-of-function mutations

It has now been widely accepted that many proteins perform more than one function, a feature deemed as "moonlighting" (*Jeffery, 2003*). By generating single surface residue substitutions, the goal is to identify alleles disrupting a given interface of the protein without completely destabilizing it, as this would perturb all of its activities. Such separation-of-function alleles allow to specifically characterize various functions of the protein. In the case of Pol12, it is thought to play a role in both DNA Replication and telomere homeostasis. Therefore, mutations tested through the ODN assay were transformed into two strains: *pol1-15 (Pol1^{TS})* and *cdc13-F684S (Cdc13^{TS})*. Both have temperature sensitive mutations impairing polymerase alpha-primase and t-RPA, respectively (*Budd et al., 1989, Paschini et al., 2012)*. As described previously, temperature sensitivity is a phenotype resulting from an overall destabilization of the protein. At permissive temperature, the protein is at or close to its native conformation and the strain behaves like WT. As the temperature increases, the protein becomes more and more destabilized, rendering it ultimately unable to perform its function.

There are three main reasons for the use of sensitized strains. Firstly, because of the presence of the endogenous WT version of the protein in the strain, very few mutations tested for ODN will have a phenotype in a non-sensitized strain. We only found disruption of active sites to give a visible growth defect in a WT strain background as these neared inviability. Secondly, as the selected strains have impaired DNA replication and telomere homeostasis respectively, the assumption is that mutants will only give an enhanced phenotype only if they're further disrupting the same pathway as the sensitized strain. Finally, the TS nature of those strains allow for easy viability comparison on permissive all the way up to non-permissive temperatures.

Material and methods: ODN assay on Pol12

All ODN analyses were performed in two temperature sensitive strains, yVL4119 (*MATa ura3-52 trp1-289 ade2-101 tyr1 gal2 can1 his3 pol1-15 leu2*Δ*::NAT*) or yVL3660 (*MATa ura3-52 lys2-801 trp-*Δ*1 his3-*Δ*200 leu2-*Δ*1 cdc13-F684S bar1*Δ*::cNAT*).

Missense mutations in Pol12 were introduced by Quickchange mutagenesis into pVL6321 (2μ LEU2 ADH-Pol12) and checked by sequencing. A standard LiAC transformation protocol was used to introduce plasmids individually into yeast alongside pVL399 (2μ LEU2 ADH) as a negative control and pVL6321 as a positive control. Cells were plated on YPD (Yeast Extract Peptone Dextrose) minus Leucine (-Leu) petri dishes, grown in duplicates overnight on YPD-Leu liquid media and gridded on YPD-Leu plates for plasmid retainment, and at increasing temperatures in ⅕ serial dilutions for readability.

Table 2.1: List of plasmids used in chapter 2

Plasmid #	Content
pVL399	*2μ LEU2 ADH*
pVL6321	*2μ LEU2 ADH-POL12*
pVL7376	*2μ LEU2 ADH-pol12-R248E*
pVL7377	*2μ LEU2 ADH-pol12-D259K*
pVL7379	*2μ LEU2 ADH-pol12-Q457E*
pVL7380	*2μ LEU2 ADH-pol12-H495E*
pVL7385	*2μ LEU2 ADH-pol12-M250E*
pVL7387	*2μ LEU2 ADH-pol12-G327E*
pVL7390	*2μ LEU2 ADH-pol12-S315K*
pVL7392	*2μ LEU2 ADH-pol12-Y616K*
pVL7925	*2μ LEU2 ADH-pol12-R322E*
pVL7932	*2μ LEU2 ADH-pol12-V326E*
pVL7953	*2μ LEU2 ADH-pol12-D303K*
pVL7954	*2μ LEU2 ADH-pol12-N312K*
pVL7954	*2μ LEU2 ADH-pol12-D676K*
pVL7955	*2μ LEU2 ADH-pol12-R329E*
pVL7963	*2μ LEU2 ADH-pol12-KKRK115-118AAAA*
pVL7964	*2μ LEU2 ADH-pol12-T190A*
pVL7965	*2μ LEU2 ADH-pol12-S290A*
pVL7966	*2μ LEU2 ADH-pol12-Q289E*
pVL7967	*2μ LEU2 ADH-pol12-Q291E*

Results: ODN assay on Pol12

The initial ODN screen performed on Pol12 followed promising results obtained from a pilot experiment performed as an undergraduate summer project. It served as an expansion from the original assay that tested 66 mutations in the *Pol1*^{TS} strain. An additional 128 mutants were designed in order to cover as many conserved surface residues as possible. These are located all throughout the sequence, including within the N-terminal region that isn't included in the crystal structure used as a guide. If the amino acid to be mutated is positively charged, a substitution

onto negatively charged Glutamic acid was performed. Negatively charged amino acids were swapped for a positively charged Lysine. For hydrophobic residues that don't have a charge, substitution onto both Lysine and Glutamic acid was performed. In addition, seven out of the eight residues hypothesized by Klinge and colleagues to be at the interface with Pol1 were also analyzed for comparison. Finally, the list included mutations of both a predicted N-terminal nuclear localization motif and several putative phosphorylation sites onto Alanine. Indeed, cell-cycle dependent changes in phosphorylation are thought to be essential for Pol12 function in DNA replication (*Foiani et al. 1995*).

New mutations were tested in the same *Pol1*^{TS} strain as the pilot study, looking at polymerase alpha-primase complex-related defects. All available mutants were also transformed in a *Cdc13*^{TS} strain, highlighting those resulting in telomere homeostasis impairment through disruption of the t-RPA complex. For every ODN experiment, viability changes were compared to an empty 2μ plasmid negative control, in case the plasmid itself affects viability, and a version containing WT Pol12, to account for potential viability changes that could arise from overexpressing the protein. In this case, the overexpression of Pol12 slightly improves viability compared to the empty vector transformed strains.

The original pilot experiment uncovered two clusters of residues that have a clear ODN phenotype in the *Pol1*^{TS}. The first (surface 1) contains multiple residues among which, most notably, arginine at position 248 (R248), methionine (M250), histidine (H495) and to a lesser degree tyrosine (Y616), and also have an ODN phenotype in a Cdc13^{TS} strain (**Figure 2.2**). Interestingly, H495 only shows an ODN phenotype when mutated onto negatively charged glutamic acid (H495E) and not with a positively charged lysine, a possible indication of a disrupted interaction with a negatively charged protein interface or DNA (**Figure 2.3**).

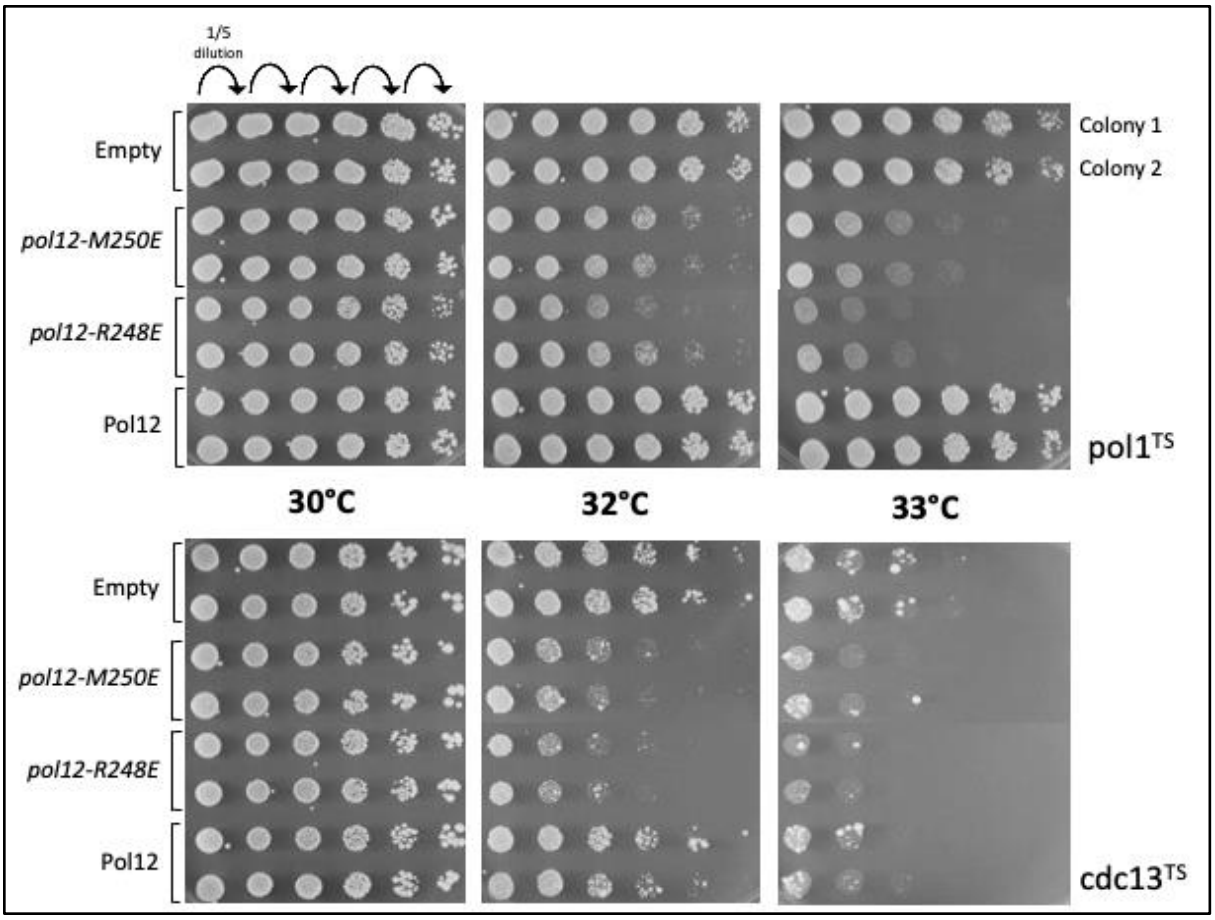

Figure 2.2: Overexpression Dominant Negative (ODN) phenotype of Pol12 surface 1 residues in both pol1TS and cdc13TS

Strains with a mutation of the gene indicated on the right side inducing a temperature-sensitive (TS) phenotype were transformed under selective marker pressure with an overexpression 2 micron (2u) vector including the content indicated on the left side. Two independent colonies were grown, replica gridded at different dilutions and grown for 3 days at a gradient of increasing temperatures ranging for permissible to non-permissible

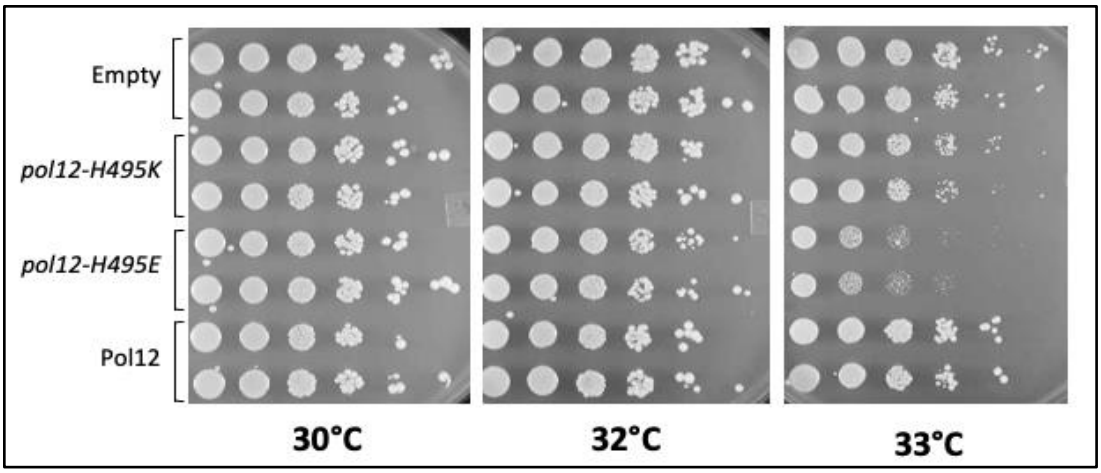

Figure 2.3: The differential ODN phenotype of pol12-H495 variants in *pol1*^{TS}
Opposite positive and negative charge variants of Pol12-H495 were transformed and analyzed as previously described in yVL4119 (pol1^{TS})

All residues of surface 1 map next to each other, although being far apart on the sequence. Residues 248 and 250 localize at the very beginning of the crystal structure of the protein, on a linker area. H495 is part of another linker whereas Y616 is on an alpha helix (**Figure 2.4**). Therefore, the phenotype is specific to their localization rather than disruption of a specific secondary structure of the protein.

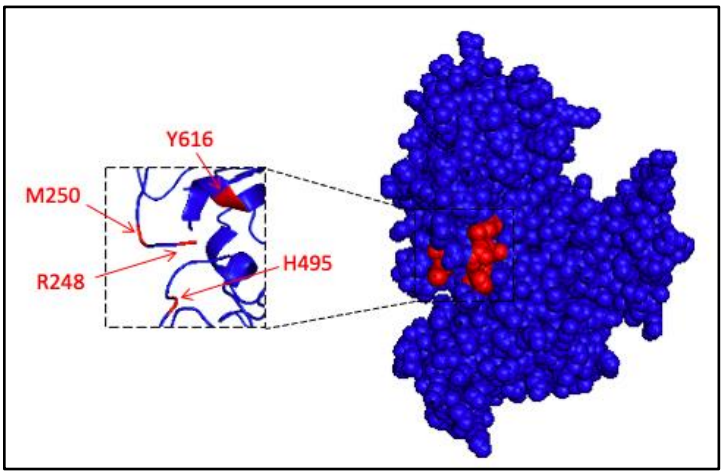

Figure 2.4: Localization of the Pol12 surface 1 residues on the surface of Pol12
Crystal structure by Klinge and Pellegrini (2009, PDB #3FLO) was visualized on Pymol. Pol12 is colored in dark blue. Residues of surface 1 are detailed in red.

Surface 2 includes aspartic acid in position 303 (D303), asparagine in 312 (N312) and surround serine 315 (S315), a potentially phosphorylatable amino acid (**Figure 2.5**). Mutating N312 onto either charge results in a similar ODN phenotype, arguing that this residue may not be a part of an interface itself but indirectly disrupt it when modified. Surfaces 1 and 2 have a similar ODN phenotype in *Pol1*^{TS} but are distinct according to the available crystal structure as they localize on opposite edges of the interface of Pol12 and Pol1 (**Figure 2.6**). Furthermore, they did not show a phenotype when transformed in the cdc13^{TS} strain in contrast to surface 1's.

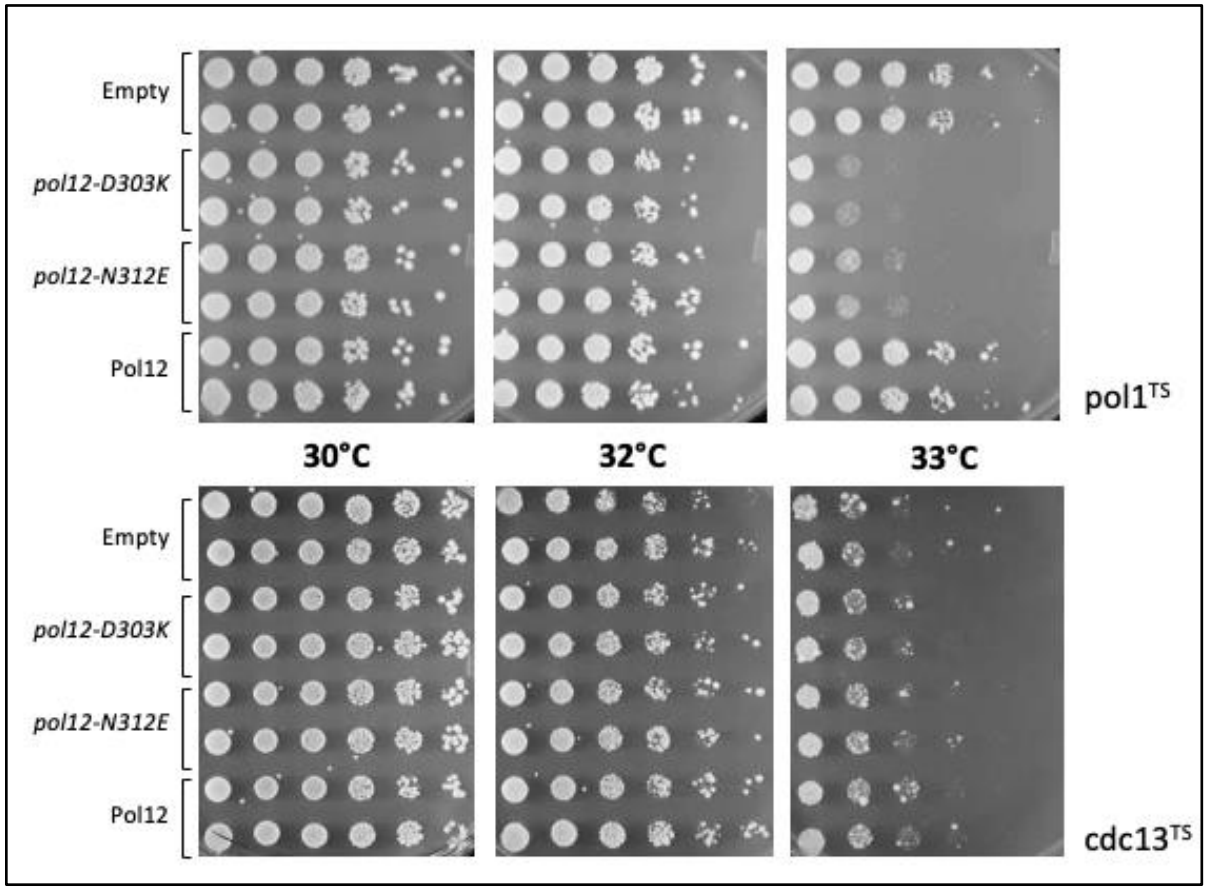

Figure 2.5: Overexpression Dominant Negative (ODN) phenotype of Pol12 surface 2 residues in pol1^{TS} but not cdc13^{TS}

Strains with a mutation of the indicated gene inducing a temperature-sensitive (TS) phenotype were transformed under selective marker pressure with an overexpression 2 micron (2u) vector including the content indicated on the left side. Two independent colonies were grown, replica gridded at different dilutions and grown for 3 days at a gradient of increasing temperatures reducing viability of the strain.

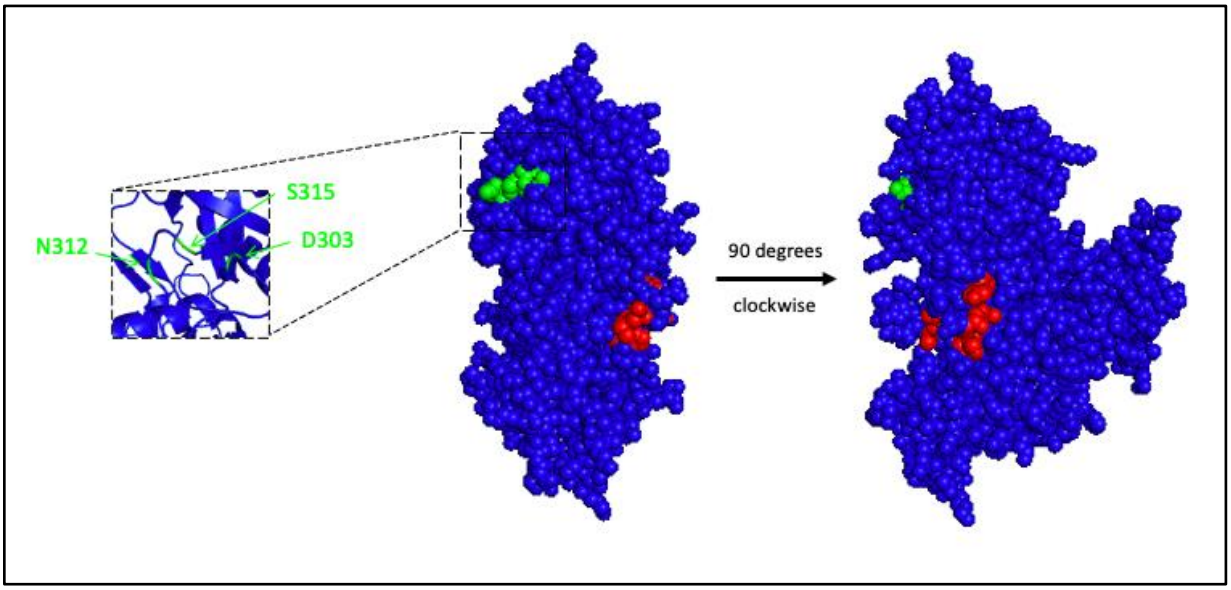

Figure 2.6: Localization of Pol12 surface 2 residues on the surface of Pol12
Crystal structure by Klinge and Pellegrini (2009, PDB #3FLO) was visualized on Pymol. Residues of surface 1 and 2 are detailed in red and green, respectively

When testing in the *Cdc13*^{TS} strain, a third surface (surface 3), including among others aspartic acid in position 259 (D259), arginine 322 (R322) and valine 326 (V326) was found (**Figure 2.7**). In contrast with surface 1, those alleles did not have a visible ODN phenotype in pol1^{TS}. Surface 3 also partially overlaps physically and phenotypically with the suspected interface area of Pol12 and Pol1 through residues E319, G327 and R329 (**Figure 2.8**). However, their lack of phenotype with pol1^{TS} reshapes the expectations about the consequences of disrupting that interface as will be discussed below.

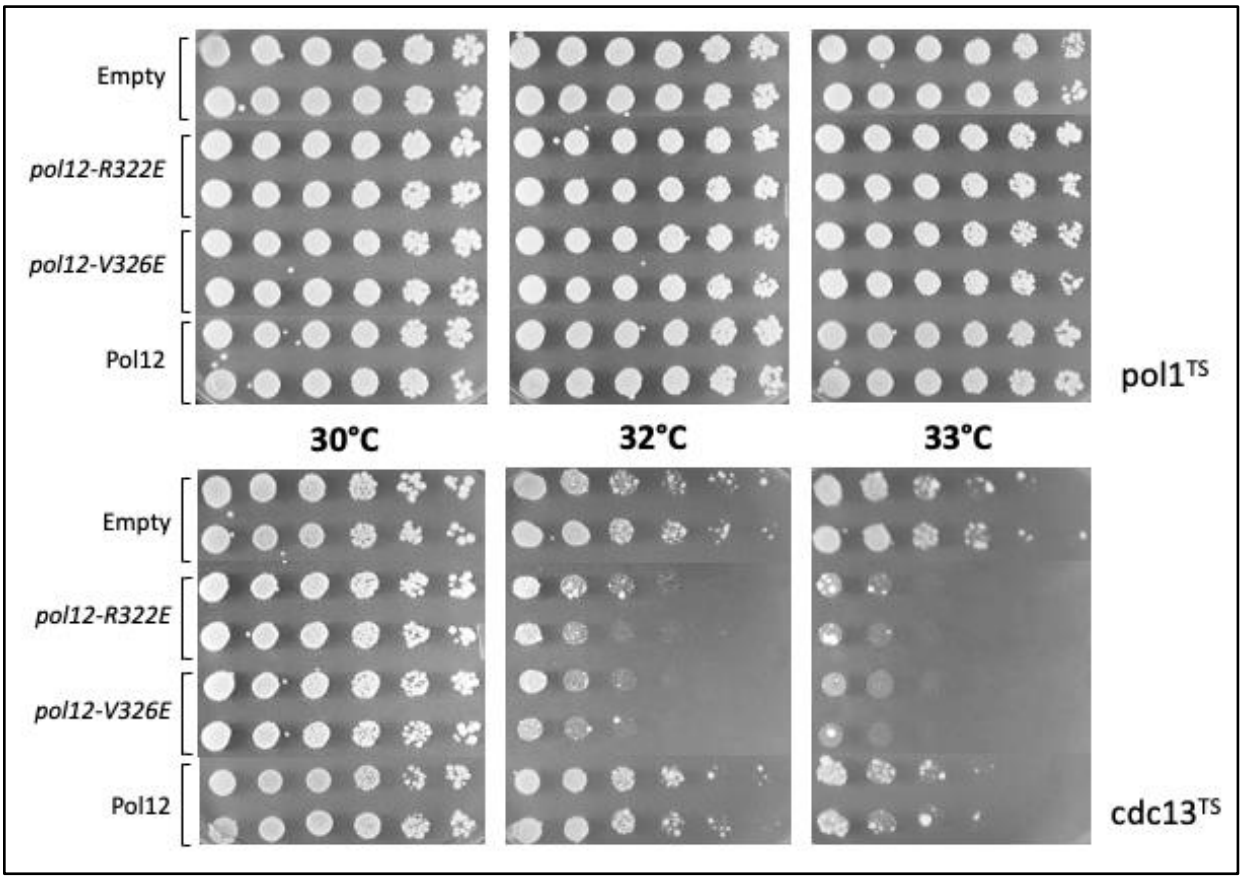

Figure 2.7: Overexpression Dominant Negative (ODN) phenotype of Pol12 surface 3 residues in cdc13^{TS} but not pol1^{TS}

Strains with a mutation of the indicated gene inducing a temperature-sensitive (TS) phenotype were transformed under selective marker pressure with an overexpression 2 micron (2u) vector including the content indicated on the left side. Two independent colonies were grown, replica gridded at different dilutions and grown for 3 days at a gradient of increasing temperatures reducing viability of the strain.

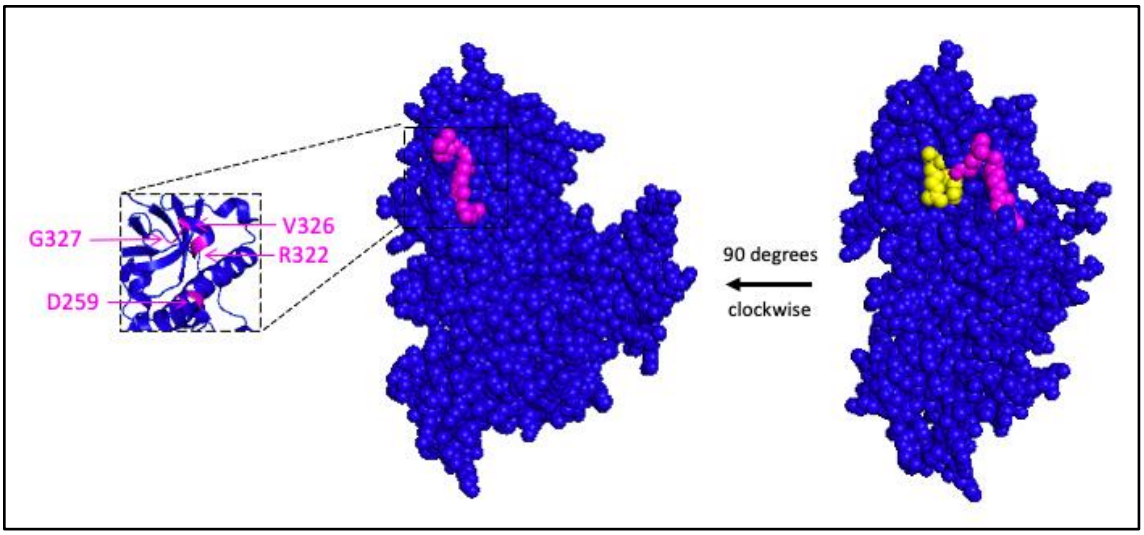

Figure 2.8: Localization of Pol12 surface 3 residues on the surface of Pol12
Crystal structure by Klinge and Pellegrini (PDB 3FLO) was visualized on Pymol. Residues of surface 3 are indicated in magenta. Residues of the expected interface of Pol12 with Pol1 with a similar phenotype are represented in yellow.

Overall, each of the 3 surfaces found had a unique pattern of ODN phenotypes and are physically distinct (**Figure 2.9** and **Table 2.2**). The complete list of ODN phenotypes of the Pol12 library is summarized in **Table 2.4**.

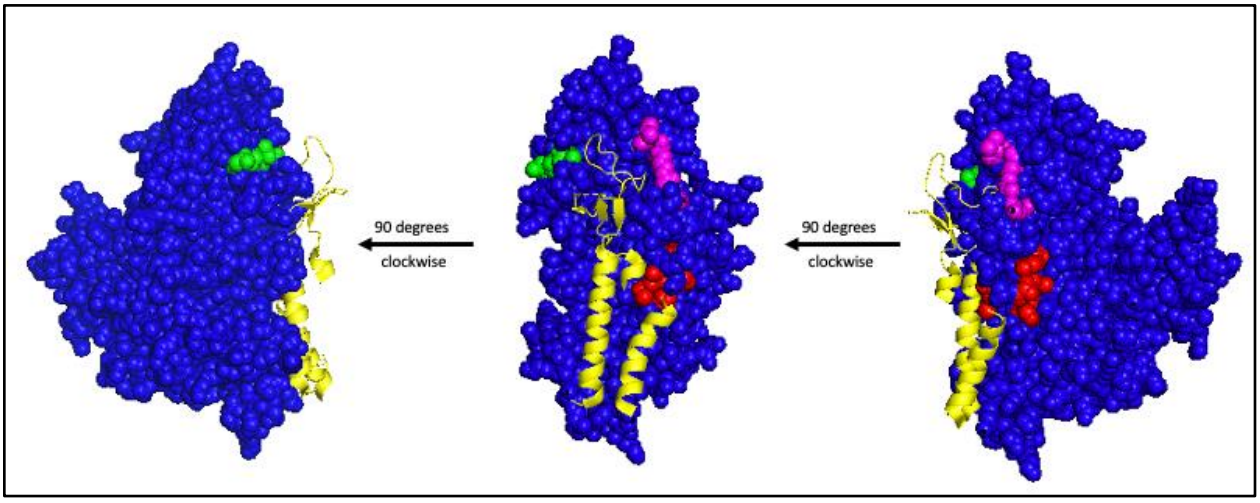

Figure 2.9: Localization of Pol12 surface residues on the surface of Pol12
Crystal structure by Klinge and Pellegrini (PDB 3FLO) was visualized on Pymol. Residues of surface 1, 2 and 3 are indicated in red, green and magenta, respectively. Residues of the expected interface of Pol12 with Pol1 are represented as yellow cartoon.

Table 2.2: Summary of main alleles of Pol12 with an ODN phenotype

Residues highlighted in yellow were previously characterized by Klinge and Pellegrini as being important for the interface with Pol1. Residues in bold were pursued for epistasis analyses described in Chapter 5.

Location	Mutation in Pol12	ODN in pol1-ts?	ODN in cdc13-ts?
Surface 1	**R248E**	YES	YES
	M250E		
	H495E		
	Y616E		
Surface 2	**D303K**	YES	NO
	N312K		
	S315K		
Surface 3	D259K	NO	YES
	R322E		
	V326E		
	G327E		

Published Pol12 residues hypothesized by Klinge and colleagues to be a part of the interface of the protein with Pol1 showed various ODN patterns. Out of the 7 residues tested, six gave a clear phenotype. Most conserved M250 shows a pattern similar to neighboring surface 1 residues as it has an ODN phenotype with both strains. On the other hand, G327 and R329 bundled physically and phenotypically with surface 3 that only has an ODN phenotype with $Cdc13^{TS}$. Finally, both charge-swapped variants of highly conserved P575 had no noticeable ODN phenotype, and the residue does not cluster with any of the surfaces found (**Figure 2.10**). Data from those residues is summarized in **Table 2.3**. This result either argues that the interface is in fact responsible for more than one interaction, or that both patterns of phenotypes are in fact the result of a similarly disrupted interaction with Pol1, possibly at different intensities. Indeed, they colocalize with different secondary structures of Pol1. Whether surfaces 1 and 3 play a similar role will be investigated in chapters 3 through 5.

Table 2.3: Summary of residues found by Klinge and Pellegrini to be important for the interface with Pol1 and their ODN phenotypes

Residue	Conservation up to Humans	ODN pol1-ts?	ODN cdc13-ts?	Colocalizes with
M250	**Invariant**	Yes	Yes	Surface 1
Q252	**Invariant**	No?	Yes	Surface 1
S258	Less conserved	No	Yes	Surface 3
L267	Less conserved	n.t.	n.t.	-
E319	**Invariant**	Yes	No	Surfaces 2 and 3
G327	**Invariant**	No	Yes	Surface 3
R329	Less conserved	No	Rescue	Surfaces 2 and 3
P575	**Invariant**	No	No	-

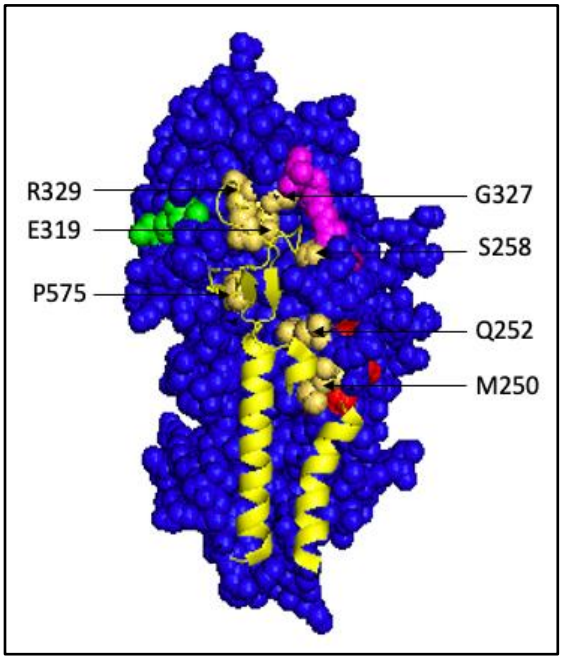

Figure 2.10: Localization of residues found by Klinge and Pellegrini to be important for the interface with Pol1 in comparison with surfaces found by ODN

Crystal structure by Klinge and Pellegrini (PDB 3FLO) was visualized on Pymol. Residues of surface 1, 2 and 3 are indicated in red, green and magenta, respectively. Residues of the expected interface of Pol12 with Pol1 are represented as yellow cartoon.

Several isolated residues were also found throughout the sequence. Most notably, *pol12-D676K* has a clear ODN phenotype in *Cdc13*^{TS} and maps on the complete opposite side of Pol12 compared to the other 3 surfaces found. *pol12-Q457E* has a similar phenotype and localizes on another edge of the protein interface with Pol1 (**Figure 2.11**). For both residues, neighboring ones did not show any growth defect when tested in either strain. However, studies have often shown protein interactions to solely depend on a single amino acid. Therefore, although potentially representative of even more functions of the protein, these residues were not given priority for further studies.

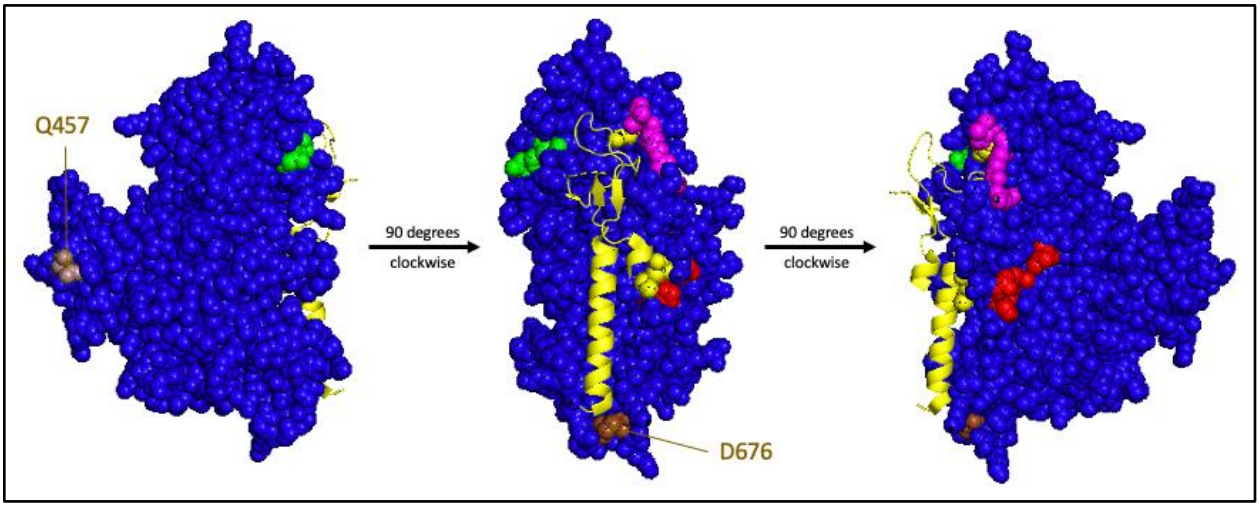

Figure 2.11: Localization of isolated residues on the surface of Pol12
Crystal structure by Klinge and Pellegrini (PDB 3FLO) was visualized on Pymol. Residues of surface 1, 2 and 3 are indicated in red, green and magenta, respectively. Residues of the expected interface of Pol12 with Pol1 are represented as yellow cartoon. Isolated residues found by ODN are indicated in brown.

Table 2.4: Summary of ODN data with Pol12 overexpression library

Viability is represented with the following nomenclature:
++++: increased viability / +++: viable / ++: slightly impaired /
+: clearly impaired / +/-: almost inviable / -: inviable / n.t.: not tested

		yVL4119 (pol1^{TS})			yVL3660 (cdc13^{TS})			
plasmid #	Mutation	RT	30°C	32°C	28°C	30°C	32°C	33°C
pVL399	Empty vector	+++	+++	++	+++	+++	++	+
pVL6321	WT Pol12	+++	+++	+++	+++	+++	++	++
pCS 146	D6K	+++	+++	+++	+++	+++	++	+
pMAM183	F11E	+++	+++	+++	+++	+++	+	+
pMAM184	F11K	+++	+++	++	+++	+++	+	+
pMAM185	D16K	+++	+++	+++	+++	+++	++	+
pMAM186	K17E	+++	+++	+++	+++	+++	++	+
pMAM187	E19K	+++	+++	+++	+++	+++	++	+
pMAM188	E25K	+++	+++	+++	+++	+++	++	+
pMAM189	K29E	+++	+++	+++	+++	+++	++	+
pMAM190	H31E	+++	+++	+++	+++	+++	++	+
pMAM191	H31K	n.t.	n.t.	n.t.	+++	+++	++	+
pCS 147	E36K	+++	+++	+++	+++	+++	+	+
pCS 148	D37K	+++	+++	+++	+++	+++	++	+
pMAM192	K41E	n.t.	n.t.	n.t.	+++	+++	++	+
pCS 149	E43K	+++	+++	+++	+++	+++	++	+
pMAM193	Q44E	+++	+++	+++	+++	+++	+	+
pMAM194	Q44K	+++	+++	+++	+++	+++	+	+
pMAM195	N60E	+++	+++	+++	+++	+++	++	+
pMAM196	N60K	+++	+++	+++	+++	+++	++	+
pMAM197	K65E	+++	+++	+++	+++	+++	++	+
pCS 150	Q69K	n.t.	n.t.	n.t.	+++	+++	++	+
pCS 151	Q69E	+++	+++	+++	+++	+++	++	+
pMAM198	E73K	+++	+++	+++	+++	+++	++	+
pMAM199	K74E	+++	+++	+++	+++	+++	+	+/-
pMAM200	R75E	+++	+++	+++	+++	+++	+	+
pMAM201	K90E	+++	+++	+++	+++	+++	+	+
pCS 153	K91E	n.t.	n.t.	n.t.	+++	+++	++	+
pMAM202	K91E	+++	+++	+++	+++	+++	++	+
pCS 154	KKRK115-118AAAA	+++	+++	++++?	+++	+++	++	++
pMAM203	K115E	+++	+++	+++	+++	+++	++	+
pMAM204	K116E	+++	+++	+++	+++	+++	++	+
pMAM205	R117E	+++	+++	+++	+++	+++	++	+
pCS 215	T190A	+++	+++	+++	n.t.	n.t.	n.t.	n.t.
pMAM206	N208E	+++	+++	+++	+++	+++	++	+
pMAM207	N208K	+++	+++	++?	+++	+++	+++	+
pMAM208	E210K	+++	+++	++?	+++	+++	++	+
pMAM209	N211E	+++	+++	+++	+++	+++	++	+
pMAM210	N211K	+++	+++	+++	+++	+++	++	+
pMAM211	E213K	+++	+++	+++	+++	+++	++	+
pMAM212	K235E	+++	+++	+++	n.t.	n.t.	n.t.	n.t.
pCS 155	D241K	+++	+++	+++	+++	+++	++	+
pCS 156	K244E	+++	+++	+++	+++	+++	+	+
pCS 157	R248E	+++	++	+/-	+++	+++	+	+
pMAM213	M250E	+++	+++	++ or +	+++	+++	+	+
pMAM215	Q252E	++?	+++	+++?	+++	+++	+	+
pMAM216	Q252K	+++	+++	+++	+++	+++	++	+
pMAM217	Q255E	+++	+++	+++	+++	+++	++	+

Table 2.4: Summary of ODN data with Pol12 overexpression library (cont.)

		yVL4119 (pol1^{TS})			yVL3660 (cdc13^{TS})			
plasmid #	Mutation	RT	30°C	32°C	28°C	30°C	32°C	33°C
pVL399	Empty vector	+++	+++	++	+++	+++	++	+
pVL6321	WT Pol12	+++	+++	+++	+++	+++	++	++
pMAM218	Q255K	+++	+++	+++	+++	+++	++	+
pMAM219	S258E	+++	+++	+++	+++	+++	++	+
pMAM220	S258K	+++	+++	+++	+++	+++	+	+/-
pCS 158	D259K	+++	+++	++	+++	+++	+/-	+/-
pCS 159	D262K	+++	+++	+	+++	+++	+/-	+/-
pCS 160	D263K	+++	+++	++	+++	+++	+	+/-
pCS 161	Q264K	+++	+++	+++	++++	++++	++	+
pCS 162	Q264E	+++	+++	+++	+++	+++	++	+
pCS 163	E266K	+++	+++	++	+++	+++	+	+/-
pMAM227	D285K	+++	+++	+++	+++	+++	+	+/-
pCS 164	Q289K	+++	+++	++	+++	+++	++	+
pCS 165	Q289E	+++	+++	+++	+++	+++	+++	++
pMAM228	Q291E	+++	+++	+++	+++	+++	+++	++
pMAM229	Q291K	+++	+++	++	+++	+++	++	+
pCS 166	E293K	+++	+++	+++	+++	+++	++	+
pCS 167	R299E	+++	+++	++	+++	+++	++	+
pCS 168	D303K	+++	++	+/-	+++	+++	++	+
pCS 169	N312K	+++	++	+	+++	+++	+++	+
pCS 170	N312E	+++	+++	+?	+++	+++	++	+
pMAM230	S315E	+++	+++	+++	+++	+++	++	+
pMAM231	S315K	+++	+++	+	+++	+++	++	+
pCS 171	E319K	+++	+++	+	+++	+++	++	+
pCS 172	R322E	+++	+++	++	+++	+++	+/-	+/-
pMAM232	V326E	+++	+++	+++	+++	+++	+/-	-
pMAM233	V326K	+++	+++	++?	+++	+++	+	-
pMAM221	G327E	+++	+++	+++	+++	+++	+	+/-
pMAM222	G327K	+++	+++	++	+++	+++	+/-	+/-
pCS 173	R329E	+++	+++	+++	+++	+++	+++	+++
pMAM234	D333K	+++	+++	+++	+++	+++	++	+
pCS 174	Q346K	+++	+++	+++	+++	+++	++	+
pCS 175	Q346E	+++	+++	+++	+++	+++	++	+
pCS 177	N354K	+++	+++	++	+++	+++	++	+
pCS 178	N354E	+++	+++	++	+++	+++	++	+
pMAM235	P369E	+++	+++	+++	+++	+++	+	+
pMAM236	P369K	+++	+++	+++	+++	+++	++	+
pMAM237	V375E	+++	+++	+++	+++	+++	++	+
pMAM238	V375K	+++	+++	+++	+++	+++	++	+
pMAM239	Q379E	+++	+++	+++	+++	+++	++	+
pMAM240	Q379K	+++	+++	+++	+++	+++	++	+
pMAM241	E380K	+++	+++	++	+++	+++	++	+
pMAM242	Q382E	+++	+++	+++	+++	+++	++	+
pCS 179	E383K	+++	+++	++++	++	++	++	+
pMAM243	Q382K	+++	+++	+++	+++	+++	++	+
pCS 180	K394E	+++	+++	+++	+++	+++	++	+
pMAM244	P401E	+++	+++	++?	+++	+++	++	+
pMAM245	P401K	+++	+++	++?	+++	+++	++	+
pMAM246	D406K	+++	+++	++?	+++	+++	++	+
pMAM247	Q414E	+++	+++	+++	+++	+++	++	+

Table 2.4: Summary of ODN data with Pol12 overexpression library (cont.)

		yVL4119 (pol1^{TS})			yVL3660 (cdc13^{TS})			
plasmid #	Mutation	RT	30°C	32°C	28°C	30°C	32°C	33°C
pVL399	Empty vector	+++	+++	++	+++	+++	++	+
pVL6321	WT Pol12	+++	+++	+++	+++	+++	++	++
pMAM248	Q414K	+++	+++	++?	+++	+++	++	+
pMAM249	E415K	+++	+++	+++	+++	+++	++	+
pMAM250	E423K	+++	+++	+++	+++	+++	++	+
pMAM251	K425E	+++	+++	+++	+++	+++	++	+
pMAM252	H427E	+++	+++	+++	+++	+++	++	+
pMAM253	H427K	+++	+++	+++	+++	+++	++	+
pMAM254	I436E	+++	+++	+++	+++	+++	++	+
pCS 181	D437K	+++	+++	++?	+++	+++	++	+
pMAM255	I436K	n.t.	n.t.	n.t.	+++	+++	+	+
pMAM256	I443E	+++	+++	+++	+++	+++	++	+
pMAM257	I443K	+++	+++	+++	+++	+++	++	+
pMAM223	S445E	+++	+++	+++	+++	+++	++	+
pMAM224	S445K	+++	+++	+++	+++	+++	++	+
pMAM258	K455E	n.t.	n.t.	n.t.	+++	+++	++	+
pCS 182	Q457K	+++	+++	+++	+++	+++	++	+
pCS 183	Q457E	+++	+++	+++	+++	+++	+	+/-
pCS 184	K459E	+++	+++	+++	+++	+++	++	+
pCS 185	D462K	+++	+++	++	+++	+++	++	+
pMAM259	K466E	+++	+++	+++	+++	+++	++	+
pMAM260	P471E	+++	+++	++	+++	+++	++	+
pMAM261	P471K	+++	+++	+++	+++	+++	++	+
pMAM262	K474E	+++	+++	+++	+++	+++	++	+
pMAM263	Q481E	+++	+++	+++	+++	+++	++	+
pMAM264	Q481K	+++	+++	+++	+++	+++	++	+
pMAM265	P486E	+++	+++	++	+++	+++	++	+
pMAM266	P486K	+++	+++	++	+++	+++	++	+
pCS 186	D490K	+++	+++	+++	+++	+++	++	+
pCS 187	H495K	+++	+++	+++	+++	+++	++	+
pCS 188	H495E	+++	++	+	+++	+++	++	+
pCS 189	Q500K	+++	+++	+++	+++	+++	++	+
pCS 190	Q500E	+++	+++	+++	+++	+++	++	+
pCS 191	R505E		+++	++	+++	+++	++	+
pCS 192	K506E	+++	+++	+++	+++	+++	++	+
pMAM267	P511E	+++	+++	+++	+++	+++	++	+
pMAM268	P511K	+++	+++	+++	+++	+++	++	+
pCS 193	R513E	+++	+++	+++	+++	+++	++	+
pMAM269	K512E	+++	+++	+++	+++	+++	++	+
pCS 194	K516E	+++	+++	+++	++++	++++	+++	++
pMAM270	P521E	+++	+++	+++	+++	+++	++	+
pMAM271	P521K	+++	+++	+++	+++	+++	++	+
pMAM272	Q525E	+++	+++	+++	+++	+++	+	+
pMAM273	Q525K	+++	+++	+++	+++	+++	++	+
pMAM274	N527E	+++	+++	+++	+++	+++	++	+
pCS 195	E528K	+++	+++	+++	+++	+++	++	+
pMAM275	N527K	+++	+++	++	+++	+++	++	+
pCS 196	D537K	+++	+++	+++	+++	+++	++	+
pMAM276	K539E	+++	+++	+++	+++	+++	+	+
pCS 197	D541K	+++	+++	+++	+++	+++	++	+
pMAM277	K543E	+++	+++	+++	+++	+++	++	+
pMAM278	E544K	+++	+++	++?	+++	+++	++	+
pMAM279	K547E	+++	+++	++?	+++	+++	++	+

Table 2.4: Summary of ODN data with Pol12 overexpression library (cont.)

		yVL4119 (pol1^{TS})			yVL3660 (cdc13^{TS})			
plasmid #	**Mutation**	**RT**	**30°C**	**32°C**	**28°C**	**30°C**	**32°C**	**33°C**
pVL399	**Empty vector**	+++	+++	++	+++	+++	++	+
pVL6321	**WT Pol12**	+++	+++	+++	+++	+++	++	++
pCS 198	R556E	+++	+++	+++	+++	+++	++	+
pCS 199	R559E	+++	+++	+++	+++	+++	+?	+
pMAM280	Q566E	+++	+++	+++	+++	+++	++	+
pMAM281	Q566K	+++	+++	+++	+++	+++	++	+
pCS 200	R568E	+++	+++	+++	+++	+++	++	++
pMAM225	P575E	+++	+++	+++	+++	+++	++	+
pMAM226	P575K	+++	+++	+++	+++	+++	++	+
pMAM282	P575E	+++	+++	++?	+++	+++	+++	+
pMAM283	P575K	+++	+++	++?	+++	+++	++	+
pMAM284	R579E	+++	+++	++?	+++	+++	++	+
pCS 201	D613K	+++	+++	+++	+++	+++	++	+
pMAM285	L612E	+++	+++	+++	+++	+++	++	+
pMAM286	L612K	+++	+++	+++	+++	+++	+	+
pMAM287	Y616E	+++	+++	+++	+++	+++	+	-
pMAM288	Y616K	+++	+++	++	+++	+++	+	-
pMAM289	L619E	+++	+++	++	+++	+++	++	+
pMAM290	L619K	+++	+++	+++	+++	+++	++	+
pCS 202	E621K	+++	+++	+++	+++	+++	+	+/-
pMAM291	V623E	+++	+++	+++	+++	+++	+	-
pMAM292	V623K	+++	+++	+++	+++	+++	+	-
pCS 203	D629K	+++	+++	+++	+++	+++	++	+
pCS 204	E636K	+++	+++	+++	+++	+++	++	++
pMAM294	L636K	+++	+++	++	+++	+++	++	+
pCS 205	R642E	+++	+++	+++	+++	+++	++	+
pMAM295	V642E	+++	+++	+++	+++	+++	++	+
pMAM296	V642K	+++	+++	+++	+++	+++	++	+
pMAM297	R656E	+++	+++	+++	+++	+++	+	+
pMAM298	Y664E	+++	+++	++	+++	+++	++	+
pMAM299	Y654K	+++	+++	+++	+++	+++	++	+
pMAM300	D673K	+++	+++	+++	+++	+++	++	+
pMAM301	E675K	+++	+++	+++	+++	+++	++	+
pMAM302	D676K	+++	+++	+++	++?	++?	+?	-
pMAM303	Y689E	+++	+++	+++	+++	+++	++	+
pMAM304	Y689K	+++	+++	+++	+++	+++	++	+
pCS 206	H692K	+++	+++	+++	+++	+++	++	++
pCS 207	H692E	+++	+++	+++	+++	+++	++	++
pCS 208	N693K	+++	+++	+++	+++	+++	++	++
pCS 209	N693E	+++	+++	+++	++	++	++	+
pCS 211	R697E	+++	+++	+++	+++	+++	++	+
pCS 212	R699E	+++	+++	+++	+++	+++	++	+
pCS 213	D701K	+++	+++	+++	+++	+++	++	+

The ODP (Overexpression Dominant positive) phenotype

The goal of the ODN assay is to uncover separation-of-function mutants that, when overexpressed, overwhelm the protein of interest's partner binding sites against WT. Although proving to be fruitful when studying essential proteins, we also encountered many mutants that resulted in the opposite growth rescue of the sensitized strain at non-permissive temperature. This ODP (Overexpression Dominant positive) phenotype was seen even in some of the original Pol12 mutants. For example, disrupting its KKRK nuclear localization partially rescues the TS of Pol1^{TS}, but not Cdc13^{TS}, compared to the empty vector growth. This puzzling observation argues that presence of extra Pol12 in the cytoplasm may increase viability, as the endogenous version of the protein is still capable of localizing properly. However, the levels of viability are very similar to the cells transformed with the overexpression vector expressing WT Pol12. Therefore, another possibility is that the mutant is still partially or fully able to localize to the nucleus and perform similar functions as WT. Additional experiments without endogenous expression of WT Pol12 are needed to gather more information about the source of the rescued viability.

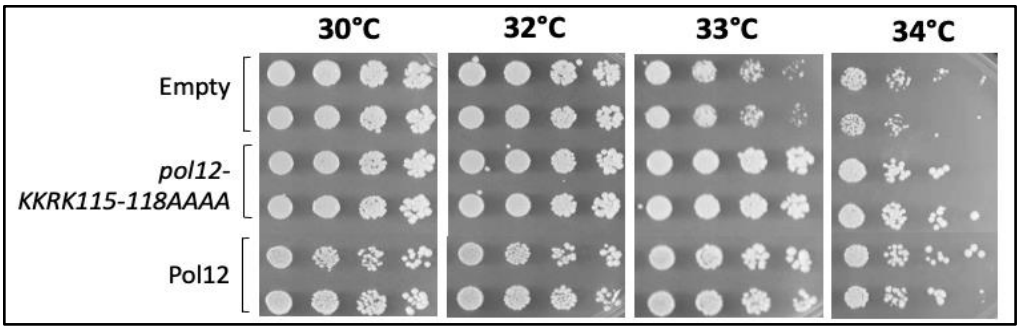

Figure 2.12: Disruption of the Pol12 nuclear localization motif KKRK rescues viability in a Pol1^{TS} strain

Pol1^{TS} was transformed under selective marker pressure with an overexpression 2 micron (2u) vector including the content indicated on the left side. Two independent colonies were grown, replica gridded at different dilutions and grown for 3 days at increasing temperatures reducing viability of the strain

Similarly, inactivating one of the putative phosphorylation sites Pol12-T190 by mutating it into Alanine results in an ODP phenotype in *Pol1*^{TS} (**Figure 2.13**). This puzzling observation argues that the increased presence of inactive Pol12 could improve viability. One possibility is that Pol12 naturally competes or interacts with another protein, such as a DNA damage response factor, and disrupting that balance improves viability. Based on previous literature about the two complexes, t-RPA's Stn1 could be that protein. To illustrate, a member of the laboratory has also observed a set of unique Replication Protein A (RPA) mutants that are able to rescue the TS phenotype of *Cdc13*^{TS} *(Moeller et al. in preparation)*. Similarly, some knock-outs of DNA repair proteins have been shown to rescue that temperature sensitivity (*Paschini et al., 2012*). It has long been suggested that, based on their structural similarities, RPA and t-RPA might compete at telomeric single-stranded DNA and such rescue could be the manifestation of a switch in that competition equilibrium. Further data looking at the possible relationship between polymerase alpha-primase, RPA and t-RPA will be discussed in chapter 5.

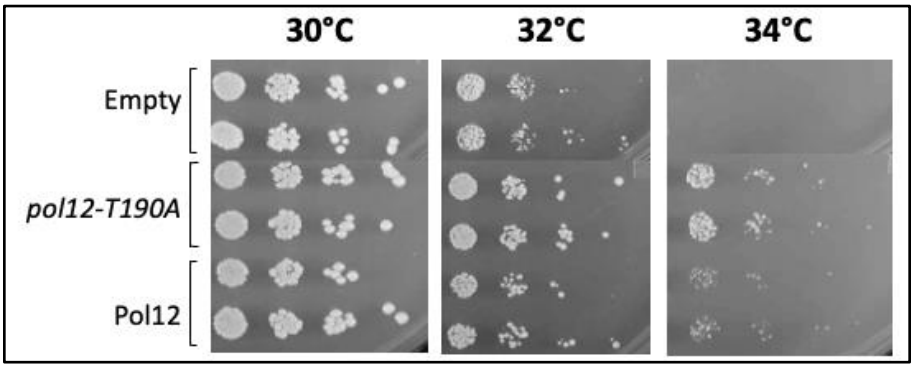

Figure 2.13: Disruption of the Pol12 suspected phosphorylation site T190 rescues viability in a Pol1^{TS} strain

Pol1^{TS} *was transformed under selective marker pressure with an overexpression 2 micron (2u) vector including the content indicated on the left side. Two independent colonies were grown, replica gridded at different dilutions and grown for 3 days at a gradient of increasing temperatures reducing viability of the strain*

Many of the ODP mutants localize close to residues showing an ODN phenotype when substituted. This observation is expected as since some separation-of-function mutations disrupt interactions, others may facilitate them. In fact, this feature has been characterized and used to generate more stable interactions to be studied biochemically (*Rao et al. 2014*). For example, R329, one of the residues predicted to be a part of the *Pol1-Pol12* interface and mapping with surface 3, gives in fact a strong ODP phenotype when swapped to glutamic acid in *Cdc13*^{TS} (**Figure 2.14**). Unlike previous alleles, this one does not rescue Pol1^{TS}. However, all other alleles are expected to alter the expression or localization of the protein rather than protein interactions.

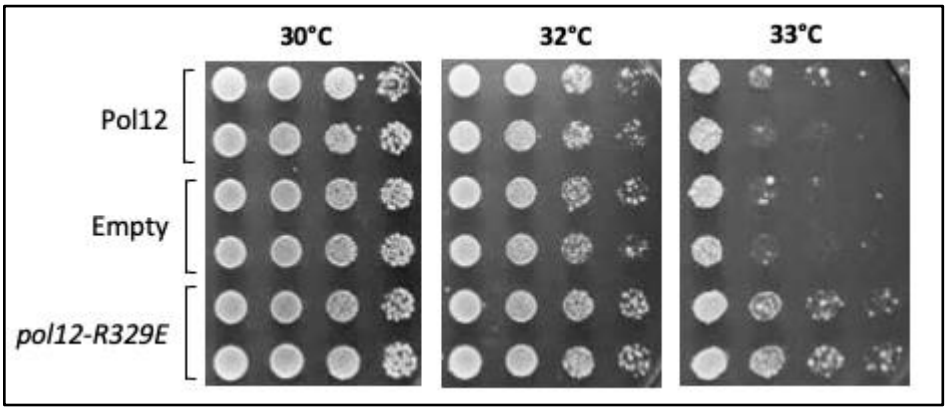

Figure 2.14: Mutation of the suspected residue playing a role in the Pol1-Pol12 interaction increases viability in a Cdc13^{TS} strain

Cdc13^{TS} was transformed under selective marker pressure with an overexpression 2 micron (2u) vector including the content indicated on the left side. Two independent colonies were grown, replica gridded at different dilutions and grown for 3 days at a gradient of increasing temperatures reducing viability of the strain

Another cluster of two residues shows a clear ODP phenotype with *Cdc13*^{TS} only. This duo maps close to surface 3 that shows an ODN phenotype in the same strain. Similarly, both polar residues flanking another predicted probable phosphorylation site S290 have a strong ODP phenotype when mutated onto negatively charged Glutamic acid, but not positively charged Lysine (*Horn et al. 2014*) (**Figure 2.15**).

As phosphorylation adds a negative charge to the target amino acid, it is possible that those mutations mimic a phosphorylated state (*Pearlman et al. 201*1). Furthermore, the predicted kinases responsible for the post-translational modification of S290 are Mec1 and Tel1. Both these proteins are essential players of replication and telomere homeostasis, respectively. The assay is therefore potentially powerful enough to be able to detect putative phosphorylation sites.

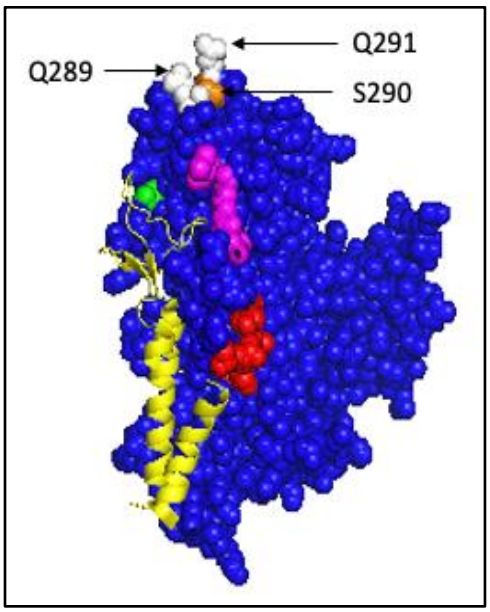

Figure 2.15: Localization of phosphorylable residue serine 290 and neighboring Glutamines on the surface of Pol12

Crystal structure by Klinge and Pellegrini (PDB 3FLO) was visualized on Pymol. Residues of surface 1, 2 and 3 are indicated in red, green and magenta, respectively. Residues of the expected interface of Pol12 with Pol1 are represented as yellow cartoon. Residues giving an ODP phenotype in cdc13^{TS} *are indicated in white whereas the putative phosphorylation site is shown in orange*

Discussion: ODN assay limits

As powerful as the ODN assay can be, it has factors and limitations to be considered. First of all, there are inherent hurdles arising from the nature of the assay itself. For example, although the point of the use of the 2 micron (2u) vector is to overflow the cells with the mutated version of the gene of interest to outcompete the endogenous WT one, the actual copy number of the plasmid is fairly variable. This feature is particularly noticeable with mutants with a strong defect, as colonies transformed synchronously may have variable sizes or levels of growth defects rendering them hard to rate and compare. To counter this, it is recommended to consistently pick the biggest colonies plated. Furthermore, the assay is performed with each mutant as a duplicate (two colonies from the same transformation) to generalize results.

Another limitation arising from the use of the 2u plasmid is the fact it can give a phenotype with a WT protein. Although our laboratory successfully screened over a dozen essential proteins with the ODN assay, it has for example not been possible to analyze Cdc13 because of the lethality resulting from the overexpression of the WT protein. Other ones can also show a slight rescue or defect through overexpression of a given protein of interest. To take this into account, the assay includes a positive control plasmid expressing the WT protein for its mutants to be compared to.

One last limitation arising from the nature of the assay is the specificity of surface residues giving a phenotype with sensitized strains. As observed with Pol12, surface 2 only has an ODN phenotype with $Pol1^{TS}$ whereas surface 3 adds to the $Cdc13^{TS}$ defect and hadn't been detected with the original pilot. Analysis of the protein, although thorough, could potentially have missed other residues important for different pathways the protein could be involved in, such as DNA damage response.

Another aspect to consider is the nature of the disruption of the mutated residues itself. Indeed, they can either abrogate the binding ability of the protein to a partner or alter a potential catalytic activity, either partially or completely. These different alterations will have different phenotypes through the ODN assay. Given the basal expression of the endogenous protein, a mutant that partially alters a binding site will outcompete the WT copy and create a phenotype. A catalytically inactive protein will also outcompete the WT copy and hog its ligand, disrupting an essential activity that will result in a nearly or fully lethal phenotype. Yet, an allele with a completely disrupted binding ability will not be able to compete with the endogenous protein and might not give a phenotype. Although possible, essential interactions between the two proteins rarely rely on a single amino acid. However, the protocol of extensively mutating conserved residues of a gene would presumably pick up neighboring ones that disrupt the interaction indirectly and/or to a milder extent.

Finally, the assay frequently uncovers temperature sensitive alleles. The matching mutated residues are often partially buried from the surface and result in an unfolding of the protein at higher temperatures. Therefore, it will show a growth phenotype independently of the strain it is tested in. Discovery of TS alleles can be a useful tool to look at consequences of a global disruption of a protein or for use as a sensitized strain.

Data from this chapter is currently in preparation to be published (Meunier and Lundblad, in preparation). The dissertation author was the primary researcher and author of this material.

CHAPTER 3:
A polymerase alpha-primase complex-wide interface performs a novel function

Abstract

Viability studies of the Pol12 alleles found by ODN argues that surfaces 1 and 3 might perform a similar essential function specific to t-RPA. This function may be distinct from that of the interface of the protein with Pol1. A broader look at the whole complex through Banavarovskiy and colleagues' crystallography work placed both of those surfaces on an interface where the DNA strand transfers from primase to polymerase during replication. After expanding the ODN protocol to the other three subunits of the complex, several mutants in Pri1, Pri2 and Pol1 with a similar sensitivity to the Cdc13 temperature sensitive strain were found. Most of those mutants cluster within that same interface and are expected to play a role in either the primase-polymerase cohesion or active sites of the complex. Therefore, the cohesion of the entire complex is expected to be important for a novel function pertaining to t-RPA.

The Loss-of-function (LOF) assay

What lead to believe surfaces found through the ODN assay encompass distinct separation-of-function alleles is their specific phenotype with different TS strains. Surface 1 and surface 2 residues give a significant growth defect in a polymerase alpha defective strain, whereas surface 1 and 3 mutants are sensitive to a disruption of t-RPA. Furthermore, although screening the protein surface pretty extensively, the residues cluster into distinct groups, all around the predicted Pol1-Pol12 interface. Various residues from that predicted interface themselves group with the different surfaces found based on their phenotype and localization, although expected to perform the same function.

In order to investigate whether the alleles are indeed separation-of-functions, we studied changes in viability by combining mutations from these distinct surfaces using a Loss-Of-Function (LOF) approach. This assay, testing for changes in viability, has been traditionally used in place of the ODN assay as a reverse genetics screening tool. It involves a knock-out strain of the gene of interest, complemented by a covering WT version of said gene if essential, like Pol12. It is based on the use of 5-Fluoroorotic Acid, a drug that kills cells containing the URA3 marker as it metabolizes it into a toxic component. As URA3 is contained within the WT Pol12 covering plasmid, exposure to the compound forces cells to shuffle it off, leaving only the mutated version to be expressed in a second plasmid. Whether the mutation is viable *in vivo* will determine whether the strain survives on 5-FOA.

Yet, when studying essential proteins, this assay doesn't distinguish between separation-of-function mutations and those creating an unfolded protein, as both result in a loss of essential functionality when solely expressed in the host cell. Nevertheless, it can be a powerful secondary method to assess whether a separation-of-function allele previously found through ODN would

result in cell lethality *in vivo*. Furthermore, as the mutated protein is expressed in the cell at basal levels through a centromeric (CEN) promoter unlike the ODN approach, its effects faithfully mimic those of the same mutation integrated onto the genome with much less work.

Material and methods: LOF

All LOF analyses were performed in yVL4931 (*MATa ura3-52 lys2-801 trp-Δ1 his3-Δ200 leu2-Δ1 pol12-Δ::KAN* complemented with pVL7267 (CEN URA3 Pol12)) and yVL4921 (*MATa ura3-52 lys2-801 trp-Δ1 his3-Δ200 leu2-Δ1 pri2-Δ::KAN* complemented with pVL7266 (CEN URA3 Pri2)).

Missense mutations in Pol12 and Pri2 were introduced by Quickchange mutagenesis into pVL7270 (CEN LEU2 Pol12) and pVL7269 (CEN LEU2 Pri2) respectively, and checked by sequencing. A standard LiAC transformation protocol was used to introduce plasmids individually into yeast alongside pVL399 as a negative control and pVL7270 or pVL7269 as a positive control. Cells were plated on YPD (Yeast Extract Peptone Dextrose) minus Leucine and Uracil (-Leu -Ura) petri dishes, grown in duplicates overnight on YPD-Leu-Ura liquid media and gridded simultaneously on -Leu-Ura plates as a control and YPD-Leu +5-Fluoroorotic Acid (5-FOA) plates in serial dilutions for readability.

All ODN analyses were performed in two temperature sensitive strains, yVL4119 (*MATa ura3-52 trp1-289 ade2-101 tyr1 gal2 can1 his3 pol1-15 leu2Δ::NAT*) or yVL3660 (*MATa ura3-52 lys2-801 trp-Δ1 his3-Δ200 leu2-Δ1 cdc13-F684S bar1Δ::cNAT*). Missense mutations in Pol1/Pri1/Pri2 were introduced by Quickchange mutagenesis into pVL6511 (2μ LEU2 ADH-

Pol12), pVL6303 (2µ LEU2 ADH-Pri1) or pVL6443 (2µ LEU2 ADH-Pri2) respectively and checked by sequencing. The rest of the protocol is described in chapter 2.

Table 3.1: List of plasmids used for the LOF assay of Pol12 and Pri2

Plasmid #	Content
pVL7266	*CEN URA3-PRI2*
pVL7267	*CEN URA3-POL12*
pVL7270	*CEN LEU2-PRI2*
pVL7270	*CEN LEU2-POL12*
pVL7495	*CEN LEU2-pri2-Y397A*
pVL7499	*CEN LEU2-pol12-R248E*
pVL7505	*CEN LEU2-pol12-R322E*
pVL7934	*CEN LEU2-pol12-R248E+R322E*
pVL7968	*CEN LEU2-pol12-L254A+F574A+P575A*
pVL7969	*CEN LEU2-pol12-R299E+E319K+R329E*
pVL7974	*CEN LEU2-pri2-C336A*
pVL7975	*CEN LEU2-pri2-C417A*
pVL7976	*CEN LEU2-pri2-C434A*
pVL7977	*CEN LEU2-pri2-C474A*
pVL7978	*CEN LEU2-pri2-C336A+C474A*

Table 3.2: List of plasmids used for the ODN assay of Pol1, Pri1 and Pri2

Plasmid #	Content
pVL6511	*2µ LEU2 ADH-POL1*
pVL6303	*2µ LEU2 ADH-PRI1*
pVL6443	*2µ LEU2 ADH-PRI2*
pVL7956	*2µ LEU2 ADH-pol1-R1366E*
pVL7957	*2µ LEU2 ADH-pol1-F1463A*
pVL7958	*2µ LEU2 ADH-pri1-D111A*
pVL7959	*2µ LEU2 ADH-pri1-D113A*
pVL7960	*2µ LEU2 ADH-pri1-D314A*
pVL7961	*2µ LEU2 ADH-pri2-Y397A*
pVL7962	*2µ LEU2 ADH-pri2-H401A*

Results: LOF assay of combination of Pol12 ODN mutants

A first step to the experiment was to check that no individual Pol12 alleles were lethal. Indeed, the key of the ODN assay includes endogenous expression of Pol12 by the cells, which prevents unfolded proteins from giving a phenotype. Therefore, severe mutations resulting in lethality by themselves might still have shown as viable through ODN although they presumably would not have shown a significant phenotype. 40 of the most notable alleles previously found were tested for LOF and found to be viable. We then looked at combinations of two strongest mutants from each individual surface by putting them onto the same Pol12 gene on the plasmid containing the LEU2 marker. Once again, all of those combination alleles were viable.

For comparison, we used data from the Klinge lab to identify residues that are most likely to interact with Pol1. This interaction is essential for the integrity of the catalytic and B subunits of all polymerases (*Garcia et al., 2004*). Without it, defects in DNA Replication result in cell lethality (*Dua et al., 1998*). Impairment of multiple residues characterized by Klinge and Pellegrini as being a part of the interface with Pol1, represented by the triple mutant *pol12-R299E+E319K+R329E*, was viable. In contrast, makeshift generation of a strongly impaired surface interaction with the zinc finger of Pol1, characterized by the triple mutant *pol12-L254A+F574A+P575A*, resulted in lethality (**Figure 3.1**). Therefore, as hypothesized in Chapter 2, either the residues disrupt the interface of Pol12 with more than just Pol1, or they disrupt it to a lesser, still viable degree by themselves.

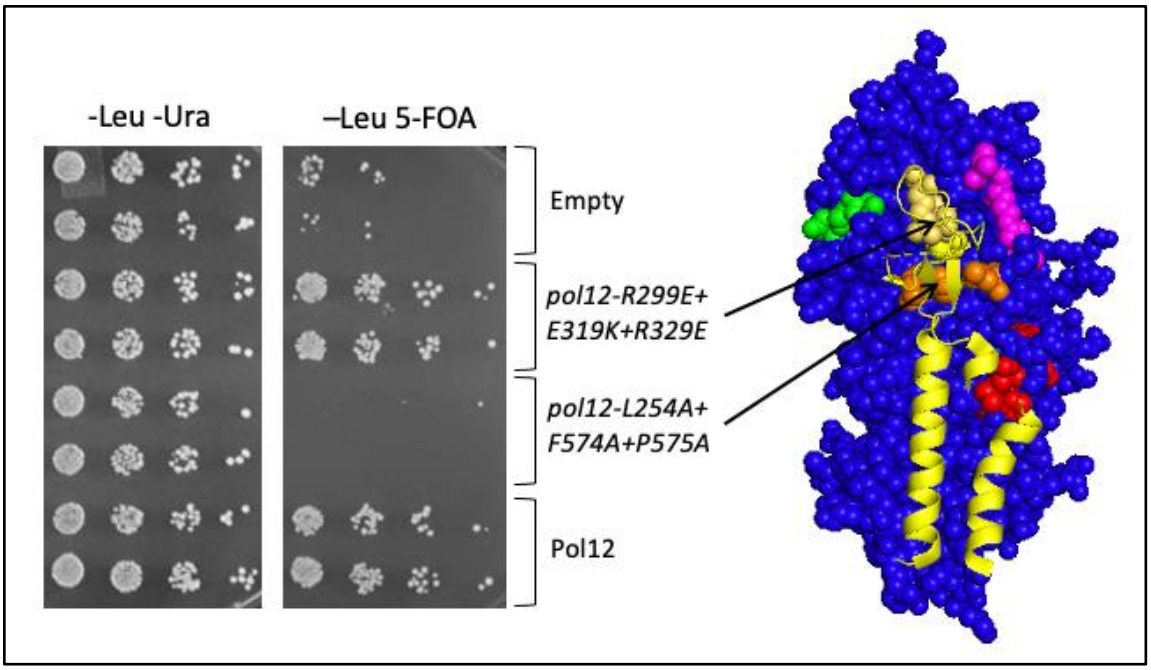

Figure 3.1: Disruption of some parts of the Pol1-Pol12 interface is lethal by LOF
(Left) A Pol12 Knock-out strain with covering CEN-URA3-Pol12 plasmid (yVL4931) was transformed with variants of CEN-LEU2 plasmids with the content indicated. Cells were grown and viability was compared on -Leu -Ura for control and -Leu 5-FOA for shuffling off the covering plasmid.
(Right) Localization of the residues mutated on the crystal structure of Pol12 interacting with Pol1 is indicated with arrows in comparison to surfaces 1, 2 and 3 found by ODN and previously described in red, green and magenta respectively (PDB 3FLO)

Finally, we combined mutants from different surfaces to address whether this might have an additive effect resulting in lethality. This would argue that those surfaces have a moderate effect on a redundant function. Indeed, if surfaces perform distinct functions, their combination would not have an additive effect as they moderately impact different functions and pathways. The combination of surface 1's *pol12-R248E* and surface 3's *pol12-R322E* was the only double mutant allele tested that resulted in lethality (**Figure 3.2**). This data, in addition to their common ODN phenotype with $Cdc13^{TS}$, leads us to believe these two surfaces may in fact be a single interface playing an important role pertaining to t-RPA and/or telomere homeostasis.

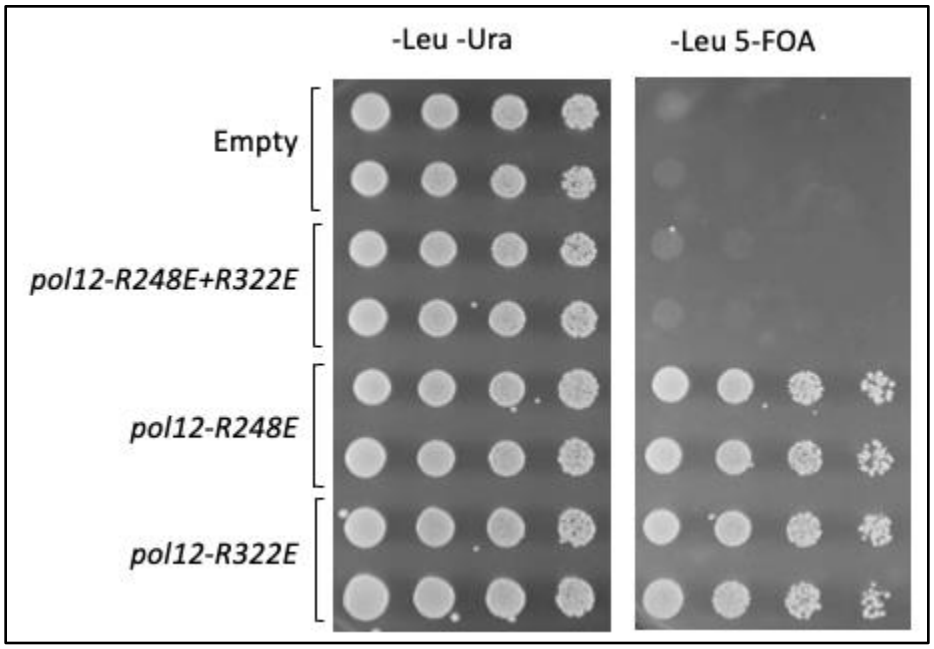

Figure 3.2: Combination of alleles of surfaces 1 and 3 found by ODN is lethal by LOF
A Pol12 Knock-out strain with covering CEN-URA3-Pol12 plasmid (yVL4931) was transformed with variants of CEN-LEU2 plasmids with the content indicated on the left. Cells were grown and viability was compared on -Leu -Ura for control and -Leu 5-FOA for shuffling off the covering plasmid.

Analysis of Pol1 subunit

A more recently published crystal structure that will extensively be used for this portion of the chapter allows to map Pol12 residues within the entire Human polymerase alpha-primase, or primosome (*Baranovskiy et al., 2016*). According to it, surface 1 and 3's clustered in a cleft in the middle of all 4 subunits. In order to address whether the function performed by the Pol12 surfaces also involves other subunits of the complex, we repeated the ODN experiment with a library of Pol1 alleles generated with a similar strategy as described above (**Figure 3.3**). It included mutants of the highly conserved very C-terminal region of the protein, as well as known active site residues.

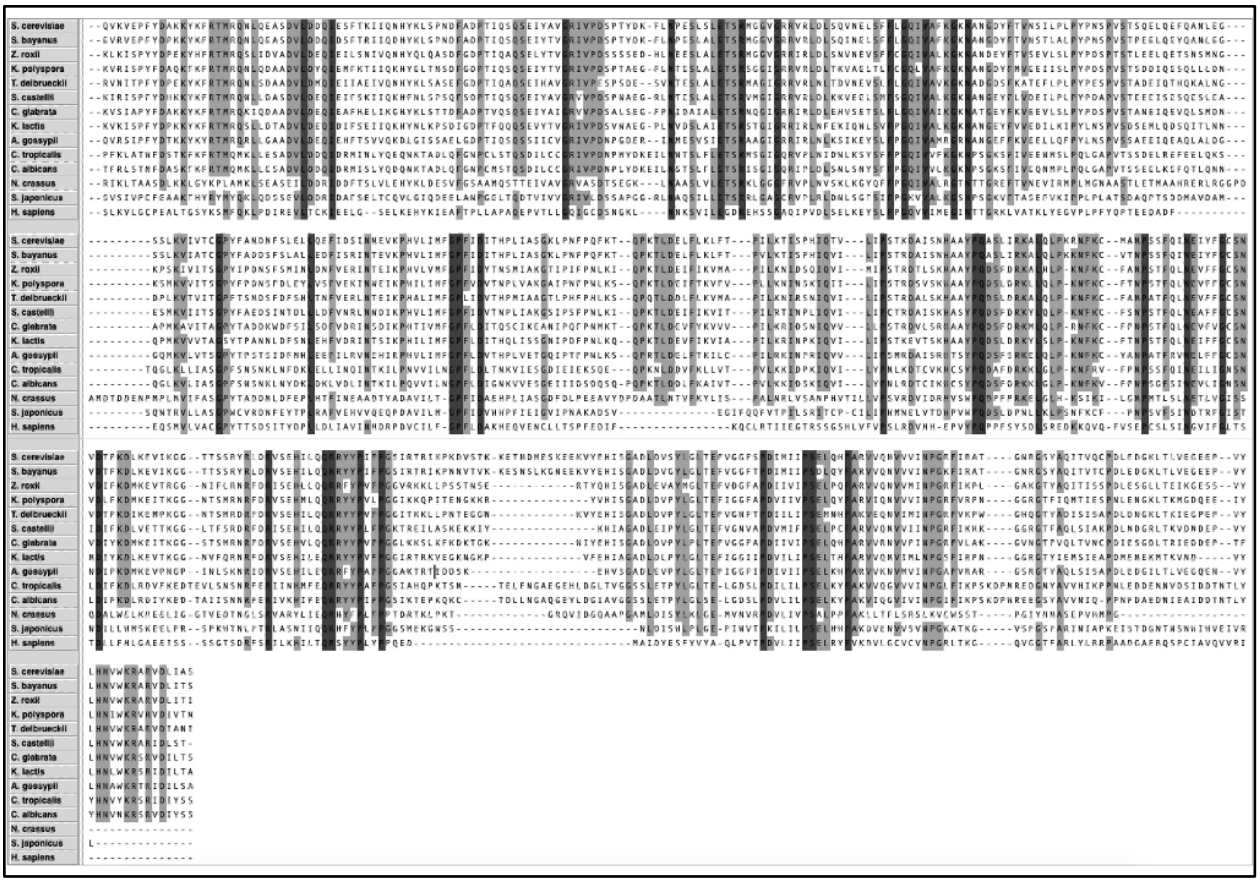

Figure 3.3: Pol1 C-terminal sequence alignment and conservation throughout 14 yeasts species

Highly Conserved and strictly conserved residues are highlighted in light grey and dark grey, respectively. Amino acids missing for a particular species compared to S. cerevisiae are indicated with a dash. Alignment was done using Macvector

Both areas tested showed a clear ODN phenotype with *Cdc13*^{TS}. This data argues that the interface found in Pol12 extends to the C-terminal domain of Pol1 and that the polymerase function is impaired by those alleles. Yet, upon testing *pol1-R1366E*, an allele expected to disrupt the Pol1-Pol12 interaction according to Klinge and Pellegrini, no ODN phenotype was observed (**Figure 3.4**). It is possible that this simple substitution is not enough to generate a phenotype. However, several single mutants of Pol12 showed a distinct growth defect through

that same assay and strain. This result therefore presumably argues that the loss of activity of the complex is distinct from the polymerase subunit's integrity.

As described by Klinge and colleagues with the help of an existing Archea's crystal structure, the interface is located between two openings, one going through primase and the other going through the polymerase subunits. It is thought to be where the DNA strand goes through in order to be replicated (*Firbank et al., 2008*). Interestingly, the possibility of an interface with DNA was already suggested in chapter 2 through the simple observation that most Pol12 residues with an ODN phenotype with $Cdc13^{TS}$ were in majority the result of a swap from a positive onto a negatively charged residue, therefore potentially generating repulsion between the mutated surface and negatively charged DNA strand.

Yet, one of the Pol1 mutants also highlighted by the ODN assay was *pol1-F1463A*, main allele of a publication arguing for its crucial importance for the polymerase-primase interaction (*Kilkenny et al., 2012*) (**Figure 3.4**). Indeed, Pol1 is thought to interact with Pri2 through the latter's very N-terminal region, while its C-terminal domain contains an iron sulfur cluster important for the priming process and interaction with the catalytic subunit Pri1. Therefore, the polymerase-primase cohesion might also specifically be what is disrupted by those alleles and the interface, beyond Pol1, should therefore also extend to the primase half of the complex. Complete data of the Pol1 ODN analysis is summarized in **Table 3.3**.

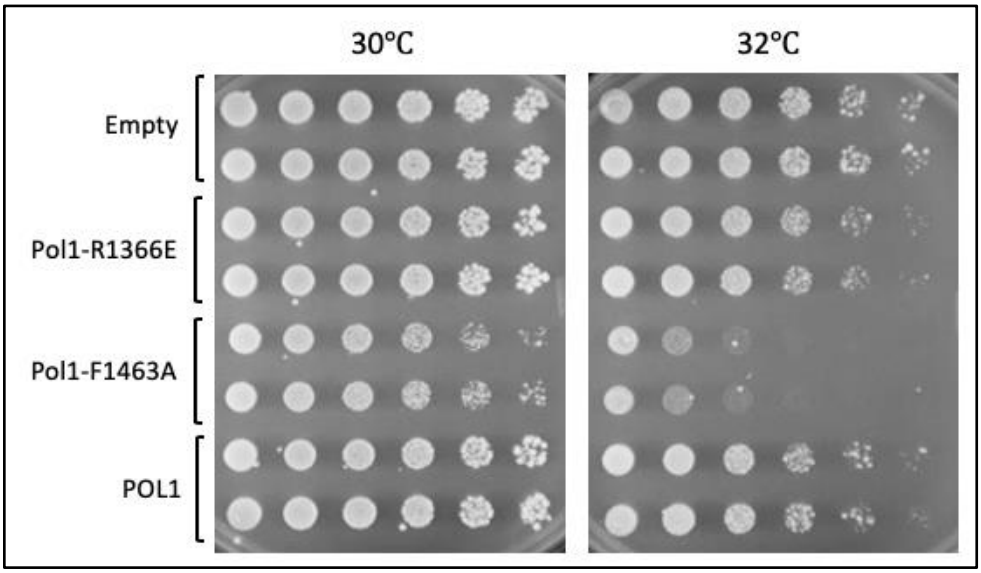

Figure 3.4: Disrupting the interaction of Pol1 with Pri2, but not Pol12, results in an ODN phenotype in a Cdc13^{TS} strain

A cdc13^{TS} strain (yVL3660) was transformed with derivatives of overexpression 2u plasmids with Pol1 (pVL6511) or empty vector (pVL399), as indicated on the left side. Cells were grown, gridded and replica plated at increasing temperatures for viability comparison

Table 3.3: Summary of ODN results of Pol1 alleles in Cdc13^{TS}

Viability is represented with the following nomenclature:
++++: increased viability / +++: viable / ++: slightly impaired /
+: clearly impaired / +/-: almost inviable / -: inviable / n.t.: not tested

		yVL3660 (cdc13^{TS})		
plasmid #	**mutation**	**30°C**	**32°C**	**33°C**
pVL399	**Empty vector**	**+++**	**+++**	**++**
pVL6511	**WT Pol1**	**+++**	**++**	**+**
pMAM716	E702K	+++	++	+
pMAM717	M703E	+++	++	+
pMAM719	R793E	+++	+	+/-
pMAM732	D864A	+++	++	+
pMAM720	R885E	+++	++	+
pMAM734	E888K	++?	+?	+/-?
pMAM735	D889K	+++	+++	++
pMAM736	D891K	+++	++	+
pMAM737	E892K	+++	++	+
pMAM740	L893K	+++	+?	+/-?
pMAM742	V896K	+++	++	+
pMAM738	E900K	+++	++	+
pMAM721	V957K	+++	++	+
pMAM722	N958K	++?	+?	+/-?
pMAM723	Y962K	+++	++	+
pMAM724	K964E	+++	++	+
pMAM743	Y962E+K964E	+++	+	+/-
pMAM745	K1365E	+++	+	+/-
pMAM725	R1366E	+++	++	+
pMAM727	K1447E	+++	++	+
pMAM731	D1458K	+++	+	+/-
pMAM726	F1463A	++	+	+/-

The ODN assay on Pri1 uncovered an extensive surface necessary for DNA priming

Both primase subunits Pri1 and Pri2 were mutated and analyzed with a process similar to that of the polymerase heterodimer. In the case of Pri1, 84 out of its 409 amino acids were tested for ODN, with roughly half of those giving a clear phenotype. A first patch of three residues located at the very N-terminal extremity of the protein maps as a novel surface with a clear ODP phenotype in *Cdc13^{TS}*. However, this region is fairly poorly conserved between yeast and human primases. Two lysines of a neighboring area have a clear ODN phenotype with *Pol1^{TS}* and *Cdc13^{TS}* when swapped to a negative charge. Interestingly, both of these residues stick out from the surface of the protein. A third cluster located ahead of the active site in the sequence has an ODN phenotype with *Cdc13^{TS}* and maps at the suggested interface with Pol1 in Humans (*Kilkenny et al., 2013*). One particular residue, K98, is at the tip of that interface but also shows an ODN phenotype with Pol1^{TS}, in contrast with the rest of the surface, but in accordance with the previously described lysine pair. Whether they highlight various degrees of importance within a single interface or pertain to two distinct ones is unclear. It is worth noting that yeast studies argue against a direct interaction between Pri1 and Pol1 and suggest that the connection between primase and polymerase happens solely through the Pri2 subunit.

Several residues located throughout the sequence and expected to affect the catalytic activity of Pri1 by altering its DNA binding ability have an ODN phenotype with both strains and map around the catalytic site. Actual substitutions of the active site residues result in near lethality even at semi-permissive temperature in the Pol1 mutant strain, but not necessarily in the Cdc13 one. In fact, only one of the 3 aspartic acids that constitutes the active site has a similar phenotype in *Cdc13^{TS} (***Figure 3.5***)*. The reason for this disparity has yet to be determined, as studies argue for loss of priming abilities when mutating any of those residues (*Kilkenny et al.,*

2013). Interestingly, no residues expected to connect Pri1 with Pri2 were found through that assay. There are also no crystal structures available in yeast that include both subunits interacting. Therefore, all surfaces found on Pri1 were summarized in **Table 3.4** mapped on a crystal structure of the protein alone (**Figure 3.6**).

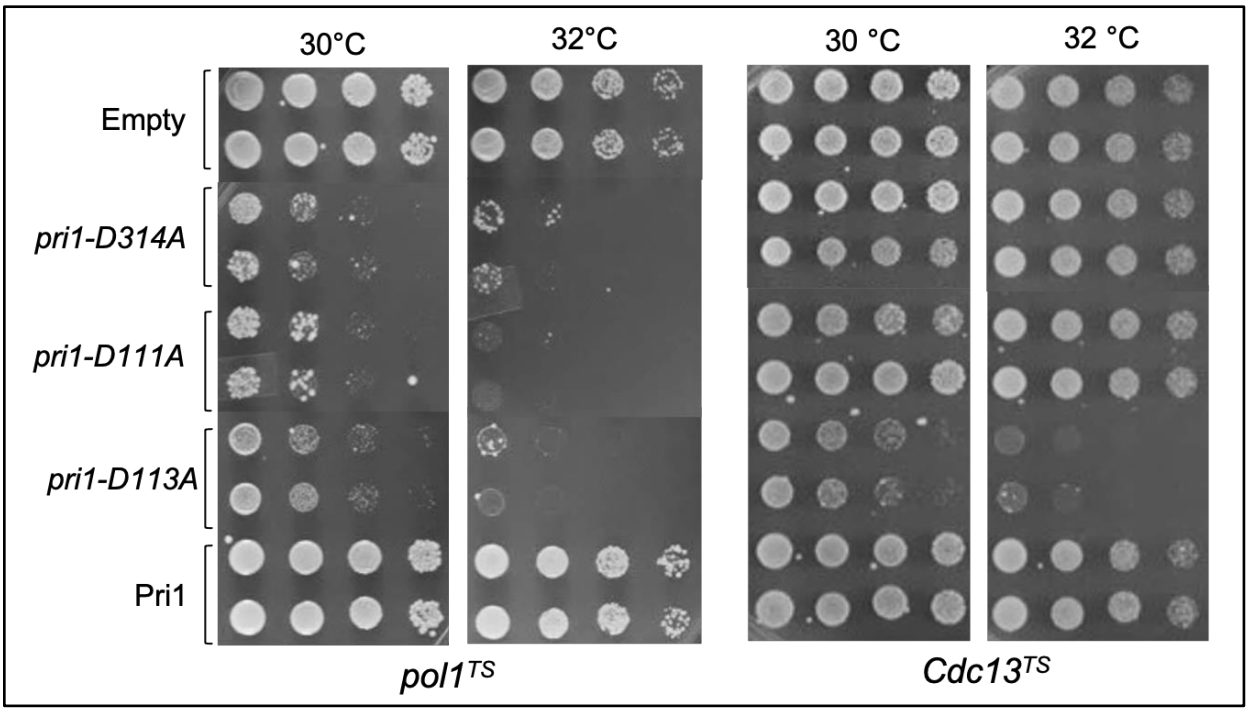

Figure 3.5: Disruption of active site residues of Pri1 gives a differential ODN phenotype in pol1^{TS} and cdc13^{TS}

A pol1^{TS} (yVL4119) and cdc13^{TS} strain (yVL3660) were transformed with derivatives of overexpression 2u plasmids with Pri1 (pVL6303) or empty vector (pVL399), as indicated on the left side. Cells were grown, gridded and replica plated at increasing temperatures for viability comparison

Histidines 186 and 323, located next to the active site, have a similar near-lethal phenotype in both strains when mutated to Alanine and have been shown to also disrupt the protein priming abilities (*Vaithiyalingam et al., 2014*). However, such growth defect observed even at permissive temperature argues that the phenotype might not be dependent on the sensitized strain but just the result of a near complete disruption of the essential function of Pri1.

Overall, all residues important for primase activity gave an ODN phenotype in both *Pol1*^{TS} and *Cdc13*^{TS}, whereas residues thought to be responsible for the protein interaction with Pol1 mostly only had an ODN phenotype with the latter. Complete data of the Pri1 ODN analysis is summarized in **Table 3.5**.

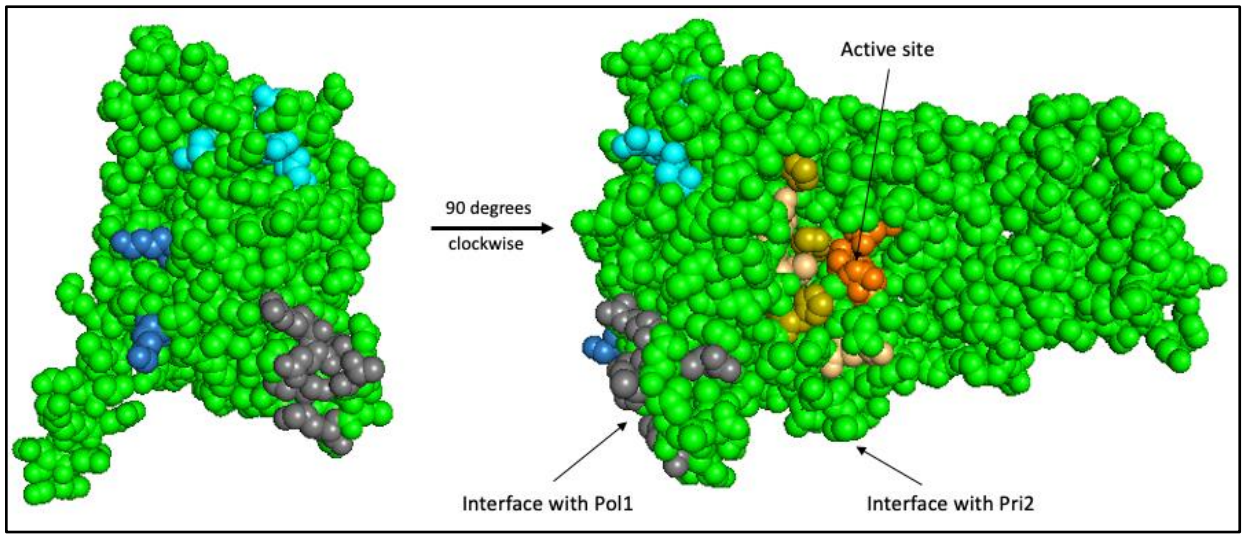

Figure 3.6: Crystal structure of Pri1 with the different surface found by the ODN assay
Pri1 surface residues are colored in green. Surface residues with an ODN phenotype are highlighted in colors as described in Table 3.4 and their predicted functions are indicated with arrows. PDB 4LIM

Table 3.4: Data summary of surfaces found on Pri1 by the ODN assay

Surface #	ODN pol1-ts?	ODN cdc13-ts?	Function
Surface 1	no	ODP	?
Surface 2	YES	YES	?
Surface 3	no?	YES	Interface with Pol1
Surface 4	YES	YES	DNA binding Domain
Surface 5	YES	YES?	Active site
Surface 6	YES	YES	Essential priming residues

Table 3.5: Summary of ODN phenotypes of Pri1 alleles

Viability is represented with the following nomenclature:
++++: increased viability / +++: viable / ++: slightly impaired /
+: clearly impaired / +/-: almost inviable / -: inviable / n.t.: not tested

		yVL4119 (pol1-ts)				yVL3660 (cdc13-ts)		
plasmid #	**Mutation**	**RT**	**30°C**	**32°C**		**30°**	**32°**	**33°**
pVL399	**Empty vector**	**++**	**++++**	**+++**		**+++**	**+++**	**+**
pVL6303	**WT Pri1**	**+++**	**+++**	**+++**		**+++**	**+++**	**+**
pEDN 13	D14K	+++	+	(+)		+++	+++	+
pMAM1	E16K	+++	+++	+++		+++	++++	+++
pMAM2	K20E	+++	+++	++		+++	+++	+
pMAM3	S21E	+++	+++	+++		+++	+++	++
pMAM4	S21K	+++	+++	+++		+++	+++	+
pEDN 14	K26E	+++	+/-	-		+++	+	+/-
pEDN 15	K37E	+++	+/-	-		+++	+++	+/-
pMAM5	S39E	+++	+++	+++		+++	++	+
pMAM124	S39K	+++	+++	+++		+++	+	+/-
pMAM6	R40E	+++	+++	+++		+++	+++	+
pEDN 16	D41K	+++	+++			+++	++	+/-
pEDN 17	R52E	+++	(+)	(+)		+++	+	+/-
pMAM125	S53K	++	+++	+++		+++	+++	+
pMAM126	S53E	+++	+++	+++		+++	+	+/-
pMAM127	G54E	+++	+++	++		+++	+	+
pMAM7	Y56E	+++	++	+/-		+++	+	+/-
pMAM8	Y56K	+++	++	+/-		+++	+	+/-
pMAM9	R58E	+++	+++	++		+++	++	+
pMAM128	N60E	+++	+++	+++		+++	+	+
pMAM129	N60K	+++	+++	+++		+++	+++	+
pEDN 18	D67K	+++	++	(+)		+++	++	+
pEDN 19	K69E	+++	++	(+)		+++	+	+/-
pMAM130	N76E	+++	+++	+++		+++	++	+
pMAM131	N76K	+++	+++	+++		+++	+++	++
pEDN 20	R79E	+++	+/-			+++	+++	+
pEDN 21	E81K	+++	++	(+)		+++	++	+
pMAM132	K88E	+++	+++	++		+++	+	+
pMAM133	R91E	+++	+++	+++		+++	+/-	-
pMAM134	E92K	+++	++	++?		+++	+/-	-
pMAM135	R93E	+++	+++	++		+++	+/-	-
pMAM136	T95E	+++	+++	+++		+++	+/-	-
pMAM137	T95K	+++	+++	+++		+++	+++	+
pEDN 22	K98E	+++	+/-	-		+++	+/-	-
PMAM10	D111A	+	+	+/-		+++?	+++?	+?
PMAM11	D113A	++	+	+/-?		+++	++	+
pMAM138	R121E	+++	+++	+++		+++	+++	+
pMAM139	Q128E	+++	+++	+++		+++	+++	+
pMAM140	Q128K	+++	+++	+++		+++	+++	+
pMAM141	K132E	+++	+++	+++		+++	+++	+
pEDN 23	K135E	+++	+++	+		+++	+++	+
pMAM142	K142E	+++	+++	+++		+++	+++	+
pMAM143	R149E	+++	+++	+++		+++	+++	+
pMAM144	E150K	+++	+++	+++		+++	+++	+
pMAM145	D151K	+++	+++	+++		+++	+++	+
pMAM146	F152E	+++	+++	+++		+++	+++	+
pMAM147	F152K	+++	+++	+++		+++	+++	+

Table 3.5: Summary of ODN phenotypes of Pri1 alleles (cont.)

		yVL4119 (pol1-ts)			yVL3660 (cdc13-ts)		
plasmid #	**Mutation**	**RT**	**30°C**	**32°C**	**30°**	**32°**	**33°**
pVL399	**Empty vector**	**++**	**++++**	**+++**	**+++**	**+++**	**+**
pVL6303	**WT Pri1**	**+++**	**+++**	**+++**	**+++**	**+++**	**+**
pMAM148	H168A	+	+	+/-	+++	+/-	-
pMAM149	D173K	+++	+++	+++	+++	+++	+
pMAM150	K174E	+++	+++	+++	+++	+++	+
pMAM151	R175E	+++	+++	+++	+++	+++	+
pMAM152	R184E	+++	+++	+++	+++	+++	+
pMAM153	N186E	+++	+++	+++	+++	+++	+
pMAM154	N186K	+++	+++	+++	+++	+++	+
pEDN 24	D189K	+++	+++	+	+++	+++	+
pEDN 25	R197E	+++	+	(+)	+++	++	+/-
pMAM155	R197E	+++	+++	+++	+++	++	+
pMAM156	N198E	+++	+++	+++	+++	+++	+
pMAM157	N198K	+++	+++	+++	+++	+++	+
pMAM158	K201E	+++	+++	+++	+++	+++	+
pEDN 26	R207E	+++	++	(+)	+++	+++	+
pMAM159	H210E	+++	+++	+++	+++	+++	+
pMAM160	H210K	+++	+++	+++	+++	+++	+
pEDN 27	R215E	+++	+++	+	+++	+++	+
pEDN 28	E231K	+++	+++	+	+++	+++	+
pMAM161	E231K	+++	+++	+++	+++	+++	+
pEDN 29	K259E	+++	+++		+++	+++	+
pMAM162	R268E	+++	+++	+++	+++	++	+
pMAM163	S269E	+++	+++	+++	+++	+++	+
pMAM164	S269K	+++	+++	+++	+++	+++	+
pMAM165	K271E	+++	+++	+++	+++	+++	+
pMAM166	E272K	+++	+++	+++	+++	+++	+
pEDN 30	K273E	+++	+++		+++	+++	+
pMAM167	N275E	+++	+++	+++	+++	+++	+
pMAM168	N275K	+++	+++	+++	+++	+++	+
pEDN 31	D278K	+++	+++		+++	+++	+
pEDN 32	D299K	+++	+++		+++	+++	+
pEDN 33	K301E	+++	+++		+++	+++	+
pEDN 34	D303K	+++	+++		+++	+++	+
pEDN 35	K312E	+++	mold	(+)	+++	+	+/-
PMAM12	D314A	+	+	-	++?	+/-?	-?
pEDN 36	E316K	+++	mold	(+)	+++	+++?	+?
pMAM169	K319E	+++	+++	+	+++	+	+/-
pMAM170	H323A	+	+/-	-	++?	-?	-?
pMAM171	L324E	++	++	+	+++	++	+
pMAM172	L325E	++	++	+/-	+++	+	-
pMAM173	K326E	+	+	+/-	+++	+?	-?
pMAM174	H332A	+++	+++	+++	+++	+	+/-
pEDN 37	N337K	+++	+++	+	+++	+++	++
pEDN 38	N337E	+++	++	(+)	+++	+++	+
pMAM175	K353E	+++	+++	+++	+++	++	+
pMAM176	E360K	+++	+++	+++	+++	+++	+
pMAM177	E362K	+++	+++	+++	+++	+++	+
pMAM178	T370E	+++	+++	+++	+++	++	+/-
pMAM179	T370K	+++	+++	+++	+++	+++	+
pEDN 39	E372K	+++	+++	+	+++	+++	++
pMAM180	Q380E	+++	+++	+++	+++	++	+
pMAM181	Q380K	+++	+++	+++	+++	+++	+
pMAM182	K388E	+++	+++	+++	+++	+	+/-
pEDN 40	E390K	+++	+++	(+)	+++	+++	+
pEDN 41	R396E	+++	+++		+++	++	+

The ODN assay on Pri2 highlighted two distinct binding sites with Pol1

Analysis of Pri2 was also a fruitful process. We created 185 single substitutions throughout the 528 amino acids making up the whole protein. A first patch of N-terminal residues shows an ODN phenotype only in *Cdc13^{TS}*. This surface isn't part of the Human primosome crystal structure except for one residue, the Human equivalent of Pri2-R39, and maps at an interface of Pri2 and Pol1. This result matches all previous observations arguing that disruption of the primase and polymerase subunits is linked to this phenotype.

The second surface area arising from the assay was at its C-terminal region, a known DNA binding domain. Mainly through its iron-sulfur (Fe-S) cluster made out of 4 Cysteines, it facilitates the RNA primer synthesis and transfer of the hybrid helix to the polymerase half of the complex. Interestingly, no ODN phenotype was observed in *Cdc13^{TS}* when mutating single Cysteine residues from the iron sulfur cluster (**Figure 3.7**). Indeed, it has been shown that this feature of the protein isn't needed for its interaction with polymerase (*Kilkenny et al., 2013*). Furthermore, mutants of the Fe-S cluster residues are viable in a LOF assay whereas alleles of some other important residues with a *Cdc13^{TS}* ODN phenotype are not. Yet, is it possible that the 4 cysteines have a redundant effect and it has been shown that no significant viability defect arises from single substitutions (*Liu et al., 2015*).

Beyond the lack of results with the Fe-S cluster of Pri2, several residues have been identified in that area as playing a crucial role for DNA replication. In particular, Y397 has been shown to be essential both in Yeast and Humans for its redox properties (*O'Brien et al., 2018*). Unlike mutants of the Fe-S cluster, *pri2-Y397A* is lethal as LOF (**Figure 3.8**).

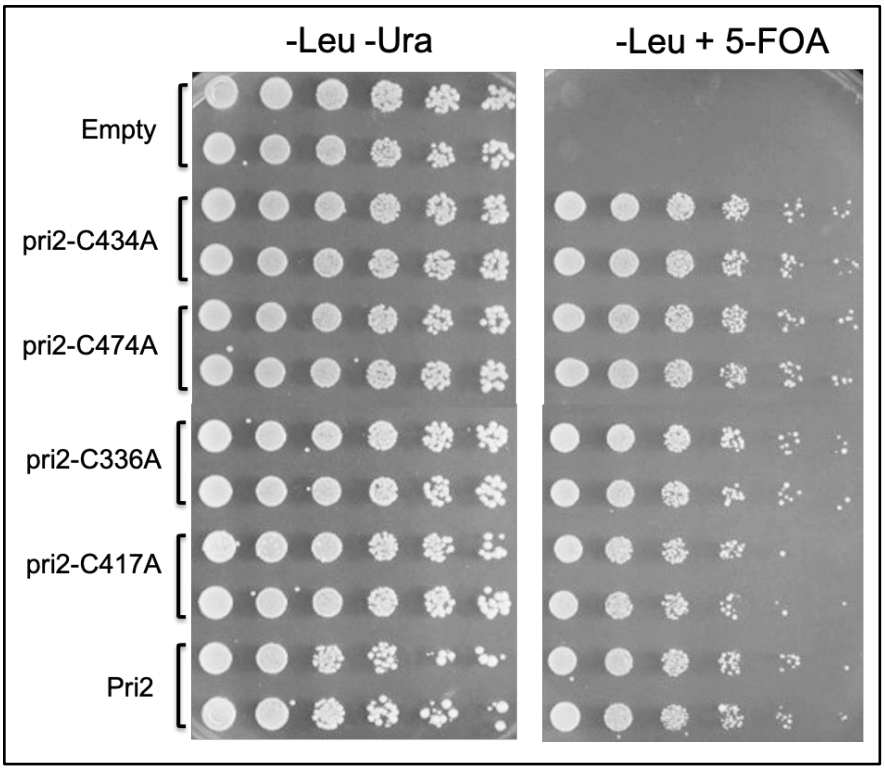

Figure 3.7: Single substitutions of the essential Pri2 iron-sulfur (Fe-S) domain are viable *in vivo*

A Pri2 Knock-out strain with covering CEN-URA3-Pri2 plasmid (yVL4921) was transformed with variants of 2u-ADH-LEU2 plasmids with the content indicated on the left. Cells were grown and viability was compared on -Leu -Ura for control and -Leu 5-FOA for shuffling off the covering plasmid at 30°C.

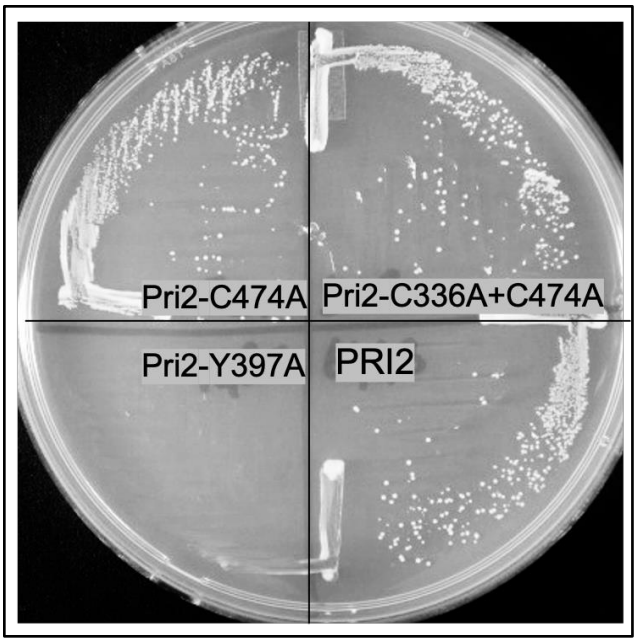

Figure 3.8: Unlike mutants of the Fe-S cluster, *pri2-Y397A* is inviable through LOF
Strains prepared and treated as described previously were streaked on -Leu 5-FOA plates for viability comparison to WT Pri2 at 30°C

Similarly, neighboring H401 has been among the first residues identified as giving the protein its essentiality (*Francesconi et al., 1991*). Both highly conserved, they are thought to be direct points of contact with the DNA strand and help it move through the complex (*Sauguet et al., 2010*). For these residues, we opted for a mutation into a non-polar alanine rather than a charge swap strategy to most efficiently abrogate their potential function without rendering the allele completely inviable. Both p*ri2-Y397A* and *pri2-H401A* had a similar extreme growth phenotype in $Cdc13^{TS}$ even at semi-permissive temperature. Although this result could relate to their overall importance for viability, independently of the nature of the sensitized strain and similarly to the Pri1 catalytic site, such intense growth phenotype wasn't observed in $Pol1^{TS}$, although a mild yet noticeable ODN phenotype was noted (**Figure 3.9**). Therefore, their essential

function seems to be distinct from that of polymerase alpha-primase and linked to telomere homeostasis and t-RPA.

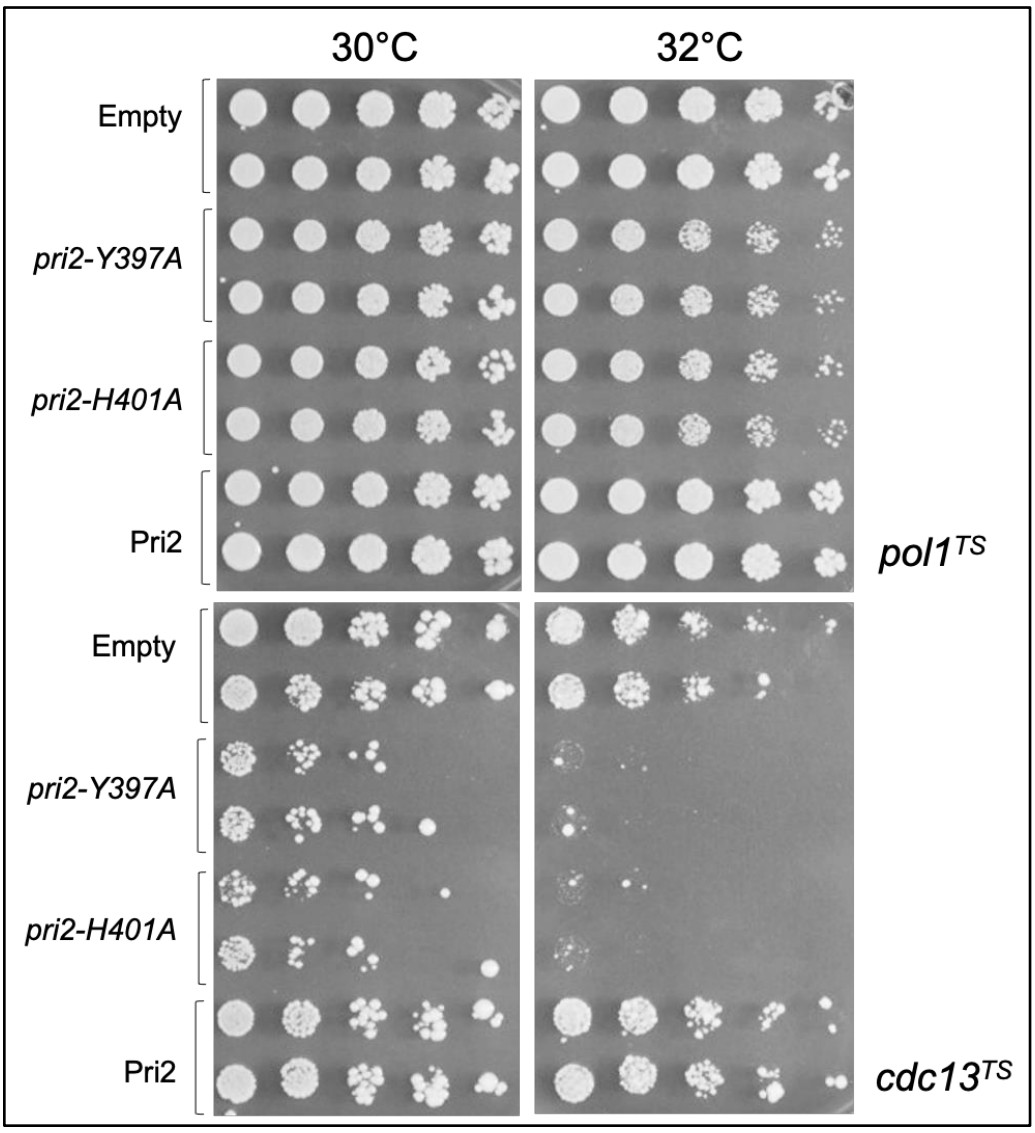

Figure 3.9: pri2 residues Y397 and H401 perform an essential function through t-RPA
A pol1^{TS} (yVL4119) and cdc13^{TS} strain (yVL3660) were transformed with derivatives of overexpression 2u plasmids with Pri2 (pVL6443) or empty vector (pVL399), as indicated on the left side. Cells were grown, gridded and replica plated at increasing temperatures for viability comparison

Table 3.6: Summary of ODN phenotypes of Pri2 alleles

Viability is represented with the following nomenclature:
++++: increased viability / +++: viable / ++: slightly impaired /
+: clearly impaired / +/-: almost inviable / -: inviable / n.t.: not tested

		yVL4119 (pol1-1)			yVL3660 (cdc13-ts)		
plasmid #	**mutation**	**RT**	**30°C**	**32°C**	**30**	**32**	**33**
pVL399	**Empty vector**	**+++**	**+++**	**++**	**+++**	**+++**	**+**
pVL6443	**WT Pri2**	**+++**	**+++**	**+++**	**+++**	**+++**	**+**
pEDN 57	R3E	n.t.	+++	?	+++	++	+/-
pEDN 58	K6E	n.t.	+++	?	+++	+++	+
pMAM13	K6E	+++	+++	+++	+++	++	+
pEDN 59	R7E	n.t.	+++	+++	+++	++	+
pEDN 60	R8E	n.t.	+++	++	+++	+	+/-
pEDN 61	R12E	n.t.	+++	+++	+++	+++	+
pEDN 62	K13E	n.t.	+++	++	+++	+++	+
pEDN 63	E39K	n.t.	+++	++	+++	++	+
pMAM14	D63K	+++	+++	+++	+++	+++	+
pMAM15	L64E	+++	+++	+++	+++	+++	+
pMAM16	E69K	+++	+++	+++	+++	+++	+
pMAM17	I70E	+++	+++	+++	+++	+++	+
pMAM18	T71E	+++	+++	+++	+++	+++	+
pMAM19	T71K	+++	+++	+++	+++	+++	+
pEDN 64	E73K	n.t.	+++	++	+++	+++	+
pMAM20	Q74E	+++	+++	+++	+++	+++	+
pMAM21	Q74K	+++	+++	+++	+++	+++	+
pEDN 65	E76K	n.t.	+++	++	+++	+++	+
pMAM22	I77E	+++	+++	+++	+++	+++	+
pEDN 66	D81K	n.t.	+++	++	+++	+++	+
pMAM23	D81K	+++	+++	+++	+++	++	+
pEDN 67	R82E	n.t.	+++	++	+++	+++	+
pEDN 68	E88K	n.t.	+++	+++	+++	+++	+
pMAM24	E88K	+++	+++	+++	+++	+++	+
pEDN 69	E90K	n.t.	+++	+	+++	+++	+
pMAM25	E90K	+++	+++	+++	+++	+++	+
pMAM26	S91E	+++	+++	+++	+++	+++	+
pMAM27	S91K	+++	+++	+++	+++	+++	++
pEDN 70	R95E	n.t.	+++	+++	+++	+++	+
pMAM28	R95E	+++	+++	+++	+++	+++	+
pEDN 71	K97E	n.t.	+++	+	+++	+++	+
pMAM29	K97E	+++	+++	+++	+++	+++	+
pEDN 72	E101K	n.t.	+++	+++	+++	+++	+
pEDN 73	E103K	n.t.	+++	+++	+++	+++	+
pEDN 74	K107E	n.t.	+++	+	+++	+++	+
pMAM30	K112E	+++	+++	+++	+++	+++	+
pEDN 75	R124E	n.t.	+++	++	+++	+++	+
pEDN 76	K125E	n.t.	+++	++	+++	+++	+
pEDN 77	K126E	n.t.	+++	++	+++	+++	+
pEDN 78	H131K	n.t.	+++	+++	+++	+++	+
pEDN 79	H131E	n.t.	+++	+++	+++	+++	+
pEDN 80	R135E	n.t.	+++	+++	+++	+++	+
pEDN 81	R140E	n.t.	+++	+	+++	+++	+
pMAM31	K142E	+++	+++	+++	+++	+++	+
pEDN 82	E143K	n.t.	+++	++	+++	++	+
pEDN 83	R145E	n.t.	+++	+++	+++	+++	+
pMAM32	R145E	+++	+++	+++	+++	+++	+
pMAM33	E146K	+++	+++	+++	+++	+++	+
pMAM34	K147E	+++	+++	++	+++	+++	+
pEDN 84	R150E	n.t.	+++	++	+++	+++	+
pMAM35	R150E	+++	+++	+++	+++	+++	+
pEDN 85	E152K	n.t.	+++	++	+++	+++	+
pEDN 86	K157E	n.t.	+++	+++	+++	+++	+
pMAM36	K157E	+++	+++	+++	+++	+++	+

Table 3.6: Summary of ODN phenotypes of Pri2 alleles (cont.)

		yVL4119 (pol1-1)				yVL3660 (cdc13-ts)		
plasmid #	**mutation**	**RT**	**30°C**	**32°C**		**30**	**32**	**33**
pVL399	**Empty vector**	**+++**	**+++**	**++**		**+++**	**+++**	**+**
pVL6443	**WT Pri2**	**+++**	**+++**	**+++**		**+++**	**+++**	**+**
pEDN 87	R159E	n.t.	+++	+++		+++	+++	+
pMAM37	R159E	+++	+++	+++		+++	+++	+
pMAM38	F160E	+++	+++	++?		+++	++	+
pMAM39	F160K	+++	+++	++?		+++	++	+
pMAM40	D167K	+++	+++	+++		+++	+++	+
pEDN 88	Q168K	n.t.	+++	+++		+++	+++	+
pEDN 89	Q168E	n.t.	+++	+++		+++	+++	+
pMAM41	T169E	+++	+++	+++		+++	+++	+
pMAM42	T169K	+++	+++	+++		+++	+++	+
pMAM43	K170E	+++	+++	+++		+++	+++	+
pMAM44	F171E	+++	+++	+++		+++	+++	+
pMAM45	F171K	+++	+++	+++		+++	++	+
pMAM46	N185E	+++	+++	+++		+++	+++	+
pMAM47	N185K	+++	+++	+++		+++	+++	+
pEDN 90	E186K	n.t.	+++	+++		n.t.	n.t.	n.t.
pMAM48	E187K	+++	+++	+++		+++	+++	+
pEDN 92	K188E	n.t.	+++	+++		+++	++	+
pMAM49	K188E	+++	+++	+++		+++	++	+
pMAM50	E211K	+++	+++	+++		+++	+++	+
pEDN 93	E212K	n.t.	+++	+++		+++	+++	+
pMAM51	E212K	+++	+++	+++		+++	+++	+
pEDN 94	R215E	n.t.	+++	++		+++	++	+
pEDN 95	E222K	n.t.	+++	++		+++	+++	+
pEDN 96	K226E	n.t.	+++	+++		+++	+++	+
pEDN 97	E230K	n.t.	+++	+++		+++	+++	+
pMAM52	E234K	+++	+++	+++		+++	++	+
pMAM53	L235E	+++	+++	+++		+++	++	+
pEDN 98	R239E	n.t.	+++	+		+++	++	+
pMAM54	L240E	+++	+++	+++		+++	+++	+
pMAM55	K244E	+++	+++	+++		+++	+++	+
pMAM56	D245K	+++	+++	+++		+++	+++	+
pMAM58	Y247K	+++	+++	++		+++	+++	+
pMAM59	Q254E	+++	+++	+++		+++	++	+
pMAM60	Q254K	+++	+++	+++		+++	+++	+
pEDN 100	Q255E	n.t.	+++	+++		+++	++	+
pMAM61	Q255E	+++	+++	++		+++	++	+
pMAM62	Q255K	+++	+++	+++		+++	+++	+
pEDN 101	E262K	n.t.	+++	++		+++	+++	+
pMAM63	E262K	+++	+++	+++		+++	++	+
pMAM64	K266E	+++	+++	+++		+++	+++	+
pMAM65	K273E	+++	+++	+++		+++	+++	+
pMAM66	Q276E	+++	+++	+++		+++	+	-
pMAM67	Q276K	+++	+++	+++		+++	+	-
pMAM68	R280E	+++	+++	+++		+++	+	-
pMAM69	N282E	+++	+++	+++		+++	+++	+
pMAM70	N282K	+++	+++	+++		+++	++	+
pMAM71	E283K	+++	+++	+++		+++	++	+
pEDN102	D284K	n.t.	+++	+++		+++	+++	+
pEDN 103	D285K	n.t.	+++	+++		+++	++	+
pEDN 104	R286E	n.t.	+++	++		+++	+++	+
pMAM72	R286E	+++	+++	+++		+++	+++	+
pMAM73	N292E	+++	+++	+++		+++	+++	++
pMAM74	N292K	+++	+++	+++		+++	+++	+
pMAM75	H293E	+++	+++	+++		+++	+++	+
pMAM76	H293K	+++	+++	+++				
pMAM77	L294E	+++	+++	+++		+++	++	+
pMAM78	K338E	+++	+++	++		+++	+++	+
pMAM79	N339E	+++	+++	+++		+++	+++	+
pMAM80	N339K	+++	+++	+++		+++	+++	+
pMAM81	E342K	+++	+++	+++		+++	+++	+
pMAM82	K345E	+++	+++	+++		+++	+++	+

Table 3.6: Summary of ODN phenotypes of Pri2 alleles (cont.)

		yVL4119 (pol1-1)			yVL3660 (cdc13-ts)		
plasmid #	**mutation**	**RT**	**30°C**	**32°C**	**30**	**32**	**33**
pVL399	**Empty vector**	**+++**	**+++**	**++**	**+++**	**+++**	**+**
pVL6443	**WT Pri2**	**+++**	**+++**	**+++**	**+++**	**+++**	**+**
pMAM83	K346E	+++	+++	+++	+++	++	+
pMAM84	N347E	+++	+++	+++	+++	+++	+
pMAM85	N347K	+++	+++	+++	+++	+++	+
pMAM86	H348E	+++	+++	+++	+++	+++	+
pMAM87	H348K	+++	+++	+++	+++	+++	+
pEDN 107	R351A	n.t.	+++	+++	+++	++	+
pMAM88	R351A	+++	+++	+++	+++	++	+
pEDN 108	Y352A	n.t.	+++	+/-?	+++	+	-
pMAM89	Y352A	+++	+++	++	+++	+	-
pMAM90	R355A	+++	+++	+	+++	+	-
pEDN109	R355A	n.t.	+++	+++	+++	+++	+
pEDN 110	K363A	n.t.	+++	++	+++	++	+
pMAM91	K363A	+++	+++	++	+++	++	+
pMAM92	D370K	+++	+++	+++	+++	+++	+
pMAM93	E379K	+++	+++	+++	+++	+++	+
pMAM94	E378K	+++	+++	++	+++	+++	+
pMAM95	E389K	+++	+++	+++	+++	+++	+
pMAM96	K390E	+++	+++	+++	+++	?	?
pMAM97	F391E	+++	+++	++	+++	?	?
pMAM98	F391K	+++	+++	++	+++	?	?
pEDN 111	K393A	n.t.	+++	++	+++	+++	+
pEDN 112	Y395A	n.t.	+++	++	+++	+	-
pMAM99	Y395A	+++	+++	+++	+++	?	?
pEDN 113	Y397A	n.t.	+++	+++	+++	+++	+
pMAM100	Y397A	+++	+++	+	+++	?	?
pMAM101	R400E	+++	+++	++	+++	+	+/-
pEDN 114	H401A	n.t.	++	+/-?	+++	+	+/-
pMAM102	H401A	+++	++	+	+++	+	+/-
pMAM103	E406K	+++	+++	++	+++	?	?
pMAM104	R409E	+++	+++	+?	+++	+	+/-
pMAM105	N411E	+++	+++	+++	+++	++	+
pMAM106	N411K	+++	+++	++	+++	+++	+
pEDN 115	Y412A	n.t.	+++	++	+++	++	+
pMAM107	Y412A	+++	+++	+++	+++	++	+
pMAM108	D416K	+++	+++	+++	+++	+++	+
pMAM109	H418E	+++	+++	+++	+++	+++	+
pMAM110	H418K	+++	+++	+++	+++	+++	+
pMAM111	S422E	+++	+++	+++	+++	+++	+
pMAM112	S422K	+++	+++	+++	+++	++	+
pMAM113	K423E	+++	+++	+++	+++	+++	+
pEDN 116	R425E	n.t.	+++	+	+++	+++	+
pEDN 117	R428E	n.t.	+++	++	+++	++	+
pMAM114	R428E	+++	+++	++	+++	++	+
pMAM115	Y431E	+++	+++	+++	+++	+++	+
pMAM116	Y431K	+++	+++	+++	+++	+++	+
pEDN 119	R437E	n.t.	+++	++	+++	++++	++
pMAM117	R437E	+++	+++	+++	+++	+++	+
pEDN 120	D438K	n.t.	+++	++	+++	++	+
pMAM118	D438K	+++	+++	+?	+++	++	+
pMAM119	E442K	+++	+++	+++	+++	++	+
pMAM120	R443E	+++	+++	+++	+++	++	+
pMAM121	S460E	+++	+++	+++	+++	+++	+
pMAM122	S460K	+++	+++	+++	+++	+++	+
pEDN 121	D463K	n.t.	+++	+++	+++	+++	++
pMAM123	D463K	+++	+++	+++	+++	+++	+
pEDN 122	E469K	n.t.	+++	+++	+++	++++	+++
pEDN 123	K476E	n.t.	+++	+++	+++	+++	+
pEDN 124	E479K	n.t.	+++	+	+++	++++	++
pEDN 125	H499K	n.t.	+++	+++	+++	+++	+
pEDN 126	H499E	n.t.	+++	+	+++	+++	+
pEDN 127	E505K	n.t.	+++	+++	+++	+++	+
pEDN 128	R506E	n.t.	+++	++	+++	+++	+
pEDN 129	R508E	n.t.	+++	++	+++	++?	-?

Conclusion: Mapping of ODN residues on the Human primosome crystal structure

The ODN assay successfully highlighted clusters of residues in each of the 4 subunits of polymerase alpha-primase. The alleles found include most of the complex known functions by encompassing the active sites of Pri1 and Pol1 as well as several interfaces between primase and polymerase. Most of those mutants cluster within a common complex-wide interface of the Human primosome structure solved by the Tahirov lab, as do the novel Pol12 surfaces 1 and 3 (**Figure 3.10**).

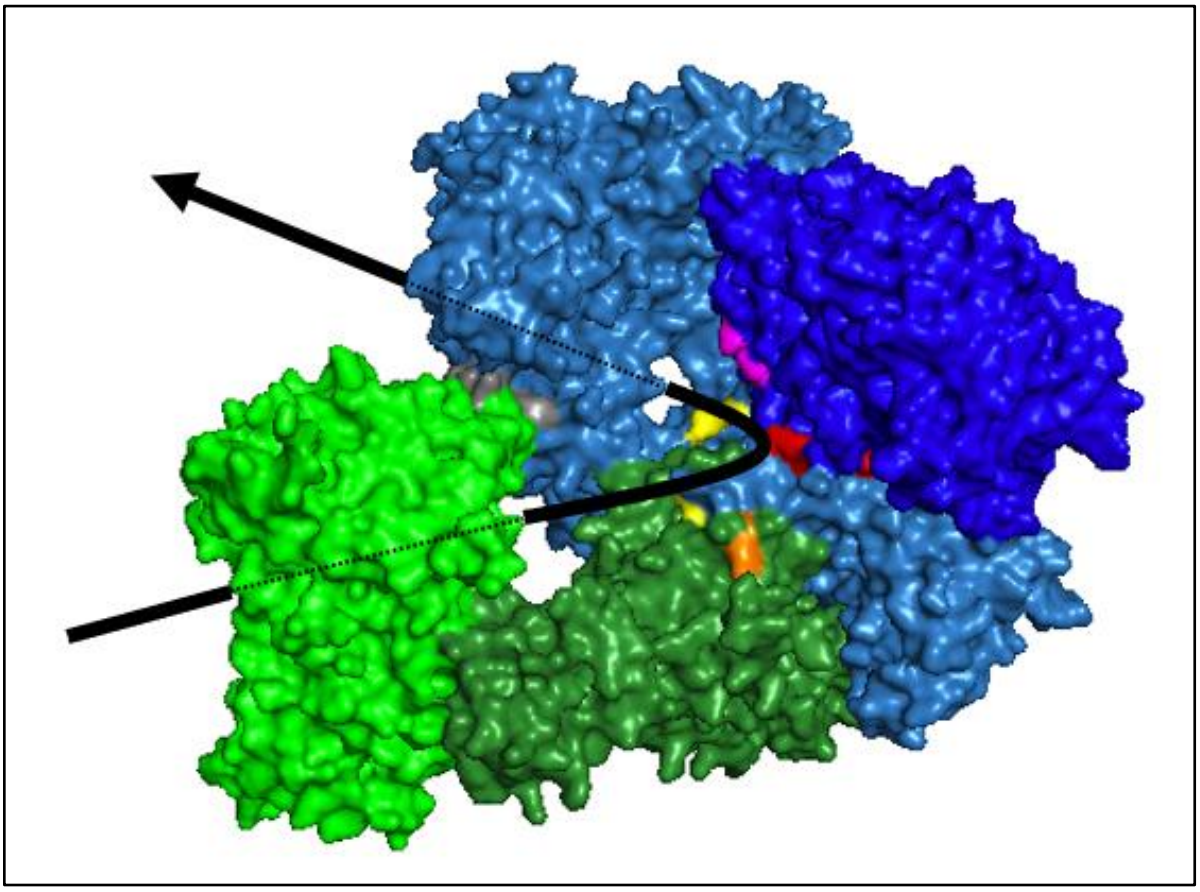

Figure 3.10: Representation of the human primosome with localization of the ODN residues and hypothesized DNA strand path

Human equivalents of Pol1, Pol12, Pri1 and Pri2 are shown in blue, dark blue, green and dark green, respectively. Surface residues with an ODN phenotype with cdc13^{TS} on Pol1, Pri1 and Pri2 are indicated in yellow, gray and orange, respectively. Surface residues with an ODN phenotype with cdc13^{TS} on Pol12 are indicated in red and magenta in accordance with previous figures. Black arrow represents the path that the lagging strand is expected to go through during replication. PDB 5EXR

In particular, Pol12-R248 and Pol12-R322, uncovered for their phenotype with *cdc13^{TS}* in surfaces 1 and 3, respectively, when mutated, are well exposed within that cleft (**Figure 3.11**).

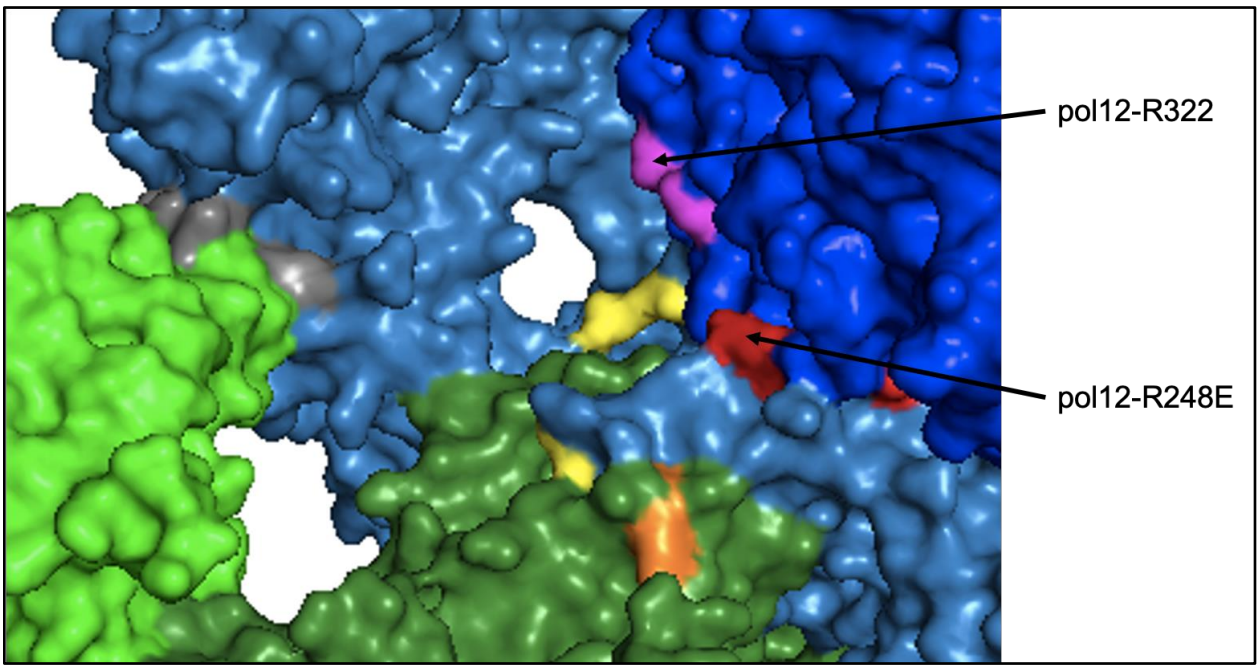

Figure 3.11: Close up of the openings going through polymerase alpha-primase and localization of surface residues with an ODN phenotype

Human equivalents of Pol1, Pol12, Pri1 and Pri2 are shown in blue, dark blue, green and dark green, respectively. Surface residues with an ODN phenotype with cdc13^{TS} on Pol1, Pri1 and Pri2 are indicated in yellow, gray and orange, respectively. Surface residues with an ODN phenotype with cdc13^{TS} on Pol12 are indicated in red and magenta in accordance with previous figures. PDB 5EXR

The only ODN residues not visible within that complex-wide interface are Pri1's active site and Pri2's known DNA Binding Domain and Fe-S cluster (**Figure 3.12**). The prior is located on the opposite side of the protein, at the entrance side of the cleft. The latter overlaps with an interface with Pol1 (**Figure 3.13**). One possible explanation for its phenotype could be found by looking at the dynamics of the Human primosome structure. This interface is independent from the characterized one between the N-terminal of Pri2 and C-terminal of Pol1. It has been shown that, as the polymerase alpha-primase complex is highly flexible throughout the replication process, so is the interface between Pol1 and Pri2 (*Nunez-Ramirez et al., 2011, Baranosvkiy et*

al., 2016). In the earlier steps of priming, Pri2 stands in the way of polymerase to keep it from elongating incomplete RNA primers. Then, the N-terminal Pri2/C-terminal Pol1 separates, facilitating the active site of polymerase contact with the primed DNA strand.

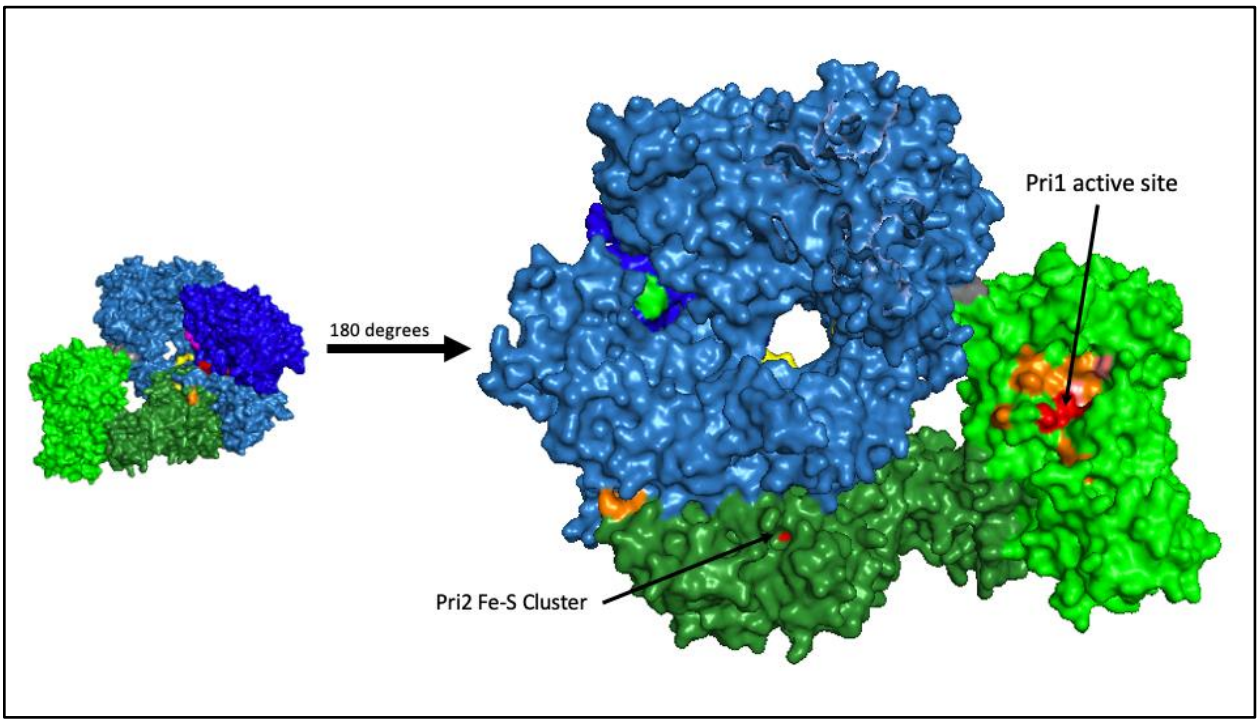

Figure 3.12: Representation of the human primosome rotated 180 degrees compared to Figure 3.10 with localization of the ODN residues

Human equivalents of Pol1, Pol12, Pri1 and Pri2 are shown in blue, dark blue, green and dark green, respectively. Active site of Pri1 and the Fe-S cluster of Pri2 are indicated with arrows. PDB 5EXR

The availability of the Human primosome structure also allows to place the *Pol1*^{TS} sensitive-only ODN Pol12 surface 2 within the complex. It shows those residues as also being a part of an interface with Pol1's amino acids ~1140 to 1145. Whether this interaction is constant, transient or an artifact has yet to be determined. Because of its lack of ODN phenotype in *Cdc13*^{TS}, mutants from surface 2 were only further investigated as a control that the phenotypes observed in the other surfaces are specific to their sensitivity to t-RPA defects. One specific synthetic phenotype pertaining to that surface only will also be discussed in chapter 5.

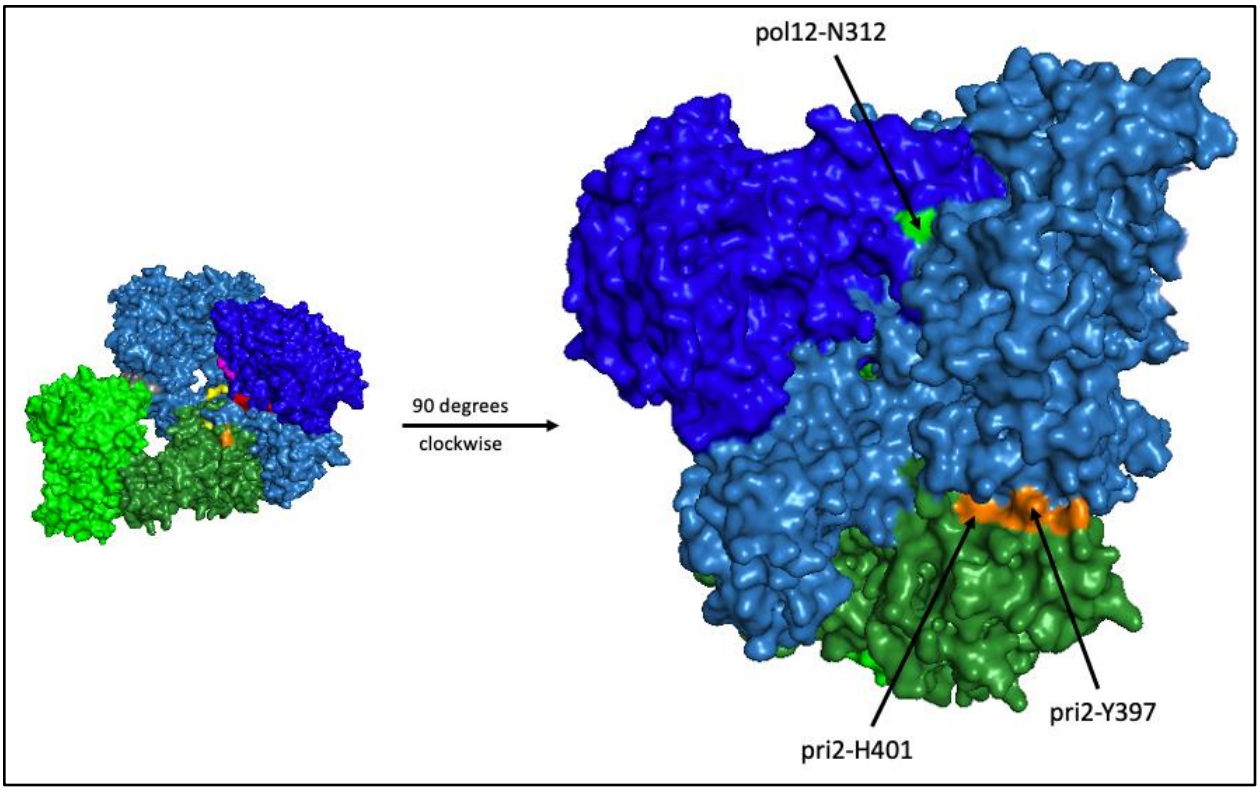

Figure 3.13: Representation of the human primosome with surface 2 residues of Pol12 and Pri2 that interact with Pol1

Human equivalents of Pol1, Pol12, Pri1 and Pri2 are shown in blue, dark blue, green and dark green, respectively. Surface residues of Pol12 with an ODN phenotype in pol1^{TS} and of Pri2 with an ODN phenotype in both pol1^{TS} and cdc13^{TS} are indicated with arrows. PDB 5EXR

Data from this chapter is currently in preparation to be published (Meunier and Lundblad, in preparation). The dissertation author was the primary researcher and author of this material.

CHAPTER 4:
Phenotypic characterization of the different Pol12 surfaces found by the ODN assay

Abstract

We investigated the nature of the defects generated by the Pol12 mutants found by the ODN assay. Although all viable *in vivo*, they resulted in a disruption of telomere homeostasis with a striking elongation phenotype for both *pol12-R248E* and *pol12-R322E*, alleles representative of surfaces 1 and 3 previously suspected to perform a similar function. In contrast, *pol12-D303K* of surface 2 has WT-looking telomeres on a Southern blot assay. A closer look into individual telomeric ends of those mutants through the use of TeloPCR shows that, although overall longer, many of those sequences are also much shorter than average, even considered critically short, a phenotype thought to trigger cell cycle arrest and DNA damage checkpoints. Furthermore, the profile of those elongated telomeres mutants closely resembles those of t-RPA mutants, arguing once again that the two complexes may act together towards a pathway that, when disrupted, gives rise to this striking phenotype.

Introduction: Yeast telomeres and t-RPA mutant telomeric defects

Based on the growth phenotype of Pol12 mutants in a t-RPA defective strain and evidence of the genetic and biochemical interaction between the two complexes, it seemed obvious to look at possible changes in telomere homeostasis arising from disruptions of the surface of the protein. To test Pol12 alleles for telomere-related phenotypes, we used the previously described Loss-of-function (LOF) strategy, with the same goal of testing a broader number of mutants without needing to integrate them onto the genome. Indeed, all of those individual mutations were found to be viable through LOF. Furthermore, the selection marker-based feature of the assay allows to maintain expression of WT Pol12 in the strain up until testing, ensuring that telomere homeostasis is maintained. Once shuffled off, the sole leftover expression of the mutated copy of the gene will potentially alter telomere homeostasis in a cell cycle dependent manner. Therefore, strains are successively streaked-out three times before analyzing telomeric DNA in order to let the mutation be expressed for roughly 60 to 75 generations (*Joseph and Hall., 2004*).

Telomeres are naturally variant, but have an overall stable average length specific to each species. In *S. cerevisiae*, the average telomere length is around 300to 350bp, as observed by Southern Blot (*Wellinger and Zakian, 2012*). This particular assay yields an image of telomeres with several bands corresponding to two main kinds of elements. The first, X elements, is a group of subtelomeric DNA with a typically set length for each of the chromosome ends. They are not affected by the end-replication problem but could potentially be altered if the replication fork isn't performing at optimal capacity. The other, Y' elements, include telomeric extremities that may strongly vary, both from replication defects and their physical localization at the

extremity of chromosomes. Y' elements therefore typically have a much broader band than X elements, highlighting this variation, even in WT strains.

Mutants of t-RPA have shown three different kinds of telomeric defects. The original allele that led to the discovery of Cdc13 showed a progressive shortening of telomeres. This senescence phenotype served as proof that the t-RPA complex plays an essential role in telomerase function (*Lendvay et al., 1996, Nugent et al., 1996*). In contrast, forcing the interaction between Cdc13 and telomerase subunit Est2 by fusing the proteins resulted in an elongation of telomeres, arguing that the role of t-RPA in recruiting telomerase is normally regulated (*Evans and Lundblad, 1999*). A second category of Cdc13 defects results in a shortening of telomeres without senescence of the cells (*Meier et al., 2001*). This observation supports the idea that it also interacts with other regulators playing a role in telomere recruitment. Finally, a subset of Cdc13 mutants elongates telomeres, a defect thought to be linked with an impaired negative regulating function of the protein (*Chandra et al., 2001*). Therefore, Cdc13 is thought to either positively or negatively regulate telomerase recruitment with different domains and under various conditions. Interestingly, overexpressing Stn1 normalizes telomere length of the last category of mutants, arguing that Cdc13 alone might have a different role than within the t-RPA complex. Mutants of Stn1 themselves showed to have overwhelmingly elongated telomeres (*Grandin et al., 1997, Grandin et al., 2000*). Finally, although less studied, Ten1 TS alleles have the same long-telomere phenotype (*Grandin et al., 2001*). Therefore, the nature of the defect in telomere homeostasis can give an indication of the possible role of the protein involved.

Material and methods: Southern Blot

All strains used for the assay were derivatives of yVL4931 (*MATa ura3-52 lys2-801 trp-Δ1 his3-Δ200 leu2-Δ1 pol12-Δ::KAN,* complemented with pVL7267 (CEN URA3 Pol12)) and yVL3734 (*MATa ura3-52 lys2-801 trp-Δ1 his3-Δ200 leu2-Δ1 rif1-Δ::KAN)* transformed with various alleles of pVL7270 (CEN LEU2 Pol12) as described in chapter 3. Strains were grown in duplicates overnight in 2mls of Yeast Extract Peptone Dextrose (YPAD) after being streaked-out 3 times. Cells and nuclei were lysed and genomic DNA was extracted to be digested with XhoI. The samples were run on an 0.8% gel, transferred on Nitrocellulose membrane and probed with a ^{32}P telomeric probe. After the appropriate washes, the blot was exposed to film and developed.

Table 4.1: List of plasmids used for Southern blot analysis and ODN assay of the Pol12-R248 variants

Plasmid #	Content
pVL399	2μ LEU2 ADH
pVL6321	2μ LEU2 ADH-POL12
pVL7267	CEN URA3-POL12
pVL7270	CEN LEU2-POL12
pVL7274	CEN LEU2-pri1-K98E
pVL7277	CEN LEU2-pri2-F391K
pVL7376	2μ LEU2 ADH-pol12-R248E
pVL7499	CEN LEU2-pol12-R248E
pVL7501	CEN LEU2-pol12-D262K
pVL7502	CEN LEU2-pol12-G327K
pVL7503	CEN LEU2-pol12-D303K
pVL7505	CEN LEU2-pol12-R322E
pVL7507	CEN LEU2-pol12-R329E
pVL7927	2μ LEU2 ADH-pol12-R248A
pVL7928	2μ LEU2 ADH-pol12-R248Q
pVL7934	2μ LEU2 ADH-pol12-R248S
pVL7979	CEN LEU2-pol12-M250E
pVL7980	CEN LEU2-pol12-Q252E
pVL7981	CEN LEU2-pol12-Q252K
pVL7982	CEN LEU2-pol12-Q255E
pVL7983	CEN LEU2-pol12-Q255K
pVL7984	CEN LEU2-pol12-S258K
pVL7985	CEN LEU2-pol12-E319K
pVL7986	CEN LEU2-pol12-P575E
pVL7987	CEN LEU2-pol12-P575K
pVL7988	2μ LEU2 ADH-pol12-R248M
pVL7989	2μ LEU2 ADH-pol12-R248N
pVL7990	2μ LEU2 ADH-pol12-R248T

Results: Southern Blot analysis of Pol12 mutants

Because of their strong ODN phenotype, high conservation throughout species and likeliness to be important for the protein interactions based on the nature of the amino acids and localization on the primosome crystal structure, we selected *pol12-R248E*, *pol12-D303K* and *pol12-R322E* to represent surfaces 1, 2 and 3, respectively. These mutations, among additional ones further described below, were expressed by exposure to 5-FOA to shuffle off the WT Pol12-containing covering plasmid, streaked for ~75 generations and ran through the Southern blot process to be analyzed. Control strains include WT, as well as a subset of the suspected

Pol12 residues involved in the interface with Pol1. Surfaces 1 and 3 mutants showed a striking elongation of telomeres. In comparison, surface 2 mutants seemed to mimic WT (**Figure 4.1**).

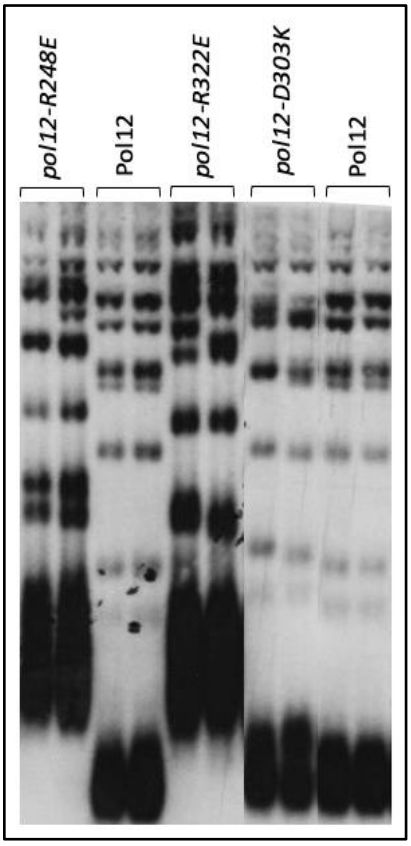

Figure 4.1: Southern blot analysis of Pol12 alleles of surfaces 1, 2 and 3 in comparison to WT shows different telomere length phenotypes

LOF assay monitoring telomere length of pol12Δ yeast strains bearing single-copy plasmids expressing mutations or WT Pol12 as described at the top. Blot was cropped for result clarity

For both *pol12-R248E* and *pol12-R322E*, main mutants representative of surfaces 1 and 3, the bottom edge of the band barely overlapped with the top part of a neighboring WT strain band, suggesting that even their shorter specimens are longer than most WT ones. This does not however show that this increase is specifically located at telomeric extremities as the internal, telomeric sequence packed X elements are also affected. It could instead be the sign of a dysregulation of all highly repetitive, difficult to replicate sequences throughout the genome, of

which telomeres are the most prominent example. Although surface 2 mutants don't display any visible increase in telomere length, it does not necessarily mean that telomeres weren't affected, as will be discussed below. Yet, the lack of visible elongation in contrast with the other two mutants argues that a different pathway might be affected, in accordance with previous results.

In addition to the main residues, the ODN assay highlighted a single substitution in Pol12 originally thought to have an ODN phenotype with both $Pol1^{TS}$ and $Cdc13^{TS}$. This residue, *pol12-D262K*, maps within surface 3, and matches the phenotypes of the cluster. Yet, it shows by Southern blot analysis an extreme elongation phenotype, different from its neighboring *pol12-R322E* but strikingly similar to mutants of two subunits of the t-RPA complex Stn1 and Ten1 (*Gelinas et al., 2009, Xu et al., 2009*) (**Figure 4.2**). A closer look at the structure argues that this residue destabilizes the protein and renders the allele temperature sensitive. Indeed, expression of the mutant by itself and not in a sensitized TS strain also results in a temperature-dependent loss of viability. This mutant illustrates how the degree of disruption of Pol12 directly correlates to telomere elongation. Whether this extreme lengthening is the direct cause of lethality or simply a side effect of disrupting an essential pathway beyond survival has yet to be understood.

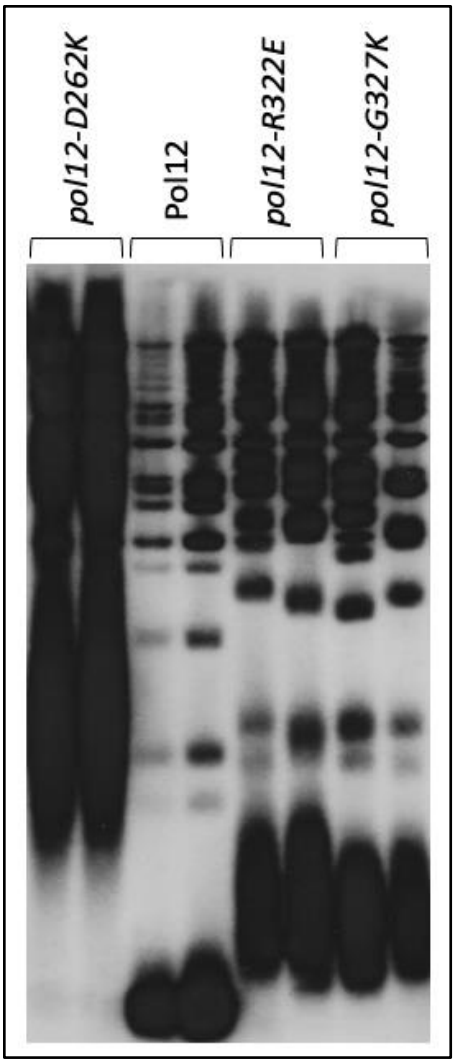

Figure 4.2: Southern blot analysis of a TS allele of Pol12 in comparison to mutations of ODN-found surface 3 shows different levels of telomere elongation

LOF assay monitoring telomere length of pol12Δ yeast strains bearing single-copy plasmids expressing mutations described above.

For confirmation of the ODN assay results that distinguish novel Pol12 alleles from characterized ones, we included the alleles characterized by Klinge and colleagues as being responsible for the interaction of Pol12 with its partner Pol1 (**Figure 4.3**). Non-polar residues were swapped onto both charges to investigate whether it may result in a differential phenotype. As shown in **Figure 4.2**, *pol12-G327K* shows the same elongated telomere phenotype as *pol12-*

R322E. However, none of the other alleles do, although Pol12-M250 and Pol12-E319 become slightly longer than WT when mutated. These residues localize close to surface 1 and 3, respectively. Highly conserved Pol12-P575 shows no elongation phenotype when mutated onto either a positively or negatively charged residue. This allele was previously discussed for its ability to disrupt the interface between Pol1 and Pol12 causing inviability when combined with substitution of neighboring residues. Therefore, disrupting the interaction of the two proteins results in a different telomere length phenotype than some of the residues found by ODN.

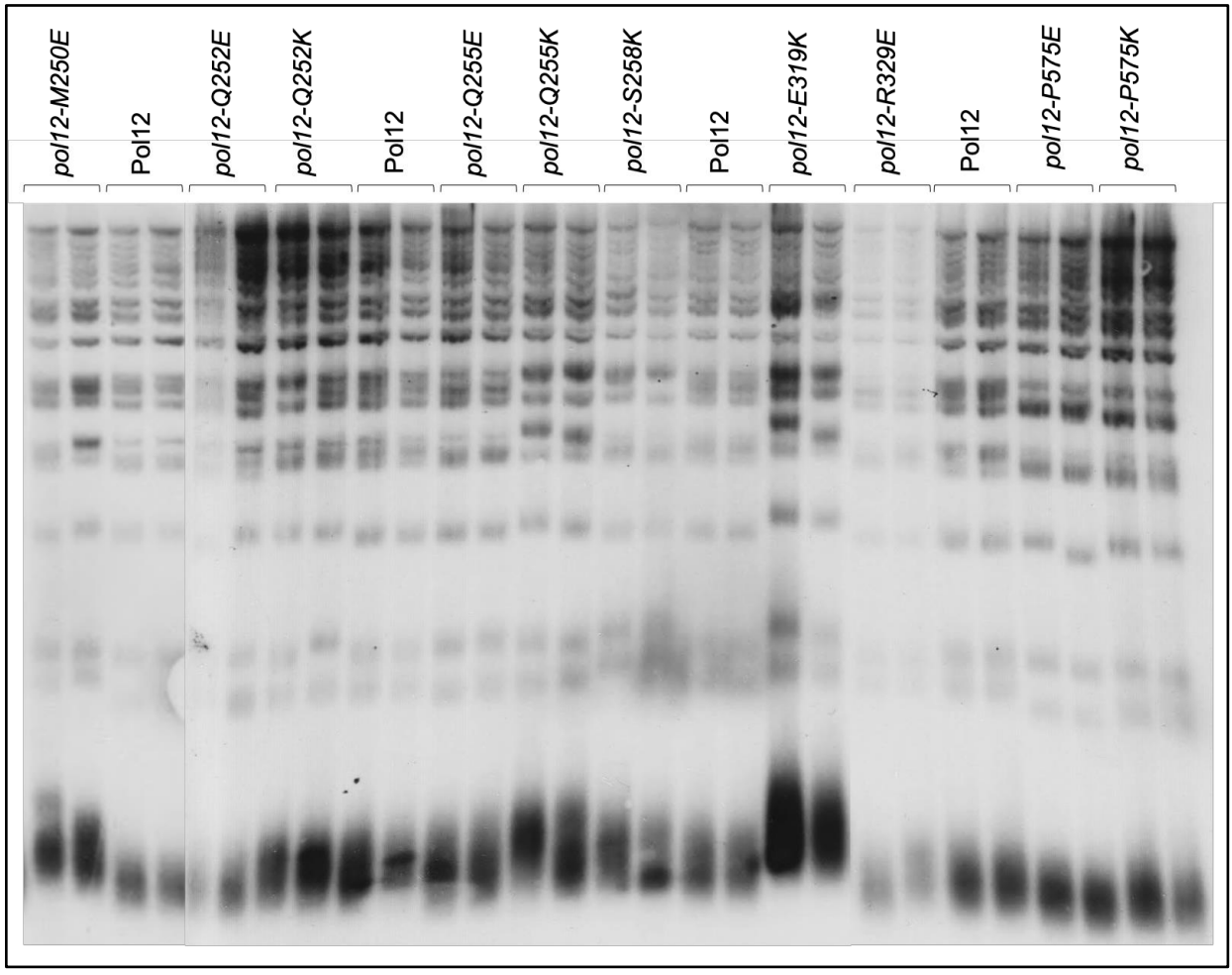

Figure 4.3: Southern blot analysis of mutants of residues thought to be important for the interface of Pol12 with Pol1 did not show a telomere elongation phenotype

LOF assay monitoring telomere length of pol12Δ yeast strains bearing single-copy plasmids expressing mutations described above.

Tracking the telomeric elongation phenotype of Pol12 mutants over generations

Although a typical Southern Blot analysis is done on strains streaked out to 3X to allow ample time for any change in telomere homeostasis to take place, we wanted to address whether the elongation phenotype observed in *pol12-R248E* and *pol12-R322E* happened progressively or as the result of a sudden event. In order to do so, we gathered, prepared and analyzed telomeric DNA of both strains in duplicates from "0X" (straight out of frozen glycerol) to 5X (5 successive streak-outs), in parallel to WT. Both mutants showed a linear increase of their telomeric DNA after each streak-out (**Figure 4.4**). Therefore, the telomere elongation phenotype is progressive, not random and cell-cycle dependent.

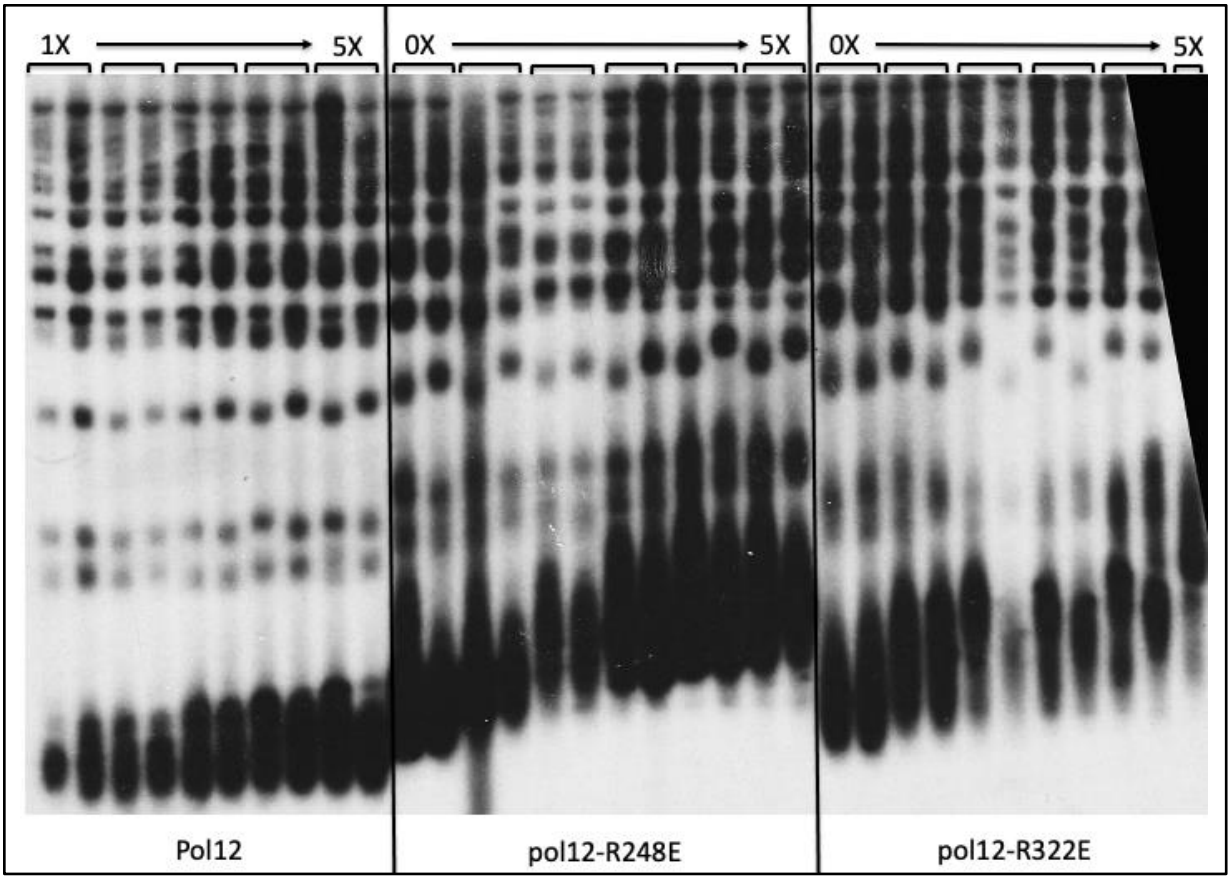

Figure 4.4: The telomere elongation phenotype of Pol12 alleles is progressive
LOF assay monitoring telomere length of pol12Δ yeast strains bearing single-copy plasmids expressing mutations described above. Strains were analyzed from frozen into glycerol (0X) for 5 successive streaked-outs (1X -> 5X).

This assay was designed with the assumption that 5 successive streak-outs might be enough generations to reach telomere homeostasis of those mutants. However, as shown by Meier and colleagues, some mutants might need more time to attain their modified telomere homeostasis, up to 225 generations or ~11 streak-outs (*Meier et al., 2001*). It is therefore difficult to conclude whether Pol12 alleles reached an equilibrium or physical limitation at 5X. Interestingly, every strain including WT showed a broadening of their Y' elements band over generations, a result presumably representative of the various events that may shorten or elongate the ends even in WT. Finally, it is important to note that the mutant strains already showed an elongation of their overall telomere length at "0X". This result can be explained by the fact that the strains were grown in liquid media overnight in order to create the frozen glycerol vial used for this experiment, which involved several rounds of cell cycle. Even though the covering plasmid with WT Pol12 was still present, the one containing the mutant version was also expressed at a basal level mimicking what a diploid heterozygous strain would look like. Therefore, the effect of the mutant isn't linked to its overexpression and the presence of WT Pol12 isn't enough to preserve telomere homeostasis, arguing that it doesn't outcompete the mutant. Furthermore, it does not behave as a recessive allele compared to WT.

Additive effect of the telomere elongation phenotype of Pol12 in the absence of negative telomerase regulator Rif1

Changes in telomere homeostasis can result in either telomere shortening (stable or senescent) or telomere lengthening depending on the allele tested which can give an indication of the pathway they might be involved in. Elongated telomeres have been reported with many

mutants, most of which are non-essential genes thought to play a role in physically binding and protecting telomeres. Mutants in all 3 subunits of t-RPA, as well as novel alleles of primase found by ODN, have exhibited "long telomeres" mutants arguing that all those distinct alleles may work together, in accordance with results described in Chapter 3 (**Figure 4.5**).

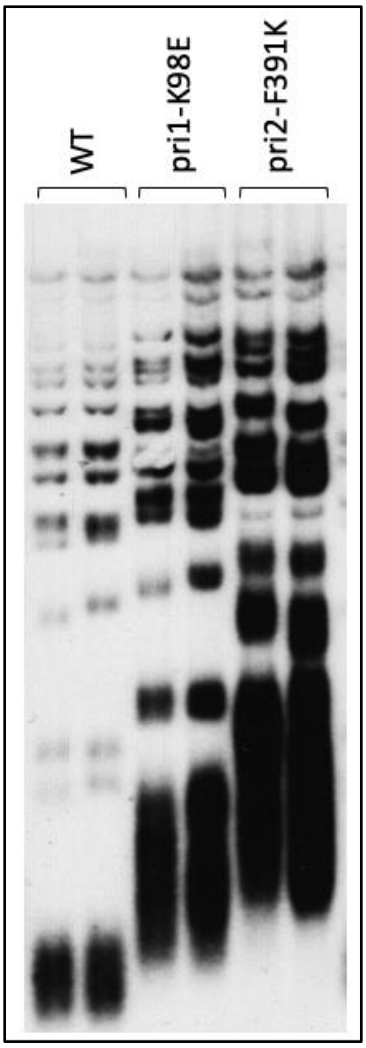

Figure 4.5: Primase alleles show a similar elongated telomere phenotype
LOF assay monitoring telomere length of pri1Δ or pri2Δ yeast strains bearing single-copy plasmids expressing mutations described above compared to WT

Among the non-essential genes resulting in telomere elongation when depleted is Rif1, which is thought to specifically localize at telomeric sequences in order to protect them from degradation (*Hardy et al., 1992*). Because the absence of this protein results in an increase in telomere length, it has been hypothesized that Rif1, alongside other telomere binding proteins, act to repress telomerase recruitment and/or activity. This long-standing "protein-counting" model argues that telomere length directly correlates with the amount of factor bound (*Marcand et al., 1997*). Therefore, the shorter the telomere, the more likely telomerase will act on it as the amount of factors bound is low. This strategy is important not only not to waste energy elongating telomeres that aren't critically short, but also as the amount of the enzyme present in a cell isn't enough to elongate every telomeric end after each round of replication (*Mozdy and Cech, 2006*). However, recent data from our laboratory has demonstrated that telomerase acted at the same likelihood at shorter and longer telomeres, in opposition with this model (*Paschini et al., 2020*). It is therefore possible that Rif1 inhibits telomerase through different means.

In order to assess whether Pol12 mutants and *rif1Δ* disrupt the same pathway giving rise to elongated telomeres, we combined both defects. If they are, one can expect the double mutant to show the same phenotype as each single allele. Although literature recorded growth reduction of *rif1Δ* with alleles of Pol12 and Pri2, such phenotype was not observed with *pol12-R248E* possibly because of the separation-of-function nature of the allele, in opposition to previously characterized TS ones (*Anbalagan et al., 2011*). Yet, Southern Blot analysis showed that telomere elongation of both single defects was additive in the context of the double mutant strain (**Figure 4.6**). This result argues that Pol12 and Rif1 may act in two distinct pathways that both result in telomere elongation when depleted.

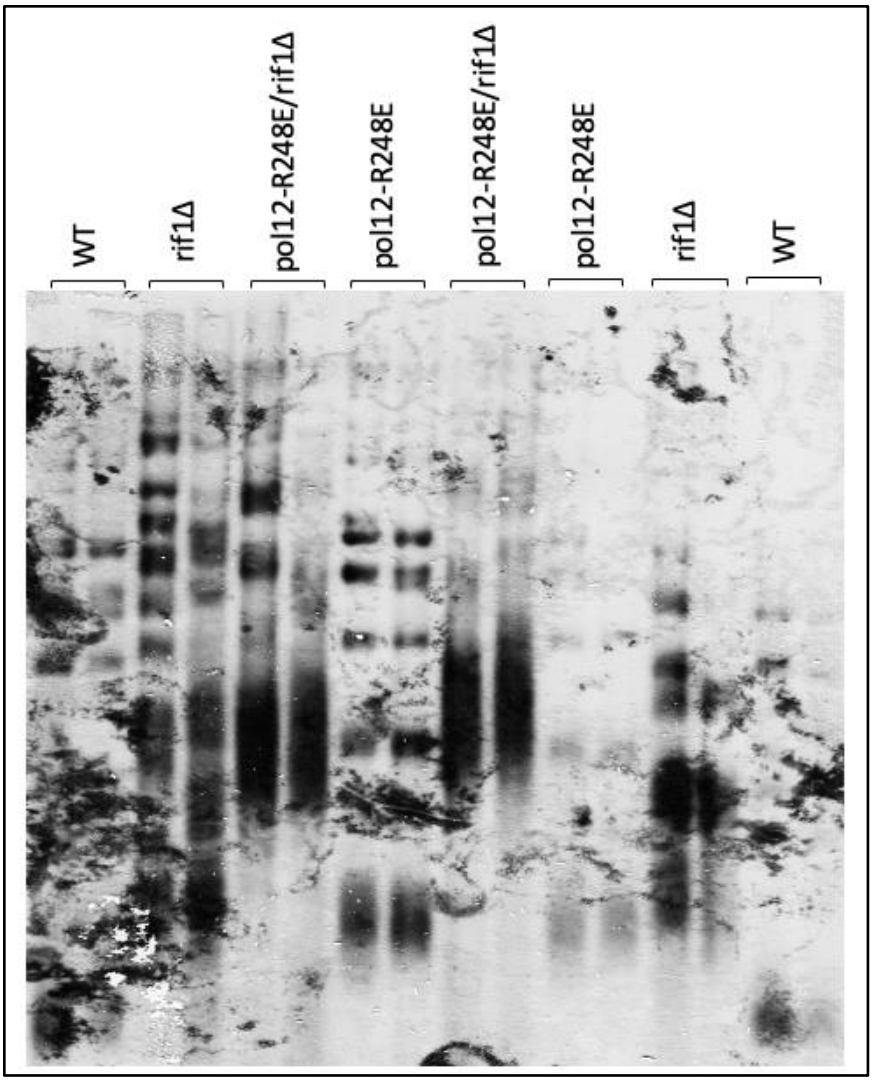

Figure 4.6: Rif1 and Pol12 influence telomere length through distinct pathways
LOF assay monitoring telomere length of rif1Δ (yVL3737), pol12Δ (yVL4931) or a combination of the two yeast strains bearing single-copy plasmids expressing mutations described above compared to WT.

Discussion: limitations of Southern Blot analysis and emergence of the TeloPCR assay

Although widely used, Southern blot analysis of telomeric DNA has drawbacks that can limit the amount of data obtained. First of all, the nature of the assay can exclude readings of critically short telomeres. Indeed, the signal is proportional to the amount of telomeric probe bound to the DNA. Therefore, shorter DNA might not be visible next to longer strands. This issue is particularly relevant in strains resulting in a drastic increase in telomere length, such as

Pol12 mutants. Getting the appropriate and/or multiple exposure(s) to limit this issue can be a delicate process as the developing step of the protocol is extremely time sensitive.

Similarly, size variations might be difficult to detect. Although telomeric repeats themselves are a few hundred base pairs long, the entire Y' element is much longer, over 1kb. The agarose gel density can make it impossible to see small changes that are still an indication of impaired telomere homeostasis or WT-length telomeres that are abnormal.

Finally, the nature of the telomere itself cannot be analyzed through this assay. More specifically, as the probe hybridizes to the C-strand, information regarding the single stranded G-tail, as well as possible changes in telomeric sequence or conformation cannot be recovered. Therefore, study of any changes in the length and/or nature of the single stranded telomeric tail is impossible through Southern Blot.

For these reasons, we added a telomere PCR (TeloPCR) based assay adapted in the laboratory (*Bennett et al., 2016*). This protocol indiscriminately isolates and amplifies hundreds of copies of a given telomeric end from a single colony. Products are subsequently cloned onto a vector to be sequenced. The resulting data can be sorted by length, creating a TeloPCR "profile". Such profiles vary greatly from strain to strain. They can be characterized by both the average telomere size, as well as the degree of variability from that mean. Our original WT strain was extensively sequenced to create baseline TeloPCR profiles for several distinct telomeric ends, mainly chromosome VI-R and I-L (*Paschini et al., 2020*). Although matching the average length of ~300bp described in the literature, the degree of variation and amount of "critically short" telomeres present even in a WT cell brings in a new vision to telomere homeostasis.

As the assay involves cloning of the PCR products, there was a specific hurdle pertaining to long-telomere strains that needed to be addressed. Indeed, there is an experimental limit for

the size of the insert that can be inserted into the vector needed to sequence it. Therefore, the risk was that the longest specimens might fall through during the process. To work around this, we created variants of a chosen ODN mutant *pol12-R248E*. The goal of such a process was to find an allele with a milder phenotype while staying representative of the impaired function of that residue. This strategy was in part inspired by a similar approach of the Wuttke laboratory working on Cdc13 and its ability to bind to DNA (*Glustrom et al., 2018*).

We created six variants of the original charge swapped residue, with substitutions into amino acids of different natures. The resulting alleles showed a wide range of severity of ODN phenotypes, ranging from the most intense being the *pol12-R248E* charge swap, to the mildest being the *pol12-R248M* allele (**Figure 4.7**).

The *pol12-R248A* allele was selected for a pilot study because of its mild yet noticeable phenotype. We analyzed its telomere length through Southern Blot and found that the overall length was close to WT, bypassing the limitations described above and allowing further analysis by TeloPCR with the expectation of still observing impaired telomere homeostasis (**Figure 4.8**). A similar result was observed with *pol12-R322E* compared to *pol12-R322A,* arguing that the defect is linked to the nature of the modified amino acid.

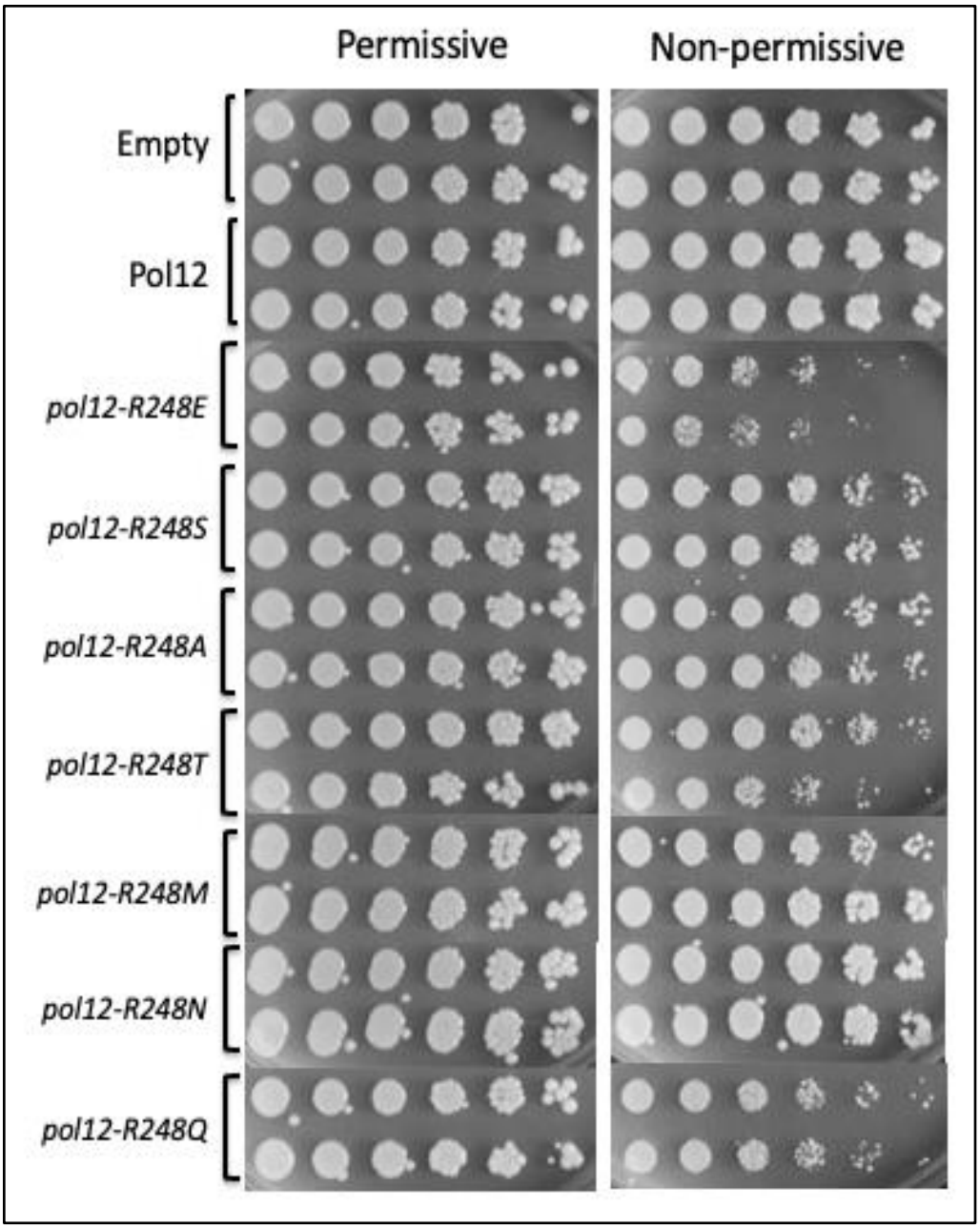

Figure 4.7: ODN analysis of variants of Pol12-R248 in a cdc13^{TS} strain shows a variety of growth phenotypes

Strains with a cdc13^{TS} mutation were transformed under selective marker pressure with an overexpression 2 micron (2u) vector including the content indicated on the left side. Two independent colonies were grown, replica gridded at different dilutions and grown for 3 days at permissive (28°C) and non-permissive (32°C) temperatures.

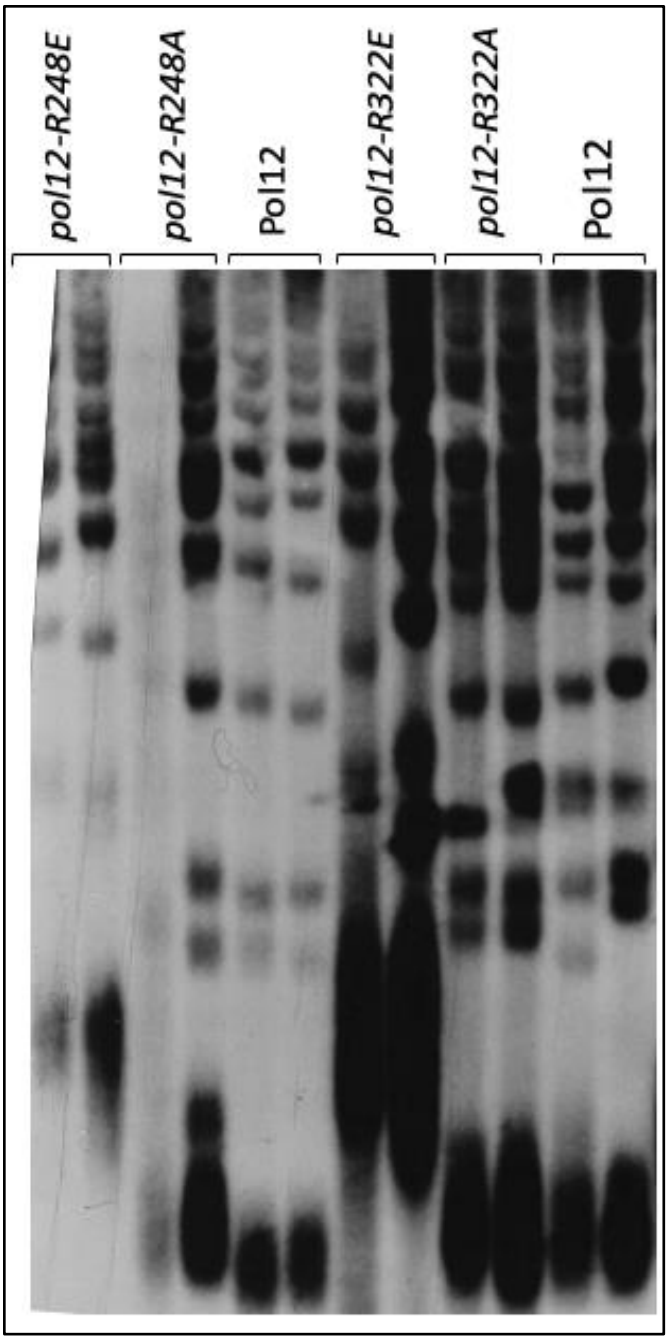

Figure 4.8: The alanine variant of key Pol12 residues does not exhibit elongated telomeres

Mutations were integrated using the pop-in pop-out method described in Chapter 5 (pol12-R248E = yVL5025, pol12-R322E = yVL5026, pol12-R248A = yVL5524, pol12-R322A = yVL5525), streaked-out 3 successives times alongside WT (yVL2967) and prepared as described in Material and methods

Material and methods: TeloPCR

All strains used for the TeloPCR assay had their mutation integrated to the genome using the pop-in pop-out method described in chapter 5. The resulting strain of interest is spread on a solid Yeast Peptone Adenine Dextrone (YPAD) media from a 40% glycerol solution stored at -80°C. Once grown at 30°C for ~72 hours, a single colony is picked and re-streaked on similar media in order to generate several distinct colonies sharing the same original founder cell. A subset of them (typically 8 to 12) are then grown individually in liquid YPAD media overnight. Cells are pelleted and their DNA is extracted and purified. Using ~150ng of template, the chromosome I left (I-L) telomeric end of each sample is amplified with Taq polymerase after addition of a C-tail using Terminal transferase (TdT) in sterile conditions. A second round of Ethanol-based purification concentrates the PCR product of which half is TA-cloned using the Thermo Fisher Scientific TA Cloning™ Kit and lab-made $CaCl_2$ *E. coli* competent cells. Clones are picked by blue-white color selection using X-Galactose and grown in prewarmed Luria-Bertani (LB) media with Carbenicillin (50mg/L) overnight to amplify the DNA. After a final round of DNA extraction using Qiagen's QIAprep Spin Miniprep Kit, samples are diluted at ~100ng/ul to be sent to sequencing by EtonBio with the universal M13-F40 primer.

Table 4.2: List of strains used for the TeloPCR studies

All strains were derived from yVL2967 and have the background genotype ura3-52 lys2-801 trp-Δ1 his3-Δ200 leu2-Δ in addition to the described point mutation

Strain #	Genotype
yVL2967	WT
yVL5524	pol12-R248A
yVL5684	pol12-D259K
yVL5782	pol12-R248Q

Results: Analysis of the pilot TeloPCR profile of pol12-R248 variants

Eight individual colonies with a common founder cell of genotype *pol12-R248A* were selected and their DNA amplified by PCR side by side with a WT strain for comparison. Prior to moving on to the cloning steps, they were run on a 2% agarose gel to check the nature and rough size of the telomeric PCR product. Every colony showed a single loose band around 500bp, with a range of up to ~200bp of variation in lengths (**Figure 4.9**).

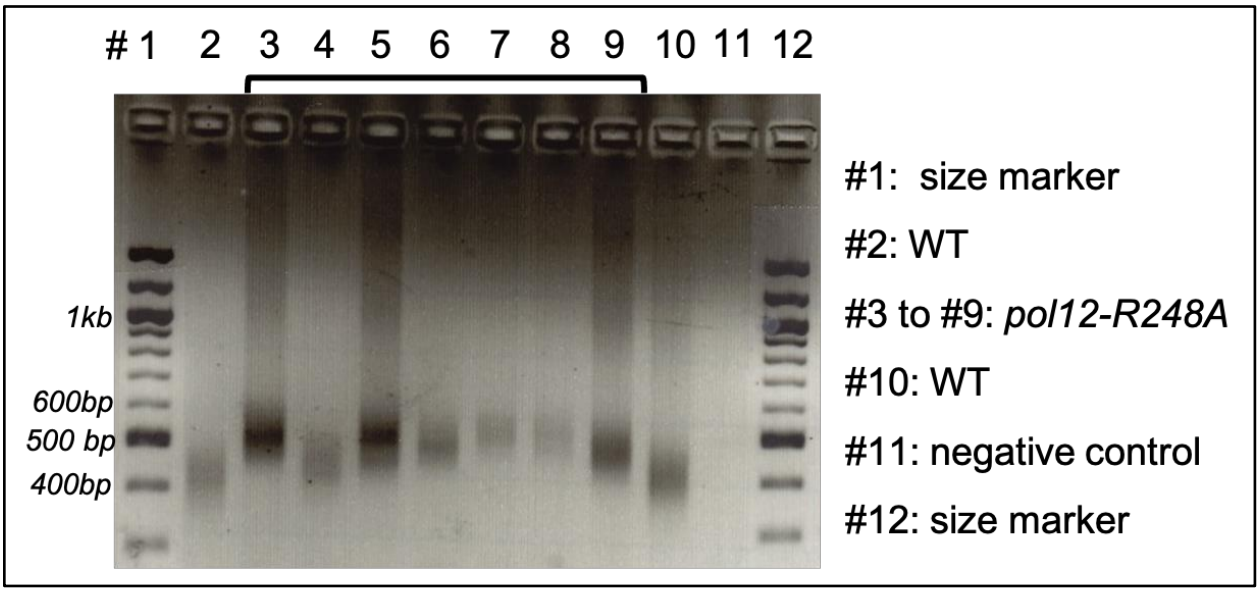

Figure 4.9: TeloPCR *pol12-R248A* samples run on a 2% agarose gel
5ul of the PCR product with the indicated template genotype was run for 2 hours at 100V on a midi 2% agarose gel alongside 5ul of 100bp size marker. Negative control = PCR sample with no template

Such variation is expected as individual colonies formed from one common cell that may have undergone different random events of replication fork stalling, DNA damage and telomerase action throughout cell cycles. Yet, as expected from previous results, every colony had an overall elongated telomere length, compared to a WT strain PCR product of ~400bp.

In order to ensure the final result to be as representative of the overall strain changes as possible, the TeloPCR profile of *pol12-R248A* was constructed by combining data of two

independent rounds of PCR using a DNA template extracted from four colonies, with a total of 145 sequences processed and sorted. The colonies were chosen based on band intensity and cleanliness of the PCR product for cloning efficiency, as well selecting bands representative of the total range of sizes found over all original colonies.

With an average length of ~340bp compared to ~310bp for WT, the teloPCR profile of *pol12-R248A* only showed a slightly elongated telomere phenotype, as previously observed by Southern blot (**Figure 4.10**). There is no obvious t-DAM (telomeric Deviation Away from the Mean), factor determined by counting the percentage of sequences that are more than 100bp longer or shorter than average. Yet, telomeres that are more than 100bp shorter than average were overall shorter in *pol12-R248A* samples compared to WT. This result goes against the protein-counting model and argues that the mutation does not solely result in elongated telomeres as observed through the Southern blot data.

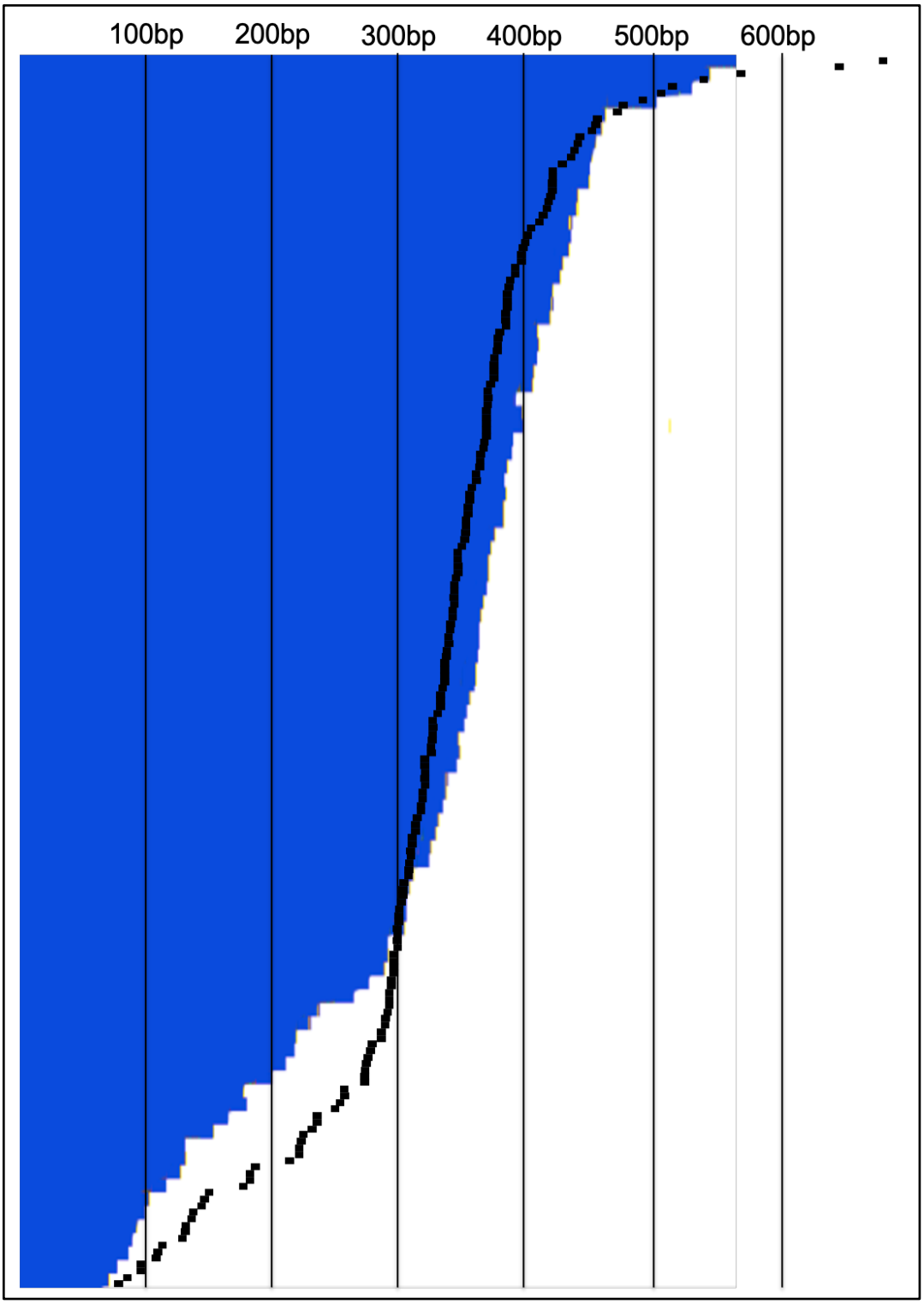

Figure 4.10: TeloPCR profile of *pol12-R248A* compared to WT

n=145 sequences from pol12-R248A (yVL5524) were individually processed and sorted by length in blue. Black curve represents the outline of a control WT (yVL2967) teloPCR profile of n=240 sequences generated by members of our laboratory (Paschini et al., 2020)

A second variant chosen to be analyzed was *pol12-R248Q*. Based on the previously shown ODN assay result, this variant has a phenotype intensity closest to *pol12-R248E*. We therefore expected this allele to show a more dramatic TeloPCR profile than *pol12-R248A*, with the possibility of missing some of the longest telomeres due to the experimental constraints of the assay previously described. To generate this profile, 127 samples were analyzed from two independent rounds of PCR protocol on three different colonies. The average of 475bp is over 50% longer than the ~310bp of WT. Telomere lengths varied from 80bp all the way up to 670bp, which is over twice the size of an average telomeric end. Strikingly, the profile appears to have two distinct slopes. Roughly two thirds of the samples are very tightly distributed between 400bp and 600bp, whereas the rest shows samples erode from 300bp all the way down to 100bp and below (**Figure 4.11**). There are several possible hypotheses to justify the obvious lack of samples ranging between 300 and 400bp, which would typically make up the majority of the samples of a WT strain. Firstly, the number of sequences could be too small and have fortuitously not covered this range. For comparison, the WT strain profiles were made using for about 250 samples. Yet, this seems unlikely as it would have necessitated over 20 additional samples to make the profile one even slope. Secondly, this could have been the result of a human error, either during PCR and/or sequencing. One again, this is unlikely as this profile was constructed from two distinct PCRs from which samples were sequenced not all at once to rule out the possibility of such issues. Therefore, the most likely explanation is that this gap is the result of the disruption of telomere homeostasis arising from the mutation. Whether there is a threshold length over/under which telomeres are recognized and treated differently is a possibility to be explored.

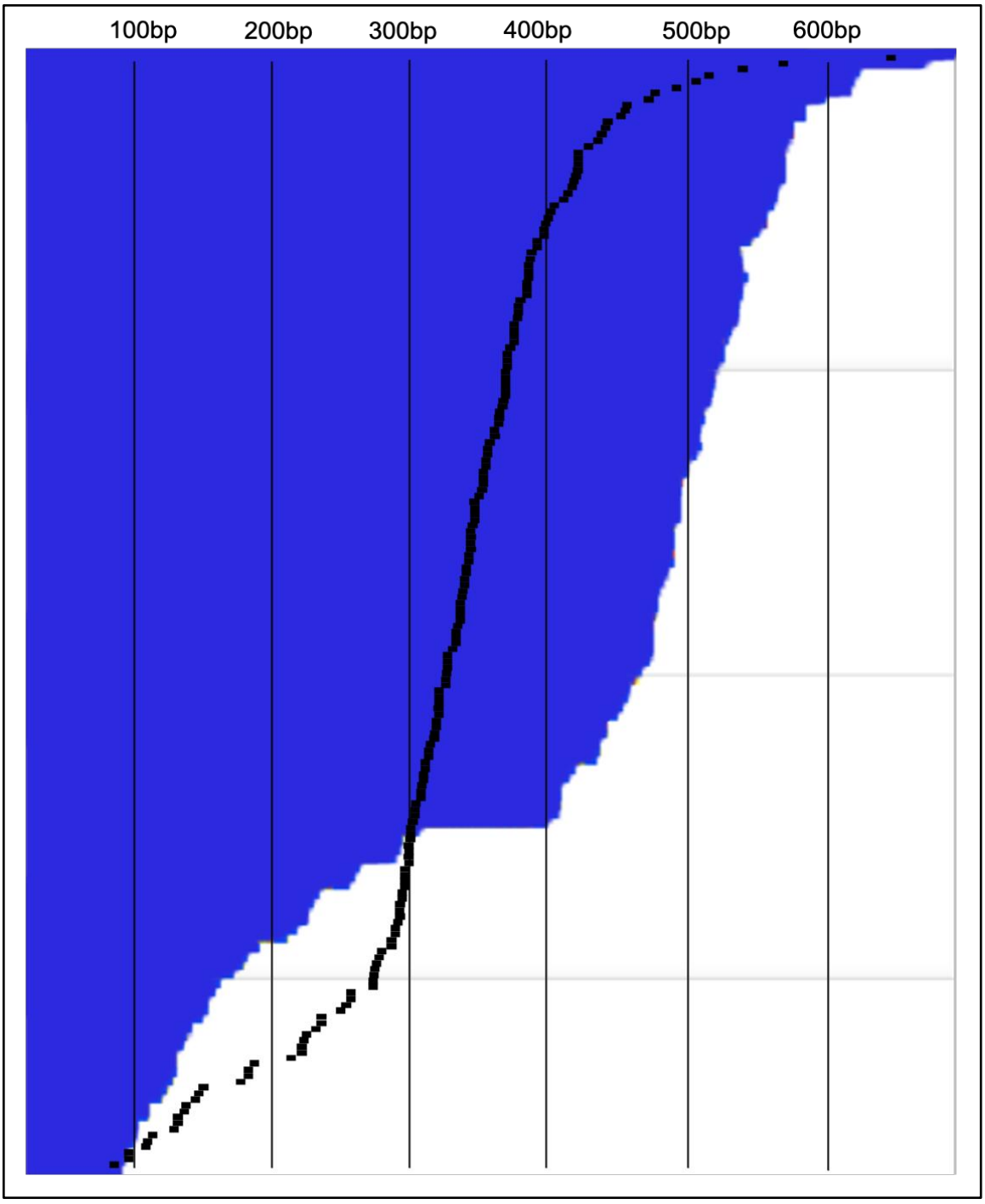

Figure 4.11: TeloPCR profile of *pol12-R248Q* compared to WT

n=127 sequences from pol12-R248Q (yVL5782) were individually processed and sorted by length. Black curve represents the outline of a control WT teloPCR profile of n=240 sequences generated by members of our laboratory (Paschini et al., 2020)

Analysis of TeloPCR profile of surface 3's pol12-D259K

The choice of the allele *pol12-D259K* to represent surface 3 for this assay was made based on the combination of its strong ODN yet mild Southern blot telomere length phenotypes. 131 samples were generated and sorted based on a similar experimental approach as described above. Lengths range from 60bp up to just over 700bp, with an average of around 350bp (**Figure 4.12**). Unlike *pol12-R248Q*, samples are distributed evenly, creating a clear t-DAM phenotype as there is ample variation from the mean. Although close to WT overall, a majority of the mutant telomeres were over or under more than 100bp from average. Finally, over 10% of them were below 100bp, a length that would be considered "critically short" in the field (*Chang et al., 2007, Teixeira 2013*).

Study of telomerase action on telomeric ends of a *pol12-R248Q* strain

The TeloPCR assay has a lot more potential than just sorting telomere populations by length. In fact, aligning sequences allows to identify points of divergence that arose from natural and/or accidental events triggering telomerase recruitment. Indeed, telomerase adds GT repeats in a slight degenerative fashion (*Singer & Gottschling, 1994*). This approach allows to sort sequences by length of non-divergent repeats and possibly identify correlation between the event position and likelihood/level of telomerase action. The TeloPCR profile of *pol12-R248Q* was re-sorted based on non-variant telomeric sequence length only (**Figure 4.13**). As previously argued by our laboratory, this order shows that telomerase does not act preferentially at shorter telomeres when an event occurs, although it seems more likely to elongate them more than longer non-divergent sequences.

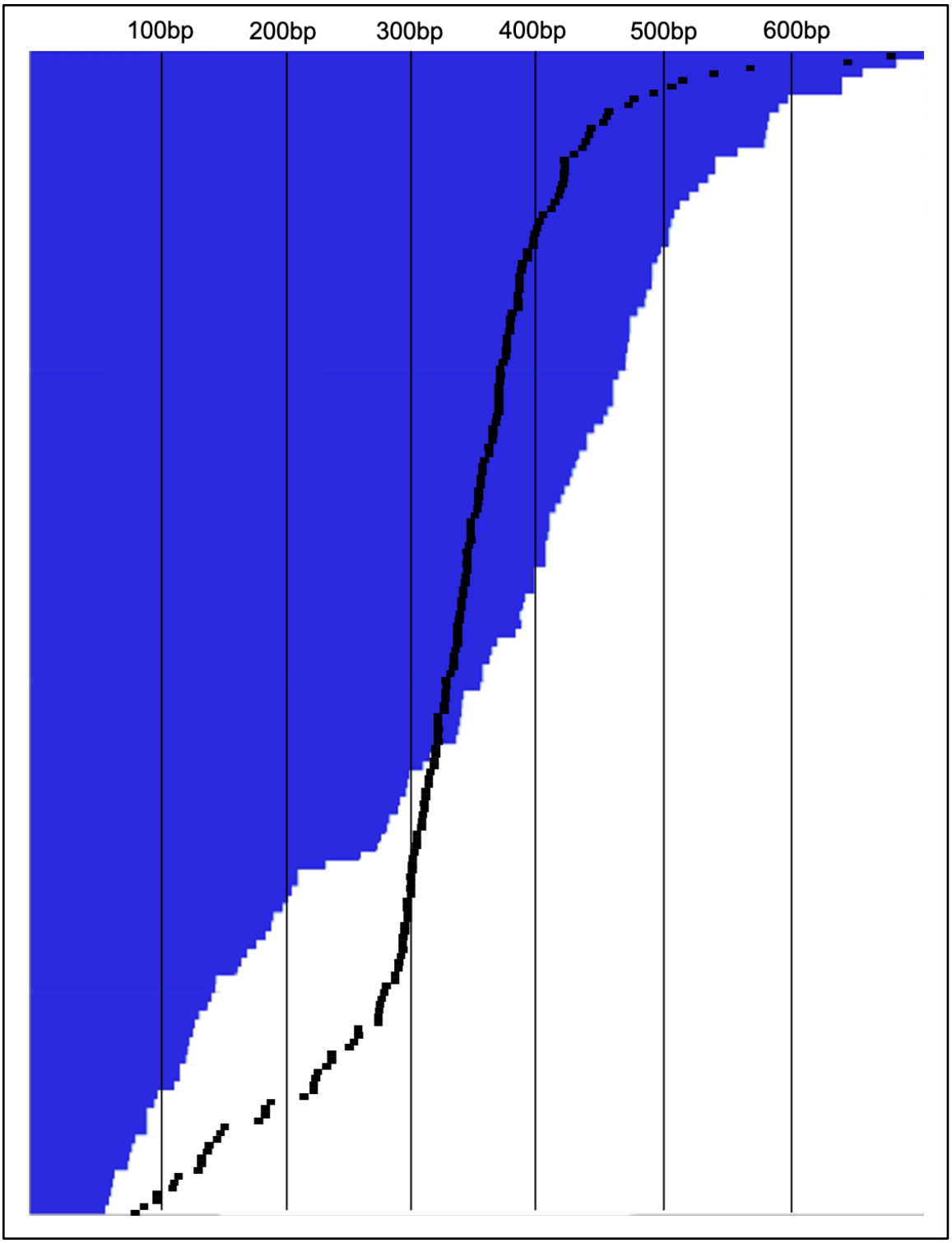

Figure 4.12: TeloPCR profile of *pol12-D259K* compared to WT

n=131 sequences were individually processed and sorted by length. Black curve represents the outline of a control WT teloPCR profile of n=240 sequences by members of our laboratory (Paschini et al., 2020)

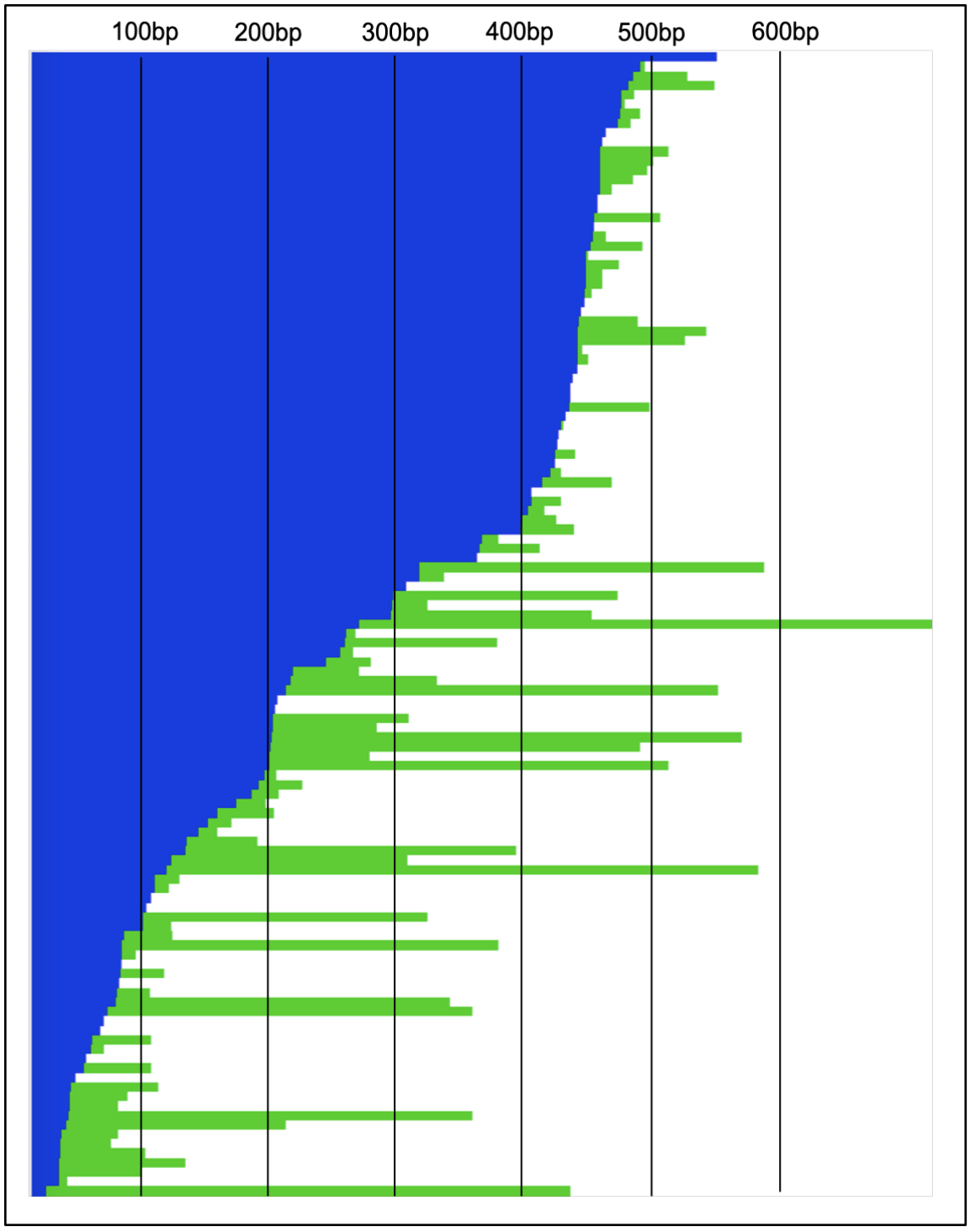

Figure 4.13: TeloPCR of *pol12-R248Q* sorted by non-variant telomeric length
Sequences that are from the founder cell are represented in blue. Sequences that are the result of telomerase action are represented in green

Conclusion: the TeloPCR profile of Pol12 mutants resemble that on a t-RPA mutant

A TeloPCR profile shows the status of telomere homeostasis of a given strain. It gives us information about the average telomere length but also the degree of variation from it. It also is able to efficiently depict critically short telomeres that might be the cause for many cell cycle defects. Data of the different Pol12 alleles described above are summarized in **Table 4.3**. Each of those mutants show an increase in average telomere length, but also a broader variation of lengths and, most importantly, a significant increase in the amount of critically short telomeric ends present in the cells.

Interestingly, comparison of *pol12-D259K's* profile with *cdc13-F539A,* courtesy of members of our laboratory, shows a striking overlap (**Figure 4.14**). This observation may argue that both defects act towards the same pathway on telomere maintenance.

Data from this chapter is currently in preparation to be published (Meunier and Lundblad, in preparation). The dissertation author was the primary researcher and author of this material.

Table 4.3: Comparison of data from the different teloPCR presented in this chapter or by our laboratory (*Paschini et al., 2020*)

Genotype	Total sequences	Average length	% sequences with t-Dam phenotype	% <100bp sequences
WT	240	~310bp	~20%	~2%
pol12-R248A	145	~340bp	~27%	~5%
pol12-R248Q	127	~475bp	~35%	~5%
pol12-D259K	131	~350bp	~60%	~11%
cdc13-F539A	251	~290bp	~80%	~14%

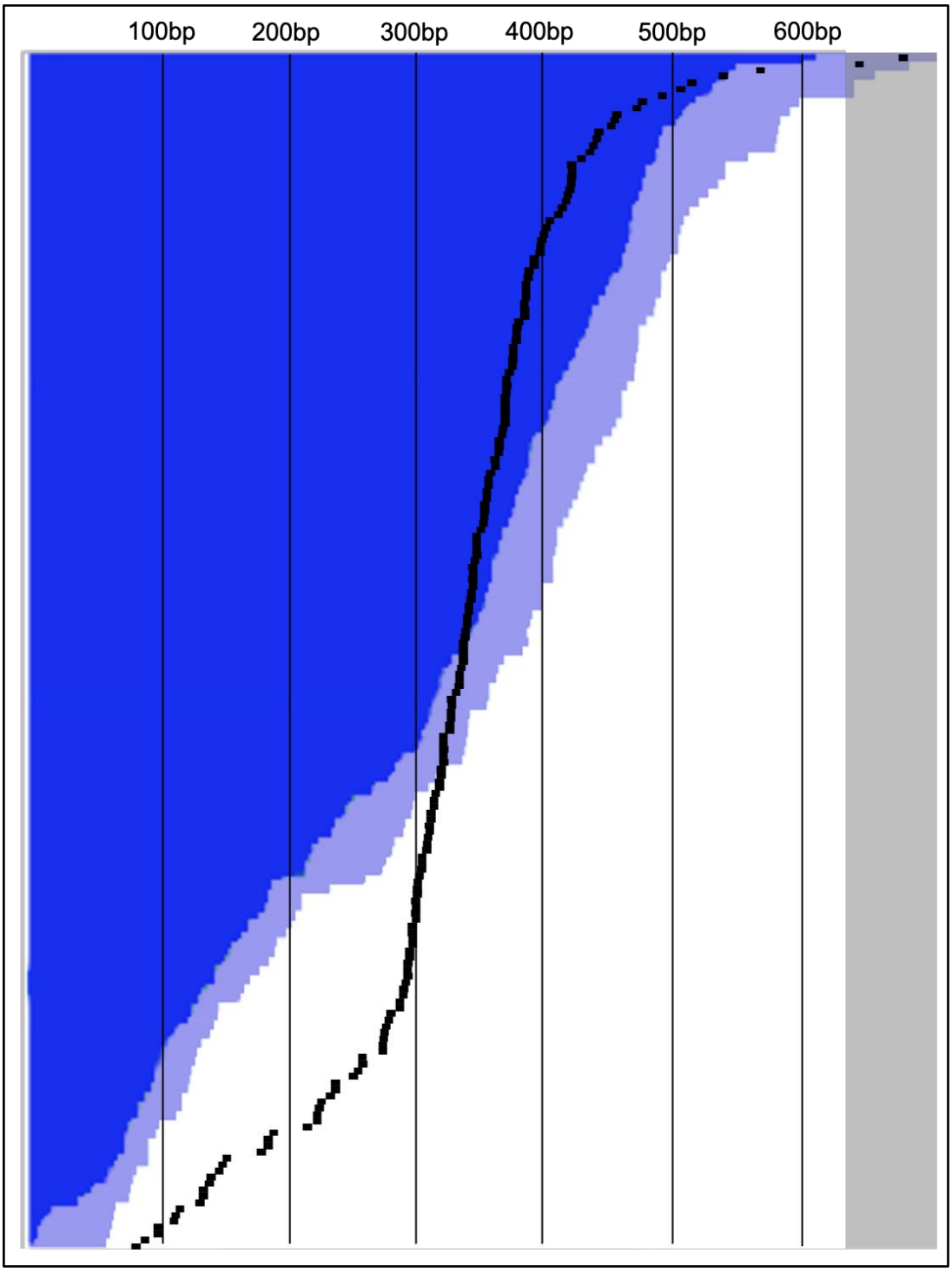

Figure 4.14: Comparison of the TeloPCR profiles of Pol12 and t-RPA mutants shows a striking overlap

The TeloPCR profile of cdc13-F539A is colored in dark blue over pol12-D259K, colored in light blue. The WT teloPCR outline is represented in black

CHAPTER 5:
Pol12 genetically interacts with t-RPA to regulate telomere length homeostasis

Abstract

We integrated key mutants of polymerase alpha-primase using the pop-in pop-out method, coupled with a known modified restriction enzyme digestion pattern for easy genotyping. Mutants of Pol12 combined with alleles of primase showed two distinct categories of double mutants. The first one, which is inviable, highlights a complex-wide essential function. The second category, which shows no additive phenotype, argues for a distinct function of Pri2 through its Fe-S cluster. Those Pol12 alleles were overwhelmingly synthetic lethal with defects of every subunit of t-RPA. This lethality seems to be linked to the binding ability of the latter complex to telomeres, as it shows to be influenced by RPA. Interestingly, some of the Pol12 alleles showed sensitivity for non-essential gene knock-outs. Among those is Okazaki fragment processing endonuclease Rad27, for which the knock-out-related phenotypes are rescued by *pol12-R248E*. This result allowed for exploration of which pathway this rescue stemmed from. We found that Pol12 seems to act to repress DNA damage checkpoint activation that would trigger repair of poorly processed lagging strand intermediates.

Introduction: epistasis principle

Saccharomyces cerevisiae is a convenient model organism to easily generate double mutants for analysis. Indeed, the species has two mating types, a and alpha, that can be combined into a diploid in a matter of hours. The resulting cell is able to go through meiosis under deprived nutritional conditions, segregating its genome randomly into 4 haploid spores to ensure survival. Physically separating the spores is an easy process done by microscopy after partial digestion of the tetrad wall, or ascus. If combining two single mutant parents, the odds of obtaining a double mutant daughter cell is 1/4 for each sporulated diploid cell.

When two individual mutations disrupting the same pathway are combined, they can result in a demultiplied effect on the resulting strain. For example, if two proteins act redundantly towards an essential function, single disruptions might have little to no effect, whereas the double mutant will be lethal. This synthetic effect, defined as epistasis, is the basis of many studies aimed at testing whether different mutants act together. Although the effect differs depending on the relationship and nature of the two genes mutated, it has shown to be a powerful genetic tool throughout fields and decades as researchers discovered that there were most often several genes responsible for a pathway to be functional. This is particularly the case for pathways essential for viability such as DNA replication and damage repair. *S. cerevisiae* is widely considered a simplified yet informative model to study those pathways.

Most of the experiments previously described involved mutations contained in plasmids expressed onto either WT, TS mutant or Knock-out (KO) strains to allow for processing of a high number of mutants. For simplicity of obtaining double mutants without having to ensure maintenance of plasmid(s), key mutations of Pol12 found in chapter 2 were integrated into the genome using the pop-in pop-out method, in order to be crossed with alleles of interest with the

goal of confirming the suspected interaction with polymerase alpha-primase and t-RPA (*Scherer and Davis, 1979*). Similarly to the LOF assay, this technique involves the use of a plasmid containing the mutation to be integrated with a URA3 marker. This construct is linearized and integrated onto the genome by homologous recombination under the selection pressure of growing the strain on a media lacking Uracil. Once "popped-in", exposure to 5-FOA forces shuffling out of the plasmid with a set odd of leaving the mutation inside the genome. In our laboratory, each mutation is paired with an additional silent mutation adding or removing a given restriction site, allowing for easy identification of the allele in sporulated cells by PCR and diagnostic digestion with a restriction enzyme (**Figure 5.1**).

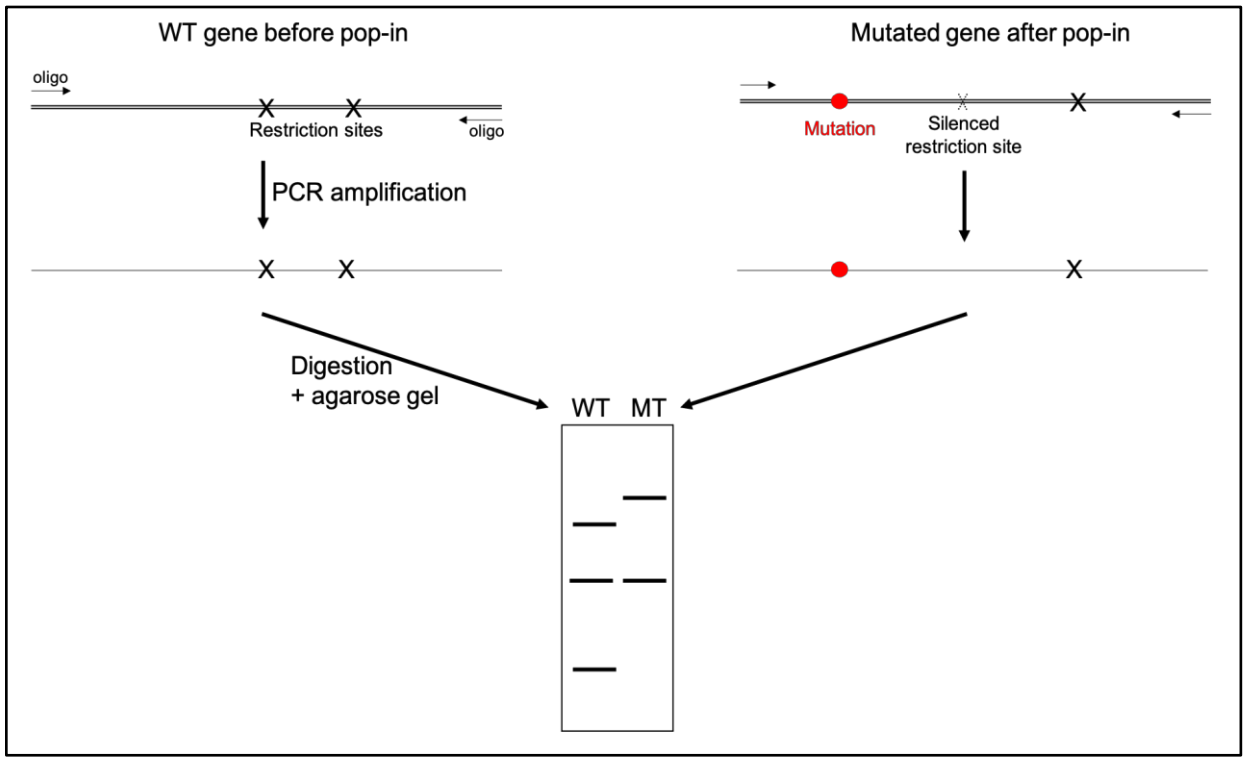

Figure 5.1: Design strategy to identify mutated alleles using restriction enzymes
A restriction site is added or removed with a silent mutation by Quickchange mutagenesis in proximity to the mutation to be integrated into the genome. When genotyping a strain for the given mutation, the gene area is PCR amplified and digested by said restriction enzyme with a different digestion pattern between WT and mutant.

Materials and methods: pop-in pop-out

All strains constructed by pop-in pop-out were derived from opposite mating types yVL2967 *(MATa ura3-52 lys2-801 trp-Δ1 his3-Δ200 leu2-Δ1)* and yVL4963 *(MATa ura3-52 lys2-801 trp-Δ1 his3-Δ200 leu2-Δ1)* transformed with derivatives of integrative plasmid Ylplac211 cloned with a gene of interest (*Gietz and Sugino, 1988*).

Table 5.1: List of the strains used for epistasis and Southern blot analysis in this chapter
All strains are derivatives of yVL2967 (ura3-52 lys2-801 trp-Δ1 his3-Δ200 leu2-Δ1)

yVL #	Mutation	Mate type
2967	WT	a
4963	WT	alpha
5025	*pol12-R248E*	alpha
5026	*pol12-R322E*	alpha
5524	*pol12-R248A*	alpha
5525	*pol12-R322A*	alpha
5027	*pol12-D303K*	alpha
4729	*pol1-1*	a
5042	*pri1-E152Q*	a
4946	*pri1-K98E*	a
4949	*pri1-D438K*	a
4256	*cdc13-Y556A+Y558A*	a
4648	*cdc13-Y556A+Y558A*	alpha
4642	*stn1-W466E*	a
5333	*rpa1-K95E*	a
5791	*ten1-E91K*	a
5184	*rpa1-K45E*	a
5498	*csm3Δ*	a
5649	*rad27Δ*	a
5795	*pol12-R248E + rad27Δ*	a
4094	*exo1Δ*	a
3736	*rad51Δ*	a
3737	*rad52Δ*	a
4881	*rad9Δ*	a
5268	*rad17Δ*	a
5502	*mec1Δ + sml1Δ*	a
5499	*ctf4Δ*	a
5244	*rad53-E365K*	a
5727	*tof1Δ*	a
5019	*mrc1Δ*	a
3815	*est2Δ*	a

Results: Epistasis analysis of Pol12 alleles with mutants of polymerase alpha primase complex

A first step in establishing the novel Pol12 mutants into a pathway is to confirm their ODN phenotype with a Pol1 TS strain once integrated into the genome. The main three alleles found by ODN, *pol12-R248E*, *pol12-D303K* and *pol12-R322E* were integrated as being representative of the phenotypes of surfaces 1, 2 and 3, respectively. They were initially crossed with *pol1-1*, allele of the catalytic polymerase subunit *(Pizzagalli et al. 1988).* The choice of this TS strain allows to compare the viability difference of the double mutant at permissive and non-permissive temperatures. For epistasis analysis, strains of opposite mating types bearing each of the two mutations to be combined were crossed for 4 hours before being microscopically picked and grown to a diploid colony. Cells were then transferred in a sporulation media deprived of nutrients for 48 hours to force meiosis. Fully sporulated tetrads were microscopically separated on YPD solid media to be grown. All the steps were performed at low permissive temperature to avoid impairments and loss of viability from the *pol1-1* TS mutation. Spores were then grown and gridded in serial dilutions at various temperatures to detect growth changes before being genotyped using the strategy described above. TS allele *pol1-1* was genotyped by patching spores at 37°C, a fully non-permissive temperature that results in complete inviability.

All three Pol12 mutants showed an additive phenotype to *pol1-1*. However, the effect was much more prominent with *pol12-R248E* and *pol12-R322E* as the double mutant was almost inviable even at room temperature (**Figure 5.2**). This result highlights previous observations arguing that TS mutants such as *pol1-1* could have a mild defect even at fully permissive temperatures (*Paschini et al., 2012*). It argues that the two proteins act redundantly for an essential function of the complex but that *pol12-D303K* is either not as severe, or that it pertains

to a different function performed by the two proteins that isn't as sensitive to an impaired Pol1. Previous ODN and Southern blot analysis results argue for the latter hypothesis.

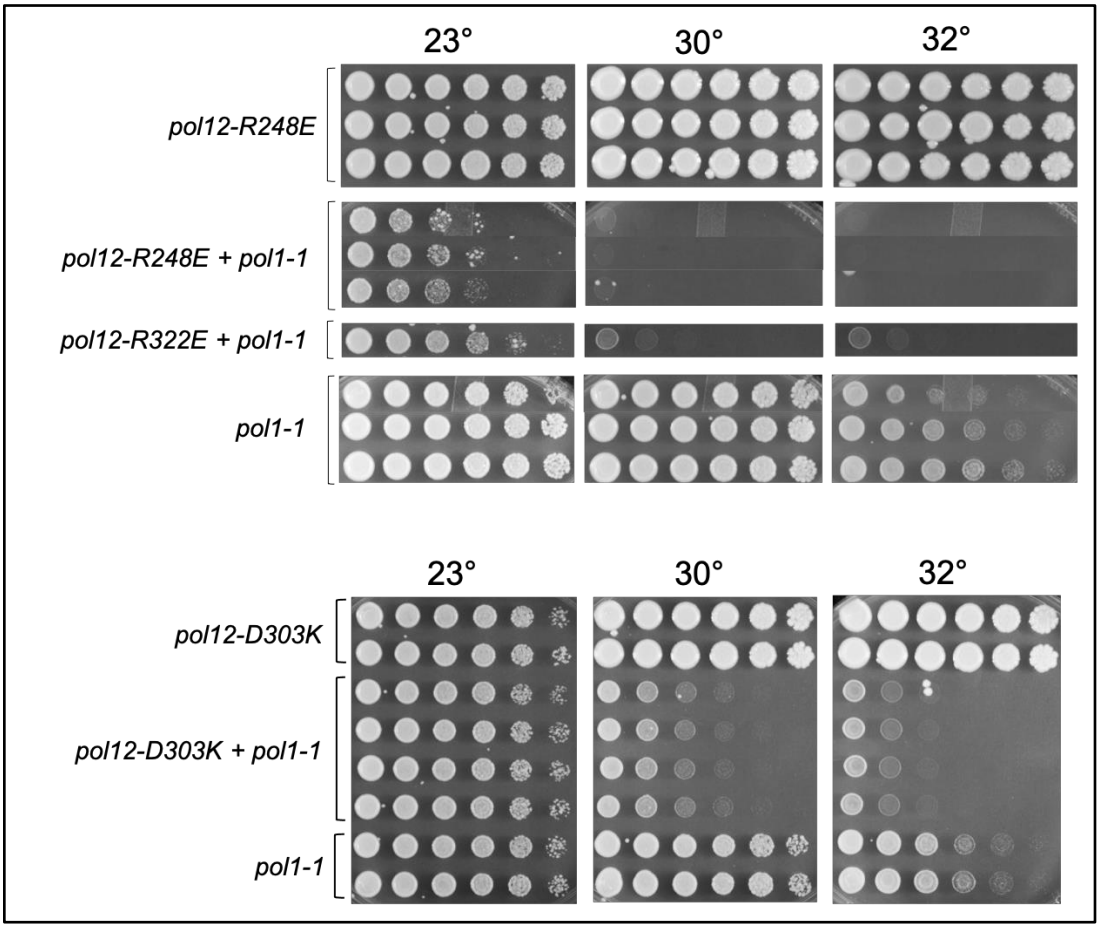

Figure 5.2: Epistasis analysis of Pol12 mutants with a TS allele of Pol1
Spores of the indicated genotype were grown at room temperature for 5 days, transferred to YPAD liquid media and replica-plated at various temperatures.

pol12-R248E and *pol12-R322E* were then tested with alleles of primase to investigate whether that essential function is specific to polymerase alpha or extends to the whole complex as argued by the ODN data. We first used *pri2-E152Q*, another TS allele expected to destabilize the protein (*Francesconi et al., 1991*). For this analysis, plates were grown at non-permissive temperature and growth differences were observed by colony size. We also crossed them with separation-of-function alleles of both subunits of primase found by ODN, represented by *pri1-*

K98E and *pri2-F391K*. Finally, *pri2-D438K* was selected for its sensitivity to cdc13^{TS}, proximity to the Fe-S cluster and long telomere phenotype as seen by Southern Blot.

Both Pol12 alleles looked synthetically lethal with the first two primase strains. However, a closer look at microcolonies showed that *pri2-E152Q/pol12-R248E* double mutants consistently arrested within the first cell division, whereas *pri2-E152Q/pol12-R322E* could progress for a few more cell cycles (**Figure 5.3**).

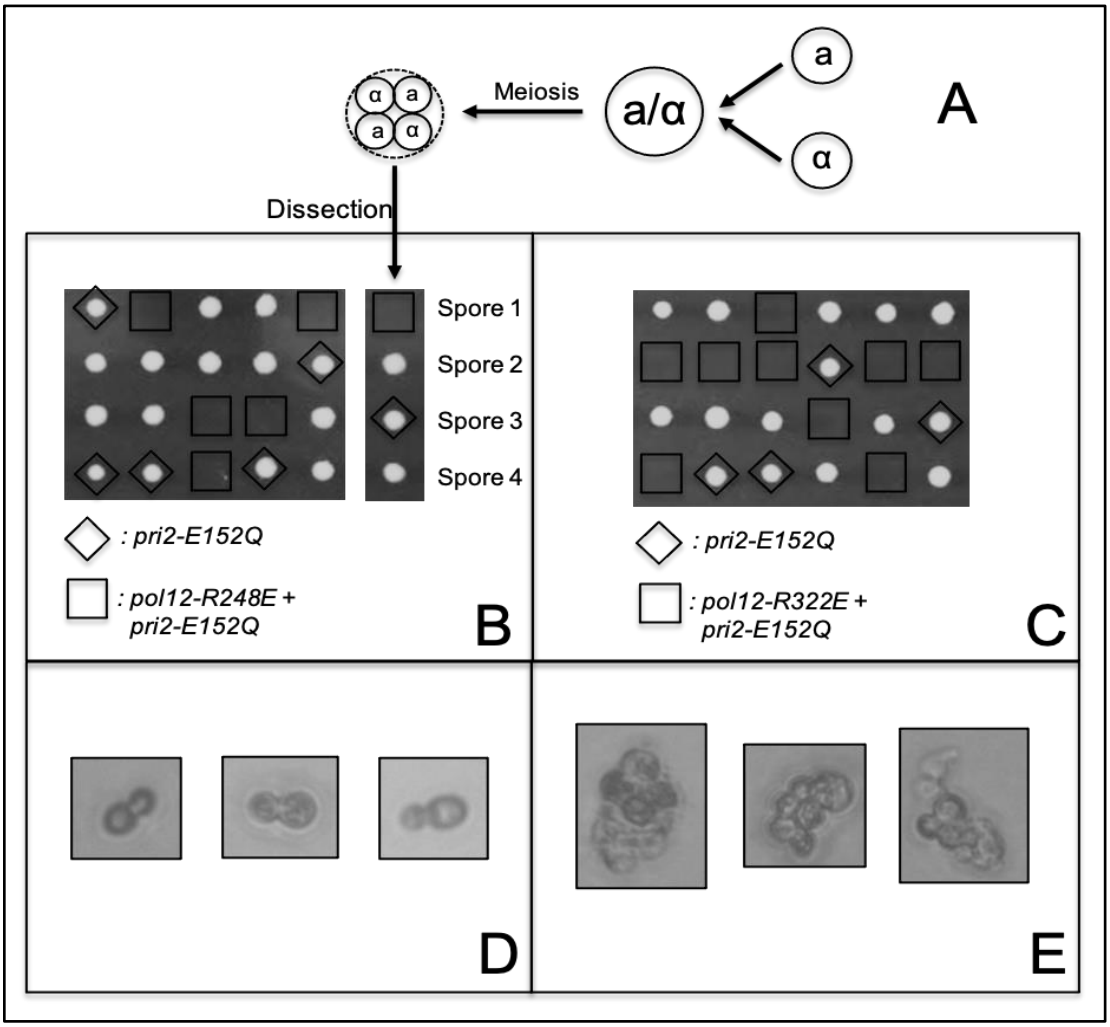

Figure 5.3: Epistasis analysis of pol12 mutants with a TS allele of Pri2
(A) Schematic representation of the process to generate double mutants (B and C) Dissected spores were grown on YPAD media for 5 days and genotyped for pol12-R248E and pol12-R322E, respectively (D and E) pictures of a subset of double mutant microcolonies were taken using a Zeiss Axioskop 50 with a Nikon Digital Sight DS-5M camera

Whether this difference in length of viability argues for two distinct functions or two levels of severity of impairment of a single function is unclear. Therefore, epistasis studies will continue to be done in parallel for *pol12-R248E* and *pol12-R322E* to try and gather further evidence for either hypothesis.

In contrast with the previous result, *pri2-F391K* had no visible additive growth phenotype with *pol12-R322E,* whereas the combination with *pol12-R248E* resulted in lethality. Although belonging to the different subunits of primase, Pri1-K98 and Pri2-F391 are both predicted to support the cohesion between primase and polymerase. Yet, as detailed in Chapter 3, it has been suggested that Pol1 binding with the latest is transient and only happens during the priming phase of lagging strand, which could explain the differential result between the two Pol12 alleles. Finally, neither strain showed an epistasis effect with *pri2-D438K*, as neither did *pri1-K98E*. This observation goes in the direction of previous observations arguing that the Fe-S cluster of Pri2 encompasses a distinct function from the cdc13^{TS} ODN alleles found in primase and polymerase alpha. However, it is also plausible that its effect simply isn't strong enough to visibly affect viability. Data from epistasis analyses within polymerase alpha-primase mutants is summarized in **Table 5.2**.

Table 5.2: Summary of epistasis analysis of combined polymerase alpha-primase mutants found by ODN

Additive growth defect is represented by crosses with the following nomenclature: -: no additive phenotype / +: slight additive phenotype / ++: clear additive phenotype / +++: synthetic lethality / n.t.: not tested

Mutant tested	Expected disruption	Epistasis with pol12-R248E	Epistasis with pol12-R322E	Epistasis with pol12-D303K
pol1-1	Unstable protein (TS)	+++	+++	++
pri1-K98E	primase-polymerase	+++	+++	n/t
pri2-E152Q	Unstable protein (TS)	+++	++	++
pri2-F391K	primase-polymerase (early replication only?)	+++	-	n/t
pri2-D438K	Fe-S cluster?	-	-	n/t

Epistasis analysis of Pol12 alleles with t-RPA mutants

The obvious next candidate for epistasis analysis was the t-RPA complex. As having been the main focus of study of several collaborators inside and outside our laboratory, many alleles of Cdc13 and Stn1 were available from targeted mutagenesis studies. Yet, no similar studies had been performed on Ten1 so far, although this subunit is also essential. Beyond containing an interface with Stn1, other functions of the protein not pertaining specifically to telomeres but affecting the whole genome have been suggested. Generation of novel Ten1 alleles and additional epistasis analyses of the protein will be discussed in detail in Appendix A.

Mutants of Cdc13 selected to be crossed disrupt the protein's DNA binding domain (DBD) to various degrees (*Glustorm et al., 2018*). These mutations are thought to alter the replication related function of the protein rather than its protective binding feature on telomeres (*Langston et al., 2020*). Little to no additive effect was observed with *pol12-D303K* and mutants of Cdc13 DBD (*cdc13*^{DBD}), in accordance with previous results. However, when combined with *pol12-R248E* and *pol12-R322E*, *cdc13*^{DBD} mutants were synthetically lethal (**Figure 5.4**). Therefore, Pol12 is necessary for viability when Cdc13 binding ability to DNA is compromised.

These Pol12 alleles were uncovered because of their ODN phenotype with *Cdc13^{TS}*. Another TS allele of Cdc13 allowed for the discovery of Stn1, as the overexpression of the protein suppressed its growth phenotype at non-permissive temperatures (*Grandin et al., 1996*). We therefore wanted to address whether the synthetic lethality observed between Pol12 and cdc13^{DBD} could similarly be rescued by overexpression of Stn1. Yet, it isn't the case, possibly arguing that Pol12 may act together with Stn1. As a result, mutants of Pol12 would prevent Stn1 from rescuing *Cdc13^{TS}*.

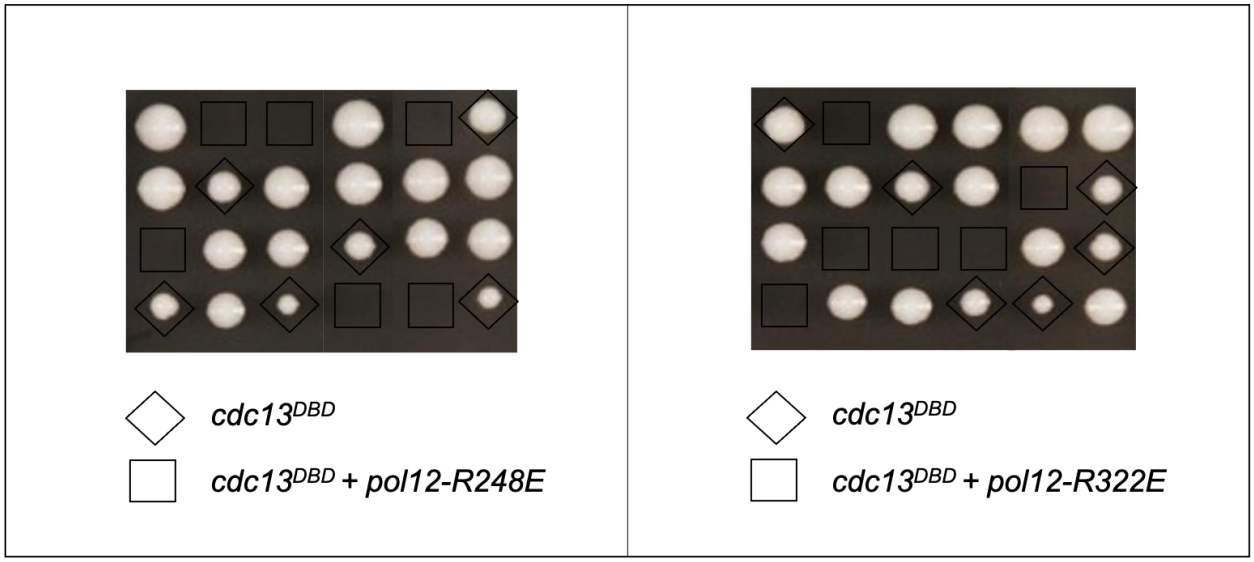

Figure 5.4: Combination of DNA binding Domain mutants of Cdc13 and Pol12 alleles showing an ODN phenotype in Cdc13^{TS} is synthetically lethal *in vivo*
6 tetrads from each combination were dissected vertically and grown on YPAD media at 30°C for 5 days and genotyped for Pol12 and Cdc13. Double mutants are indicated with a square shape

Several other mutations of Cdc13 were identified through their synthetic lethal phenotype with a deletion of Yku70, arguing that their role at telomeres is distinct from long telomere alleles such as *cdc13-1* (*Chandra et al., 2001*). Indeed, Yku proteins play an important role in binding telomeres and recruiting telomerase (*Gravel et al., 1998, Lemon et al., 2019*). As these mutants exhibit a different telomere length phenotype from Pol12 ones, we wanted to confirm

that these were indeed affecting telomeres through different pathways. The lack of synthetic effect of Pol12 alleles with *yku70Δ* confirms this assumption that the synthetic lethal phenotype of Pol12 alleles with Cdc13 is linked to a replication defect rather than a lack of physical protection of telomeres.

A similar synthetic lethal phenotype was also observed with Stn1 and Ten1 mutants (**Figure 5.5**). For the former, most mutations localize on its winged Helix-Loop-Helix domain ($Stn1^{wHLH}$), thought to play a role in both interacting with Cdc13 and DNA. For the latter, mutations were found on the OB-fold domain ($Ten1^{OB}$) making up the majority of the protein, and for which the only known role is to allow interaction with Stn1.

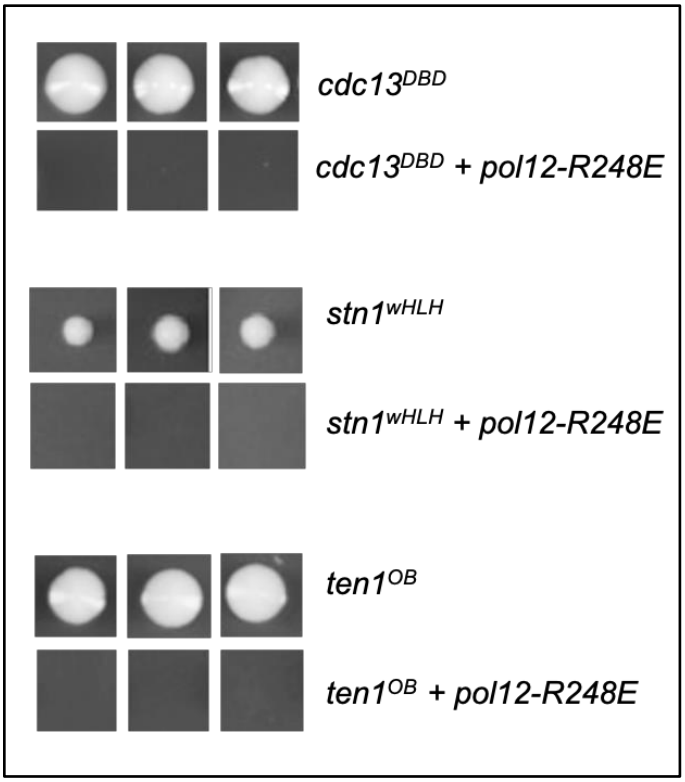

Figure 5.5: Epistasis analysis of *pol12-R248E* with mutants of the t-RPA complex shows broad synthetic lethality

Tetrads were dissected and grown on YPAD media at 30°C for 5 days before being photographed and genotyped. Spore genotype is indicated on the right of the pictures

All the mutations of t-RPA that are synthetically lethal with *pol12-R248E* and *pol12-R322E* pertain to either the complex integrity or its binding ability to DNA. Therefore, Pol12 plays an essential role in either facilitating or compensating for a lack of proper localization of t-RPA that results in elongated telomeres.

Because of their synthetic lethal phenotype, those double mutants cannot be further studied for characterization of the essential function they disrupt. Therefore, we repeated crosses with alanine mutant versions of the Pol12 allele rather than charge swaps. Indeed, as shown in Chapter 4, these had a milder set of phenotypes. As expected, the alanine version attenuated the growth defect of the double mutants to close to WT levels (**Figure 5.6**). This result illustrates the advantages of straying away from the typical mutagenesis strategy onto alanine, as well as brings up the idea of a "dial" combination strategy for synthetically lethal double mutants.

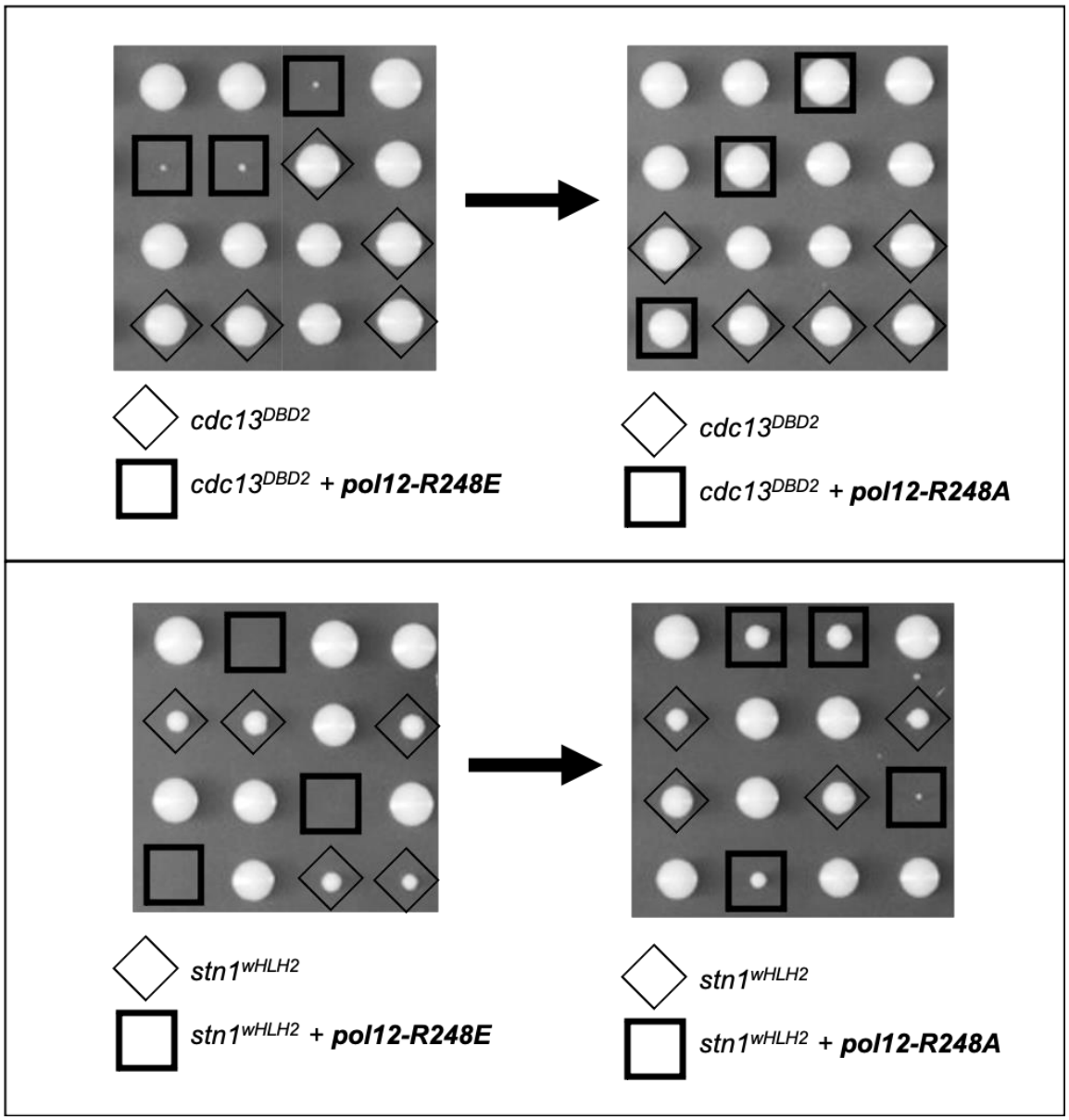

Figure 5.6: Alanine variants of Pol12 alleles show a milder synthetic phenotype with t-RPA mutants compared to charge swap

4 tetrads from each combination were dissected vertically and grown on YPAD media at 30°C for 5 days before being photographed and genotyped for Pol12 and Cdc13 or Stn1

Epistasis analysis of Pol12 alleles with RPA mutants

All t-RPA subunits include at least one Oligosaccharide-Binding (OB) fold domain. This structure is thought to allow specific binding to DNA, RNA and/or proteins (*Brennan, 1993*, *Theobald et al., 2003*). Interactions within the complex also happen through parts of their respective OB-folds (*Sun et al., 2009*). In fact, the OB-fold organization dictates the protein interactions (*Lin et al., 2008, Mason et al., 2013*). Many of the t-RPA mutants studied in this chapter affect those structures, highlighting their importance for the telomere homeostasis function of the complex. OB-folds are a feature conserved from the Replication Protein A (RPA) complex, single stranded DNA binding complex also independently present on the replisome in *S. cerevisiae* (*Flynn and Zhou, 2011*). Beyond this particular domain, the overall structural similarities between the RPA and t-RPA complexes have been striking (*Gelinas et al., 2009)*. Evidence of an overlapping role has also been shown. Indeed, Rpa1 can recruit telomerase subunit Est1 in a similar fashion as Cdc13 (*Schramke et al., 2004*). Furthermore, the ~100bp N-terminal area of Rpa1 has been characterized early on as stimulating activity of polymerase alpha, in a similar fashion to how t-RPA was originally discovered (*Goulian et al. 1990, Kim et al., 1996*, *Braun et al., 1997*). Yet, the existence and conservation of both complexes all the way up to Humans argues that they each may have evolved to perform distinct functions, characterized by a difference in preferential DNA sequence binding (*Gelinas et al., 2009)*. Yet, antagonistic phenotypes have also argued that the two complexes might physically compete at the telomeres (*Flynn et al., 2012, Grandin and Charbonneau, 2013, Moeller et al., in preparation*). Given the extreme synthetic phenotype of Pol12 mutants with t-RPA, we investigated whether a similar result could be observed with mutants of equivalent domains of the RPA proteins.

One of the original alleles discovered in Rpa1, *Rpa1-D223Y*, showed to be synthetically lethal with a temperature sensitive allele of Pol12, *pol12-100* (*Smith et al., 2000*). Interestingly, the mutation is not part of the region of the protein that stimulates polymerase alpha's activity. Instead, this mutant disrupts the binding of the protein to ssDNA (*Audry et al., 2015*). However, the short telomere phenotype of this allele does not match what has been observed with Pol12 and t-RPA alleles, arguing that it may result in lethality through a different process. Furthermore, similarly to *cdc13-1*, this Rpa1 allele is genetically linked to the action of Yku proteins, with which no synthetic effect has been observed when combined with Pol12 mutants. Finally, the TS nature of the *pol12-100* allele does not exclude that the synthetic lethality phenotype is linked to another function of the protein from the one studied in this thesis, or its overall instability.

A point mutant of the N-terminal region of Rpa1, *rpa1-t11,* sequenced as *rpa1-K45E*, was uncovered by EMS mutagenesis and characterized by its sensitivity to DNA damage agents (*Umezu et al., 1998*). This phenotype was also observed in another allele from that same study affecting L221, a neighboring residue of the *Rpa1-D223Y* allele described above. Yet, *rpa1-t11* showed once again no synthetic effect with our Pol12 alleles.

ODN analysis of the N-terminal of Rpa1 performed by another member of the laboratory uncovered additional residues with a similar phenotype pattern to *rpa1-t11*. Surprisingly, one of those alleles, *rpa1-K95E,* exhibited long telomeres whereas *rpa1-t11* telomeres were roughly of WT length (**Figure 5.7**). Although having no synthetic effect with Pol12 mutants, this strain alone has poor viability and highlights an essential function of Rpa1 pertaining to telomeres. Further studies of Rpa1 were performed and will be discussed in Appendix B in the context of DNA damage response pathways.

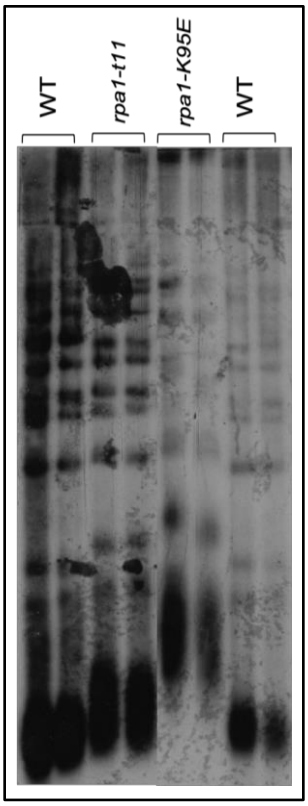

Figure 5.7: Similarly to Pol12, Rpa1 alleles show different telomere length phenotypes as shown by Southern Blot

Strains of the indicated genotype were streaked-out 3 successive times alongside WT (yVL2967) and processed as described in Chapter 4

That same ODN screening of Rpa1 that uncovered *Rpa1-K95E* also found further alleles in the middle ssDNA binding domain of the protein. These alleles have the ability to rescue Cdc13^{DBD} mutants, a feature arguing one again for a competition of binding of the two proteins at single stranded telomeric sequences. Given the extreme opposite phenotypes observed between *pol12-R248E* and Rpa1^{DBD} with Cdc13^{DBD} mutants, we investigated the effect of combining all 3 mutants within a strain. Interestingly, the triple mutant colonies were viable. This argues that the deadly defect of *pol12-R248E* with Cdc13^{DBD} could be the result of a failure of t-RPA to bind to telomeres against RPA. A similar rescue was observed with a Ten1 allele that has a moderate growth phenotype with *pol12-R248E* (**Figure 5.8**).

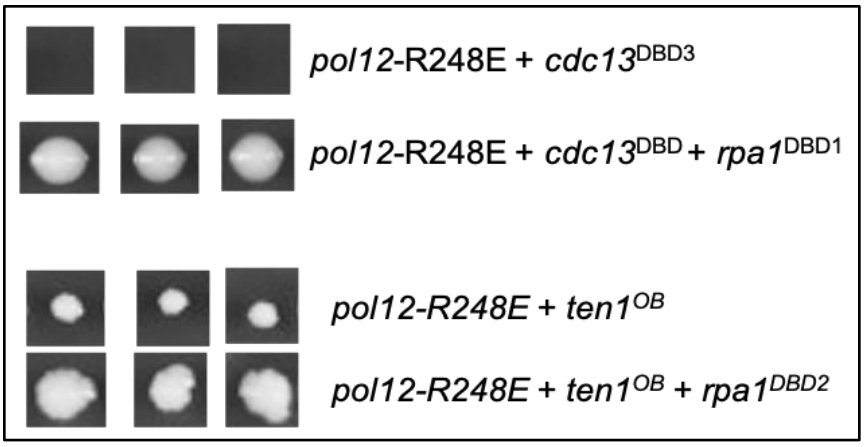

Figure 5.8: Some rpa1^{DBD} mutants can rescue the synthetic growth phenotype of t-RPA mutant combinations with *pol12-R248E*

Tetrads were dissected and grown on YPAD media at 30°C for 5 days before being photographed and genotyped. Spore genotype is indicated on the right of the pictures

However, other mutants of Rpa1 and Rpa2 showed the opposite worsening phenotype with similar combinations of *pol12-R248E* and t-RPA mutants (**Figure 5.9**). This result may be the manifestation of an overall lack of protection of single stranded DNA because of RPA not being compensated by binding of t-RPA. Overall, there seems to be a subtle balance between t-RPA and RPA binding that Pol12 plays a role in.

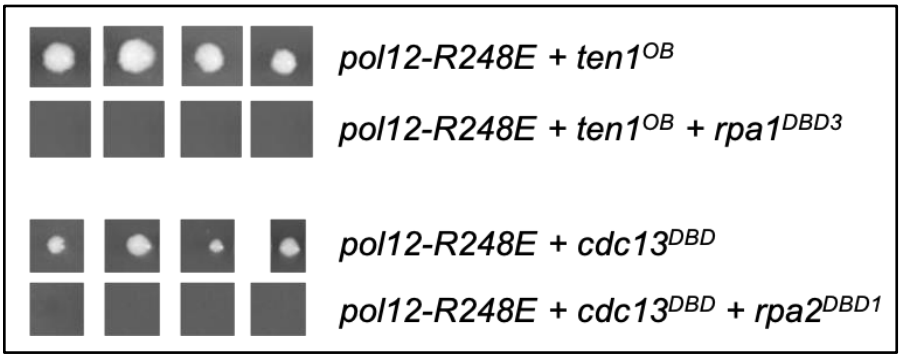

Figure 5.9: Other rpa1^{DBD} and rpa2^{DBD}mutants worsen the synthetic growth phenotype of t-RPA mutant combinations with *pol12-R248E*

Tetrads were dissected and grown on YPAD media at 30°C for 5 days before being photographed and genotyped. Spore genotype is indicated on the right of the pictures

Epistasis analysis of Pol12 alleles with non-essential genes

Crosses with *pol12-R248E* were repeated with multiple non-essential genes, with a particular focus on DNA damage repair and checkpoint proteins. Indeed, the suspected common role of both polymerase alpha-primase and t-RPA in the C-strand fill-in mechanism as well as their elongated telomere phenotype may argue for a defect dependent on those proteins for survival. This screen looked for obvious changes in viability of the double mutant and uncovered two main alleles.

A first gene was detected for its synthetic effect with *pol12-R248E* when knocked-out. It encodes for Csm3, a known replication factor with a role in signaling stress and damage through the DNA replication checkpoint pathway (*Xu et al., 2004*). It was originally characterized in a genome-wide screen looking at cell cycle defects and was therefore named for its importance on chromosome segregation during meiosis (CSM) (*Rabitsch et al., 2001*). Interestingly, the synthetic growth defect of *csm3Δ* was also observed in *pol12-D303K* as the double mutant was inviable. In contrast, *pol12-R322E* showed no additive phenotype (**Figure 5.10**).

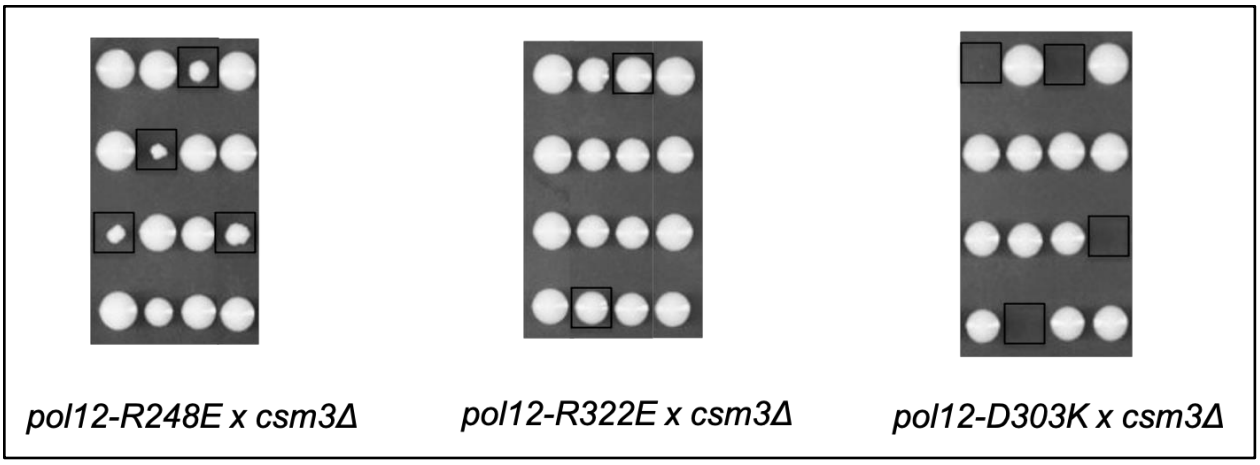

Figure 5.10: Pol12 alleles sensitive to *Pol1*^{TS} depend on Csm3 for viability
4 tetrads from each combination were dissected vertically and grown on YPAD media at 30°C for 5 days and genotyped for Pol12 and Csm3. Double mutants are indicated with a square shape

Interestingly, knock-out of Csm3 does not result in elongated telomeres when analyzed by Southern blot (**Figure 5.11**). This result is in contrast to synthetic defects observed with t-RPA and polymerase alpha-primase alleles. Furthermore, its lack of additive growth phenotype with *pol12-R322E*, highlighted in the ODN assay for its sensitivity for cdc13^{TS} only, argues that the reduced viability is linked to the essential function of Pol12 in DNA replication. Indeed, csm3Δ has shown impaired growth when combined with TS alleles of both polymerase alpha and primase (*Costanzo et al., 2010, Dubarry et al., 2015*).

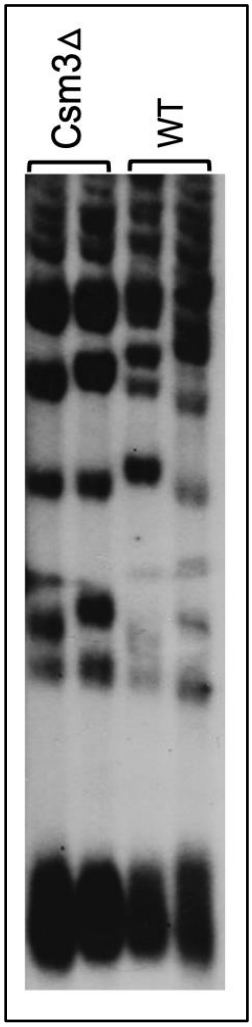

Figure 5.11: Southern blot analysis of Csm3Δ shows a telomere length similar to WT
Csm3Δ (yVL5498) was streaked-out 3 successive times alongside WT (yVL2967) and processed as described in Chapter 3

Proteins of the CSM family are all non-essential and only Csm3 physically interacts with the replication fork (*Calzada et al., 2005*). Their non-essentiality argues for either a degree of redundancy or alternative existing pathway that keeps the cell from death when disrupted. However, high-throughput studies have identified many other factors of the replication fork that show a synthetic effect with *csm3Δ*, rendering further experiments complicated. However, no synthetic effect was observed with knock-outs of either of its main known interacting partners Mrc1 and Tof1 with *pol12-R248E and pol12-D303K (Dubarry et al., 2015)*. Therefore, the growth defect might be linked to a distinct function of the protein yet to be investigated.

Epistasis analyses of *pol12-R248E* have so far only given synthetic growth defects with very specific strains of t-RPA and the replication fork factor Csm3. However, a striking synthetic rescue phenotype was observed when combined with a knock-out of Rad27 (**Figure 5.12**). This gene encodes a nuclease necessary for DNA damage repair and normal processing of lagging strand Okazaki fragments (*Goulian et al., 1990, Reagan et al., 1995*). Interestingly, *rad27Δ* gives rise to elongated telomeres, potentially arguing that it pertains to a similar regulating pathway as Pol12 (*Gatbonton et al., 2006*).

Although playing a role in an essential step of lagging strand replication and resulting in temperature and DNA damage sensitivity, budding yeast Rad27 is disposable whereas its Human equivalent, FEN1, is essential (*Zheng et al., 2011*). Indeed, the endonuclease role of Rad27 shows some redundancy with Dna2, although the latter also carries additional essential functions (*Budd and Campbell, 1997, Ayyagari et al., 2003*). That same endonuclease function is also

partially complemented by Exo1, another exonuclease known for its ability to resect single-stranded telomeric sequences (*Tran et al., 2002, Sun et al., 2003).*

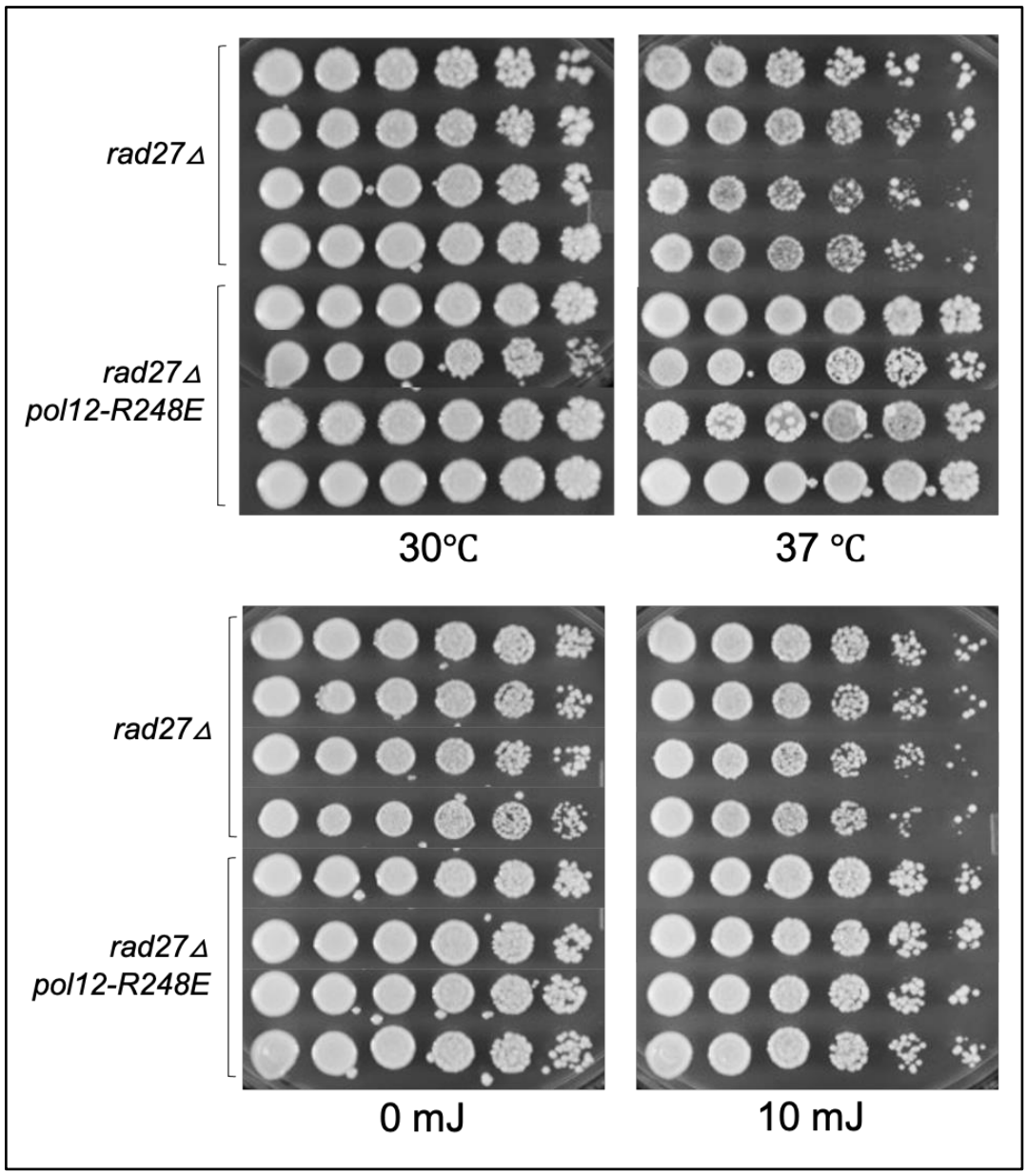

Figure 5.12: *pol12-R248E* rescues both the temperature and DNA damage sensitivity defects of a *rad27Δ* strain

Strains of the indicated genotype were gridded in ⅕ serial dilutions on YPAD plates and grown under different conditions of temperature or ultraviolet (UV) DNA damage inducing exposure for 3 days

The rescue of its DNA sensitivity is specific to Rad27 as *pol12-R248E* alone shows no particular resistance to Ultraviolet (UV) or Hydroxyurea (HU)-induced DNA damage (**Figure 5.13**).

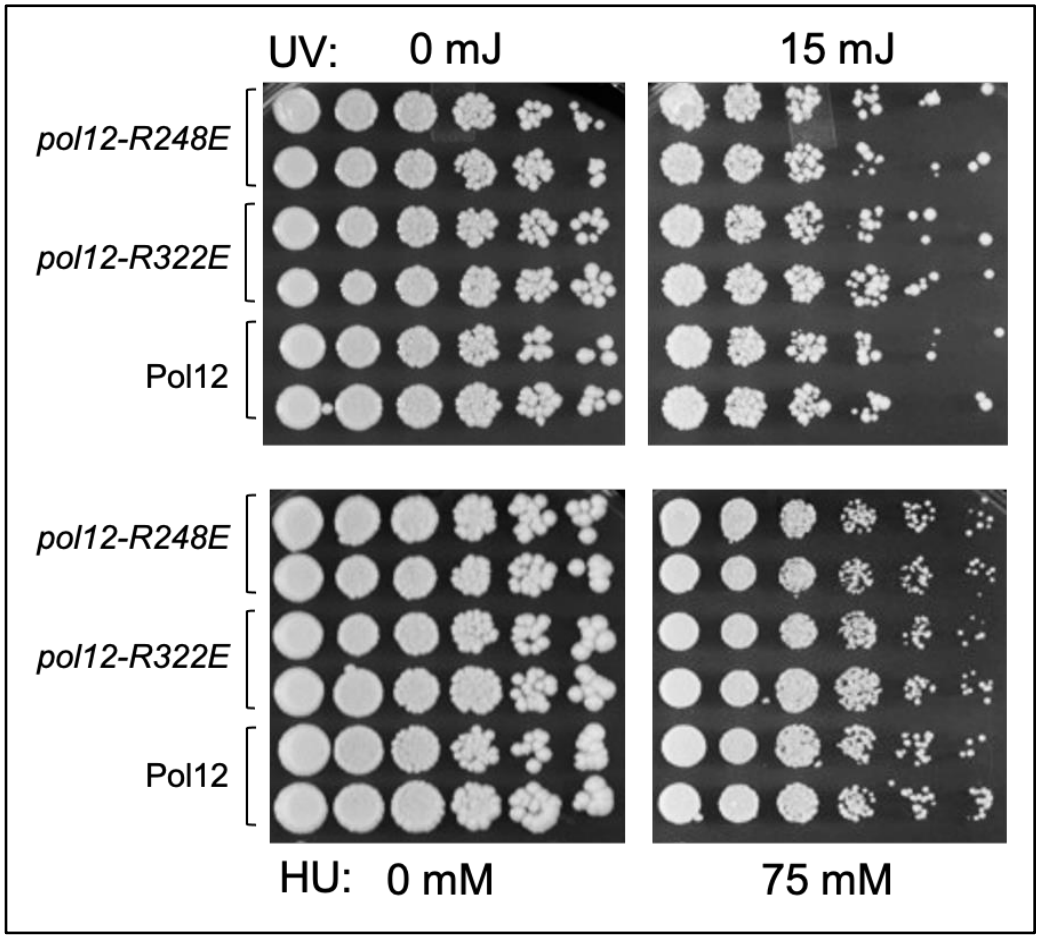

Figure 5.13: Pol12 alleles found by ODN did not show sensitivity to DNA damaging agents by themselves

Strains of the indicated genotype were gridded in ⅕ serial dilutions on YPAD plates and grown under different conditions of DNA damage inducing UV exposure or presence of Hydroxyurea (HU) for 3 days

Unlike the previous crosses widely resulting in lethality, the strong viability of this double mutant allowed for further analyses. We sought to understand which pathway is being rescued by *pol12-R248E* in the absence of Rad27. In order to do so, we established a list of alleles shown to be synthetically lethal with *rad27Δ* to be tested as a triple mutant strain. Indeed,

such additive phenotype with Rad27 argues that both genes either act redundantly or towards alternate pathways necessary for survival. We therefore generated a subset of those double mutants strains and studied whether addition of the Pol12 allele rescued their synthetic lethal phenotype.

As a control, we generated a *pol12-R248E*, *rad27Δ*, *exo1Δ* strain. As described above, Rad27 and Exo1 have a partial redundant endonuclease function and their combined knock-out is expected to be lethal, also some double knock-out spores turned out to be slightly viable. However, the triple mutant was consistently clearly viable and healthier than those double mutants (**Figure 5.14**). This result argues that Pol12 acts to repress the pathway arising from improper Okazaki fragment processing by endonucleases. However, the triple mutant colonies were consistently smaller than WT, which can either be the result of other non-viability threatening defects resulting from either mutant, or simply the result of slower growth from having to activate alternate pathways to bypass the absence of Okazaki fragments processing. Defects in Dna2 were not tested because the gene is essential for viability although separation-of-function alleles have been characterized (*Budd et al., 2000*). However, these alleles argue that the nuclease function of Dna2 itself is essential to viability (*Lee et al., 2000*).

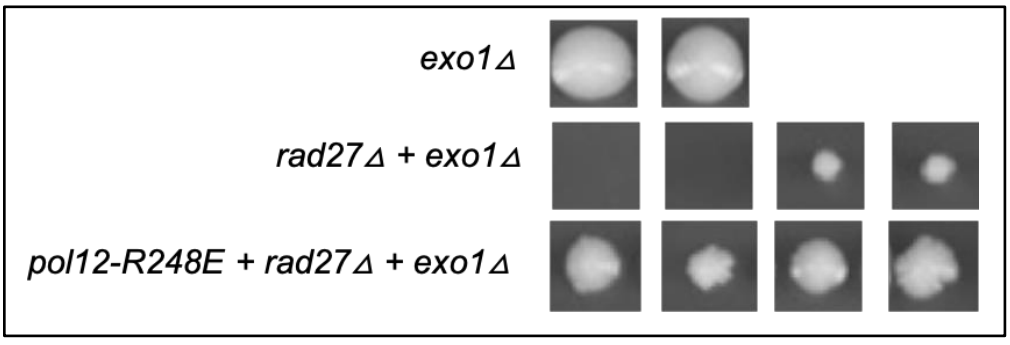

Figure 5.14: Disrupting Pol12 improves viability in the absence of Okazaki fragment processing endonucleases

Spores of the indicated genotype were grown for 5 days before being genotyped and photographed

Since unprocessed Okazaki fragments would be recognized as DNA damage, we then investigated the impact of disrupting factors that would typically bind to exposed DNA. Combination of rad27Δ with either *rad51Δ* or *rad52Δ* is inviable (*Tishkoff et al., 1997*). Indeed, Rad51 physically binds to single-stranded DNA and acts with Rad52 to trigger repair by homologous recombination (*Mortensen et al., 1996*). This method of strand repair is thought to be the main and only way for cells to correct unprocessed Okazaki fragments. To our surprise, *pol12-R248E* is able to slightly but consistently rescue the lethal combination of *rad27Δ* with *rad51Δ* but not *rad52Δ* (**Figure 5.15**). One possible explanation for the lethality of the latter triple mutant strain could be explained by the observation that unprocessed binding of Rad51 to DNA by Rad52 creates a toxic filament structure (*Veaute et al., 2003*). However, there is also evidence that Rad52 influences alternative methods of DNA repair, independently of Rad51 (*Symington, 2002*). The details of these differential results have yet to be investigated.

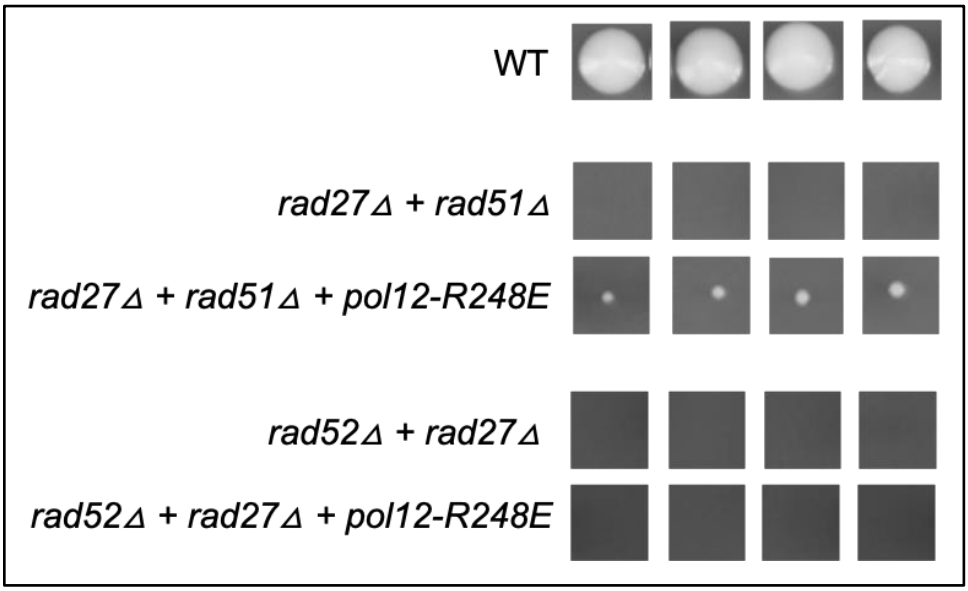

Figure 5.15: Disrupting Pol12 improves viability in the absence of processing of Okazaki fragments and Rad51, but not Rad52

Spores of the indicated genotype were grown for 5 days before being genotyped and photographed

Finally, we combined *pol12-R248E* and *rad27Δ* with DNA damage checkpoint genes knock-outs. It has been shown that activation of the checkpoint as a result of the detection of damaged DNA is necessary for cell survival (*Paulovich et al., 1998, Loeillet et al., 2005*). This cell arrest depends on several proteins, among which Rad9, Rad17 and Rad24. The combination of either protein with *rad27Δ* is once again lethal (*Paulovich et al., 1997*). A viable triple mutant was observed for both *rad9Δ* and *rad17Δ*, while *rad24Δ* was not tested but expected to give a similar result (**Figure 5.16**). Interestingly, *rad24Δ* had previously been studied in our laboratory for its ability to rescue the lack of essential Cdc13 or Stn1 (*Paschini et al., 2012*). Whether it could rescue the synthetic lethality phenotype of Pol12 and t-RPA alleles described above has yet to be determined but would argue that the lack of genetic interaction between the two complexes results in DNA damage checkpoint activation.

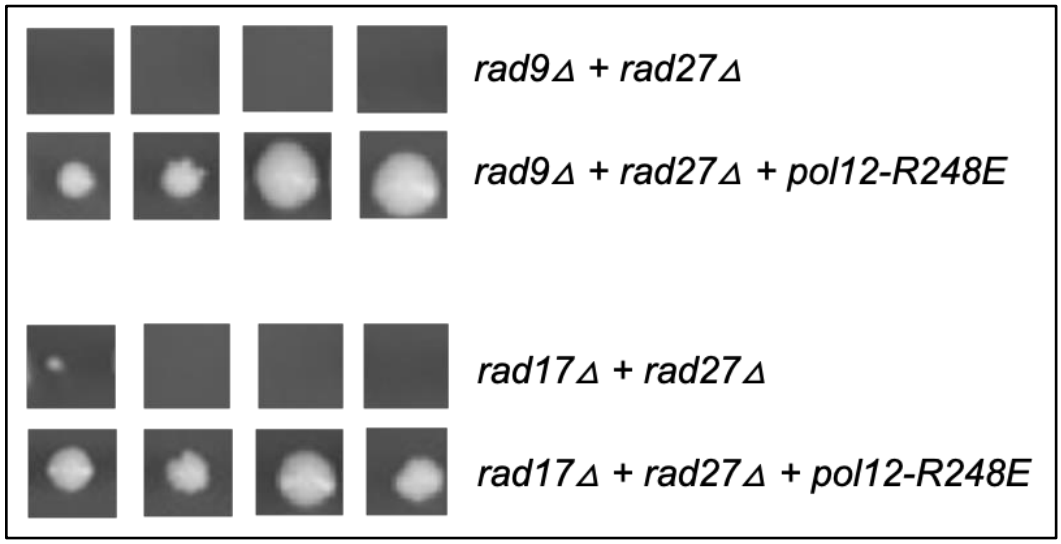

Figure 5.16: Disrupting Pol12 improves viability in the absence of processing of Okazaki fragments and key DNA damage checkpoint proteins
Spores of the indicated genotype were grown for 5 days before being genotyped and photographed

Additional alleles of genes also known for their importance in DNA repair were also found to be viable as a triple mutant. The list includes *mec1Δ* (solely viable with *sml1Δ*), *ctf4Δ* (but not *ctf18Δ),* and a well characterized DNA repair defective allele of Rad53. However, *pol12-R248E* also rescues the growth defect caused by *rad53-21* alone in the presence of Rad27 (**Figure 5.17**). This confirms that Pol12 inhibits a DNA repair-related pathway.

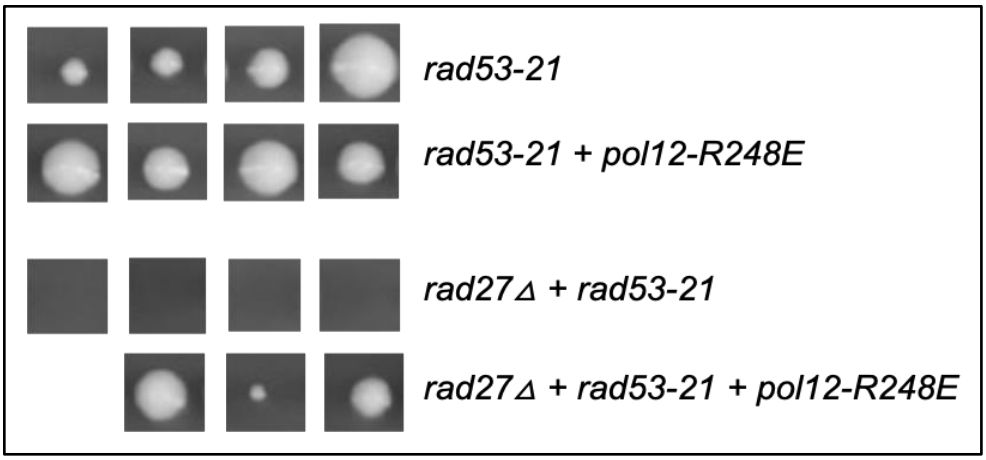

Figure 5.17: Disrupting Pol12 improves viability of a DNA damage repair impaired allele of Rad53 both in the presence and absence of Rad27
Spores of the indicated genotype were grown for 5 days before being genotyped and photographed

Interestingly, lack of Csm3 rescues both *rad27Δ* and the double mutant *pol12-R248E*/rad27Δ although showing a strong decrease in growth with *pol12-R248E* alone, as described above (**Figure 5.18**). This puzzling result may argue that Csm3 acts with Rad27 downstream from Pol12. However, this result was not observed with a knock-out of Tof1 or Mrc1, main partners of Csm3 (*Bando et al., 2009*). Therefore, this genetic interaction might be linked to a specific function of the protein although the number of spores analyzed was very limited. The use of separation-of-function alleles of Rad27 might help unravel that function (*Karanja and Livingston, 2009*).

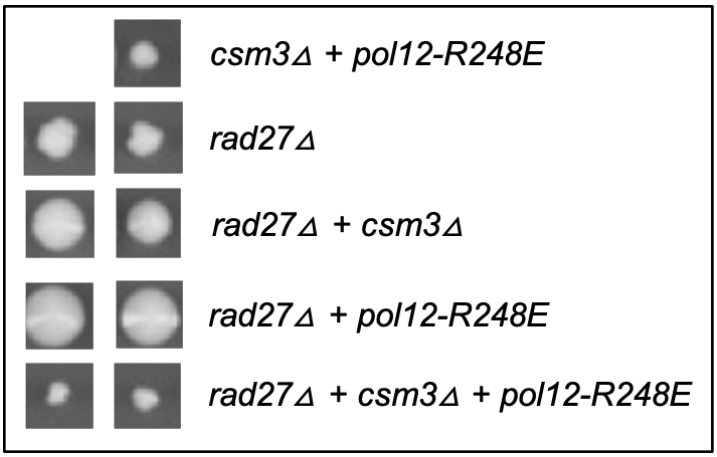

Figure 5.18: The intriguing epistatic relationship between Pol12, Csm3 and Rad27
Spores of the indicated genotype were grown for 5 days before being genotyped and photographed

Data pertaining to triple mutant viability analysis are summarized in **Table 5.3**.

Table 5.3: Summary of the rescue status of typically synthetic lethal double mutant combinations with *rad27Δ* when adding *pol12-R248E*

Pol12-R248E + rad27Δ combined with	Rescue?
Ctf4Δ	**Yes**
Ctf18Δ	No
Ddc1Δ	No
Exo1Δ	**Yes**
Mec1Δ (sml1Δ)	**Yes**
Mre11Δ	No
Rad9Δ	**Yes**
Rad17Δ	**Yes**
Rad50Δ	No
Rad51Δ	**Yes**
Rad52Δ	No
Rad53-21	**Yes**
Srs2Δ	No
Tof1Δ	No

Epistasis analysis of the influence of Pol12 on senescence of est2Δ

We sought to investigate whether *pol12-R248E* modifies the senescence speed of a telomerase null strain. Indeed, a mutant that accelerates or slows the rate at which cells with no active telomerase senesces indicates how the protein is part of a pathway that shortens or lengthens the telomeres, respectively (*Ballew and Lundblad, 2013*). To replicate the absence of telomerase, we generated a knock-out of Est2, one of the subunits of the enzyme. Once generated, double mutant cells were propagated for ~75 generations in parallel to *est2Δ* single mutants for blind senescence rate comparison, using a colony growth rating scale ranging from 5 (like WT) to 1 (fully senesced).

We found that *pol12-R248E* accelerates the senescence rate of *est2Δ* during the first ~ 25 generations, although the relative senescence ratio of the double mutant compared to est2Δ only reduces as cell division progresses (**Figure 5.19**). This result could argue that Pol12 normally slows replicative senescence, but does not play a direct role in telomerase recruitment. One hypothesis to explain this trend can be found by observing individual telomeric ends through the TeloPCR assay, as detailed in Chapter 4. Indeed, although Pol12-R248 mutants exhibit overall elongated telomeres, they also generate an increased amount of critically short ends. These could be the result of increased major loss of telomeric repeats and will likely be subject to senescence after fewer cell cycles if not compensated. For comparison, Ballew and Lundblad analyzed the senescence rate of a knock-out of Tlc1, RNA template of telomerase, combined with well characterized alleles *rif1Δ* or *rif2Δ* that also exhibit elongated telomeres. They found that, although Rif1 does not influence the rate of senescence, Rif2 acts to slow it by repressing the DNA double-strand break repair complex MRX (*Gobbini et al., 2016*). As described previously,

data indicates that Pol12 might have a similar repressing action on the DNA damage checkpoint, which would be impaired by *pol12-R248E*, independently of Rif1.

Data from this chapter is currently in preparation to be published (Meunier and Lundblad, in preparation). The dissertation author was the primary researcher and author of this material.

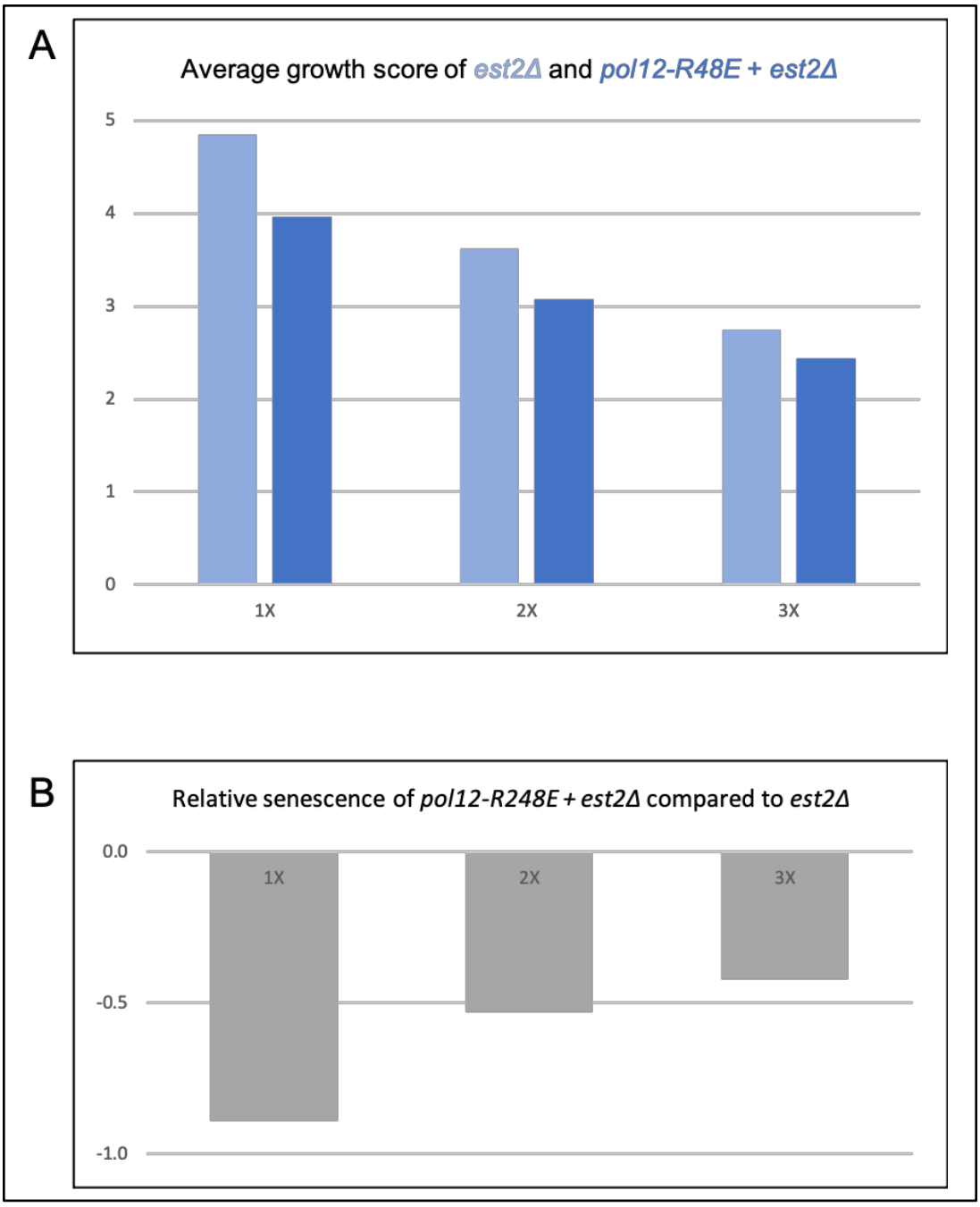

Figure 5.19: Statistical analysis of the senescence rate of est2Δ in the presence or absence of *pol12-R248E*

(A) The average growth score between 1 (inviable) and 5 (like WT) was recorded for n=45 individual spores genotyped for est2Δ::KAN through 3 successives streak-outs (1X to 3X). At 3X, spores were genotyped for pol12-R248E by PCR and restriction enzyme digestion. Scores were averaged for both est2Δ n=20) and est2Δ + pol12-R248E (n=25) (B) Average senescence score of the double mutant was subtracted with the average score of est2Δ only for each 1X - 3X streak-outs. A negative score is indicative of accelerated senescence of the double mutant strain

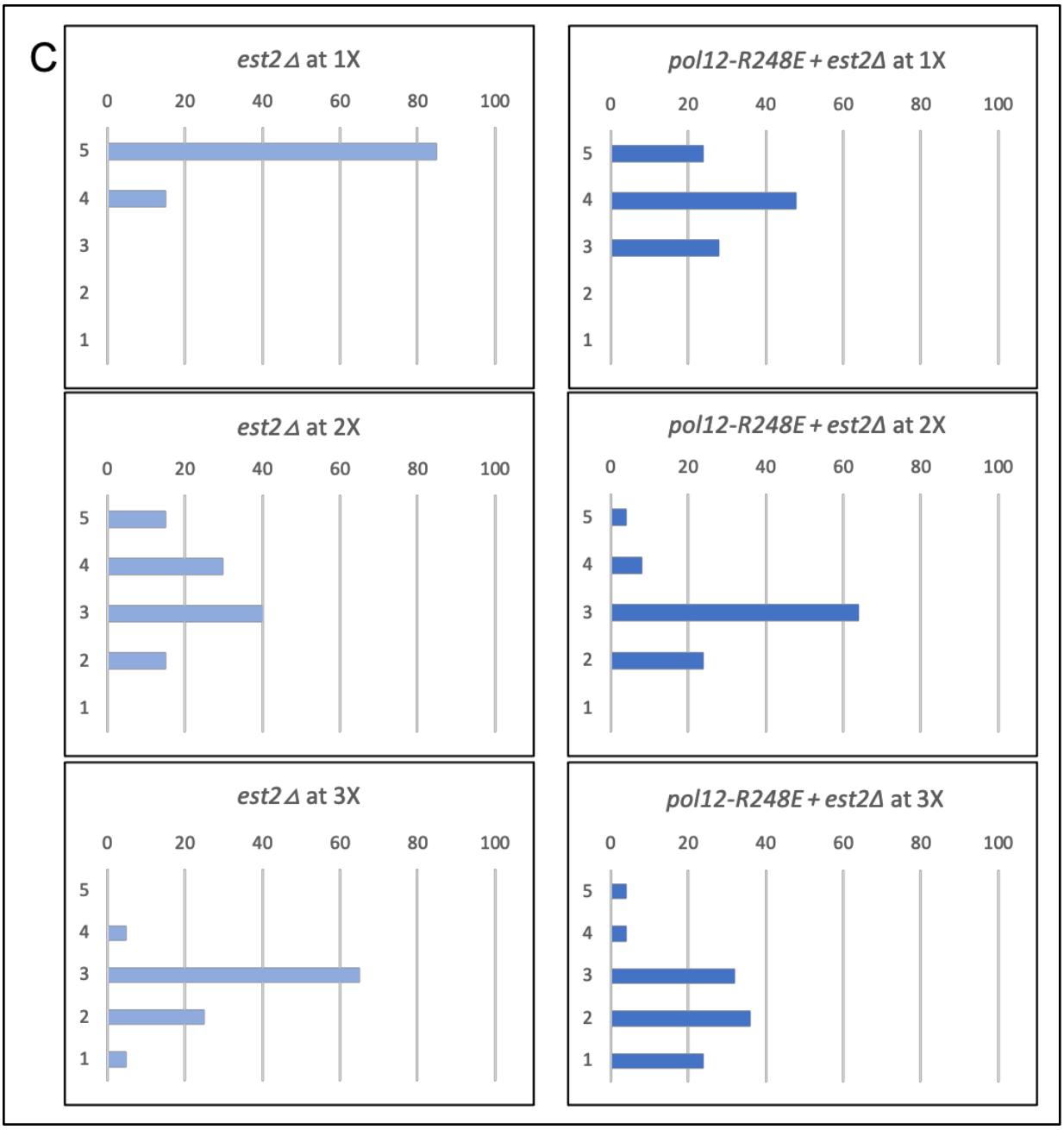

Figure 5.19 (cont.)

(C) Distribution of the viability scores of 1 to 5 of est2Δ (n=20) and pol12-R28E + est2Δ (n=25) at each streak out 1X to 3X. Scores were normalized using percentages to compare the two genotypes

CHAPTER 6:
Pol12 physically interacts with t-RPA to regulate telomere length homeostasis

Abstract

We tested the less characterized N-terminal region of Pol12 and showed it did not play a role in the protein interaction with Pol1. However, the presence of highly conserved residues and motifs argues that it performs another function that has yet to be investigated. On the other hand, *pol12-R248E* was shown to be essential for the protein interaction with t-RPA subunit Stn1. Once again, the details of this interaction are unclear. Particularly, previous studies have highlighted a physical interaction between the two complexes through Pol1 and Cdc13. Therefore, whether those interactions are direct or indirect is unknown. Furthermore, the localization of *pol12-R248E* and a published Pol12 allele that lost interaction with Stn1 argues that the mutants found might in fact disrupt the interaction with Stn1 but only because the interaction with Pol12 and Pol1 is lost. Therefore, whether the two complexes interact through one or more regions has not been resolved yet. Studies of additional mutants found by ODN or high-throughput analyzes such as Mass spectrometry could help understanding the physical dynamics between polymerase alpha-primase and t-RPA. Furthermore, it could help find potential new partners of the protein, using for example mutants found in Surface 2 by ODN or isolated mutants of Pol12.

Introduction: existing evidence of physical interactions between polymerase alpha and t-RPA

The link between polymerase alpha-primase and t-RPA has long been suggested. Indeed, most of the ~300bp of telomeric sequences are duplicated normally by the replication machinery. If active, telomerase can then be recruited at the end of a newly replicated telomere by t-RPA to further elongate its G-rich telomeric strand. Filling of the complementary C-strand depends on the action of polymerase-alpha primase. Disruption of either complex results in a similar elongated telomere phenotype that may arise from a defect in C-strand fill-in. It is therefore believed that the two complexes interact genetically but also physically.

Direct interaction between t-RPA and polymerase alpha was first characterized by the Zakian laboratory (*Qi and Zakian, 2000*). This study defined a function for the N-terminal of Pol1 as a direct interface with Cdc13. Interestingly, mutations disrupting the interaction of Pol1 with either primase or Cdc13 as well as impairment of its catalytic domain all resulted in elongated telomeres, in a fashion dependent on telomerase (*Adams and Holm, 1996*). Finally, it also highlighted a possibly overlapping interface of Cdc13 with Pol1 and Est1, a subunit of telomerase. Further studies later confirmed the plurality of interacting partners of the protein, while narrowing down the interface area to its 250bp N-terminal OB-fold region (*Hsu et al., 2004*). Eventually, a crystal structure of the Cdc13-Pol1 dimer was generated (*Sun et al., 2011*). However, none of the mutations found, although for some almost fully abrogating the Pol1-Cdc13 interaction *in vitro*, showed to be lethal. Since the essential function of Cdc13 pertains to telomere maintenance, given how overexpression of Est1 specifically rescues *cdc13-1* growth defects, they argued that its interaction with Pol1 wasn't the sole link between the two complexes.

As the interest for polymerase alpha and its importance for telomere homeostasis grew, the Shore laboratory generated a novel non-TS allele in Pol12 (*Grossi et al., 2004*). Although exhibiting elongated telomeres, the point mutation did not generate overall replication defects seen in Pol1 TS alleles. In contrast to the previous study, this separation-of-function mutant is inviable when specifically combined with TS alleles of the t-RPA subunit Stn1. Additional studies confirmed that the two proteins interacted independently of Cdc13 and through the N-terminal half of Pol12. Whether this interaction occurs with the N and/or C-terminal half of Stn1 has been subject to debate (*Petreaca et al., 2006, Puglisi et al,. 2008, Lue et al., 2014*). This synthetic lethal effect is not observed with more severe alleles of polymerase alpha, arguing that this interaction pertains to a distinct essential function indirectly regulating telomere homeostasis. Grossi and coworkers brought up the hypothesis that Pol12 and Stn1 may need to interact in response to DNA damage signals, as data from Chapter 5 similarly suggested. However, further work has shown that their interaction was necessary for a mechanism able to partially bypass the absence of Cdc13 with an overexpression of Stn1-Ten1 (*Petreaca et al., 2006*).

Therefore, although characterized, many details of those interactions with t-RPA and polymerase alpha remain unclear. In particular, studies of interactions of Pol12 only used a broad truncation of the protein in half. Although most of the alleles found in the protein localize between amino acids ~250-350, there are several conserved residues ahead of that area that play a significant role, as described in Chapter 2. In particular, we wanted to investigate whether the N-terminal of Pol12 played a role in its interactions. We also wanted to confirm our hypothesis that all the phenotypes observed throughout Chapter 2 through 5 argue that *pol12-R248E* disrupts the protein interaction with Stn1.

Material and methods: Western Blot

Whole-cell extracts of WT and mutants were prepared from two independent 200 ml YPAD liquid cultures (OD ~0.8–0.9) and processed in parallel. Cells were pelleted at low temperature, washed in TMG200 buffer (10 mM Tris-HCl pH 8, 5% glycerol, 1mM MgCl2, 200mM NaCl) with protease inhibitors, and resuspended in 1 ml of the same buffer. Extracts were prepared by grinding this suspension in a mortar with liquid nitrogen until the suspension formed a fine powder. Extracts were thawed and clarified by doing two 15 min cold spins at max speed. Supernatants were mixed with Tween 20 to a final concentration of 0.1% and subjected to IP by incubation with anti-Flag M2 affinity gel (Sigma), in TMG200 buffer with protease inhibitors for 2 hours at 4°C on a roller. Beads were washed in TMG200 + 0.5% Tween 20, and eluted for 4 min at 99°C with SDS loading buffer. Immunoprecipitated proteins were run on a 6% (for detection of Est1, Est2, or Pol1), 10% (for detection of Stn1) or 16% (for detection of Pol12) SDS-PAGE and once transferred to nitrocellulose membranes, probed with antibodies anti-myc 2272 (Cell Signaling Technology) at 1:1000 or anti-Flag F7425 (Sigma) at 1:10,000 dilution, followed by anti-rabbit HRP conjugate (Promega) at 1:10,000. Chemiluminescence (ECL) was used for antibody detection using film.

Table 6.1: yVL strains used in this chapter

All strains are derivatives of AVL78 (leu2 trp1 ura3-52 GAL+ prb- prc- pep4-3)

Strain ID	Biochemistry construct(s)	
yMAM384	*Pol1-13Myc-kanMX6*	*Pol12(1-244)-FLAG (in 2u LEU2 ADH plasmid)*
yMAM386	*Pol1-13Myc-kanMX6*	*Pol12(1-215)-FLAG (in 2u LEU2 ADH plasmid)*
yMAM388	*Pol1-13Myc-kanMX6*	*Pol12(1-122)-FLAG (in 2u LEU2 ADH plasmid)*
yVL3382	*Pol12-mycX13::KAN*	-
yVL3383	*Pol12-mycX13*	*Stn1-G8-FLAG3*
yVL3528	*Est1-G6-myc12*	*(FLAG)3-myc12-G6-Est2*
yVL5678	*pol12-R248E-mycX13*	*Stn1-G8-FLAG3*

Results: Studying the interaction of N-term truncations of Pol12 with Pol1

Truncations were designed to optimize peptide stability by identifying conserved areas to stop protein expression after. We designed three versions of the truncated protein, including amino acids 1 to 122, 210 and 241 of the *S. cerevisiae* Pol12 gene, respectively (**Figure 6.1**).

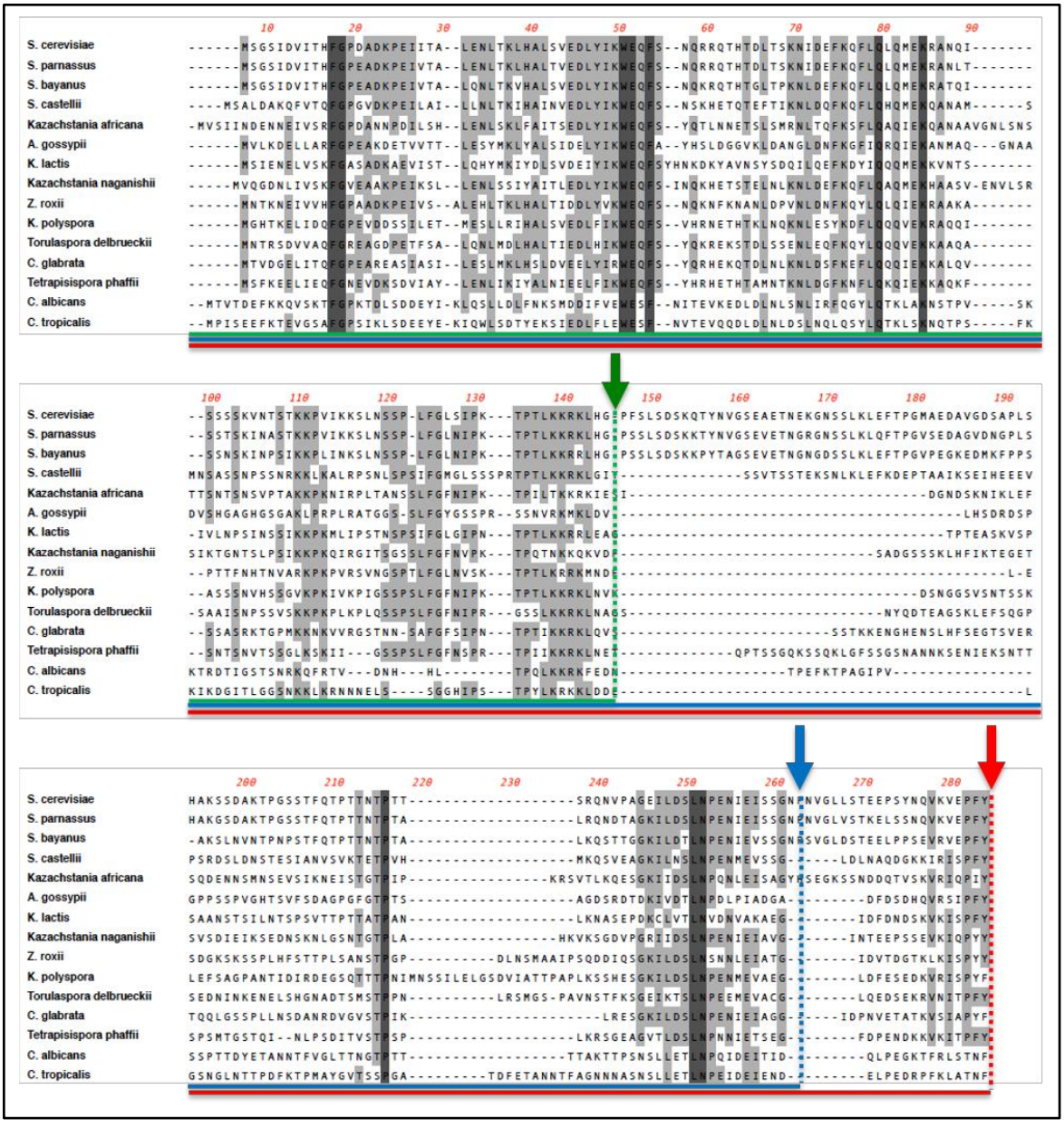

Figure 6.1: Alignment of the N-terminal region of Pol12 throughout 15 yeasts species

The localization of the truncations at amino acids 122, 210 and 241 is indicated in green, blue and red, respectively. Highly conserved amino acids are indicated in light grey. Strictly conserved amino acids are indicated in dark grey.

The shortest construct contains a sequence that is overall fairly conserved without significant addition of residues throughout species. It includes a nuclear localization motif and several strictly conserved individual or paired residues which could also constitute potential motifs for binding or modifications. The intermediate sized truncated N-terminal Pol12 includes T177, T185 and particularly T190, a potential phosphorylation site that gives a strong ODP phenotype in *pol1*^{TS} when disrupted. Interestingly, the predicted kinase responsible for this modification is of the Cyclin-Dependent Kinases (CDK) family (*Horn et al., 2014*). Among those proteins is Cdk1, which has been thought to play a crucial role in telomere homeostasis (*Liu et al., 2014*). Finally, the bigger truncation includes almost the entire N-terminal area of Pol12 that has no existing crystal structure.

As those truncations wouldn't be viable *in vivo*, the strain analyzed still contains WT Pol12 and the constructs are expressed through an overexpression plasmid, similarly to the ODN process. Each of the three constructs yielded moderately stable peptides with sizes matching their respective sequence length. Yet, they showed a total absence of interaction with Pol1 (**Figure 6.2**). This result argues that amino acids 1-240 of Pol12 are not enough for the polymerase alpha heterodimer cohesion. This result does not exclude the possibility of an experimental flaw as this pilot experiment lacked a full Pol12 construct as control. Furthermore, this construct showed signs of degradation that could be the result of an unstable peptide. However, the presence of the Est1-Est2 control bands rules out the possibility of an immunoprecipitation issue.

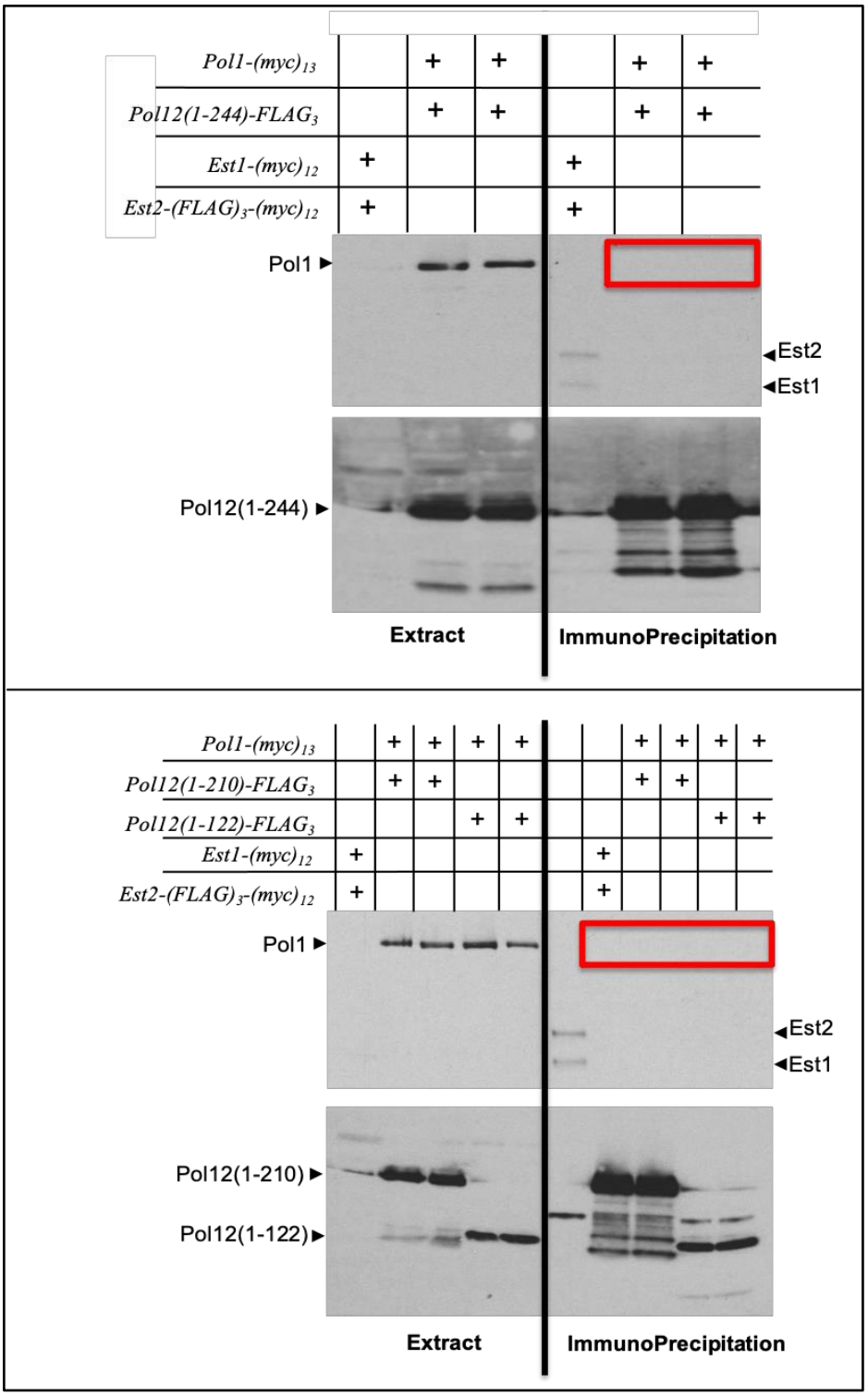

Figure 6.2: Pol1 does not interact with the N-terminal of Pol12

Strains of the indicated construct were immunoprecipitated for FLAG with a Myc co-Immunoprecipitation. Expected localization of the proteins is indicated with arrows. Expected localization of Pol1 is indicated with a red outline

Pol12-R248 is important for the interaction of the protein with Stn1

We next wanted to address whether *pol12-R248E* impacts the interaction of Pol12 and Stn1. Indeed, its elongated telomere phenotype matches that of the characterized separation-of-function *pol12-216,* shown to disrupt that binding (*Grossi et al., 2004*). This allele contains a point mutation in G325. Although half buried, this residue maps under surface 3's R322 and V326, and next to one of the predicted Pol1-Pol12 important interface residues G327 (*Klinge et al., 2009*) (**Figure 6.3**).

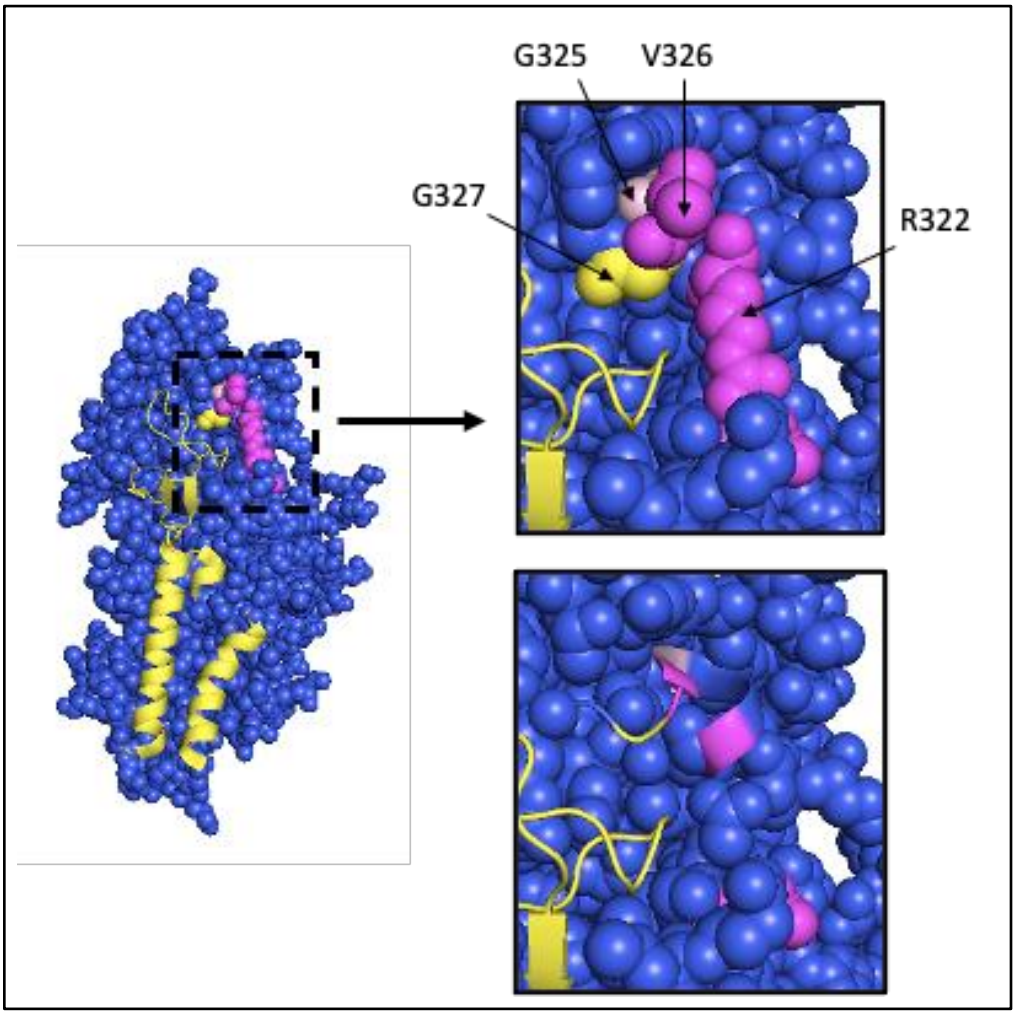

Figure 6.3: pol12-216 allele mutation localizes with surface 3 residues found by ODN
Crystal structure by Klinge and Pellegrini (PDB 3FLO) was visualized on Pymol. Residues of surface 3 are indicated in magenta. Residues of the expected interface of Pol12 with Pol1 are represented in yellow. G325 Residue mutated in pol12-216 is represented in light pink.

The introduction of charge swap *pol12-R248E* significantly reduced the protein binding to Stn1 (**Figure 6.4**). Although it hasn't been verified whether the mutation might render the peptide unstable, the presence of a clear single band as well as previous studies have argued that ODN alleles expressed stably folded proteins consistently (*Lubin et al., 2013*). The Pol12-Myc-containing plasmid itself was successfully tested by previous members of the laboratory. This result confirms that pol12-R248 is important for the protein's binding with Stn1, although the experiment does not elucidate whether the interaction is direct or indirect. Furthermore, this argues that surfaces 1 and 3 both play a role in the interaction between Pol12 and Stn1, for which there has been conflicting data discussed in chapter 5.

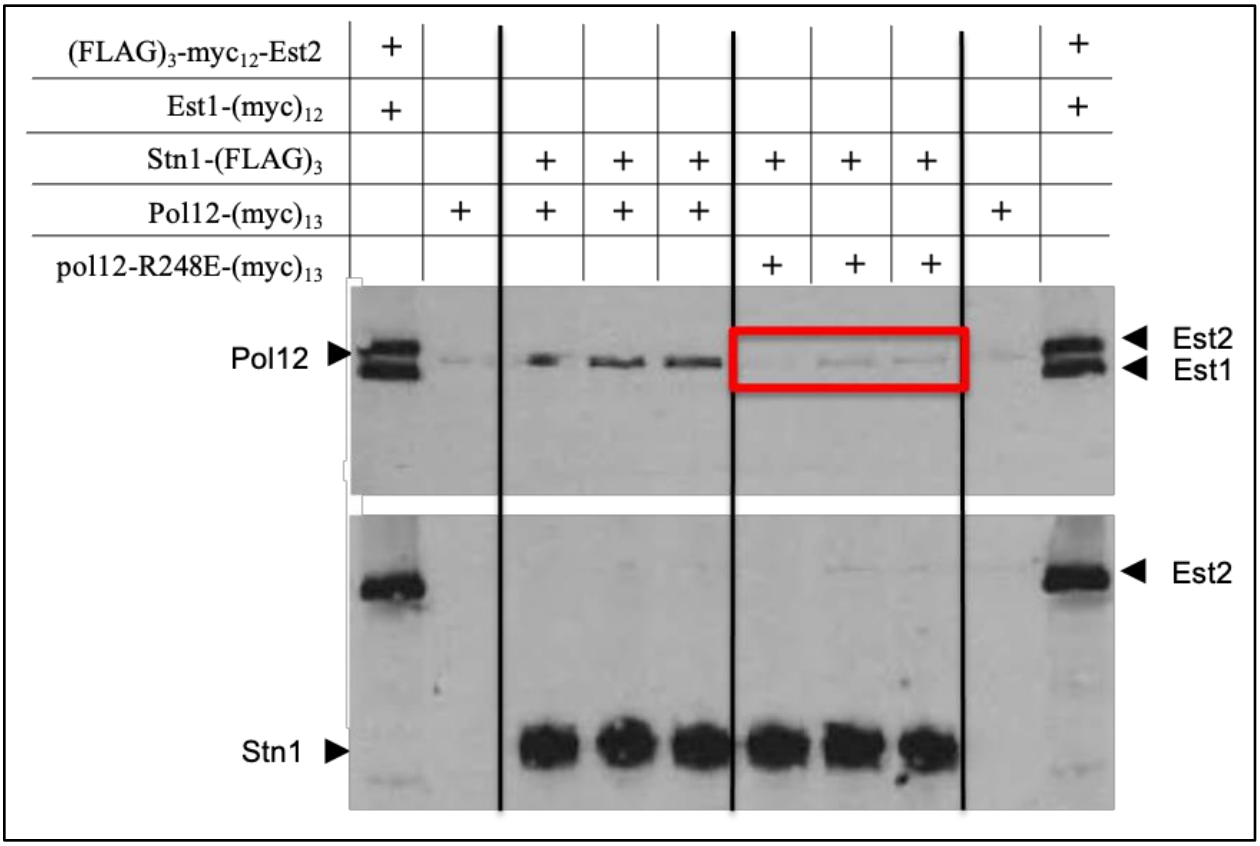

Figure 6.4: *pol12-R248E* disrupts the interaction of the protein with Stn1
Strains of the indicated construct were immunoprecipitated for FLAG with a Myc co-Immunoprecipitation. Expected localization of the proteins is indicated with arrows. Expected localization of Stn1 is indicated with a red outline

Conclusion and future directions

The results presented in this chapter bring up numerous questions and additional experiments that would be needed in order to get a better understanding of the mode of binding of Pol12. First of all, our results argue that the first 240 amino acids of the protein don't contribute to its binding to Pol1. These residues have so far been excluded from crystal structure studies that could help give this region a function through possible known secondary structures. Furthermore, it is overall fairly conserved and contains several suspected phosphorylation sites. It is believed that those sites are phosphorylated following binding of Pol1 and Pol12 (*Ferrari et al., 1996*). Therefore, it is possible that this step is a precursor for binding to another protein that has yet to be determined. As the two bigger truncations gave rise to some proteomic degradation, it seems unlikely that those alleles could be studied *in vivo*.

The same lack of answer comes from the western blotting analysis of *pol12-R248E* and Stn1. Indeed, this residue is located at the edge of the protein's suspected interface with Pol1 as is *pol12-216*, the original allele used to characterize the interaction. Although we were not able to replicate the experiment using *pol12-R322E* because of construct issues, we would strongly expect to see a similar loss of interaction with Stn1, in accordance with previous results and extreme proximity of the residue with *pol12-216*. There are several scenarios of which proteins are directly binding to explain this result. It seems unlikely that Pol1 and Pol12 would not directly interact as their dimerization is needed for the polymerase function to take place, although there is in fact only one high-throughput study looking at their direct interaction *in vitro* in yeast (*Yu et al., 2008*). The existence of a co-crystal structure of both proteins constitutes the strongest argument for their direct interaction, although downsides and possible artifacts of such an assay were highlighted in Chapter 2. Therefore, the most likely hypothesis is that the Pol12

interaction with Pol1 is necessary for that with Stn1. One experiment to investigate this would be to test the Pol1 immunoprecipitation levels of *pol12-R248E*. It is worth noting that many mutants from every other subunit of the complex with a specific ODN phenotype in a *cdc13*^{TS} strain pointed at areas that are important for the primase cohesion with Pol1. Interestingly, past studies have argued that Pol12 isn't necessary for that complex formation (*Brooke and Dumas, 1991*). Thus, another question to address is whether that more global cohesion of the complex may be important for the interaction between Pol12 and Stn1. Finally, it would be interesting to test whether the disruption of that interaction has consequences on that of Pol1 with Cdc13. Indeed, studies have shown that the subunits Stn1-Ten1 may exist independently of the third t-RPA subunit, even able to partially perform the complex function at telomeres in its absence. Whether the interaction between Cdc13 and Stn1 depends on polymerase alpha would reshape the basis of the complex's function at telomeres. Finally, the differential phenotypes observed for *pol12-D303K* make it an interesting candidate for testing. Indeed, its localization and strong ODN phenotype with a pol1^{TS} strain make it likely to disrupt the interaction between the two proteins. However, whether it also disrupts that with Stn1 or not could help us distinguish between a direct and indirect contact of the two proteins. Possible scenarios of the interaction between polymerase alpha-primase and t-RPA are shown in **Figure 6.5**.

In addition to unraveling the interaction specifics of polymerase alpha and t-RPA, investigating whether Pol12 mutations may destabilize the binding to other factors could be useful to understand the possible multiple protein functions affected. A classical approach to such a question would be to perform a mass spectrometry experiment. As these usually yield a very high number of candidates with lots of artifacts, it is best to compare the hits of a mutant allele to those of the WT protein. There are several likely proteins and complexes suggested to

interact with Pol12 specifically. Among those is Ctf4, early characterized as POB1 (Polymerase One Binding) for its ability to bind polymerase alpha (*Miles and Formosa, 1991*). This protein is thought to be the link between this complex and several others who play a crucial role in replication fork integrity. Ctf4 was also highlighted as one of the factors who's synthetic lethality with *rad27Δ* is rescued by *pol12-R248E* in the previous chapter. A similar comparative mass spectrometry experiment of Pol12 with mutations that mimic either the presence or absence of phosphorylation through its N-terminal Tyrosines could also yield novel candidates and broaden the function of the protein to other pathways.

Data from this chapter is currently in preparation to be published (Meunier and Lundblad, in preparation). The dissertation author was the primary researcher and author of this material.

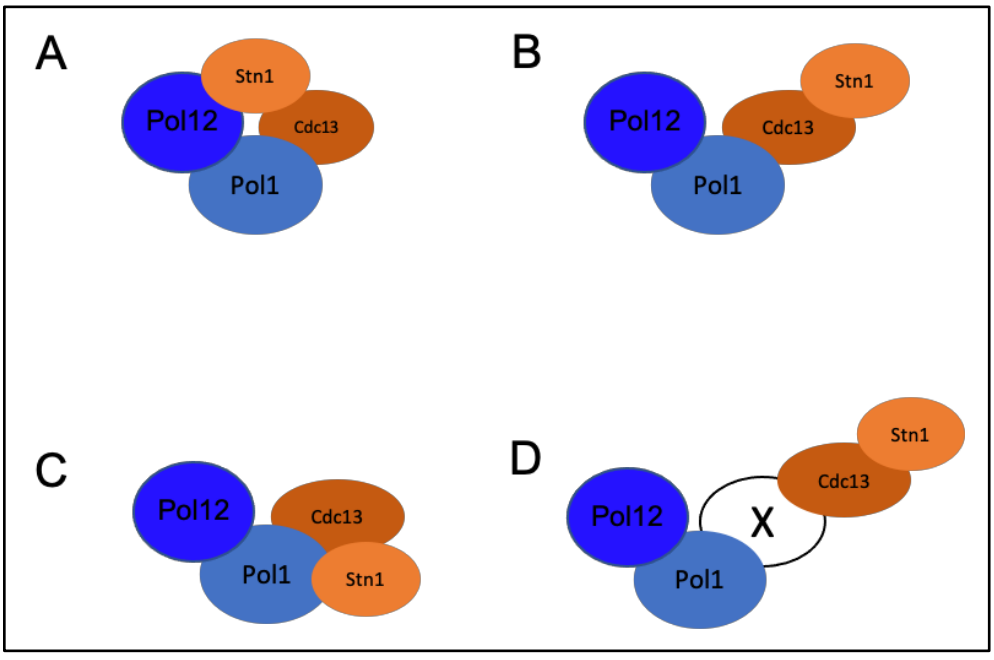

Figure 6.5: Possible interactions for Pol1, Pol12, Cdc13 and Stn1
(A) Pol12 interacts with Stn1 directly and independently of Pol1,
(B) Pol12 interacts with Stn1 indirectly and dependently of Pol1, Stn1 and Pol1 don't interact
(C) Pol12 interacts with Stn1 indirectly and dependently of Pol1, Stn1 and Pol1 interact
(D) Pol12 interacts with Stn1 indirectly and dependently of Pol1, through another factor

CHAPTER 7:
Conclusion

A novel interface of polymerase alpha-primase plays a role in telomere homeostasis with t-RPA

Polymerase alpha-primase had long only been known for its lagging-strand replication function within the replisome. Evidence slowly built up for a similar replication function of the complex, possibly independently of some or all of the replisome, taking place at the newly replicated telomeres. This mechanism is intended to counter the end-replication problem induced by that same complex that results in a progressive shortening of telomeres. It is thought to involve t-RPA, and previous proofs of physical interactions between polymerase alpha's Pol1 and Pol12 with t-RPA's Cdc13 and Stn1, respectively, were uncovered. However, the exact interface of Pol12 responsible for this interaction with Stn1 was never investigated, and, more generally, no real function for the essential protein was argued since.

Using the ODN assay that was perfected in our laboratory, I extensively mutagenesized the surface of Pol12. It highlighted residues that show a sensitivity to a t-RPA defect. Most of those residues happened to cluster around the predicted interface of Pol12 with its main catalytic partner Pol1. Pursuing our study to the rest of the complex showed that this sensitivity extends to every subunit of polymerase-alpha primase. Therefore, this entire complex is genetically involved with t-RPA. A closer look at the phenotypes of mutants of those residues showed a striking elongation of the telomeres, although this phenotype was overshadowing a matching increase of the critically short telomeres amount in the cells. Such a phenotype has been similarly observed in t-RPA mutants. Indeed, combination of key Pol12 alleles found by ODN with known t-RPA mutants resulted in synthetic lethality. Using biochemistry, we found that this lethality was the result of a loss of interaction between Pol12 and Stn1. This indicates that both complexes interact to work within a similar pathway.

Disrupting the interaction between Pol12 and Stn1 does not influence levels of fork collapse

There are two possible pathways in which polymerase alpha-primase and t-RPA might need to interact. Our laboratory recently published data arguing that t-RPA plays a key role during DNA replication with the machinery. On the other hand, the evidence for a post replicative pathway taking place to elongate the telomeres piles up. Thanks to another assay developed by a previous collaborator, we were able to conclude on the question. Indeed, we have the ability to monitor fork collapse levels to determine which factors play a role in that process. However, because of the synthetic lethality phenotype widely observed between mutants of Pol12 and all three subunits of t-RPA, we had to select mutants of Cdc13 resulting in a very mild disruption of the DNA binding ability of the protein in order to obtain a viable double mutant. Analysis of fork collapse levels of the resulting strain showed no significant increase compared to the single mutants. Therefore, the most likely explanation for the phenotypes observed is that they're acting towards a similar pathway independent of the replication fork and that affects telomere homeostasis.

The C-strand filling mechanism: existing data

Evidence of a mechanism for telomere processing by polymerase alpha distinct from the replication machinery arose in early 2010's (*Price et al., 2010, Chow et al., 2012*), although the independent process of C-strand fill-in was long described (*Price et al., 1994, Fan and Price, 1997, Reveal et al., 1997*). It highlighted the recruiting role of t-RPA, as the two complexes had been found to physically interact. More recently, data argued for a particular role for Stn1 and Ten1 in the process (*Feng et al., 2018*). This result goes with previous work hypothesizing that Cdc13 was partially dispensable by polymerase alpha-primase binding to telomeres alongside Stn1, although the DNA binding domain involved is unclear (*Petreaca et al., 2006*). The dual

role of Cdc13 at recruiting telomerase and acting on the C-strand fill-in process would explain that mutants of the protein were found having opposite telomere defects. In contrast, every mutant found in Stn1 and Ten1 showed the same elongated telomere phenotype as observed with alleles of polymerase alpha-primase, arguing for a common role. Indeed, if telomerase recruitment is unaffected but C-strand fill-in is impaired, the result will be an elongated but single stranded telomere. This hypothesis is confirmed by the observations that the elongation is solely dependent on telomerase, and that the action of single-stranded exonuclease on t-RPA mutant telomeres cleaves them back to WT levels.

Evidence of a link between C-strand fill-in and DNA damage checkpoint/repair

The synthetic lethality phenotype of combinations of mutants of polymerase alpha-primase and t-RPA is expected to be the result of an activation of the DNA damage checkpoint. Indeed, loss of any checkpoint protein has been shown to bypass growth defects in Cdc13 DBD mutants (*Zubko et al., 2004, Paschini et al., 2012, Holstein et al., 2017*). In parallel, we showed how *pol12-R248E* is able to partially rescue the deadly defect induced by a lack of proper processing of Okazaki fragments and impaired DNA damage checkpoint. Therefore, Pol12 normally acts to repress a parallel DNA repair pathway. The role for this protein in damage processing has long been suggested, as its very first allele was characterized by an increased level of unresolved Holliday Junctions (*Zou and Rothstein, 1997*). This result argues that Pol12 normally acts to either solve those structures or prevent their formation altogether. It has also very recently been argued that the Human equivalent of Pol12, POLA2, played a helping role in double strand break (DSB) repair (*Dang and Morales, 2020*). The two main repair mechanisms for such type of damage are specifically controlled at telomeres (*Doksani and de Lange, 2014*).

When triggered, they involve formation of a Holliday Junction. Therefore, it seems plausible that Pol12 acts to repress activation of those pathways. Whether it is linked to its binding properties to t-RPA or an independent function has yet to be investigated. Yet, it seems clear that such checkpoint activation is the result of increased single-stranded DNA resulting from an impaired C-strand fill-in.

Model

All the data described above allowed for generation of a model linking polymerase alpha-primase and the t-RPA complex in the context of C-strand fill-in. Under normal conditions, Cdc13 binds to the newly replicated single-strand G-rich overhang (**Figure 7.1A**). It has the ability to recruit telomerase through direct binding with its Est1 subunit (**Figure 7.1B**). Telomerase generates *de novo* telomeric repeats onto the G-rich strand and it then either released or displaced by polymerase alpha-primase, with data arguing that Cdc13 binds both Est1 and Pol1 through the same region (**Figure 7.1C**). Once together, t-RPA and polymerase alpha-primase allow for the complementary C-strand fill-in (**Figure 7.1D**) until reaching the double-stranded telomeric region (**Figure 7.1E**). As generation of the C-strand goes against the natural directionality of the machinery and similarly to lagging strand replication, the product includes RNA-DNA hybrids that have to be processed through action of endonuclease and ligase (**Figure 7.1F**). The whole processed results in an elongated telomere in comparison to that resulting of regular replication.

Figure 7.1: Schematic representation of t-RPA, telomerase and the polymerase alpha primase interactions during the C-strand fill in process

A/ After the replication fork machinery has finished lagging strand replication, Cdc13 is bound to the single-stranded telomeric end and recruits telomerase Est1, B/ Telomerase elongates the single-stranded G-rich strand, C/ Pol1 removes telomerase from binding to Cdc13 and brings the t-RPA complex together, D/ Polymerase alpha primase performs 3' to 5' C-strand fill-in with Okazaki fragments (represented in red), E/ Endonucleases and ligase process the Okazaki fragments , F/ Final elongated telomere

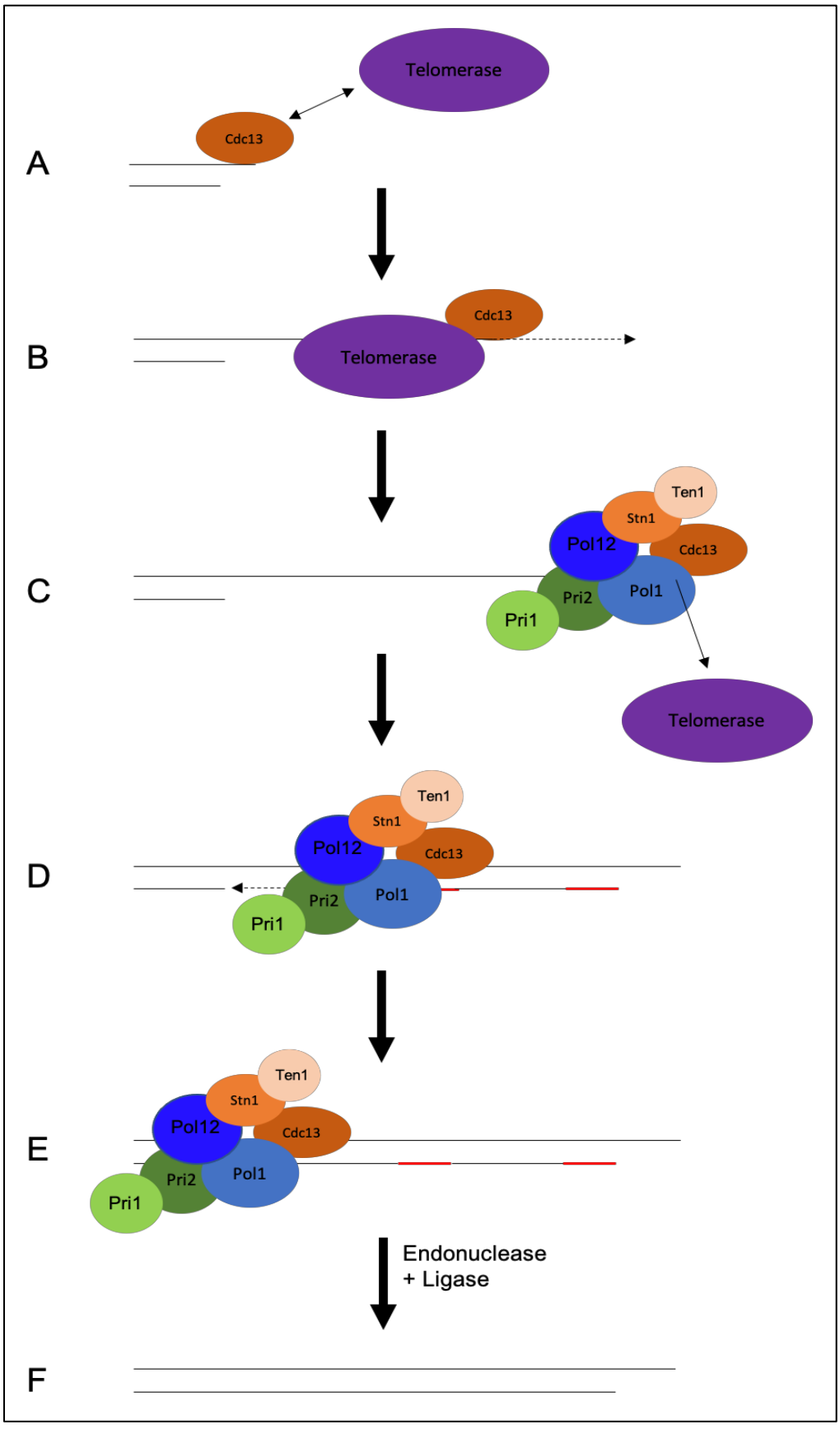
A
Telomerase
Cdc13
B
Cdc13
Telomerase
C
Ten1
Stn1
Pol12
Cdc13
Pri2
Pol1
Pri1
Telomerase
D
Ten1
Stn1
Pol12
Cdc13
Pri2
Pol1
Pri1
E
Ten1
Stn1
Pol12
Cdc13
Pri2
Pol1
Pri1
Endonuclease
+ Ligase
F

Mutations of subunits of the complexes that are important on C-strand fill-in have distinct consequences on telomere length. Literature on Cdc13 alleles show that depending on the region of the protein that is altered, telomeric length will either be shortened or elongated. Such phenotypes argue for two altered stages of C-strand fill-in process. In the first case scenario, short telomeres could be the representation of a lessened successful recruitment of telomerase by Cdc13. In the other case scenario, elongated telomeres are the consequence of an impaired C-strand fill-in. Indeed, studies have shown that those telomeres are in fact single-stranded. Whether this impairment is the result of a disruption of the t-RPA-polymerase alpha binding integrity through Cdc13 and Pol1 has yet to be investigated (**Figure 7.2**).

Figure 7.2: Schematic representation of t-RPA with a Cdc13 mutant, telomerase and the polymerase alpha primase interactions during the C-strand fill in process

A/ After the replication fork machinery has finished lagging strand replication, Cdc13 is bound to the single-stranded telomeric end and recruits telomerase Est1, B/ Telomerase elongates the single-stranded G-rich strand, C/ Pol1 cannot bind to Cdc13 but is still partially able to bind to single-stranded DNA, D/ Polymerase alpha primase performs 3' to 5' C-strand fill-in with Okazaki fragments (represented in red), E/ Endonucleases and ligase process the Okazaki fragments , F/ Final elongated telomere

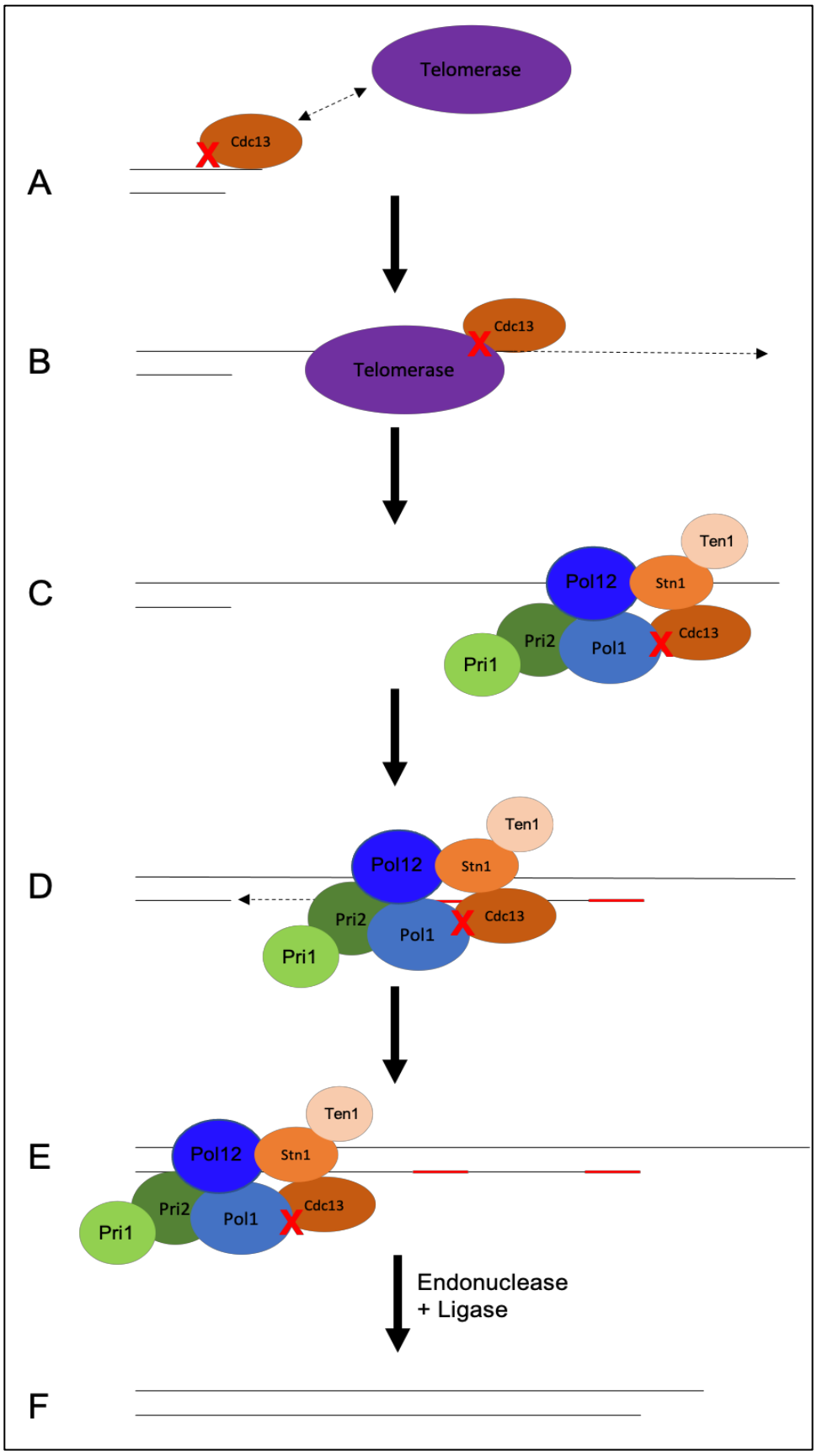
Telomerase
Cdc13
A
B
Telomerase
Cdc13
C
Ten1
Pol12
Stn1
Pri2
Pol1
Cdc13
Pri1
D
Ten1
Pol12
Stn1
Pri2
Pol1
Cdc13
Pri1
E
Ten1
Pol12
Stn1
Pri2
Pol1
Cdc13
Pri1
Endonuclease
+ Ligase
F

Data discussed throughout this thesis described newly generated Pol12 alleles thought to disrupt the protein interaction with Stn1. Mutations of both protein result in an increase in telomere length with the prediction that those repeats are single-stranded. Therefore, similarly to some Cdc13 mutants, it argues for a defect in the C-strand fill-in (**Figure 7.3**).

Figure 7.3: Schematic representation of t-RPA, telomerase and the polymerase alpha primase with a Pol12 mutant interactions during the C-strand fill in process

A/ After the replication fork machinery has finished lagging strand replication, Cdc13 is bound to the single-stranded telomeric end and recruits telomerase Est1, B/ Telomerase elongates the single-stranded G-rich strand, C/ Pol12 and Stn1 cannot bind but Pol1 can still bind partially Cdc13, D/ Polymerase alpha primase performs 3' to 5' C-strand fill-in with Okazaki fragments (represented in red), E/ Endonucleases and ligase process the Okazaki fragments, F/ Final elongated telomere

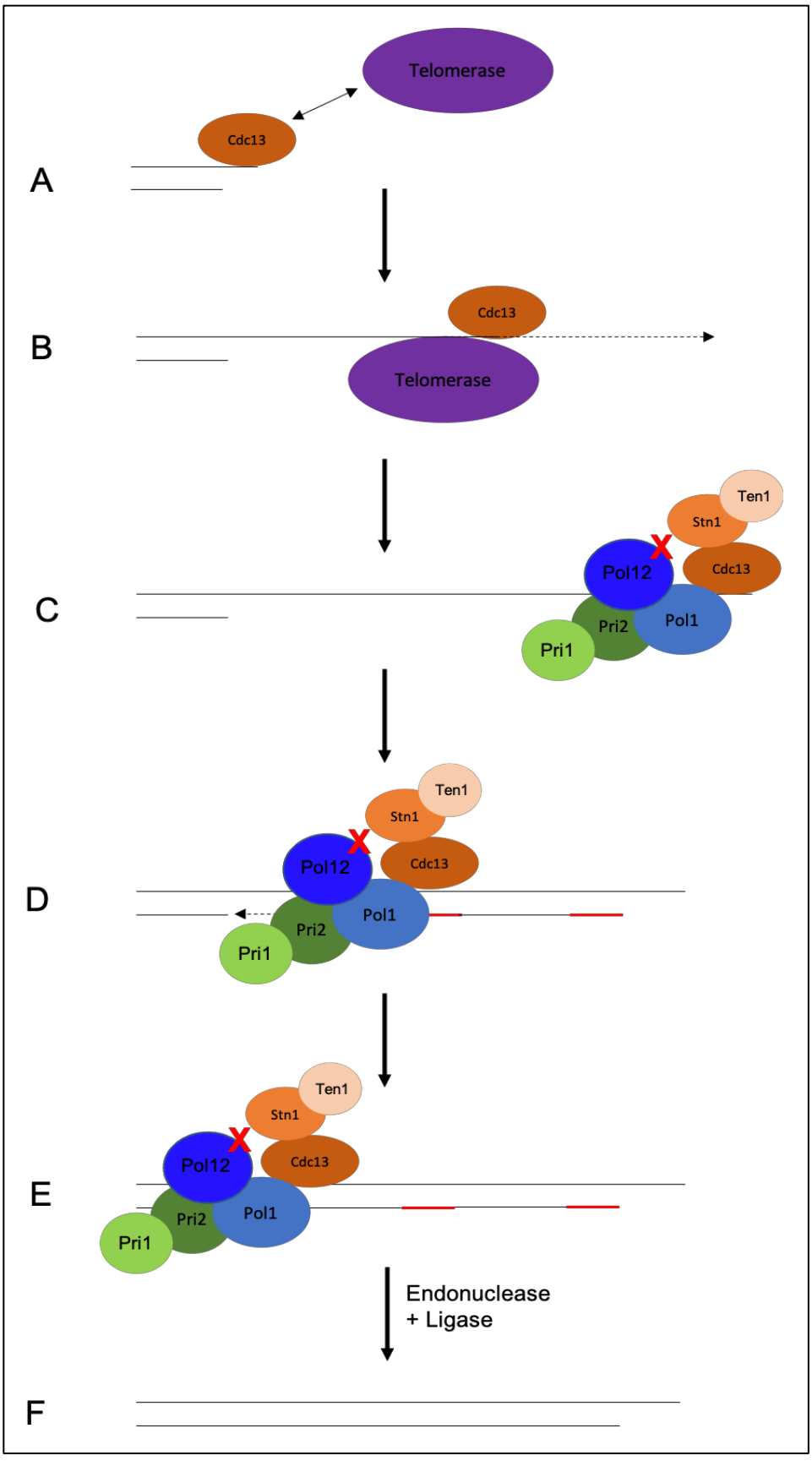
Telomerase
Cdc13
A
B
Cdc13
Telomerase
C
Ten1
Stn1
Pol12
Cdc13
Pri2
Pol1
Pri1
D
Ten1
Stn1
Pol12
Cdc13
Pri2
Pol1
Pri1
E
Ten1
Stn1
Pol12
Cdc13
Pri2
Pol1
Pri1
Endonuclease
+ Ligase
F

One of the most striking phenotypes of those novel Pol12 alleles is the synthetic lethality observed when combined with mutants of each of the subunits of t-RPA. Based on the localization of the various mutants involved in those inviable strains, this result argues that the interaction between t-RPA and polymerase alpha-primase needed for the C-strand fill-in to occur normally involves several points of contact. For example, combinations of Cdc13 and Pol12 mutants results in a lessened or completely abrogated interaction between the two complexes (**Figure 7.4**). Complete lack of C-strand fill-in leaves excess single-stranded DNA that is detected as DNA damage and triggers cell arrest through checkpoint.

Figure 7.4: Schematic representation of a t-RPA's Cdc13 and polymerase alpha primase's Pol12 synthetically lethal double mutant

A/ After the replication fork machinery has finished lagging strand replication, Cdc13 is bound to the single-stranded telomeric end and recruits telomerase Est1, B/ Telomerase elongates the single-stranded G-rich strand, C/ Pol1 cannot bind to Cdc13 and Pol12 cannot bind to Stn1, D/ C-strand fill-in cannot take place, E/ unprocessed single-stranded DNA activates DNA damage checkpoint

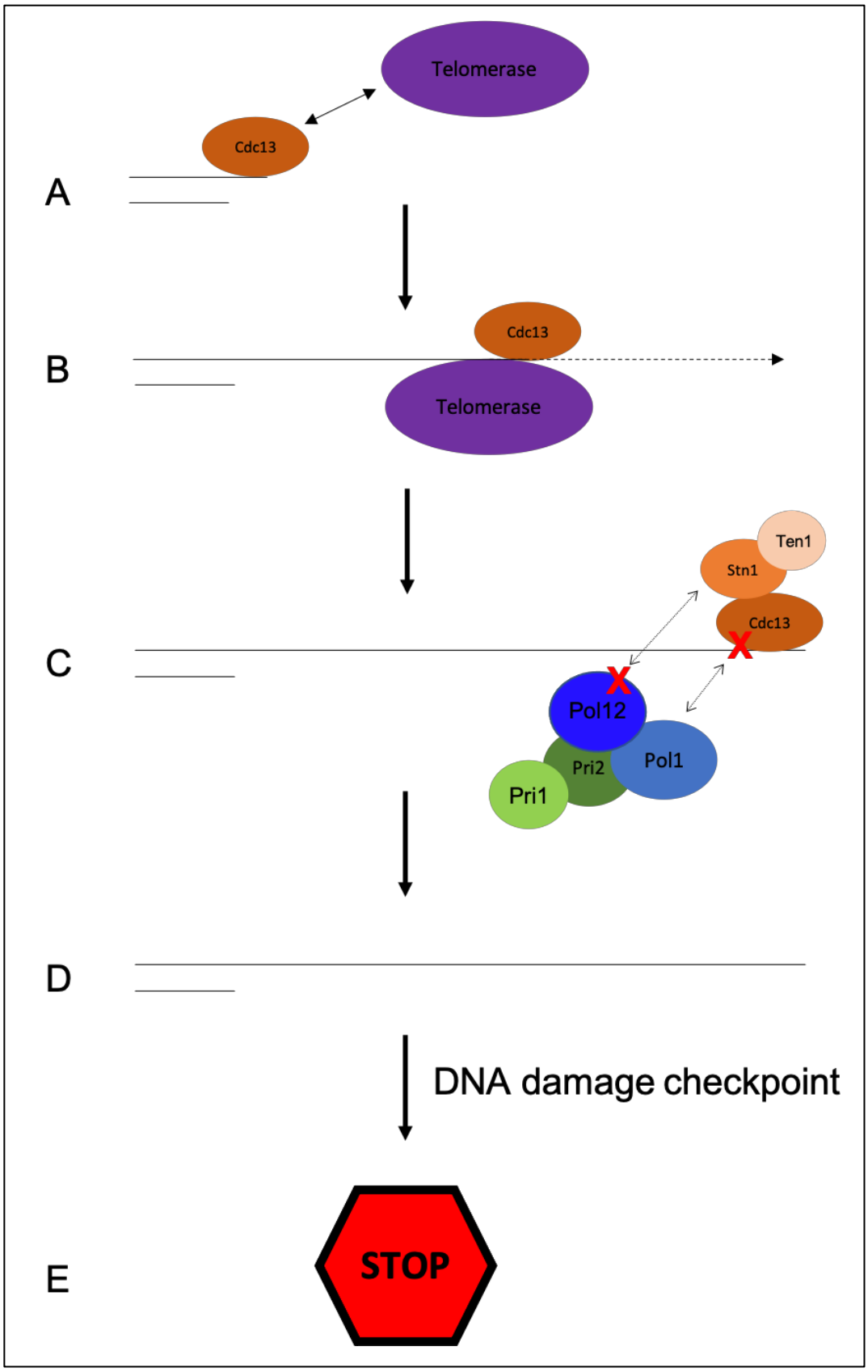
Telomerase
Cdc13
A
Cdc13
B
Telomerase
Ten1
Stn1
Cdc13
C
Pol12
Pri2
Pol1
Pri1
D
DNA damage checkpoint
STOP
E

Similarly, combination of Pol12 and Stn1 mutants is inviable. This result argues that Stn1 and/or Ten1 are essential for the C-strand fill-in process (**Figure 7.5**). Indeed, there are no evidence that Ten1 interacts with t-RPA through Cdc13, and its presence would therefore be dependent on Stn1's Whether either of the two proteins is important for stability or plays a specific role in the process is unclear. However, lethal combination of Ten1 and Pol12 mutants brings novel information in which Ten1 is essential as well for the process (**Figure 7.6**).

Figure 7.5: Schematic representation of a t-RPA's Stn1's and polymerase alpha primase's Pol12 synthetically lethal double mutant

A/ After the replication fork machinery has finished lagging strand replication, Cdc13 is bound to the single-stranded telomeric end and recruits telomerase Est1, B/ Telomerase elongates the single-stranded G-rich strand, C/ Stn1 cannot bind to either Cdc13 nor Pol12, D/ C-strand fill-in cannot take place, E/ unprocessed single-stranded DNA activates DNA damage checkpoint

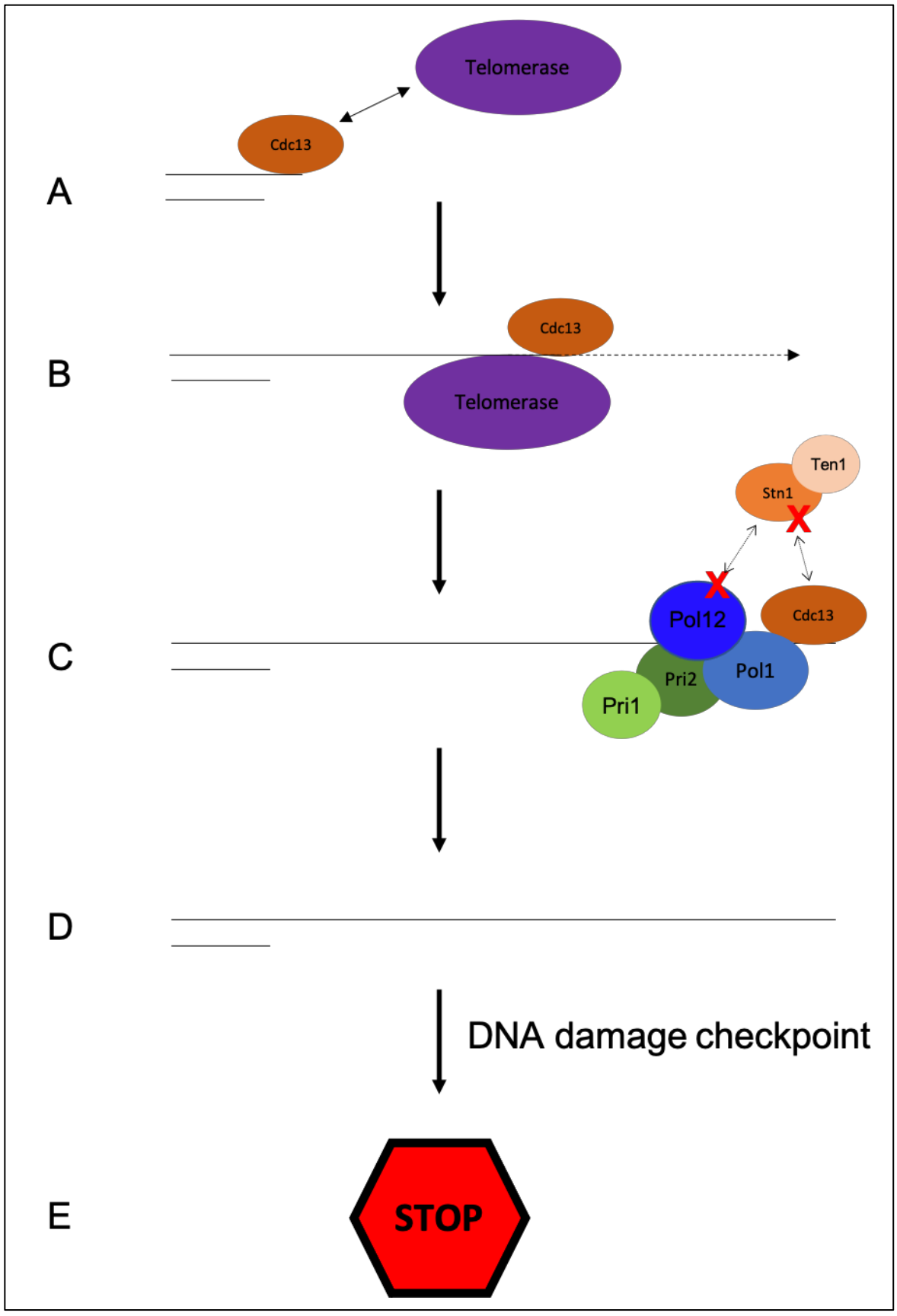
Telomerase
Cdc13
A
Cdc13
B
Telomerase
Ten1
Stn1
X
X
Pol12
Cdc13
Pri2
Pol1
Pri1
C
D
DNA damage checkpoint
STOP
E

Figure 7.6: Schematic representation of a t-RPA's Ten1's and polymerase alpha primase's Pol12 synthetically lethal double mutant

A/ After the replication fork machinery has finished lagging strand replication, Cdc13 is bound to the single-stranded telomeric end and recruits telomerase Est1, B/ Telomerase elongates the single-stranded G-rich strand, C/ Ten1 cannot bind to Stn1, D/ C-strand fill-in cannot take place, E/ unprocessed single-stranded DNA activates DNA damage checkpoint

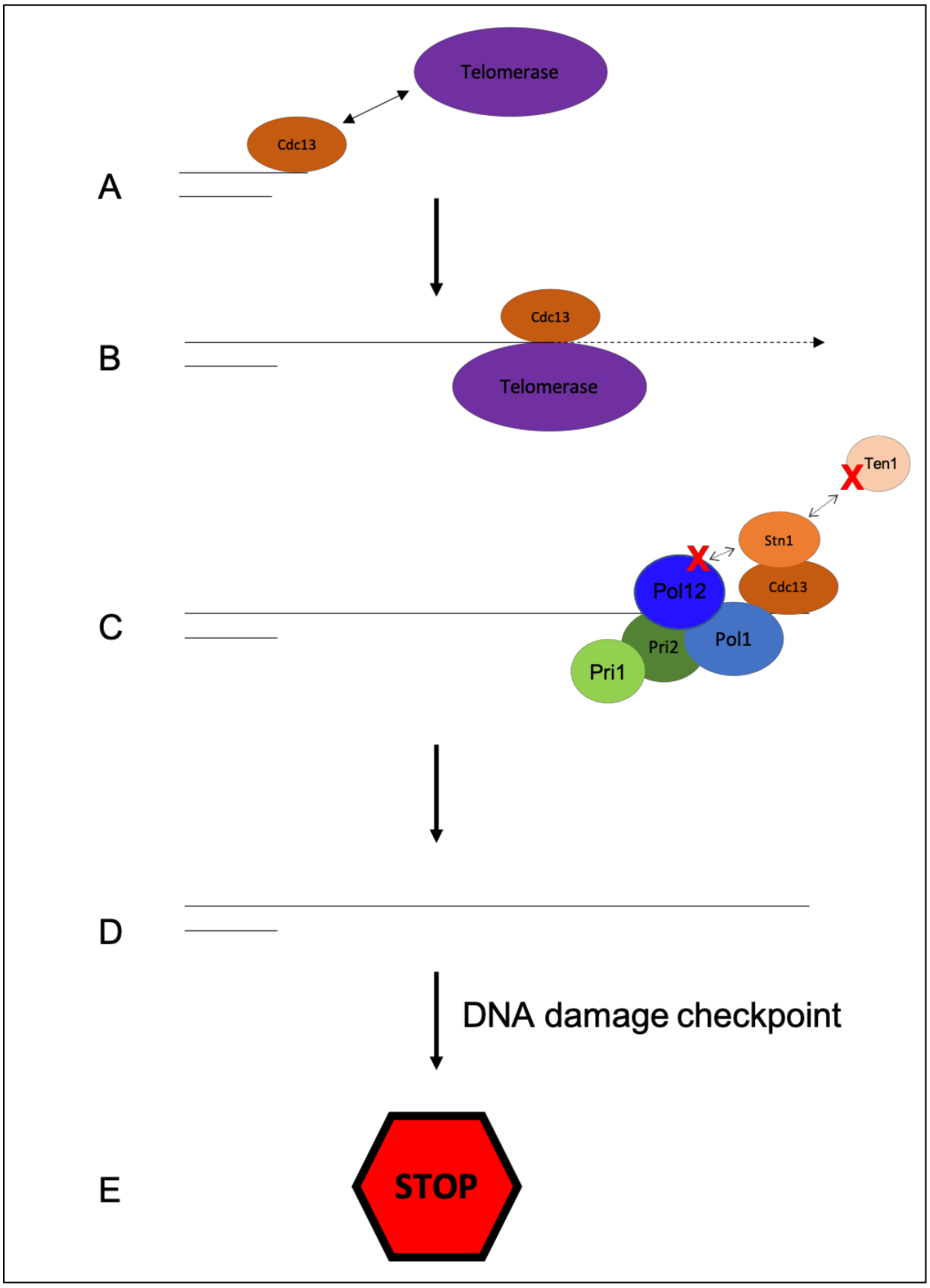
Telomerase
Cdc13
A
Cdc13
B
Telomerase
Ten1
X
Stn1
X
Pol12
Cdc13
C
Pri2
Pol1
Pri1
D
DNA damage checkpoint
E
STOP

Applications to Humans diseases

Telomere homeostasis is crucial for survival as it protects coding DNA of the linear chromosomes from degradation. Yet, they naturally shorten overtime, as cells majoritarily lack active telomerase (*Collins and Mitchell, 2002*). The likelihood of developing one of many neurodegenerative diseases also increases with age. Whether short telomeres are the cause, a consequence or simply correlate with the appearance of such pathologies have been subject to debate (*Eitan et al., 2015*). However, it is widely understood that the chances of accumulating deleterious mutations increase overtime, especially when critically shortened telomeres become unable to perform their protective function. The chances of developing cancer also closely relate to age as each round of cell cycle is susceptible to generate oncogenic mutations. Cancerous cells divide uncontrollably and at a much faster pace than regular cells. In the very vast majority of cancers, telomerase has been hijacked and re-activated (*Kim et al., 1994*). This prevalence varies slightly depending on the type of tissue affected, correlating with data arguing that telomere length is tissue specific (*Friedrich et al., 2000*). Indeed, various types of tissues are exposed to various additional environmental and epigenetics factors that also influence genome stability.

Polymerase alpha is a central player of cancer biology. Its action during lagging strand replication makes it a possible culprit for novel mutations, especially considering its lack of proofreading ability and error rate of 1/10,000 (*Kunkel, 2004*). Yet, beyond its role in DNA replication, this thesis highlighted its importance in telomere homeostasis through interaction with t-RPA during C-strand fill-in. The elongated nature of the telomeres arising from mutants of those complexes does not match the short telomeres phenotype often used as a biomarker for diseases. Furthermore, their single-strandedness makes them susceptible to telomere fusion between chromosomes, with grim potential consequences during mitosis. Finally, increasing

evidence for a role of Pol12 and its Human equivalent in controlling mutation prone DNA repair pathways demonstrates how the protein participates in genome stability at many levels. However, possibly because of the lack of recognition of its impact, research of potential disease-causing alleles of the protein has been limited.

Telomere syndromes, or telomeropathies, are inherited diseases linked to the presence of extremely short telomeres. They mainly result from mutations of telomerase or components of telomeric-bound proteins, named shelterin in humans. Although the homologs of t-RPA subunits are distinct from shelterin, mutations of CTC1, equivalent of Cdc13, and STN1 are a known cause of several telomeropathies such as Coats Plus and Dyskeratosis congenita (*Chen et al., 2013, Ganduri and Lue, 2017*). Similarly to observations done in *S. cerevisiae*, human STN1 plays a role in stimulating the activity of polymerase alpha-primase that is disrupted in those disease-causing alleles. Therefore, it is likely that reciprocal mutants on POLA2, the human equivalent of Pol12, exist but haven't been investigated yet.

On the other hand, defects of POLA1, catalytic subunit of polymerase alpha and human equivalent of Pol1, are a known cause of a syndrome causing immunodeficiency, X-linked reticulate pigmentary disorder (*Starokadomskyy et al., 2016*). More recently, another disease-causing intellectual disability has been suggested to be the result of a mutation altering the splicing of POLA1 (*Esch et al., 2019*). Both of those pathologies are X-linked, in accordance with the localization of the gene on chromosome X, rendering its identification easier as several men of the same family are likely to be affected. However, they're not considered telomeropathies. In contrast, cases of X-linked dyskeratosis congenita have also been found but were solely linked to a mutation in DKC1, named after the defect it creates when altered (*Townsley et al., 2014*). Interestingly, it is suggested that diseases caused by mutations of

POLA1 are the result of an impaired interferon production resulting in immunodeficiency. This phenotype brings up a whole new function of the protein in the immune system that has yet to be investigated further but does not seem to involve POLA2. Although mostly unknown as disease-causing alleles, POLA2 is increasingly studied as a cancer biomarker. An allele of the protein, resulting in altered localization of the protein in the cytoplasm rather than the nucleus, has been shown to correlate with a better prognosis in patients with non-small cell lung cancer (*Mah et al., 2014*). This result is also interesting from a genetic standpoint as the single substitution responsible for mislocalization maps next to a suspected phosphorylation site, away from the protein interface with its catalytic partner. It was later shown that normally localized POLA2 interferes with a commonly used drug for that type of cancer, and is therefore a biomarker to take into account (*Koh et al., 2016*). Finally, recent work identified POLA2 as a collateral target for another type of drug used for that same kind of cancer, once again highlighting its potential as a biomarker for drug efficiency (*Kim et al., 2020*). However, as the protein is needed for replication in every cell, it does not constitute an ideal therapeutic target, in contrast to telomerase that is inactive in most somatic tissues but active in most cancers.

APPENDIX A:
Genetic analysis of Ten1, subunit of the t-RPA complex

Introduction: Ten1

The t-RPA or CST complex is made out of 3 subunits: Cdc13, Stn1 and Ten1. Whereas the first two have been extensively studied, knowledge about Ten1 is comparatively limited. It is an essential small protein originally discovered for its ability to rescue TS mutants of Stn1. Although Ten1 overexpression doesn't rescue *cdc13-1* unlike overexpression of Stn1 does, its combination with overexpressed Stn1 rescues the growth defect greatly more than Stn1 alone (*Grandin et al., 2001*). The two proteins have been shown to directly interact (*Gao et al., 2007, Paschini et al., 2010*). When disrupted, Ten1 shows an elongated telomere phenotype, similarly to Stn1 and a subset of Cdc13 DBD mutants (*Xu et al., 2009*). More recently, a specific function of Stn1-Ten1 has been suggested as necessary for recruitment of Polymerase alpha-Primase during the C-strand fill-in process, independently of telomerase action (*Feng et al., 2018*). It has also long been suggested that Ten1 performs essential functions independently of the t-RPA complex (*Kasbek et al., 2013*). Such a function could possibly be attributed to the Transcription process through RNA polymerase II as of recent data (*Calvo et al., 2019*).

Our laboratory successfully identified many alleles of t-RPA subunits Cdc13 and Stn1 by targeted mutagenesis as described throughout this thesis. The decision to study Ten1 arose for several reasons. First of all, the role of Ten1 in and outside of the context of t-RPA is still unclear. Furthermore, to this day, all existing alleles of Ten1 were generated through random mutagenesis although crystal structures of the peptide have been readily available both in various yeast species and Humans (*Sun et al., 2009*, *Bryan et al., 2013, Ge et al., 2020*). Most recently, collaboration work between the Cech and Wuttke laboratories even produced a complete structure of CST, the Human equivalent of t-RPA (*Lim et al., 2020*). Finally, its physical and

genetic proximity to Stn1 and long telomere phenotype makes it a strong potential interacting partner to Pol12.

Choice of residues to mutate on Ten1 was made by using a combination of sequence alignments throughout 27 species of yeasts, with the help of a *C. tropicalis* structure to identify surface and interface residues with Stn1 (**Figure A.1**). Since this study, a similar crystal structure of the complex in *K. Lactis* has been published (*Ge et al., 2020*). Ten1 is a notably short yet very conserved protein of only 160 amino acids. Therefore, one might expect most of the sequence to be important for its function(s) and potentially lethal if disrupted. Furthermore, although being successful with most essential proteins, the ODN assay could not yield results with Cdc13 as overexpression of the protein affects viability. Overexpression of Ten1 has also been shown to have an effect on t-RPA binding abilities. For these reasons, the use of a LOF assay using a basal-expressing centromeric (CEN) promoter was preferred.

Material and methods: Ten1

13 mutant alleles of 10 residues located throughout the sequence of Ten1 were generated and tested for LOF. All Loss-of-function (LOF) analyses were performed in yVL2082 (*MATa ura3-52 lys2-801 trp-Δ1 his3-Δ200 leu2-Δ1 ten1-Δ::KAN*, complemented with pVL1808 (CEN URA3 Ten1)). Missense mutations in Ten1 were introduced by Quickchange mutagenesis into pVL3779 (CEN TRP1 Ten1) and checked by sequencing. A standard LiAC transformation protocol was used to introduce plasmids individually into yeast alongside pVL399 as a negative control and pVL3779 as a positive control. Cells were plated on YPD (Yeast Extract Peptone Dextrose) minus Tryptophan and Uracil (-Trp -Ura) petri dishes, grown in duplicates overnight

on YPD-Trp-Ura liquid media and gridded simultaneously on -Trp-Ura plates as a control and YPD-Trp +5-Fluoroorotic Acid (5-FOA) plates in ⅕ serial dilutions for readability.

For epistasis analyses, mutations were integrated into the genome using the pop-in pop-out method as previously described.

Table A.1: List of plasmids used in this appendix

Plasmid #	Content
pVL399	*2μ LEU2 ADH*
pVL3779	*2μ LEU2 ADH-TEN1*
pMAM629	*2μ LEU2 ADH-ten1-S2E*
pMAM630	*2μ LEU2 ADH-ten1-D7K*
pMAM631	*2μ LEU2 ADH-ten1-R41E*
pMAM632	*2μ LEU2 ADH-ten1-R43E*
pMAM633	*2μ LEU2 ADH-ten1-R47E*
pMAM634	*2μ LEU2 ADH-ten1-D50K*
pMAM635	*2μ LEU2 ADH-ten1-D50A*
pMAM636	*2μ LEU2 ADH-ten1-F51E*
pMAM637	*2μ LEU2 ADH-ten1-F51A*
pMAM638	*2μ LEU2 ADH-ten1-E91K*
pMAM639	*2μ LEU2 ADH-ten1-D110K*
pMAM640	*2μ LEU2 ADH-ten1-E127K*
pMAM641	*2μ LEU2 ADH-ten1-E127A*

Table A.2: List of strains used in this appendix

All strains are derivatives of yVL2967 (ura3-52 lys2-801 trp-Δ1 his3-Δ200 leu2-Δ1)

yVL #	Mutation	Mate type
2082	*Ten1Δ (CEN-URA3-Ten1)*	a
2967	WT	a
5025	*pol12-R248E*	alpha
5026	*pol12-R322E*	alpha
5027	*pol12-D303K*	alpha
5788	*ten1-F51E*	a
5791	*ten1-E91K*	a
5796	*ten1-D7K*	a
5797	*ten1-D50K*	a

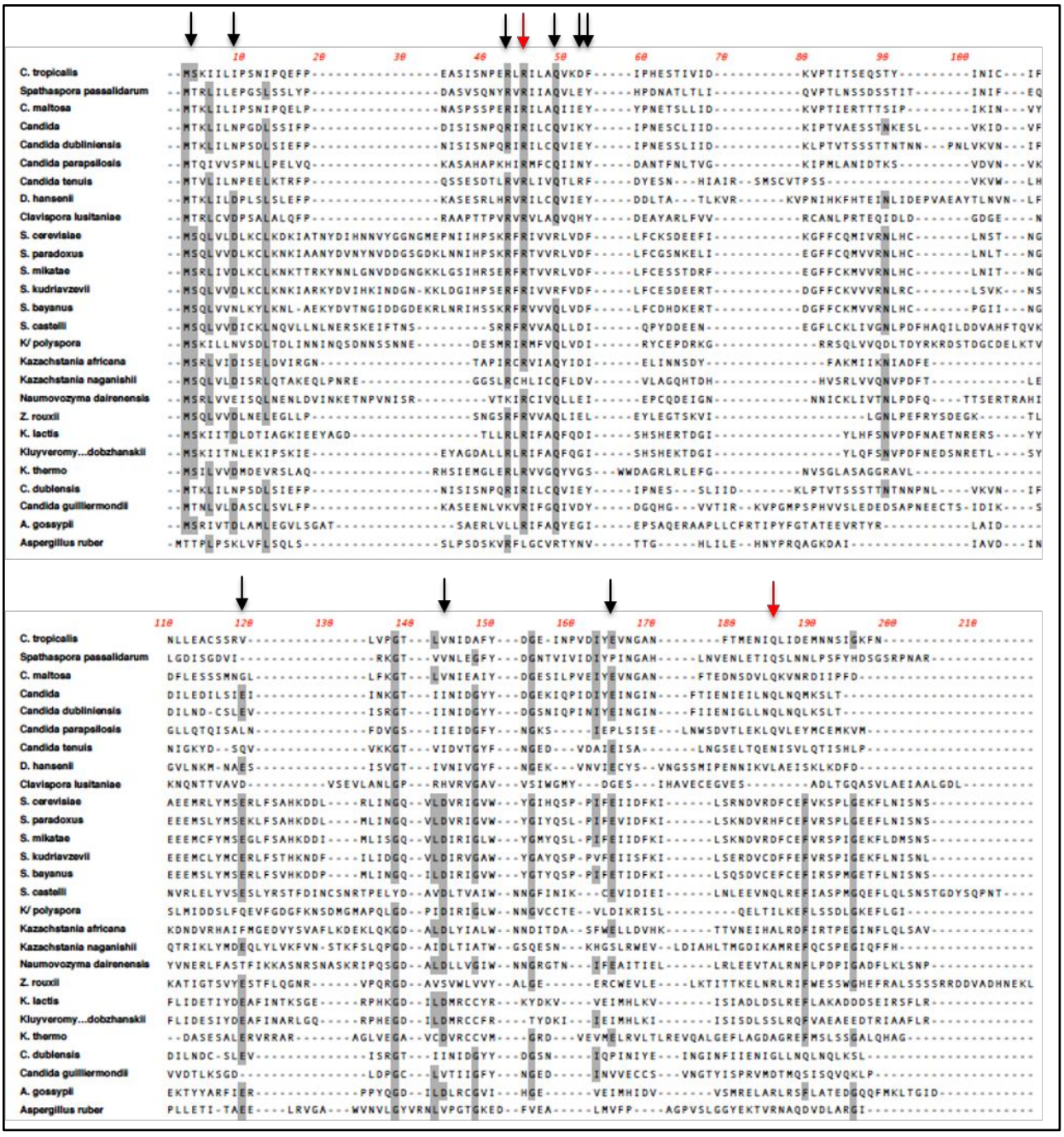

Figure A.1: Ten1 sequence alignment and conservation throughout 27 yeasts species.

Highly Conserved and strictly conserved residues are highlighted in light grey and dark grey, respectively. Amino acids missing for a particular species compared to S. cerevisiae are indicated with a dash. Alignment was done using Macvector.

Results of the Loss-of-function (LOF) screening of Ten1

Out of the ten residues of Ten1 tested, only four were viable through LOF when mutated, whereas six were inviable (**Figure A.2** and **Table A.3**).

Table A.3: Summarized results of the Loss-of-function viability status of novel Ten1 alleles
Strains were tested on -Trp 5-FOA at 30 and 34°C to identify possible TS alleles. Viability was tracked with the following nomenclature: -: inviable, +/-: sick, +: viable

	Viability at	
Ten1 allele	30°C	34°C
S2E	-	-
D7K	+/-	+/-
R41E	-	-
R43E	-	-
R47E	-	-
D50K	+	+
D50A	+	+
F51E	+/-	+/-
F51A	+	+
E91K	+	+
D110K	-	-
E127K	-	-
E127A	-	-

Among those are residues known or suspected to be important for the interaction between Ten1 and Stn1. This observation of a majority of alleles being inviable is fairly expected given the highly conserved nature of the protein, as well as the fact these mutants weren't tested for ODN prior. Indeed, one can expect many of those alleles to affect the essential function(s) of Ten1, which would result in cell death. All of the inviable mutants localized at the interface of Ten1 and Stn1, although another allele was found away from it. This result either argues that there is another essential interface of the protein besides its binding to Stn1, or that the interface

extends beyond what the crystal structure captures. A known allele previously detected in our laboratory, Ten1-D138, also localized at that interface as expected (*Paschini et al., 2010*).

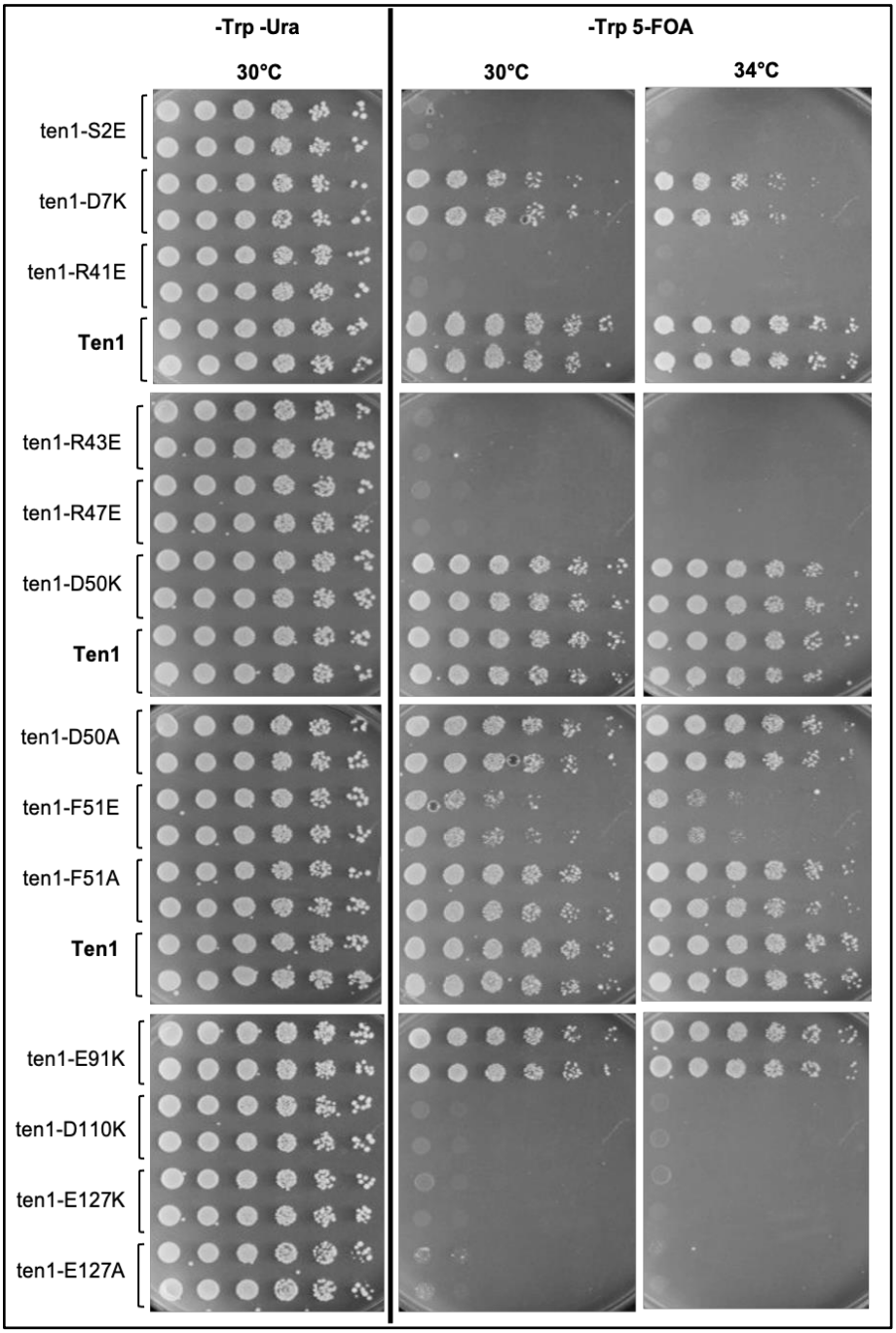

Figure A.2: Loss-of-function testing results of the novel Ten1 mutants

A Ten1 Knock-out strain with covering CEN-URA3-Pol12 plasmid (yVL4931) was transformed with variants of CEN-LEU2 plasmids with the content indicated. Cells were grown and viability was compared on -Leu -Ura for control and -Leu 5-FOA for shuffling off the covering plasmid.

Every viable allele mapped on the surface away from the interface with Stn1 but did not cluster in a particular area of the protein. It is possible that, although highly conserved throughout species, some of these mutants do not perform any essential or particular function. It is also possible that they also disrupt the protein interaction with Stn1 but to an extent that isn't inviable. Their extremely long telomeres as seen by Southern Blot analysis supports the latest idea as it matches a similar phenotype seen in Stn1 and Pol12 mutants (**Figure A.3**).

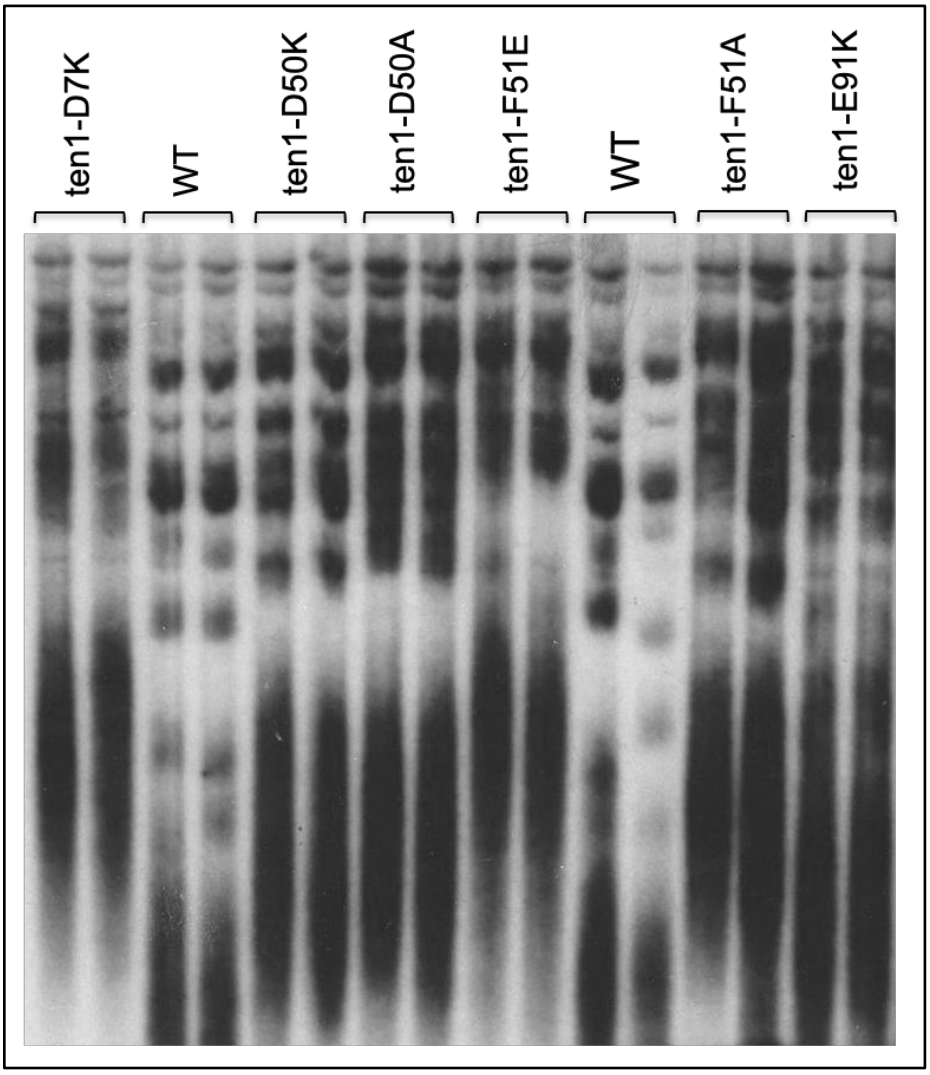

Figure A.3: Viable Ten1 alleles have extremely elongated telomeres

LOF assay monitoring telomere length of ten1Δ yeast strain (yVL2082) bearing single-copy plasmids expressing mutations described above.

When mapped on the crystal structure of *K. lactis*, every single inviable allele of the Ten1 homolog localized on a five-sheet beta-barrel formed by the peptide (**Figure A.4**). The two viable but sick residues when mutated immediately flank that secondary structure that is a part of the protein's OB-fold. This result highlights its importance for the function of Ten1, presumably through interaction with Stn1. In contrast, the four previously found TS alleles of Ten1 are complex to characterize (*Xu et al., 2009*). Indeed, one of them is made out of a buried residue and presumably is truly TS. Yet, for the other three, evidence has shown that they might actually be partial loss-of-function mutants (*Paschini et al., 2012*). However, they're made out of combinations of several substitutions which, although all surfaces, make it hard to pinpoint which are responsible for the defect. Finally, and fascinatedly, their fourth allele encodes for a premature STOP codon resulting in the truncation of an entire α-helix that interacts with Stn1. It includes E127 and D138, two residues shown by our laboratory to be essential for the proteins to interact. How this mutant could be viable is unclear, although it may argue that another part of the surface can take over the essential interaction with Stn1.

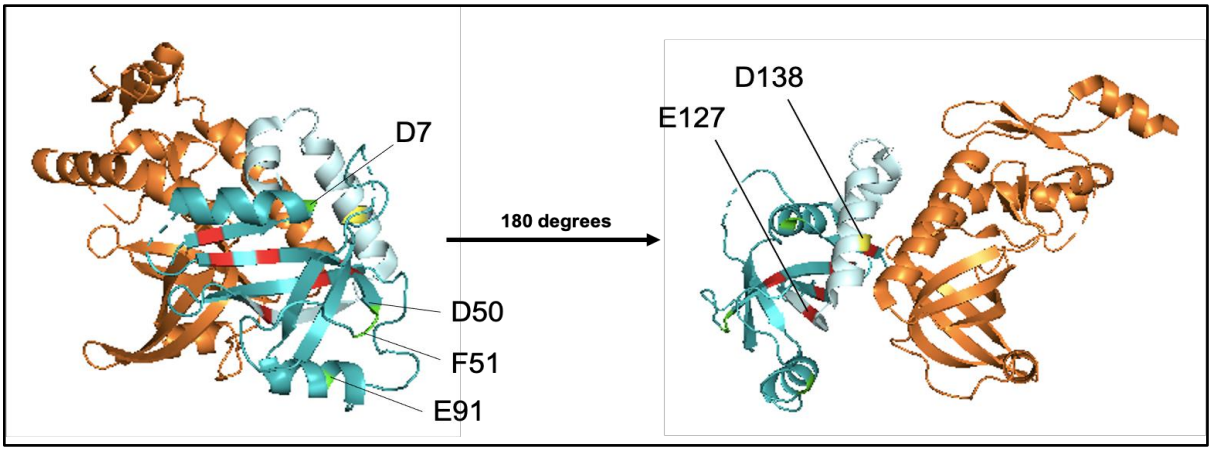

Figure A.4: Representation of the novel Ten1 alleles on the K. Lactis crystal structure
Stn1 and Ten1 are represented in orange and cyan, respectively. Alleles that are inviable through LOF are indicated in red whereas viable mutants are indicated in green. A previously characterized residue known for its importance in the interaction with Stn1 is highlighted in yellow. Estimated truncation area of the TS ten1-106 allele from Nugent and coworkers is shown in light cyan. PDB: 6LBU

Results of the epistasis analysis of Ten1

The inviable alleles were not pursued further as they logically cannot be successfully integrated into the genome. For mutants that were viable through LOF, the possibility that they might result in a severe defect could also make them inviable or temperature sensitive once integrated into the genome. Particularly, two of the mutants, *ten1-D7K* and *ten1-F51E*, were shown viable but sick and had the longest looking telomeres when run on a Southern blot. The F51A variant was viable and healthy on the LOF assay, therefore highlighting the idea of a greater defect on the surface when introducing a negative charge through *ten1-F51E*. We selected the sicker allele to be integrated, as it could potentially yield more noticeable phenotypes. Furthermore, its immediate proximity to the sequence and structure to another viable allele, *ten1-D50K*, as well as to the essential beta-barrel structure, renders the area particularly interesting for further studies.

All 4 viable alleles were successfully integrated using the standard pop-in pop-out protocol without giving an obvious or TS phenotype on their own, arguing against the possibility of an unstable protein. Those newly generated strains were crossed with key alleles for epistasis analysis. The initial goal of the experiment was to address whether the specific striking additive phenotype observed by *pol12-R248E* with mutants of Cdc13 and Stn1 could be generalized to all subunits of the t-RPA complex. As expected, their combination with The Pol12 defect resulted in a similar phenotype, with a viability of the double mutants ranging from sick to lethal after a couple cell divisions, in accordance with the severity of phenotypes observed for the individual Ten1 alleles when tested for LOF (**Table A.4**). This result argues that the viable allele found by LOF do affect an important function of the protein.

Table A.4: Size of the double mutant combinations of Pol12 and Ten1 alleles found

Pictures of 4 double mutant spores of the indicated single mutant crosses are shown. n.t. = not tested

Mutant	*ten1-D7K*	*ten1-D50K*	*ten1-F51E*	*ten1-E91K*
pol12-R248E		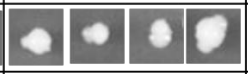	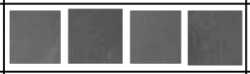	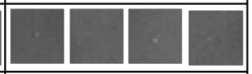
pol12-R322E	n.t.	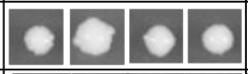		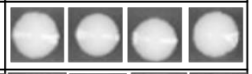
pol12-D303K	n.t.	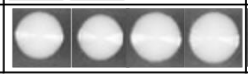	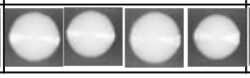	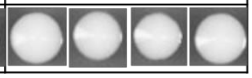

The variation of synthetic growth phenotype varied between *pol12-R248E* and *pol12-R322E* for each of the Ten1 mutants. *Ten1-F51E* was the most severe allele as its combination with either does not give rise to visible colonies. Yet, a closer look at the nature of the microcolonies of the double mutants shows that *pol12-R248E*'s stopped growing at no more than 5 cell divisions whereas *pol12-R322's* consistently divided a few more times, although never enough to be visible after 5 days of growth (**Figure A.5**).

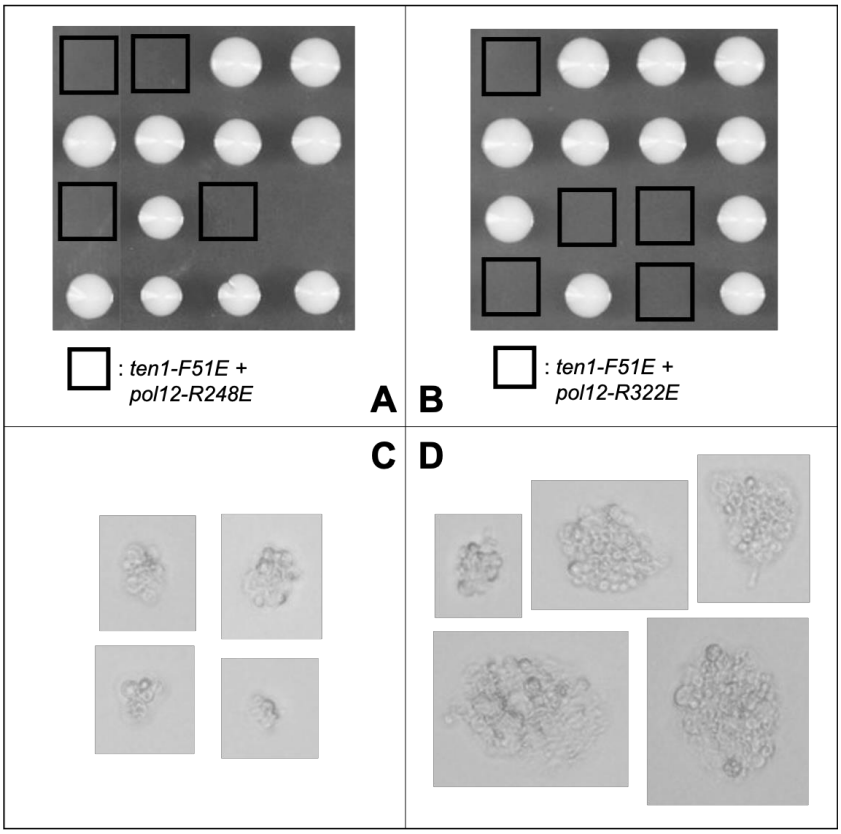

Figure A.5: Mutants of Ten1 are synthetically lethal with cdc13^{TS}-sensitive Pol12 alleles
Dissected spores were grown on YPAD media for 5 days and genotyped for (A) pol12-R248E and (B) pol12-R322E respectively (C and D) pictures of a subset of double mutant microcolonies were taken using a Zeiss Axioskop 50 with a Nikon Digital Sight DS-5M camera

However, the double *ten1-E91K* and *pol12-R248E* barely formed visible colonies whereas *ten1-E91K* and *pol12-R322E* grew to almost WT size (**Figure A.6**). This result may argue for a distinct function of Ten1 being altered compared to the previous allele. Indeed, this residue is the only one not closely located to the beta-barrel structure of the protein, although being a part of a helix thought to be important for the OB-fold stability (*Bryan et al., 2013*). This result cannot be due to an experimental error in strain-making as all individual mutants were previously tested and showed different growth phenotypes compared with the double mutants.

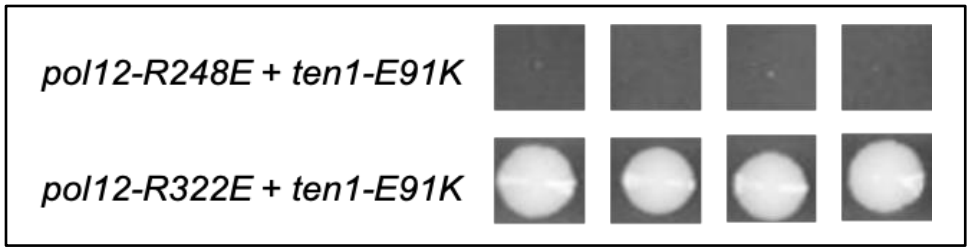

Figure A.6: Size comparison of the combination of *ten1-E91K* with Pol12 alleles
Spores of the indicated genotype were grown for 5 days before being genotyped and photographed

Finally, although close in size, the double mutants of *Ten1-D50K* crossed with both Pol12 alleles were very irregular in shape compared to that with *pol12-D303K*. This phenotype could possibly be the sign of an uneven, chaotic cell cycling happening in the cells. It has indeed been shown that the genotype can influence colony morphology. This feature has even been used as a selection tool for genetic suppressor screenings (*Granek and Magwene, 2010, Furukawa, 2011*). However, this allele of Ten1, as well as the others, showed no effect with *rad27Δ*, arguing for a distinct function from *pol12-R248E* that is able to rescue the knock-out through activation of the DNA damage checkpoint repair pathway.

APPENDIX B:
Genetic analysis of Pol30, processivity factor of the replisome

Introduction: PCNA

Proliferating Cell Nuclear Antigen (PCNA) is a ring-shaped complex that surrounds the DNA strand and guides the fork machinery throughout replication. In *S. cerevisiae*, it is made out of a homotrimer of Pol30 (*Bauer & Burgers, 1990*). PCNA is essential, highly conserved up to Humans, and thought to have important functions in recruiting proteins necessary for DNA replication and repair (*Maga and Hubscher, 2003*). It is indeed necessary for activation of post-replicative repair processes, which happens among others when Okazaki fragments aren't processed properly (*Nguyen et al., 2013, Becker et al., 2015*). The protein is post-translationally modified through ubiquitination, sumoylation and/or acetylation of well characterized residues in order to perform its post-replication DNA damage protein recruitment function (*Stelter and Ulrich, 2003*). Although not a direct player of telomere homeostasis, it is known to interact with factors resulting in elongated telomeres when disrupted (*Adams and Holm, 1996, Johnson et al., 2016*). According to recent studies, this phenotype is also thought to be linked to a defect in stress response (*Henninger et al., 2020, Shen et al., 2021*).

Yet, similarly to Pol12 and Ten1, the rest of the surface stays fairly unexplored. To this day, there are a few studies looking at surface residues of the protein beyond the post-translationally modified ones, while mostly focusing on DNA damage defects (*Ayyagari et al., 1995*, *Lau et al., 2002, Bowman et al., 2004, Halmai et al., 2016, Jiang et al., 2019*). We therefore wanted to investigate whether the ODN assay could yield novel or known alleles of the protein that could help us understand its function within the replication fork and how it may impact telomere homeostasis.

Material and methods: Pol30

Table B.1: List of plasmids used for the ODN assay in this appendix

Plasmid #	Content
pVL399	*2μ LEU2 ADH*
pVL6304	*2μ LEU2 ADH-POL30*
pBMB68	*2μ LEU2 ADH-pol30-E3K*
pBMB76	*2μ LEU2 ADH-pol30-R61E*
pMAM475	*2μ LEU2 ADH-pol30-K107R*
pMAM477	*2μ LEU2 ADH-pol30-K164R*
pMAM686	*2μ LEU2 ADH-pol30-D41A*
pBMB75	*2μ LEU2 ADH-pol30-D41K*
pMAM687	*2μ LEU2 ADH-pol30-D42A*
pMAM470	*2μ LEU2 ADH-pol30-D42K*
pMAM471	*2μ LEU2 ADH-pol30-D41A+D42A*
pMAM478	*2μ LEU2 ADH-pol30-L126A+I128A*
pMAM479	*2μ LEU2 ADH-pol30-P252A K253A*
pMAM596	*2μ LEU2 ADH-pol30-K20A*
pMAM594	*2μ LEU2 ADH-pol30-K13A*
pBMB78	*2μ LEU2 ADH-pol30-K77E*
pMAM598	*2μ LEU2 ADH-pol30-K146A*
pBMB89	*2μ LEU2 ADH-pol30-D124K*

Table B.2: List of strains used for epistasis analysis in this appendix

Strain #	Mutation	Mate type
yMAM360	*cdc9-1*	alpha
yMAM392	*pol30-D41A*	a
yMAM393	*pol30-D42K*	a
yMAM394	*pol30-D41A+D42A*	a
yMAM396	*pol30-D42A*	a
yVL2967	*WT*	a
yVL3584	*tlc1Δ*	alpha
yVL3737	*rad52Δ*	a
yVL4649	*cdc13-YYAA*	a
yVL4940	*pol32Δ*	a
yVL5025	*pol12-R248E*	alpha
yVL5026	*pol12-R322E*	alpha
yVL5027	*pol12-D303K*	alpha
yVL5184	*rpa1-t11*	a
yVL5411	*cdc2-2*	a
yVL5429	*pol30-R61E*	alpha
yVL5430	*pol30-K164R*	alpha
yVL5548	*pol30-K20A*	a
yVL5550	*cdc2-2*	alpha
yVL5552	*pol30-R61E*	a
yVL5558	*pol30-K20A*	alpha
yVL5562	*pol30-K164R*	a
yVL5648	*rad27Δ*	alpha

Results of the ODN assay on Pol30

A pilot study performed in our laboratory in 2012 looked at 100 mutants of the 258 amino acids protein using the ODN assay with a *cdc2-2* TS ($cdc2^{TS}$) strain. Cdc2 is a subunit of the polymerase delta complex, main partner of Pol30 during lagging strand replication (*Bauer & Burgers, 1990*). Polymerase delta is thought to take the place of polymerase alpha-primase to elongate Okazaki fragments using its proofreading activity (*Waga and Stillman 1998, Stodola and Burgers, 2017*). Using this strain for the ODN assay therefore highlighted potential mutants of Pol30 playing a role in lagging strand replication and possible related defects. It is worth noting that overexpression of Pol30 slightly impaired growth. This observation can be explained by its binding affinity for DNA, which may turn the protein into a physical obstacle when present at very high quantities in the cells. As detailed in chapter 2, analysis of ODN phenotypes is made in comparison to a control strain that overexpresses the WT protein for that reason.

The assay identified seven residues with a strong ODN phenotype in $cdc2^{TS}$ when mutated. All of them are located on the outer ring or side of the homotrimer. The list includes K164, sole ubiquitination site and unarguably the most characterized residue of the protein (*Hoege et al., 2002*). In contrast, another known post-translationally modified residue, K107, did not give such a phenotype when mutated. This result argues for distinct functions linked to those kind of post-translational modifications (**Figure B.1**)

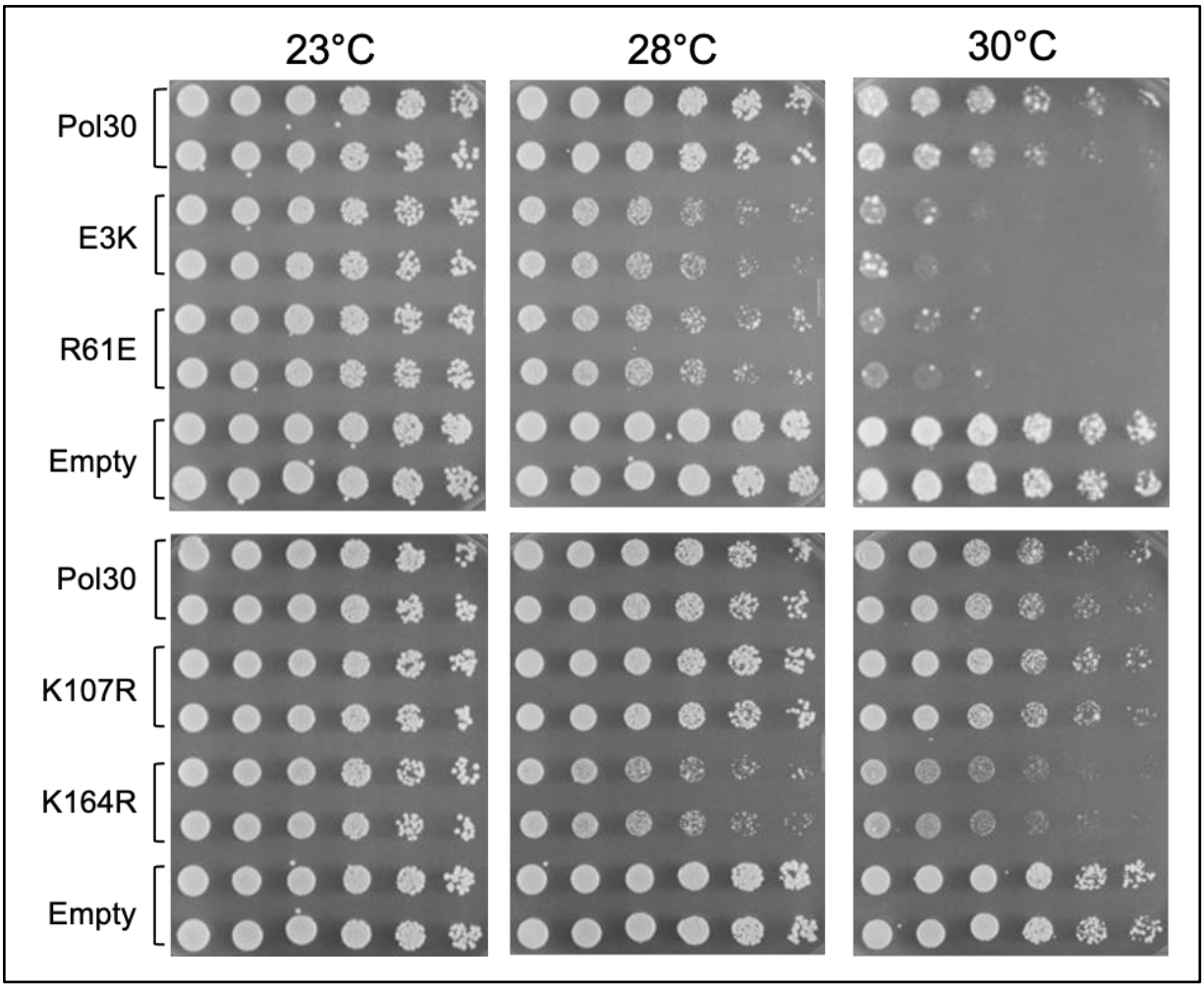

Figure B.1: Mutant of the outer ring of PCNA show an ODN phenotype with *cdc2^{TS}*
Strains with a mutation of Cdc2 inducing a temperature-sensitive (TS) phenotype were transformed under selective marker pressure with an overexpression 2 micron (2u) vector including the content indicated on the left side. Two independent colonies were grown, replica gridded at different dilutions and grown for 3 days at a gradient of increasing temperatures reducing viability of the strain.

The assay also found a residue of the Inter-Domain Connecting Loop (IDCL), through which most proteins, including Cdc2, are thought to interact with PCNA (*Eissenberg et al., 1997*). A closely located loop made of two arginines appears to be necessary for the complex recruitment by Replication Factor C (RFC) and was also highlighted by this assay (*Bowman et*

al., 2004). Interestingly, those two residues seem to give a different phenotype depending on the nature of the substitution (**Figure B.2**).

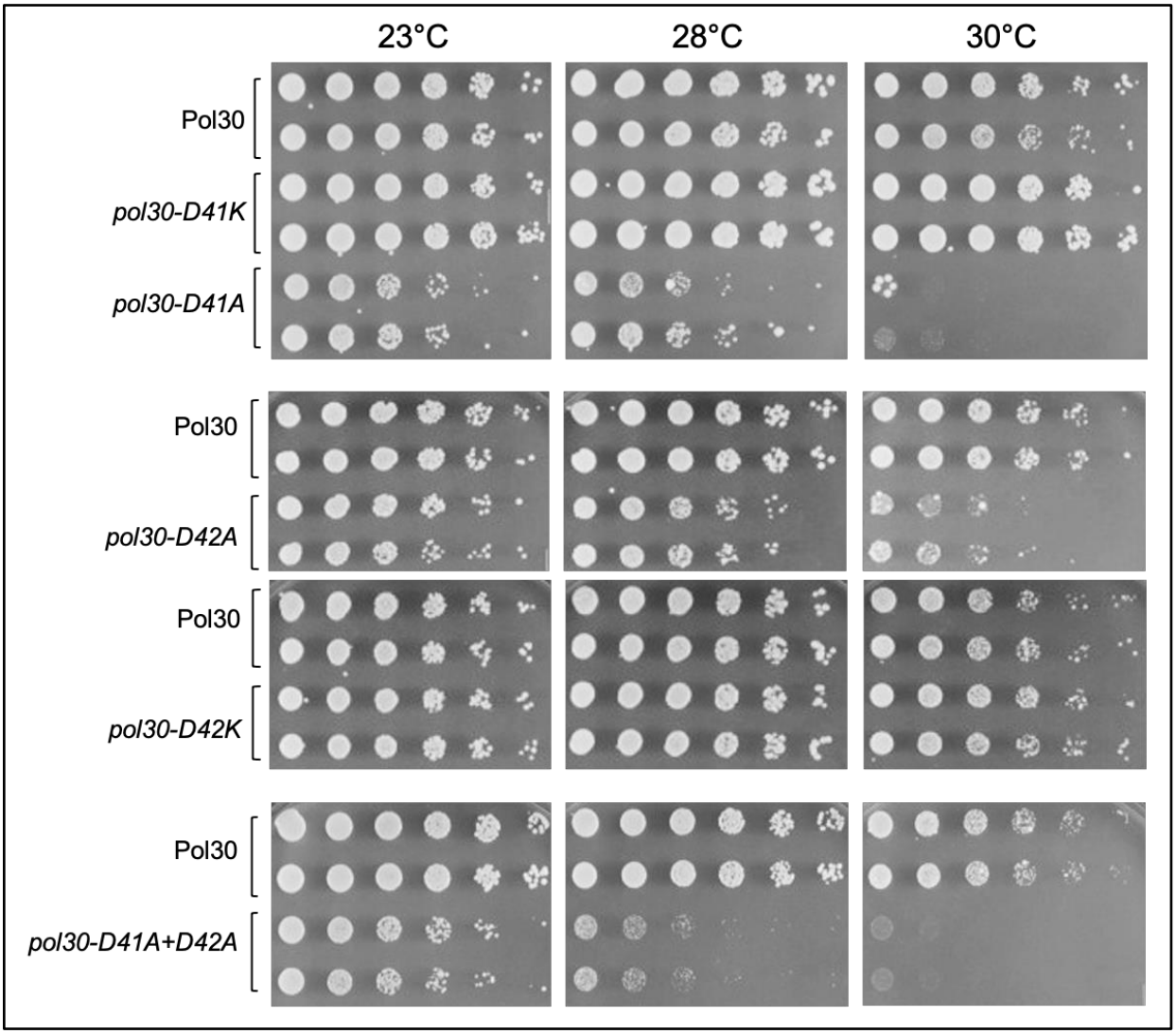

Figure B.2: IDCL residues D41 and D42 show opposite phenotypes with cdc2^{TS} depending on the nature of the mutation

Strains with a mutation of Cdc2 inducing a temperature-sensitive (TS) phenotype were transformed under selective marker pressure with an overexpression 2 micron (2u) vector including the content indicated on the left side. Two independent colonies were grown, replica gridded at different dilutions and grown for 3 days at a gradient of increasing temperatures reducing viability of the strain.

Similarly, neighboring published allele *pol30-L126A-I128A* gave an ODP phenotype in *cdc2*^{TS}. These mutants have since been characterized as pertaining to the same function in stabilizing the genome (*Brothers and Rine, 2019*). This is in contrast with another characterized double mutant, *pol30-K252A-P253A,* which although thought to play a similar role showed no ODN phenotype in that strain (**Figure B.3**).

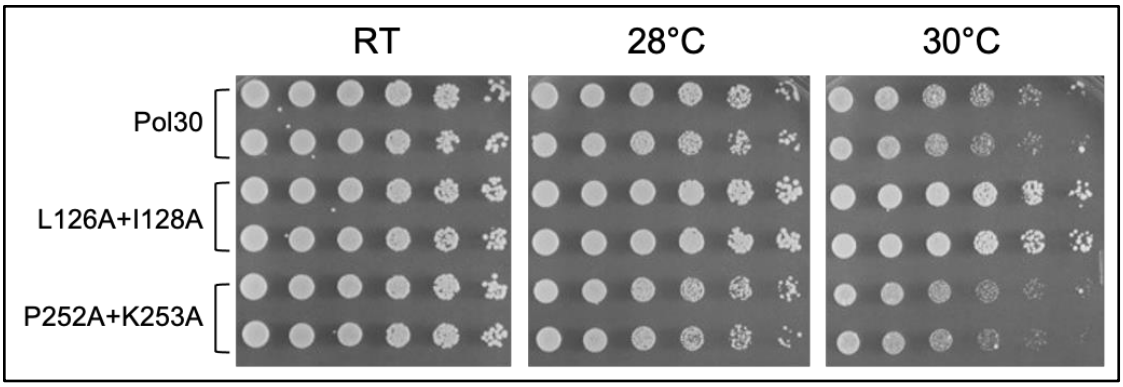

Figure B.3: Phenotype of characterized Pol30 alleles in cdc2^{TS}
Strains with a mutation of Cdc2 inducing a temperature-sensitive (TS) phenotype were transformed under selective marker pressure with an overexpression 2 micron (2u) vector including the content indicated on the left side.

Finally, a cluster of three polar residues known to disrupt gene silencing was highlighted *(Kondratick et al., 2018*). Every key residue found by this ODN assay was able to be placed on the existing yeast structure (**Figure B.4**).

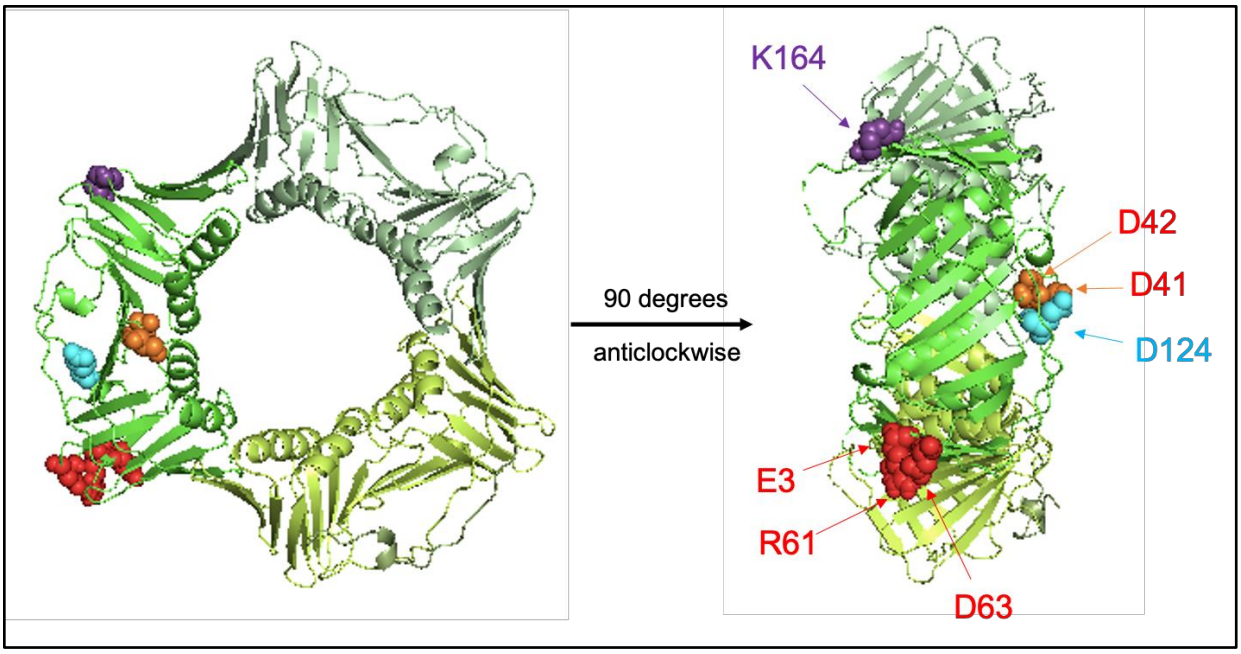

Figure B.4: Localization of the mutant showing an ODN phenotype in *cdc2^{TS}*
Each Pol30 molecule of the PCNA homotrimer is colored in a different shade of green. PDB# 3K4X

Following the promising pilot results, study of Pol30 was extended to additional residues in 2015 to be tested in a *cdc9^{TS}* allele. Cdc9 encodes DNA Ligase I, an enzyme that fuses the processed Okazaki fragments into the continuous replicated lagging strand (*Johnston and Nasmyth, 1978*). Study of new Pol30 alleles highlighted a novel cluster, located on the inner ring of the trimer. Those residues showed a striking ODP phenotype, rescuing the temperature sensitivity nature of the sensitized strain. In Particular, it identified lysines K13, K20, K77 and K146 that are highly conserved up to Humans and directly interacts with the negatively charged DNA that PCNA surrounds (*McNally et al., 2010*). One particular residue, K20, has since been described as being acetylated and, because of its phenotype with *cdc9^{TS}*, was selected for further studies (*Billon et al., 2017*) (**Figure B.5**).

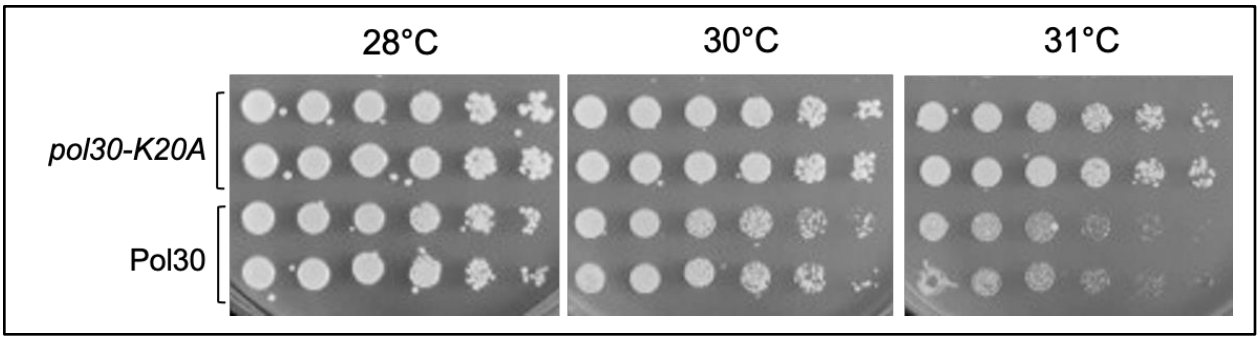

Figure B.5: Mutations of inner ring lysine residues rescue the TS phenotype of cdc9^{TS}
Strains with a mutation of Cdc9 inducing a temperature-sensitive (TS) phenotype were transformed under selective marker pressure with an overexpression 2 micron (2u) vector including the content indicated on the left side.

For comparison, none of the alleles found colocalized with the predicted Pol30-Cdc9 interface located at the C-terminal of the sequence, arguing that their effect pertains to DNA binding abilities rather than direct protein interaction (*Vijayakumar et al., 2007*). Interestingly, another lysine K107 was identified as giving a similar rescue phenotype in Cdc9 mutants (*Nguyen et al., 2013*). This particular residue isn't a part of the *K. lactis* crystal structure of PCNA, possibly arguing that it is on a highly mobile portion of the surface. Although not being a part of the inner ring of the complex, it localizes on the *S. cerevisiae* structure fairly close to the other lysines and could therefore possibly perform a singular function (**Figure B.6**). On that same crystal, the DNA strand that PCNA surrounds appears to directly interact with that area. Therefore, this function could be to bind DNA or help proteins bind to the DNA. Details of the residues found by ODN are detailed in **Table B.3**. Complete list of residues tested and their phenotypes can be found in **Table B.4**.

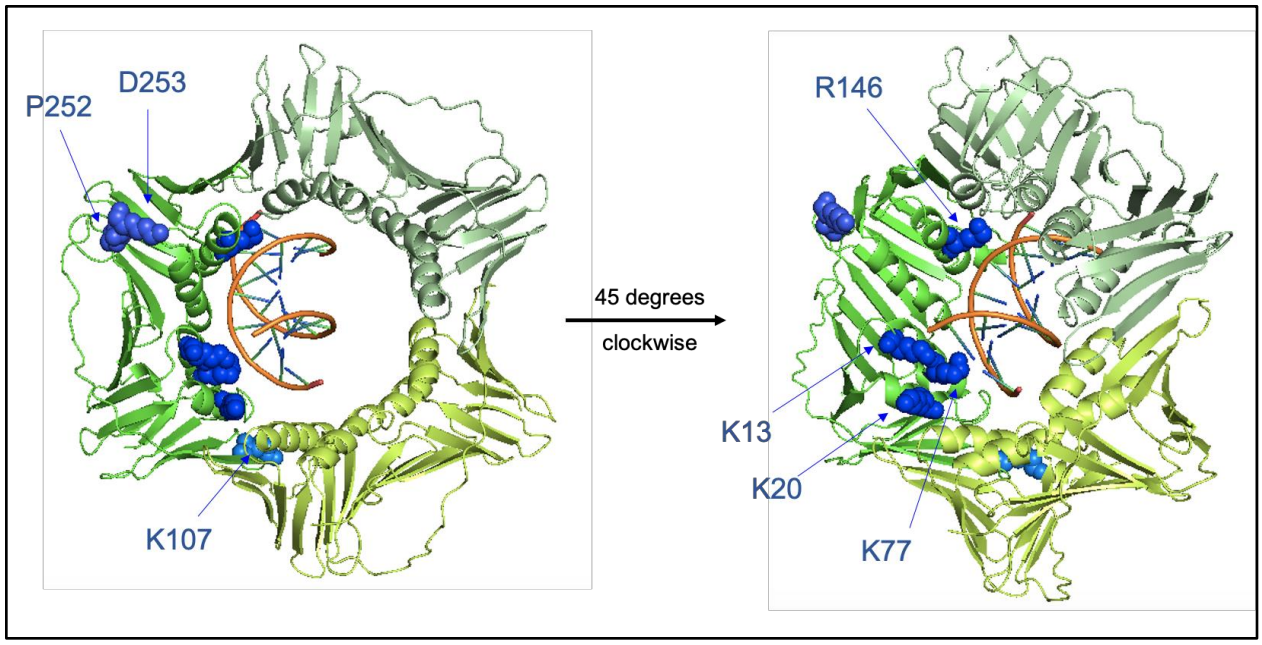

Figure B.6: Localization of the residues rescuing cdc9^{TS} on PCNA, in comparison to the DNA strand and known residues interacting with Cdc9

Each Pol30 molecule of the PCNA homotrimer is colored in a different shade of green. DNA strand is represented in orange. Known residues are indicated on the left structure. Residues with an ODN phenotype in cdc9^{TS} are indicated on the right structure. PDB 3K4X

Table B.3: Summary of the ODN assay on Pol30 and expected localization of the residues

Phenotypes were summarized using the following nomenclature:
no: no difference in growth phenotype compared to positive control (strain overexpressing Pol30)
n.t.: not tested
ODN: overexpression of the mutant results in lessened viability compared to positive control
ODP: overexpression of the mutant results in increased viability compared to positive control

Allele	Phenotype in $cdc2^{TS}$	Phenotype in $cdc9^{TS}$	Localization
E3K	ODN	no	Outer ring
R61E	ODN	no	Outer ring
D63K	ODN	no	Outer ring
K107R	no	n.t.	Outer ring
K164R	ODN	n.t.	Outer ring
P252A D253A	no	n.t.	Outer ring
K13A	n.t.	ODP	Inner ring
K20A	ODP	ODP	Inner ring
K77R	no	ODP	Inner ring
K146A	no	ODP	Inner ring
D41K	ODP	ODP	IDCL
D42K	ODN	n.t.	IDCL
D124K	ODN	ODN	IDCL
L126A I128A	ODP	n.t.	IDCL

Table B.4: Complete list of ODN assay results in Pol30

		yVL4090 (cdc2^{ts})				yVL4088 (cdc9^{ts})		
Plasmid #	**Mutation**	**RT**	**28°**	**30°**		**28°**	**30°**	**32°**
pVL399	**empty vector**	**++**	**++**	**++**		**++**	**++**	**+**
pVL6304	**WT Pol30**	**++**	**++**	**+**		**++**	**+**	**+/-**
pBMB 68	E3K	++	+	+/-		++	+	+/-
pMAM466	E3A	++	+	+/-		n.t.	n.t.	n.t.
pBMB 69	K5E	++	++	+/-		++	+	+/-
pMAM467	E3A + K5A	++	+	+/-		n.t.	n.t.	n.t.
pNAE 1	E7K	n.t.	n.t.	n.t.		++	+	+/-
pNAE 2	E8K	n.t.	n.t.	n.t.		++	+	+/-
pBMB 70	K13E	++	++	+/-		+++	++	+
pMAM594	K13A	n.t.	n.t.	n.t.		+++	++	++
pBMB 71	R14E	++	++	+/-		+++	++	+
pMAM595	R14A	n.t.	n.t.	n.t.		+++	++	+
pBMB 72	D17K	++	++	-/+		++	+	+/-
pBMB 73	K20E	++	++	+/-		+++	++	+
pMAM596	K20A	n.t.	n.t.	n.t.		+++	+++	++
pBMB 74	D21K	++	++	-/+		++	+	+/-
pMAM563	Q29K	n.t.	n.t.	n.t.		++	++	+
pNAE 3	K31E	n.t.	n.t.	n.t.		++	+	+/-
pNAE 4	E32K	n.t.	n.t.	n.t.		++	+	+/-
pNAE 5	D33K	n.t.	n.t.	n.t.		++	+	+/-
pMAM564	I36E	n.t.	n.t.	n.t.		++	++	+
pBMB 75	D41K	++	++	++		+++	++	+
pMAM470	D42K	++	++	+		n.t.	n.t.	n.t.
pMAM471	D41A D42A	(+)	+/-	-		n.t.	n.t.	n.t.
pMAM565	R44E	n.t.	n.t.	n.t.		+++	+++	++
pNAE 6	E51K	n.t.	n.t.	n.t.		++	+	+/-
pNAE 7	E55K	n.t.	n.t.	n.t.		++	+	+/-
pBMB 76	R61E	++	+	+/-		++	+	+/-
pMAM468	R61A	++	+	+/-		n.t.	n.t.	n.t.
pBMB 77	D63K	++	+	+/-		++	+	+/-
pMAM469	R61A D63A	++	+	+/-		n.t.	n.t.	n.t.
pNAE 10	H64E	n.t.	n.t.	n.t.		++	(+)?	+/-
pNAE 9	H64K	n.t.	n.t.	n.t.		n.t.	n.t.	n.t.
pMAM566	T67E	n.t.	n.t.	n.t.		++	++	+
pBMB 78	K77E	++	++	-/+		+++	++	+
pMAM597	K77A	n.t.	n.t.	n.t.		+++	++	+
pMAM472	R80E	++	++	+		n.t.	n.t.	n.t.
pMAM473	R80A	++	++	+		n.t.	n.t.	n.t.
pBMB 79	D86K	++	++	-/+		++	+	+/-
pMAM567	T89E	n.t.	n.t.	n.t.		++	++	+
pMAM568	T89K	n.t.	n.t.	n.t.		++	++	+
pBMB 80	D93K	++	++	-/+		++	+	+/-
pNAE 12	N94E	n.t.	n.t.	n.t.		++	+	+/-
pNAE 11	N94K	n.t.	n.t.	n.t.		++	+	+/-
pBMB 81	D97K	++	++	+		++	++	+/-
pMAM569	I100E	n.t.	n.t.	n.t.		++	++	+
pMAM570	L102E	n.t.	n.t.	n.t.		++	++	+
pBMB 82	E104K	++	+	-/+		++	+	+/-

Table B.4: Complete list of ODN assay results in Pol30 (cont.)

		yVL4090 (cdc2^{ts})				yVL4088 (cdc9^{ts})		
Plasmid #	**Mutation**	**RT**	**28°**	**30°**		**28°**	**30°**	**32°**
pVL399	**empty vector**	**++**	**++**	**++**		**++**	**++**	**+**
pVL6304	**WT Pol30**	**++**	**++**	**+**		**++**	**+**	**+/-**
pMAM474	E104A D105A	++	++	+		n.t.	n.t.	n.t.
pMAM475	K107R	++	++	+		n.t.	n.t.	n.t.
pBMB 83	D109K	++	+	-/+		++	+	+/-
pBMB 84	R110E	++	++	+/-		+++	++	+
pMAM571	I111K	n.t.	n.t.	n.t.		++	++	+
pBMB 85	E113K	++	++	-/+		++	+	+/-
pMAM573	S115P	n.t.	n.t.	n.t.		+++	+++	++
pBMB 86	K117E	++	+	-/+		++	+	+/-
pBMB 87	D120K	++	++	+/-		++	+	+/-
pBMB 88	D122K	++	++	-/+		++	+	-
pBMB 89	D124K	++	+/-	-		++	+	+/-
pMAM478	I126A L128A	++	++	++		n.t.	n.t.	n.t.
pMAM574	K127R	n.t.	n.t.	n.t.		++	++	+
pMAM575	E129K	n.t.	n.t.	n.t.		++	++	+
pMAM576	E130K	n.t.	n.t.	n.t.		++	++	+
pMAM577	T136E	n.t.	n.t.	n.t.		++	++	+
pBMB 90	E143K	++	++	-/+		++	+	+/-
pBMB 91	K146E	++	++	-/+		++	++	+/-
pMAM598	K146A	n.t.	n.t.	n.t.		++	++	++
pBMB 92	D150K	++	++	-/+		++	+	+/-
pMAM579	N159K	n.t.	n.t.	n.t.		++	++	+
pMAM580	M161K	n.t.	n.t.	n.t.		++	++	+
pBMB 93	K164E	++	++	-/+		++	+	+/-
pMAM477	K164R	++	+	+/-		n.t.	n.t.	n.t.
pMAM481	T166E	n.t.	n.t.	n.t.		++	++	+
pBMB 94	K168E	++	++	+/-		++	+	+/-
pBMB 95	D174K	++	++	+/-		++	+	+/-
pMAM582	S177E	n.t.	n.t.	n.t.		++	++	+
pMAM583	S179E	n.t.	n.t.	n.t.		++	++	+
pMAM584	I181E	n.t.	n.t.	n.t.		++	++	+
pMAM585	K196A	n.t.	n.t.	n.t.		++	++	+
pMAM586	E198K	n.t.	n.t.	n.t.		++	++	+
pMAM587	D204K	n.t.	n.t.	n.t.		++	++	+
pMAM588	T206K	n.t.	n.t.	n.t.		++	++	++
pBMB 96	K210E	++	++	-/+		++	++	+
pMAM599	K210A	n.t.	n.t.	n.t.		++	++	+
pMAM589	R224E	n.t.	n.t.	n.t.		++	++	+
pMAM590	R228E	n.t.	n.t.	n.t.		++	++	+
pMAM591	D240K	n.t.	n.t.	n.t.		++	++	+
pMAM592	F245E	n.t.	n.t.	n.t.		++	++	+
pMAM593	F245K	n.t.	n.t.	n.t.		++	++	+
pMAM480	F248A F249A	++	++	+		n.t.	n.t.	n.t.
pMAM481	A251V	++	++	+		n.t.	n.t.	n.t.
pMAM479	P252A K253A	++	++	+		n.t.	n.t.	n.t.
pBMB 98	K253E	++	++	-/+		++	++	+
pBMB 99	D256K	++	++	-/+		++	+	+/-
pBMB 100	E257K	++	++	-/+		++	+	+/-
pBMB 101	E258K	++	++	-/+		++	+	+

Results of the epistasis analysis of Pol30

The ODN assay highlighted four categories of residues on the surface of Pol30. The first category is located throughout the outer ring of the trimer, and contains residues known to be post-translationally modified. The second cluster is also on the outer ring but thought to play a distinct role in gene silencing. A third category of mutants alters the Inter-Domain Connecting Loop (IDCL) that is used for interactions with several proteins, such as RFC, through a recognition motif. Finally, a group of lysines cluster on the inner side of the ring-shaped complex where it interacts with DNA.

A representative subset of those residues found on Pol30 were integrated into the genome using the previously described pop-in pop-out protocol in order to be tested for epistasis analysis with key mutants. Strains were initially crossed with polymerase delta mutant *cdc2*^{TS}, in order to confirm the phenotypes found by the ODN assay. As expected, alanine mutants of the IDCL aspartic acids were synthetically lethal with the TS mutation. This result illustrates how important the PCNA-Cdc2 interaction is for viability. In fact, the IDCL is close to the C-terminal residues of Pol30 thought to be necessary for both proteins to interact. However, a single specific charge swap of the area, *pol30-D42K*, gave an opposite rescue phenotype (**Figure B.7**). This switch highlights the crucial importance of the residue, although whether it influences the interaction directly or indirectly is unclear.

Residues of the N-terminal outer ring cluster gave a similar synthetic lethal phenotype when disrupted. In fact, most of those allele combinations were fully lethal even at permissive temperature. Therefore, both regions of the proteins genetically interact towards a similar essential pathway. Interestingly, mutations of the inner ring residues rescued the TS phenotype, although to a lesser degree than *pol30-D42K*. This observation potentially indicates that the

DNA strand and Cdc2 sterically impede each other *in vivo*. Finally, mutation of ubiquitinated K164 had no synthetic effect although showing an ODN phenotype with the same strain, indicating that the result might have been linked to the overexpression of the mutated protein. For example, one could hypothesize that *pol30-K164R* accumulates on the DNA while not being able to activate post-replication repair processes, hindering viability, similarly to the overexpression of WT Pol30. Indeed, the residue is a target of polyubiquitination, degradation signal for the proteasome (*Haracska et al., 2004*).

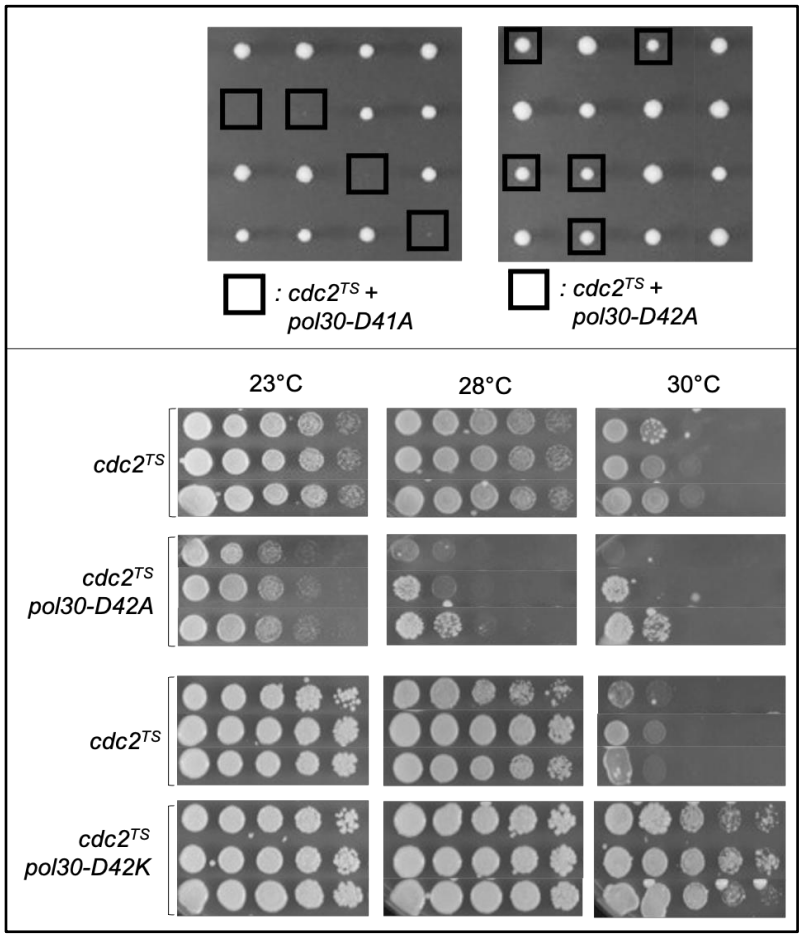

Figure B.7: IDCL residue D41 gives various phenotypes based on the nature of its mutation
(Top) 4 tetrads of cdc2^{TS} crossed with pol30-D41A (Left) or pol30-D42A (Right) were dissected vertically and grown at 30°C for 5 days before being photographed. Double mutant spores are indicated with a square. (Bottom) Spores of the indicated genotype were grown at room temperature (23°C) before being gridded and replica plated at serial dilutions and temperature

Pol30 mutant strains were also tested with a knock-out of non-essential Pol32. This gene encodes for one of the three subunits of polymerase delta, alongside Pol31 and Cdc2. Dispensability of a subunit is a surprising feature for the polymerase family. Its main role is to bind PCNA, and combinations of *pol32Δ* with some Pol30 mutants is inviable (*Johansson et al., 2004*). This epistasis analysis may therefore allow to identify additional areas of Pol30 that are essential for that interaction. Interestingly, Pol32 is also thought to interact with polymerase alpha through Pol1, and its absence leads to elongation of the telomeres, a phenotype extensively described throughout this thesis.

Interestingly, mutants of the IDCL that were lethal with $cdc2^{TS}$ showed no synthetic phenotype with *pol32Δ*. However, in complete opposition to the previous results, the *pol30-D42K* variant was close to inviable with the knock-out (**Figure B.8**). This striking result might indicate that the rescue phenotype of $cdc2^{TS}$ by *pol30-D42K* might depend on the presence of Pol32. This hypothesis could be tested by generation of the triple mutant. Similarly, mutants of the N-terminal gene silencing cluster did not have an additive phenotype with *pol32Δ*.

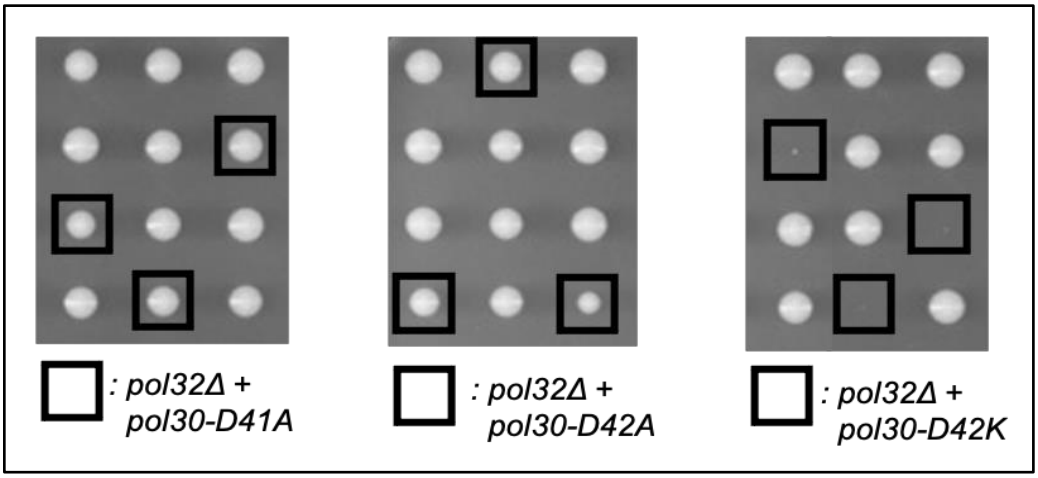

Figure B.8: IDCL residues had opposite phenotypes with pol32Δ compared to $cdc2^{TS}$
3 tetrads of pol32Δ crossed with mutants of Pol30-D41 and D42 were dissected vertically and grown at 30°C for 5 days before being photographed. Double mutant spores are indicated with a square.

Similar results were observed with two TS mutant strains of Cdc9, which encodes for Ligase I. This argues that the lowered interaction between PCNA and the DNA strand may facilitate protein interactions with the IDCL. In fact, epistasis analysis with several strains tested showed an additive growth defect with mutants of the PIP-box interacting domain found in the IDCL. Furthermore, they were also sick when combined with *rad27Δ*, an endonuclease that works with Cdc9 to process Okazaki fragments, as previously described (*Karanja and Livingston, 2004*).

Another notable result was found when crossing the Pol30 alleles with *rfa1-t11*. This previously characterized allele of the main subunit of Rpa1 is thought to also play a role in DNA repair pathways. Mutants of the N-terminal cluster of the outer ring of PCNA show a clear growth defect with the RPA allele. With that allele, mutation of K164 but not K107 was also sick. The exact same phenotype was observed with *rad52Δ* arguing that both alleles may pertain to the same pathway. Finally, the triple mutant was inviable, arguing for a possible redundancy of the proteins within an essential pathway (**Figure B.9**).

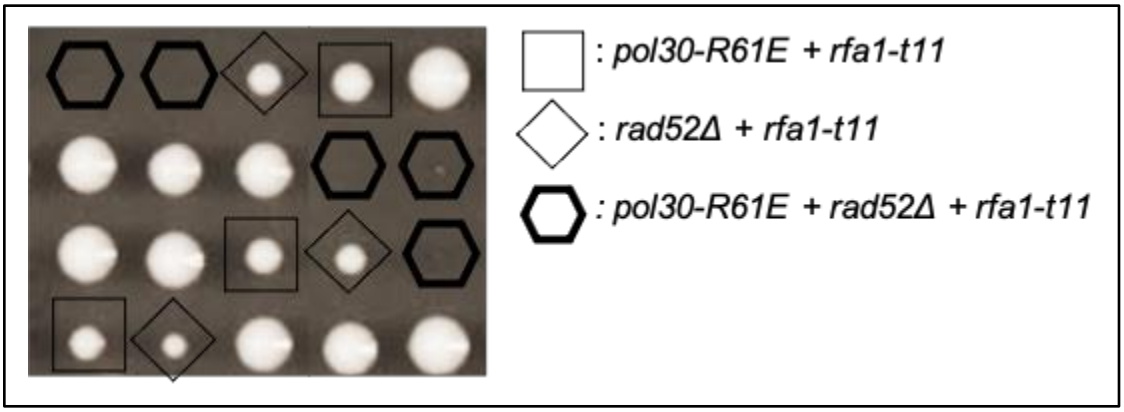

Figure B.9: Triple epistasis analysis of *pol30-R61E* with *rad52Δ* and *rpa-t11*
5 tetrads of diploid cells containing pol30-R61E, rfa1-t11 and rad52Δ were dissected vertically and grown at 30°C for 5 days before being photographed. Mutant spores genotype are indicated with various shapes.

Interestingly, this surface of Pol30 is mainly characterized by its ability to bind chromatin assembly factor Pop2 (*Zhang et al., 2000*). Its disruption results in a newly discovered impaired gene silencing linked to the lack of proper chromatin assembly (*Kondratick et al., 2018, Janke et al., 2018, Brothers and Rine, 2019*). On the other hand, RPA and Rad52 closely interact for homologous recombination (*Sugiyama et al., 1998*). The only existing evidence linking the two processes suggests the existence of a shared unknown pathway (*Schild 1995*). Whether PCNA is the link between the two processes for that unknown pathway has yet to be further investigated.

Finally, strains were tested on their influence on the senescence rate of a *tlc1Δ* strain. Surprisingly, strains that had shown opposite phenotypes with other mutants showed a similar acceleration of the senescence rate of the double mutant (**Figure B.10**).

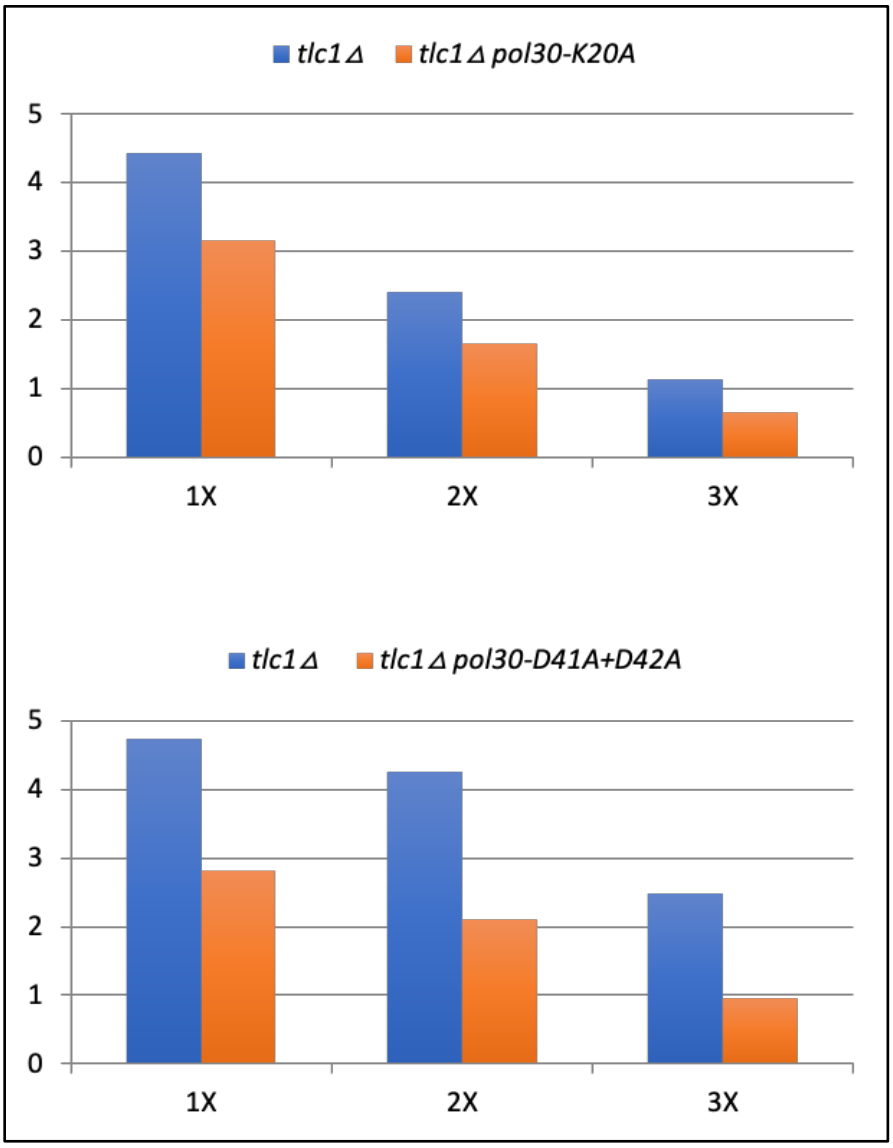

Figure B.10: Comparison of the average senescence rate of tlc1Δ in the presence or absence of (Top) pol30-K20A or (Bottom) pol30-D41A+D42A

The average growth score between 1 (inviable) and 5 (like WT) was recorded for n=40 (Top) and n=40 (bottom) individual spores genotyped for tlc1Δ::KAN through 3 successive streak-outs (1X to 3X). At 3X, spores were genotyped for Pol30 by PCR and restriction enzyme digestion. Scores were averaged for both tlc1Δ (n=27) and tlc1Δ + Pol30 mutant (n=13)

Interestingly, mutants of the N-terminal outer cluster and post-translationally modified residue K164 did not show such phenotype (**Figure B.11**).

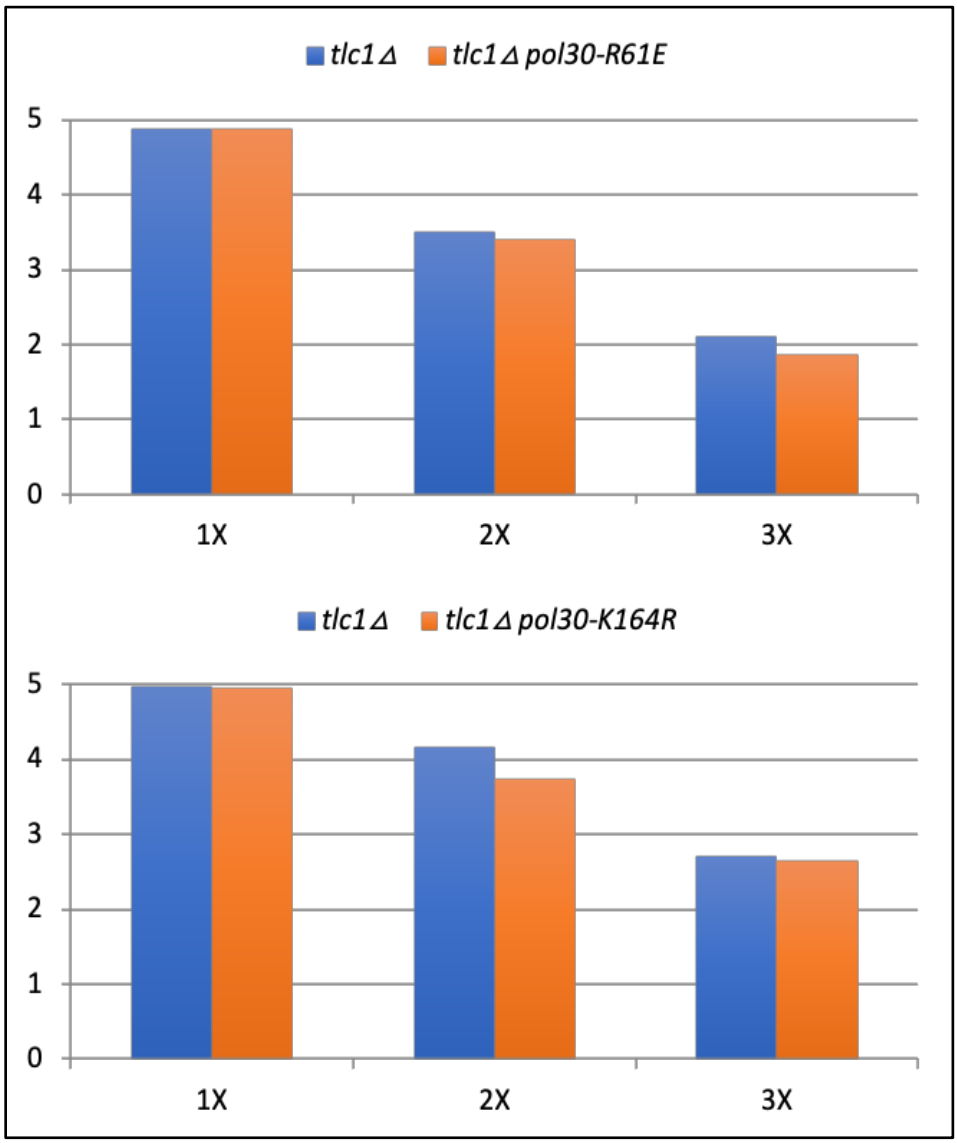

Figure B.11: Comparison of the average senescence rate of tlc1Δ in the presence or absence of pol30-R61E (Top) or pol30-K164R (Bottom)

The average growth score between 1 (inviable) and 5 (like WT) was recorded for n=52 (Top) and n=48 (Bottom) individual spores genotyped for tlc1Δ::KAN through 3 successive streak-outs (1X to 3X). At 3X, spores were genotyped for Pol30 by PCR and restriction enzyme digestion. Scores were averaged for both tlc1Δ (n=36 (Top) and n=33 (Bottom)) and tlc1Δ + pol30-R61E (n=16) or pol30-K164R (n=15)

Overall, the ODN assay highlighted many residues, some of which were already characterized, whereas others hadn't been discovered at the time. Epistasis analysis of Pol30 has brought up many hints as to what functions the different key residues and surface of the complex might perform. These functions ensure that the replication fork travels through the DNA strand smoothly. However, it also showed to have an impact on telomere length. As some mutants of Pol30 result in a premature senescence, it implies that Pol30 acts to positively regulate telomere length, although this regulation is presumably indirect. Indeed, mutants of Pol30 themselves do not show an obvious telomere homeostasis dysregulation that may have been observed in t-RPA or polymerase alpha-primase (**Figure B.12**).

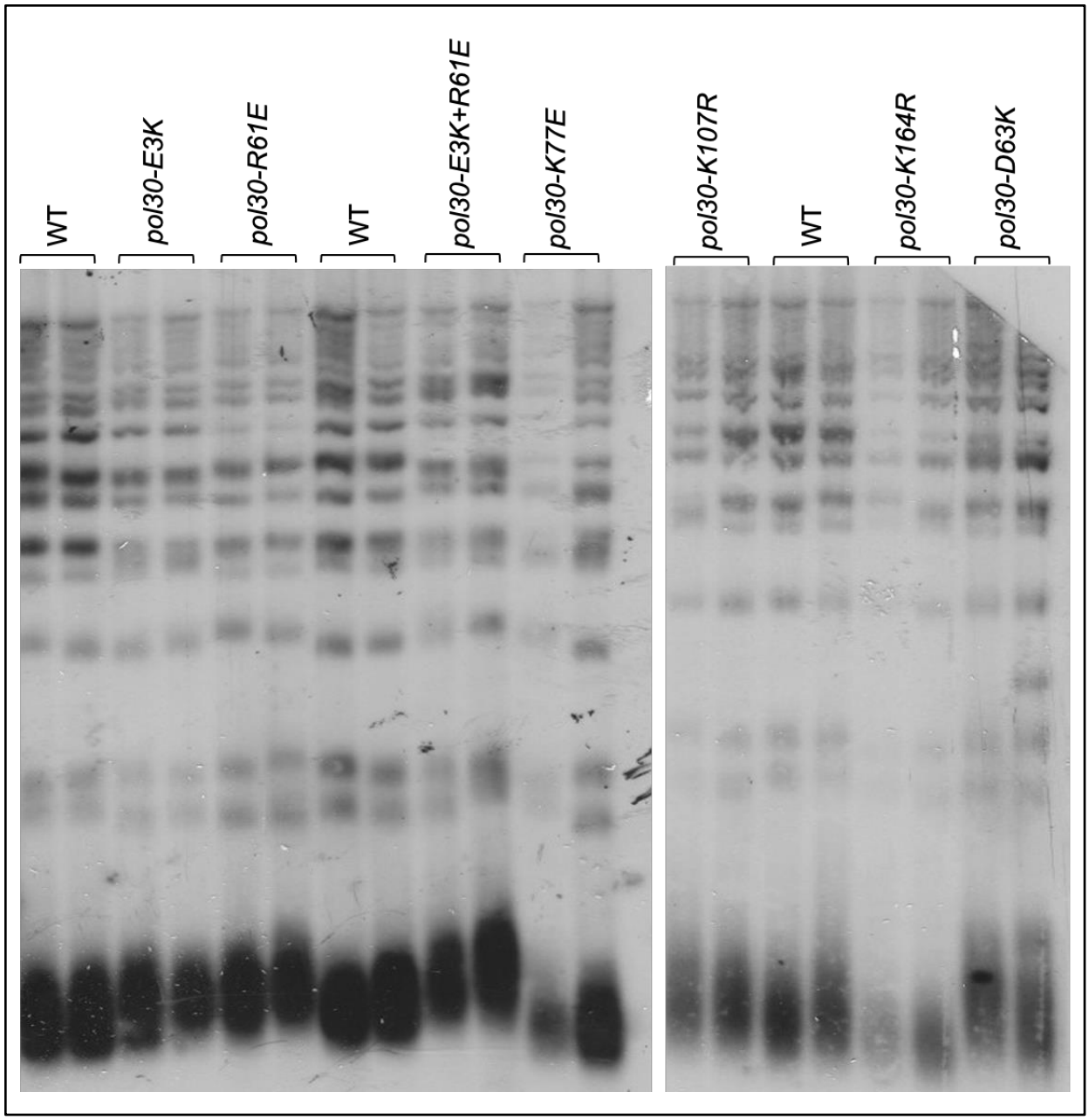

Figure B.12: Mutants of Pol30 do not show an obvious change in overall telomere length, as shown by Southern blot

Mutants of Pol30 or WT strains (yVL2967) are described above the blot.

Furthermore, mutants of those two complexes were crossed with key Pol30 alleles and did not show any significant growth differences. Therefore, it seems likely that this impact on telomere length is linked to the ability of the complex to interact with proteins that can help maintain homeostasis. Among those candidates are several proteins responsible for DNA damage processing. Epistasis analyses with those candidates are summarized in **Table B.5**.

Table B.5: Summary of epistasis analyses of Pol30

Expected function	Mutant	*Cdc2^{TS}*	*pol32Δ*	*Cdc9^{TS}*	*rad27Δ*	*Rpa1-t11*	*tlc1Δ*
DNA contact	*pol30-K20A*	*Rescue*	No effect	*Rescue*	No effect	No effect	Senesces faster
Protein contact	*pol30-D41A*	**Lethal**	No effect	**Lethal**	**sick**		Senesces faster
	pol30-D42A	**Lethal**	No effect	**Lethal**	**sick**		Senesces faster
	pol30-D42K	*Rescue*	**Lethal**		No effect		No effect
Gene silencing	*pol30-R61E*	**Lethal**	No effect	**Lethal**	No effect	**sick**	No effect
DNA repair	*pol30-K164R*	No effect	No effect	No effect	No effect	**sick**	No effect

References

Adams AK, Holm C. Specific DNA replication mutations affect telomere length in Saccharomyces cerevisiae. Mol Cell Biol. 1996;16(9):4614-4620.

Anbalagan S, Bonetti D, Lucchini G, Longhese MP. Rif1 supports the function of the CST complex in yeast telomere capping. PLoS Genet. 2011;7(3):e1002024.

Aravind L, Koonin EV. Phosphoesterase domains associated with DNA polymerases of diverse origins. Nucleic Acids Res. 1998;26(16):3746-52.

Audry, J., Maestroni, L., Delagoutte, E., Gauthier, T., Nakamura, T. M., Gachet, Y., Saintomé, C., Géli, V., & Coulon, S. (2015). RPA prevents G-rich structure formation at lagging-strand telomeres to allow maintenance of chromosome ends. The EMBO journal, 34(14), 1942–1958.

Ayyagari R, Impellizzeri KJ, Yoder BL, Gary SL, Burgers PM. A mutational analysis of the yeast proliferating cell nuclear antigen indicates distinct roles in DNA replication and DNA repair. Mol Cell Biol. 1995;15(8):4420-4429.

Ayyagari R, Gomes XV, Gordenin DA, Burgers PMJ. Okazaki fragment maturation in yeast. I. Distribution of functions between FEN1 AND DNA2. J Biol Chem. 2003;278(3):1618-1625.

Ballew BJ, Lundblad V. Multiple genetic pathways regulate replicative senescence in telomerase-deficient yeast. Aging Cell. 2013;12(4):719-727.

Bando, M., Katou, Y., Komata, M., Tanaka, H., Itoh, T., Sutani, T., & Shirahige, K. (2009). Csm3, Tof1, and Mrc1 form a heterotrimeric mediator complex that associates with DNA replication forks. The Journal of biological chemistry, 284(49), 34355–34365.

Baranovskiy, A. G., Babayeva, N. D., Zhang, Y., Gu, J., Suwa, Y., Pavlov, Y. I., & Tahirov, T. H. (2016). Mechanism of Concerted RNA-DNA Primer Synthesis by the Human Primosome. The Journal of biological chemistry, 291(19), 10006–10020.

Bauer GA, Burgers PM. Molecular cloning, structure and expression of the yeast proliferating cell nuclear antigen gene. Nucleic Acids Res. 1990;18(2):261-265.

Becker, J. R., Pons, C., Nguyen, H. D., Costanzo, M., Boone, C., Myers, C. L., & Bielinsky, A. K. (2015). Genetic Interactions Implicating Postreplicative Repair in Okazaki Fragment Processing. PLoS genetics, 11(11), e1005659.

Bernad A, Zaballos A, Salas M, Blanco L. Structural and functional relationships between prokaryotic and eukaryotic DNA polymerases. EMBO J. 1987;6(13):4219-25.

Bennett HW, Liu N, Hu Y, King MC. TeloPCR-seq: a high-throughput sequencing approach for telomeres.
FEBS Lett. 2016;590(23):4159-4170.

Billon P, Li J, Lambert JP, Chen Y, Tremblay V, Brunzelle JS, Gingras AC, Verreault A, Sugiyama T, Couture JF, Côté J. Acetylation of PCNA Sliding Surface by Eco1 Promotes Genome Stability through Homologous Recombination. Mol Cell. 2017 Jan 5;65(1):78-90.

Boeke JD, Trueheart J, Natsoulis G, Fink GR. 5-Fluoroorotic acid as a selective agent in yeast molecular genetics. Meth Enzymol. 1987;154:164-75.

Braun KA, Lao Y, He Z, Ingles CJ, Wold MS. Role of protein-protein interactions in the function of replication protein A (Rpa): RPA modulates the activity of DNA polymerase alpha by multiple mechanisms. Biochemistry. 1997;36(28):8443-8454.

Brooke RG, Dumas LB. Reconstitution of the Saccharomyces cerevisiae DNA primase-DNA polymerase protein complex in vitro. The 86-kDa subunit facilitates but is not required for complex formation. J Biol Chem. 1991;266(16):10093-10098.

Brothers M, Rine J. POL30 alleles in Saccharomyces cerevisiae reveal complexities of the cell cycle and ploidy on heterochromatin assembly. bioRxiv. Published online June 22, 2019:679829.

Bryan C, Rice C, Harkisheimer M, Schultz DC, Skordalakes E. Structure of the human telomeric Stn1-Ten1 capping complex. PLoS One. 2013;8(6):e66756.

Budd ME, Wittrup KD, Bailey JE, Campbell JL. DNA polymerase I is required for premeiotic DNA replication and sporulation but not for X-ray repair in Saccharomyces cerevisiae. Mol Cell Biol. 1989;9(2):365-376.

Budd ME, Campbell JL. A yeast replicative helicase, Dna2 helicase, interacts with yeast FEN-1 nuclease in carrying out its essential function. Mol Cell Biol. 1997;17(4):2136-2142.

Budd ME, Choe W c, Campbell JL. The nuclease activity of the yeast DNA2 protein, which is related to the RecB-like nucleases, is essential in vivo. J Biol Chem. 2000;275(22):16518-16529.

Calvo, O., Grandin, N., Jordán-Pla, A., Miñambres, E., González-Polo, N., Pérez-Ortín, J. E., & Charbonneau, M. (2019). The telomeric Cdc13-Stn1-Ten1 complex regulates RNA polymerase II transcription. Nucleic acids research, 47(12), 6250–6268.

Calzada A, Hodgson B, Kanemaki M, Bueno A, Labib K. Molecular anatomy and regulation of a stable replisome at a paused eukaryotic DNA replication fork. Genes Dev. 2005;19(16):1905-1919.

Carson MJ, Hartwell L. CDC17: an essential gene that prevents telomere elongation in yeast. Cell. 1985;42(1):249-57.

Chandra A, Hughes TR, Nugent CI, Lundblad V. Cdc13 both positively and negatively regulates telomere replication. Genes Dev. 2001;15(4):404-414.

Chang M, Arneric M, Lingner J. Telomerase repeat addition processivity is increased at critically short telomeres in a Tel1-dependent manner in Saccharomyces cerevisiae. Genes Dev. 2007;21(19):2485-2494.

Chen L-Y, Majerská J, Lingner J. Molecular basis of telomere syndrome caused by CTC1 mutations. Genes Dev. 2013;27(19):2099-2108.

Collins K, Mitchell JR. Telomerase in the human organism. Oncogene. 2002;21(4):564-579.

Costanzo M, Baryshnikova A, Bellay J, Kim Y, Spear ED, Sevier CS, Ding H, Koh JL, Toufighi K, Mostafavi S, Prinz J, St Onge RP, VanderSluis B, Makhnevych T, Vizeacoumar FJ, Alizadeh S, Bahr S, Brost RL, Chen Y, Cokol M, Deshpande R, Li Z, Lin ZY, Liang W, Marback M, Paw J, San Luis BJ, Shuteriqi E, Tong AH, van Dyk N, Wallace IM, Whitney JA, Weirauch MT, Zhong G, Zhu H, Houry WA, Brudno M, Ragibizadeh S, Papp B, Pál C, Roth FP, Giaever G, Nislow C, Troyanskaya OG, Bussey H, Bader GD, Gingras AC, Morris QD, Kim PM, Kaiser CA, Myers CL, Andrews BJ, Boone C. The genetic landscape of a cell. Science. 2010 Jan 22;327(5964):425-31. doi: 10.1126/science.1180823.

Cunningham BC, Wells JA. High-resolution epitope mapping of hGH-receptor interactions by alanine-scanning mutagenesis. Science. 1989;244(4908):1081-5.

Dang TT, Morales JC. Involvement of pola2 in double strand break repair and genotoxic stress. Int J Mol Sci. 2020;21(12).

Djinovic-carugo K, Carugo O. Missing strings of residues in protein crystal structures. Intrinsically Disordered Proteins. 2015;3(1):e1095697.

Doksani Y, de Lange T. The role of double-strand break repair pathways at functional and dysfunctional telomeres. Cold Spring Harb Perspect Biol. 2014;6(12).

Dua R, Levy DL, Campbell JL. Role of the putative zinc finger domain of Saccharomyces cerevisiae DNA polymerase epsilon in DNA replication and the S/M checkpoint pathway. J Biol Chem. 1998;273(45):30046-30055.

Dubarry M, Lawless C, Banks AP, Cockell S, Lydall D. Genetic networks required to coordinate chromosome replication by dna polymerases α, δ, and ε in saccharomyces cerevisiae. G3 (Bethesda). 2015;5(10):2187-2197.

Eissenberg JC, Ayyagari R, Gomes XV, Burgers PM. Mutations in yeast proliferating cell nuclear antigen define distinct sites for interaction with DNA polymerase delta and DNA polymerase epsilon. Mol Cell Biol. 1997;17(11):6367-6378.

Eitan E, Hutchison ER, Mattson MP. Telomere shortening in neurological disorders: an abundance of unanswered questions. Trends Neurosci. 2014;37(5):256-263.

Van Esch H, Colnaghi R, Freson K, Starokadomskyy P, Zankl A, Backx L, Abramowicz I, Outwin E, Rohena L, Faulkner C, Leong GM, Newbury-Ecob RA, Challis RC, Õunap K, Jaeken J, Seuntjens E, Devriendt K, Burstein E, Low KJ, O'Driscoll M. Defective DNA Polymerase α-Primase Leads to X-Linked Intellectual Disability Associated with Severe Growth Retardation, Microcephaly, and Hypogonadism. Am J Hum Genet. 2019 May 2;104(5):957-967. doi: 10.1016/j.ajhg.2019.03.006.

Evans SK, Lundblad V. Est1 and Cdc13 as co-mediators of telomerase access. Science. 1999;286(5437):117-20.

Fan X, Price CM. Coordinate regulation of G- and C strand length during new telomere synthesis. Mol Biol Cell. 1997;8(11):2145-2155.

Farrow MA, Somasundaran M, Zhang C, Gabuzda D, Sullivan JL, Greenough TC. Nuclear localization of HIV type 1 Vif isolated from a long-term asymptomatic individual and potential role in virus attenuation. AIDS Res Hum Retroviruses. 2005;21(6):565-74.

Feng X, Hsu S-J, Bhattacharjee A, Wang Y, Diao J, Price CM. CTC1-STN1 terminates telomerase while STN1-TEN1 enables C-strand synthesis during telomere replication in colon cancer cells. Nat Commun. 2018;9(1):2827.

Ferrari M, Lucchini G, Plevani P, Foiani M. Phosphorylation of the DNA polymerase alpha-primase B subunit is dependent on its association with the p180 polypeptide. J Biol Chem. 1996;271(15):8661-8666.

Foiani M, Marini F, Gamba D, Lucchini G, Plevani P. The B subunit of the DNA polymerase alpha-primase complex in Saccharomyces cerevisiae executes an essential function at the initial stage of DNA replication. Mol Cell Biol. 1994;14(2):923-33.

Foiani M, Liberi G, Lucchini G, Plevani P. Cell cycle-dependent phosphorylation and dephosphorylation of the yeast DNA polymerase alpha-primase B subunit. Mol Cell Biol. 1995;15(2):883-91.

Firbank SJ, Wardle J, Heslop P, Lewis RJ, Connolly BA. Uracil recognition in archaeal DNA polymerases captured by X-ray crystallography. J Mol Biol. 2008;381(3):529-539.

Flynn RL, Zou L. Oligonucleotide/oligosaccharide-binding (Ob) fold proteins: a growing family of genome guardians. Crit Rev Biochem Mol Biol. 2010;45(4):266-275.

Flynn RL, Chang S, Zou L. RPA and POT1: friends or foes at telomeres? Cell Cycle. 2012;11(4):652-657.

Furukawa K, Furukawa T, Hohmann S. Efficient construction of homozygous diploid strains identifies genes required for the hyper-filamentous phenotype in Saccharomyces cerevisiae. PLoS One. 2011;6(10):e26584.

Futcher AB. The 2 micron circle plasmid of Saccharomyces cerevisiae. Yeast. 1988;4(1):27-40.

Francesconi S, Longhese MP, Piseri A, Santocanale C, Lucchini G, Plevani P. Mutations in conserved yeast DNA primase domains impair DNA replication in vivo. Proc Natl Acad Sci U S A. 1991;88(9):3877-3881.

Friedrich U, Griese E, Schwab M, Fritz P, Thon K, Klotz U. Telomere length in different tissues of elderly patients. Mech Ageing Dev. 2000;119(3):89-99.

Ganduri S, Lue NF. STN1–POLA2 interaction provides a basis for primase-pol α stimulation by human STN1. Nucleic Acids Res. 2017;45(16):9455-9466.

Gao H, Cervantes RB, Mandell EK, Otero JH, Lundblad V. RPA-like proteins mediate yeast telomere function. Nat Struct Mol Biol. 2007;14(3):208-214.

Garcia JS, Ciufo LF, Yang X, Kearsey SE, MacNeill SA. The C-terminal zinc finger of the catalytic subunit of DNA polymerase δ is responsible for direct interaction with the B-subunit. Nucleic Acids Res. 2004;32(10):3005-3016.

Garvik B, Carson M, Hartwell L. Single-stranded DNA arising at telomeres in cdc13 mutants may constitute a specific signal for the RAD9 checkpoint. Mol Cell Biol. 1995;15(11):6128-38.

Gatbonton T, Imbesi M, Nelson M, Akey JM, Ruderfer DM, Kruglyak L, Simon JA, Bedalov A. Telomere length as a quantitative trait: genome-wide survey and genetic mapping of telomere length-control genes in yeast. PLoS Genet. 2006 Mar;2(3):e35. doi: 10.1371/journal.pgen.0020035.

Ge Y, Wu Z, Chen H, Zhong Q, Shi S, Li G, Wu J, Lei M. Structural insights into telomere protection and homeostasis regulation by yeast CST complex. Nat Struct Mol Biol. 2020 Aug;27(8):752-762. doi: 10.1038/s41594-020-0459-8.

Gelinas AD, Paschini M, Reyes FE, Héroux A, Batey RT, Lundblad V, Wuttke DS. Telomere capping proteins are structurally related to RPA with an additional telomere-specific domain. Proc Natl Acad Sci U S A. 2009 Nov;106(46) 19298-19303. doi:10.1073/pnas.0909203106.

Gietz RD, Sugino A. New yeast-Escherichia coli shuttle vectors constructed with in vitro mutagenized yeast genes lacking six-base pair restriction sites. Gene. 1988;74(2):527-534.

Glustrom LW, Lyon KR, Paschini M, Reyes CM, Parsonnet NV, Toro TB, Lundblad V, Wuttke DS. Single-stranded telomere-binding protein employs a dual rheostat for binding affinity and specificity that drives function. Proc Natl Acad Sci U S A. 2018 Oct 9;115(41):10315-10320. doi: 10.1073/pnas.1722147115.

Gobbini E, Cassani C, Villa M, Bonetti D, Longhese MP. Functions and regulation of the MRX complex at DNA double-strand breaks. Microb Cell. 2016;3(8):329-337.

Goulian M, Heard CJ. The mechanism of action of an accessory protein for DNA polymerase alpha/primase. J Biol Chem. 1990;265(22):13231-9.

Goulian M, Heard CJ, Grimm SL. Purification and properties of an accessory protein for DNA polymerase alpha/primase. J Biol Chem. 1990;265(22):13221-30.

Goulian M, Richards SH, Heard CJ, Bigsby BM. Discontinuous DNA synthesis by purified mammalian proteins. J Biol Chem. 1990;265(30):18461-18471.

Grandin N, Reed SI, Charbonneau M. Stn1, a new Saccharomyces cerevisiae protein, is implicated in telomere size regulation in association with Cdc13. Genes Dev. 1997;11(4):512-27.

Grandin N, Damon C, Charbonneau M. Cdc13 cooperates with the yeast Ku proteins and Stn1 to regulate telomerase recruitment. Mol Cell Biol. 2000;20(22):8397-8408.

Grandin N, Damon C, Charbonneau M. Ten1 functions in telomere end protection and length regulation in association with Stn1 and Cdc13. EMBO J. 2001;20(5):1173-83.

Grandin N, Charbonneau M. RPA provides checkpoint-independent cell cycle arrest and prevents recombination at uncapped telomeres of Saccharomyces cerevisiae. DNA Repair (Amst). 2013;12(3):212-226.

Granek JA, Magwene PM. Environmental and genetic determinants of colony morphology in yeast. PLOS Genetics. 2010;6(1):e1000823.

Gravel S, Larrivée M, Labrecque P, Wellinger RJ. Yeast Ku as a regulator of chromosomal DNA end structure. Science. 1998;280(5364):741-744.

Grossi S, Puglisi A, Dmitriev PV, Lopes M, Shore D. Pol12, the B subunit of DNA polymerase alpha, functions in both telomere capping and length regulation. Genes Dev. 2004;18(9):992-1006.

Halling SM, Sanchez-Anzaldo FJ, Fukuda R, Doi RH, Meares CF. Zinc is associated with the beta subunit of DNA-dependent RNA polymerase of Bacillus subtilis. Biochemistry. 1977;16(13):2880-2884.

Halmai M, Frittmann O, Szabo Z, Daraba A, Gali VK, Balint E, Unk I. Mutations at the Subunit Interface of Yeast Proliferating Cell Nuclear Antigen Reveal a Versatile Regulatory Domain. PLoS One. 2016 Aug 18;11(8):e0161307. doi: 10.1371/journal.pone.0161307.

Haracska L, Torres-Ramos CA, Johnson RE, Prakash S, Prakash L. Opposing effects of ubiquitin conjugation and sumo modification of pcna on replicational bypass of dna lesions in saccharomyces cerevisiae. Mol Cell Biol. 2004;24(10):4267-4274.

Hardy CF, Sussel L, Shore D. A RAP1-interacting protein involved in transcriptional silencing and telomere length regulation. Genes Dev. 1992;6(5):801-14.

Hartwell LH, Culotti J, Reid B. Genetic control of the cell-division cycle in yeast. I. Detection of mutants. Proc Natl Acad Sci USA. 1970;66(2):352-9.

Hartwell LH, Mortimer RK, Culotti J, Culotti M. Genetic control of the cell division cycle in yeast: v. Genetic analysis of cdc mutants. Genetics. 1973;74(2):267-286.

Erin E. Henninger, Pascale Jolivet, Emilie Fallet, Mohcen Benmounah, Zhou Xu, Stefano Mattarocci, Maria Teresa Teixeira Maturation of telomere 3'-overhangs is linked to the replication stress response bioRxiv 2020.08.27.269621; doi: https://doi.org/10.1101/2020.08.27.269621

Herskowitz I. Functional inactivation of genes by dominant negative mutations. Nature. 1987;329(6136):219-22.

Hoege C, Pfander B, Moldovan G-L, Pyrowolakis G, Jentsch S. RAD6-dependent DNA repair is linked to modification of PCNA by ubiquitin and SUMO. Nature. 2002;419(6903):135-141.

Holstein EM, Ngo G, Lawless C, Banks P, Greetham M, Wilkinson D, Lydall D. Systematic Analysis of the DNA Damage Response Network in Telomere Defective Budding Yeast. G3 (Bethesda). 2017 Jul 5;7(7):2375-2389. doi: 10.1534/g3.117.042283.

Holt LJ, Tuch BB, Villén J, Johnson AD, Gygi SP, Morgan DO. Global analysis of Cdk1 substrate phosphorylation sites provides insights into evolution. Science. 2009;325(5948):1682-6.

Horn H, Schoof EM, Kim J, Robin X, Miller ML, Diella F, Palma A, Cesareni G, Jensen LJ, Linding R. KinomeXplorer: an integrated platform for kinome biology studies. Nat Methods. 2014 Jun;11(6):603-4. doi: 10.1038/nmeth.2968.

Hsu C-L, Chen Y-S, Tsai S-Y, Tu P-J, Wang M-J, Lin J-J. Interaction of Saccharomyces Cdc13p with Pol1p, Imp4p, Sir4p and Zds2p is involved in telomere replication, telomere maintenance and cell growth control. Nucleic Acids Res. 2004;32(2):511-521.

Huang H, Weiner BE, Zhang H, Fuller BE, Gao Y, Wile BM, Zhao K, Arnett DR, Chazin WJ, Fanning E. Structure of a DNA polymerase alpha-primase domain that docks on the SV40 helicase and activates the viral primosome. J Biol Chem. 2010 May 28;285(22):17112-22. doi: 10.1074/jbc.M110.116830.

Janke R, King GA, Kupiec M, Rine J. Pivotal roles of PCNA loading and unloading in heterochromatin function. Proc Natl Acad Sci U S A. 2018;115(9):E2030-E2039.

Jeffery CJ. Moonlighting proteins: old proteins learning new tricks. Trends in Genetics. 2003;19(8):415-417.

Jiang Q, Zhang W, Liu C, Lin Y, Wu Q, Dai J. Dissecting PCNA function with a systematically designed mutant library in yeast. J Genet Genomics. 2019;46(6):301-313.

Johansson E, Garg P, Burgers PMJ. The Pol32 subunit of DNA polymerase delta contains separable domains for processive replication and proliferating cell nuclear antigen (Pcna) binding. J Biol Chem. 2004;279(3):1907-1915.

Johnson C, Gali VK, Takahashi TS, Kubota T. Pcna retention on dna into g2/m phase causes genome instability in cells lacking elg1. Cell Rep. 2016;16(3):684-695.

Johnston LH, Nasmyth KA. Saccharomyces cerevisiae cell cycle mutant cdc9 is defective in DNA ligase. Nature. 1978;274(5674):891-3.

Joseph SB, Hall DW. Spontaneous mutations in diploid saccharomyces cerevisiae. Genetics. 2004;168(4):1817-1825.

Karanja KK, Livingston DM. C-terminal flap endonuclease (Rad27) mutations: lethal interactions with a dna ligase i mutation (Cdc9-p) and suppression by proliferating cell nuclear antigen (Pol30) in saccharomyces cerevisiae. Genetics. 2009;183(1):63-78.

Kasbek C, Wang F, Price CM. Human TEN1 maintains telomere integrity and functions in genome-wide replication restart. J Biol Chem. 2013;288(42):30139-30150.

Kawasaki Y, Sugino A. Yeast replicative DNA polymerases and their role at the replication fork. Mol Cells. 2001;12(3):277-85.

Kilkenny ML, De Piccoli G, Perera RL, Labib K, Pellegrini L. A conserved motif in the C-terminal tail of DNA polymerase α tethers primase to the eukaryotic replisome. J Biol Chem. 2012;287(28):23740-23747.

Kilkenny ML, Longo MA, Perera RL, Pellegrini L. Structures of human primase reveal design of nucleotide elongation site and mode of Pol α tethering. Proc Natl Acad Sci U S A. 2013;110(40):15961-15966.

Kim NW, Piatyszek MA, Prowse KR, Harley CB, West MD, Ho PL, Coviello GM, Wright WE, Weinrich SL, Shay JW. Specific association of human telomerase activity with immortal cells and cancer. Science. 1994 Dec 23;266(5193):2011-5. doi: 10.1126/science.7605428.

Kim DK, Stigger E, Lee SH. Role of the 70-kDa subunit of human replication protein A (I). Single-stranded dna binding activity, but not polymerase stimulatory activity, is required for DNA replication. J Biol Chem. 1996;271(25):15124-15129.

Kim TY, Ji ES, Lee JY, Kim JY, Yoo JS, Szasz AM, Dome B, Marko-Varga G, Kwon HJ. DNA Polymerase Alpha Subunit B Is a Binding Protein for Erlotinib Resistance in Non-Small Cell Lung Cancer. Cancers (Basel). 2020 Sep 13;12(9):2613. doi: 10.3390/cancers12092613.

Klinge S, Hirst J, Maman JD, Krude T, Pellegrini L. An iron-sulfur domain of the eukaryotic primase is essential for RNA primer synthesis. Nat Struct Mol Biol. 2007;14(9):875-7.

Klinge S, Núñez-ramírez R, Llorca O, Pellegrini L. 3D architecture of DNA Pol alpha reveals the functional core of multi-subunit replicative polymerases. EMBO J. 2009;28(13):1978-87.

Koh V, Kwan HY, Tan WL, Mah TL, Yong WP. Knockdown of POLA2 increases gemcitabine resistance in lung cancer cells. BMC Genomics. 2016;17(Suppl 13):1029.

Kondratick CM, Litman JM, Shaffer KV, Washington MT, Dieckman LM. Crystal structures of PCNA mutant proteins defective in gene silencing suggest a novel interaction site on the front face of the PCNA ring. PLoS One. 2018;13(3):e0193333.

Kumar NV, Govil G. Theoretical studies on protein-nucleic acid interactions. I. Interaction of positively charged amino acids with nucleic acid fragments. Biopolymers. 1984;23(10):1979-93.

Kunkel TA. Dna replication fidelity. Journal of Biological Chemistry. 2004;279(17):16895-16898.

Langston RE, Palazzola D, Bonnell E, Wellinger RJ, Weinert T. Loss of Cdc13 causes genome instability by a deficiency in replication-dependent telomere capping. PLoS Genet. 2020;16(4).

Lau PJ, Flores-Rozas H, Kolodner RD. Isolation and characterization of new proliferating cell nuclear antigen (Pol30) mutator mutants that are defective in dna mismatch repair. Mol Cell Biol. 2002;22(19):6669-6680.

Lee, K. H., Kim, D. W., Bae, S. H., Kim, J. A., Ryu, G. H., Kwon, Y. N., Kim, K. A., Koo, H. S., & Seo, Y. S. (2000). The endonuclease activity of the yeast Dna2 enzyme is essential in vivo. Nucleic acids research, 28(15), 2873–2881.

Lendvay TS, Morris DK, Sah J, Balasubramanian B, Lundblad V. Senescence mutants of Saccharomyces cerevisiae with a defect in telomere replication identify three additional EST genes. Genetics. 1996;144(4):1399-412.

Lim CJ, Barbour AT, Zaug AJ, Goodrich KJ, McKay AE, Wuttke DS, Cech TR. The structure of human CST reveals a decameric assembly bound to telomeric DNA. Science. 2020 Jun 5;368(6495):1081-1085. doi: 10.1126/science.aaz9649.

Lin Y, Lin LJ, Sriratana P, Coleman K, Ha T, Spies M, Cann IK. Engineering of functional replication protein a homologs based on insights into the evolution of oligonucleotide/oligosaccharide-binding folds. J Bacteriol. 2008 Sep;190(17):5766-80. doi: 10.1128/JB.01930-07.

Liu C-C, Gopalakrishnan V, Poon L-F, Yan T, Li S. Cdk1 regulates the temporal recruitment of telomerase and cdc13-stn1-ten1 complex for telomere replication. Mol Cell Biol. 2014;34(1):57-70.

Liu L, Huang M. Essential role of the iron-sulfur cluster binding domain of the primase regulatory subunit Pri2 in DNA replication initiation. Protein Cell. 2015;6(3):194-210.

Loeillet S, Palancade B, Cartron M, Thierry A, Richard GF, Dujon B, Doye V, Nicolas A. Genetic network interactions among replication, repair and nuclear pore deficiencies in yeast. DNA Repair (Amst). 2005 Apr 4;4(4):459-68. doi: 10.1016/j.dnarep.2004.11.010.

Longhese MP, Jovine L, Plevani P, Lucchini G. Conditional mutations in the yeast DNA primase genes affect different aspects of DNA metabolism and interactions in the DNA polymerase alpha-primase complex. Genetics. 1993;133(2):183-91.

Lubin JW, Rao T, Mandell EK, Wuttke DS, Lundblad V. Dissecting protein function: an efficient protocol for identifying separation-of-function mutations that encode structurally stable proteins. Genetics. 2013;193(3):715-25.

Lucchini G, Francesconi S, Foiani M, Badaracco G, Plevani P. Yeast DNA polymerase--DNA primase complex; cloning of PRI 1, a single essential gene related to DNA primase activity. EMBO J. 1987;6(3):737-42.

Lucchini G, Mazza C, Scacheri E, Plevani P. Genetic mapping of the Saccharomyces cerevisiae DNA polymerase I gene and characterization of a pol1 temperature-sensitive mutant altered in DNA primase-polymerase complex stability. Mol Gen Genet. 1988;212(3):459-65.

Lue NF, Chan J, Wright WE, Hurwitz J. The CDC13-STN1-TEN1 complex stimulates Pol α activity by promoting RNA priming and primase-to-polymerase switch. Nat Commun. 2014;5:5762.

Maga G, Hubscher U. Proliferating cell nuclear antigen (Pcna): a dancer with many partners. J Cell Sci. 2003;116(Pt 15):3051-3060.

Mah TL, Yap XN, Limviphuvadh V, Li N, Sridharan S, Kuralmani V, Feng M, Liem N, Adhikari S, Yong WP, Soo RA, Maurer-Stroh S, Eisenhaber F, Tong JC. Novel SNP improves differential survivability and mortality in non-small cell lung cancer patients. BMC Genomics. 2014;15 Suppl 9(Suppl 9):S20. doi: 10.1186/1471-2164-15-S9-S20.

Marcand S, Gilson E, Shore D. A protein-counting mechanism for telomere length regulation in yeast. Science. 1997;275(5302):986-90.

Mason, M., Wanat, J. J., Harper, S., Schultz, D. C., Speicher, D. W., Johnson, F. B., & Skordalakes, E. (2013). Cdc13 OB2 dimerization required for productive Stn1 binding and efficient telomere maintenance. Structure (London, England : 1993), 21(1), 109–120.

Matsumoto T, Eki T, Hurwitz J. Studies on the initiation and elongation reactions in the simian virus 40 DNA replication system. Proc Natl Acad Sci USA. 1990;87(24):9712-6.

McNally R, Bowman GD, Goedken ER, O'Donnell M, Kuriyan J. Analysis of the role of PCNA-DNA contacts during clamp loading. BMC Struct Biol. 2010;10:3.

Meier B, Driller L, Jaklin S, Feldmann HM. New function of CDC13 in positive telomere length regulation. Mol Cell Biol. 2001;21(13):4233-4245.

Miles J, Formosa T. Protein affinity chromatography with purified yeast DNA polymerase alpha detects proteins that bind to DNA polymerase. Proc Natl Acad Sci U S A. 1992;89(4):1276-1280.

Morris CF, Sinha NK, Alberts BM. Reconstruction of bacteriophage T4 DNA replication apparatus from purified components: rolling circle replication following de novo chain initiation on a single-stranded circular DNA template. Proc Natl Acad Sci USA. 1975;72(12):4800-4.

Mortensen UH, Bendixen C, Sunjevaric I, Rothstein R. DNA strand annealing is promoted by the yeast Rad52 protein. Proc Natl Acad Sci U S A. 1996;93(20):10729-10734.

Mozdy AD, Cech TR. Low abundance of telomerase in yeast: implications for telomerase haploinsufficiency. RNA. 2006;12(9):1721-37.

Nakayama N, Arai N, Kaziro Y, Arai K. Structural and functional studies of the dnaB protein using limited proteolysis. Characterization of domains for DNA-dependent ATP hydrolysis and for protein association in the primosome. J Biol Chem. 1984;259(1):88-96.

Nguyen HD, Becker J, Thu YM, Costanzo M, Koch EN, Smith S, Myung K, Myers CL, Boone C, Bielinsky AK. Unligated Okazaki Fragments Induce PCNA Ubiquitination and a Requirement for Rad59-Dependent Replication Fork Progression. PLoS One. 2013 Jun 18;8(6):e66379. doi: 10.1371/journal.pone.0066379.

Nugent CI, Hughes TR, Lue NF, Lundblad V. Cdc13p: a single-strand telomeric DNA-binding protein with a dual role in yeast telomere maintenance. Science. 1996;274(5285):249-52.

Núñez-Ramírez, R., Klinge, S., Sauguet, L., Melero, R., Recuero-Checa, M. A., Kilkenny, M., Perera, R. L., García-Alvarez, B., Hall, R. J., Nogales, E., Pellegrini, L., & Llorca, O. (2011). Flexible tethering of primase and DNA Pol α in the eukaryotic primosome. Nucleic acids research, 39(18), 8187–8199.

O'Brien E, Salay LE, Epum EA, Friedman KL, Chazin WJ, Barton JK. Yeast require redox switching in DNA primase. PNAS. 2018;115(52):13186-13191.

Olovnikov AM. A theory of marginotomy. The incomplete copying of template margin in enzymic synthesis of polynucleotides and biological significance of the phenomenon. J Theor Biol. 1973;41(1):181-90.

Okazaki R, Okazaki T, Sakabe K, Sugimoto K, Sugino A. Mechanism of DNA chain growth. I. Possible discontinuity and unusual secondary structure of newly synthesized chains. Proc Natl Acad Sci USA. 1968;59(2):598-605.

Paschini M, Mandell EK, Lundblad V. Structure prediction-driven genetics in Saccharomyces cerevisiae identifies an interface between the t-RPA proteins Stn1 and Ten1. Genetics. 2010;185(1):11-21.

Paschini M, Toro TB, Lubin JW, Braunstein-ballew B, Morris DK, Lundblad V. A naturally thermolabile activity compromises genetic analysis of telomere function in Saccharomyces cerevisiae. Genetics. 2012;191(1):79-93.

Margherita Paschini, Cynthia M. Reyes, Abigail E. Gillespie, Karen A. Lewis, Leslie W.Glustrom, Tatyana O. Sharpee, Deborah S. Wuttke, Victoria Lundblad Spontaneous replication fork collapse regulates telomere length homeostasis in wild type cells bioRxiv 2020.08.05.237172; doi: https://doi.org/10.1101/2020.08.05.237172

Paulovich AG, Margulies RU, Garvik BM, Hartwell LH. RAD9, RAD17, and RAD24 are required for S phase regulation in Saccharomyces cerevisiae in response to DNA damage. Genetics. 1997;145(1):45-62.

Paulovich AG, Armour CD, Hartwell LH. The Saccharomyces cerevisiae RAD9, RAD17, RAD24 and MEC3 genes are required for tolerating irreparable, ultraviolet-induced DNA damage. Genetics. 1998;150(1):75-93.

Pearlman SM, Serber Z, Ferrell JE. A mechanism for the evolution of phosphorylation sites. Cell. 2011;147(4):934-46.

Petreaca RC, Chiu H-C, Eckelhoefer HA, Chuang C, Xu L, Nugent CI. Chromosome end protection plasticity revealed by Stn1p and Ten1p bypass of Cdc13p. Nat Cell Biol. 2006;8(7):748-755.

Pizzagalli A, Valsasnini P, Plevani P, Lucchini G. DNA polymerase I gene of Saccharomyces cerevisiae: nucleotide sequence, mapping of a temperature-sensitive mutation, and protein homology with other DNA polymerases. Proc Natl Acad Sci USA. 1988;85(11):3772-6.

Price CM, Adams AK, Vermeesch JR. Accumulation of telomerase RNA and telomere protein transcripts during telomere synthesis in Euplotes. J Eukaryot Microbiol. 1994;41(3):267-275.

Price CM, Boltz KA, Chaiken MF, Stewart JA, Beilstein MA, Shippen DE. Evolution of CST function in telomere maintenance. Cell Cycle. 2010;9(16):3157-3165.

Puglisi A, Bianchi A, Lemmens L, Damay P, Shore D. Distinct roles for yeast Stn1 in telomere capping and telomerase inhibition. EMBO J. 2008;27(17):2328-2339.

Qi H, Zakian VA. The Saccharomyces telomere-binding protein Cdc13p interacts with both the catalytic subunit of DNA polymerase alpha and the telomerase-associated est1 protein. Genes Dev. 2000;14(14):1777-88.

Rabitsch KP, Tóth A, Gálová M, Schleiffer A, Schaffner G, Aigner E, Rupp C, Penkner AM, Moreno-Borchart AC, Primig M, Esposito RE, Klein F, Knop M, Nasmyth K. A screen for genes required for meiosis and spore formation based on whole-genome expression. Curr Biol. 2001 Jul 10;11(13):1001-9. doi: 10.1016/s0960-9822(01)00274-3.

Rao T, Lubin JW, Armstrong GS, Tucey TM, Lundblad V, Wuttke DS. Structure of Est3 reveals a bimodal surface with differential roles in telomere replication. Proc Natl Acad Sci USA. 2014;111(1):214-8.

Reagan MS, Pittenger C, Siede W, Friedberg EC. Characterization of a mutant strain of Saccharomyces cerevisiae with a deletion of the RAD27 gene, a structural homolog of the RAD2 nucleotide excision repair gene. J Bacteriol. 1995;177(2):364-371.

Reveal PM, Henkels KM, Turchi JJ. Synthesis of the mammalian telomere lagging strand in vitro. J Biol Chem. 1997;272(18):11678-11681.

Roberts JJ, Warwick GP. Mode of action of alkylating agents: formation of S-ethylcysteine from ethyl methane-sulphonate in vivo. Nature. 1957;179(4571):1181-2.

Rupert CS. Repair of ultraviolet damage in cellular DNA. J Cell Comp Physiol. 1961;58(3)Pt 2:57-68.

Sauguet L, Klinge S, Perera RL, Maman JD, Pellegrini L. Shared active site architecture between the large subunit of eukaryotic primase and dna photolyase. PLoS One. 2010;5(4).

Scherer S, Davis RW. Replacement of chromosome segments with altered DNA sequences constructed in vitro. Proc Natl Acad Sci U S A. 1979;76(10):4951-4955.

Scherzinger E, Lanka E, Hillenbrand G. Role of bacteriophage T7 DNA primase in the initiation of DNA strand synthesis. Nucleic Acids Res. 1977;4(12):4151-63.

Schild D. Suppression of a new allele of the yeast RAD52 gene by overexpression of RAD51, mutations in srs2 and ccr4, or mating-type heterozygosity. Genetics. 1995;140(1):115-127.

Schramke V, Luciano P, Brevet V, Guillot S, Corda Y, Longhese MP, Gilson E, Géli V. RPA regulates telomerase action by providing Est1p access to chromosome ends. Nat Genet. 2004 Jan;36(1):46-54. doi: 10.1038/ng1284.

Singer MS, Gottschling DE. TLC1: template RNA component of Saccharomyces cerevisiae telomerase. Science. 1994;266(5184):404-409.

Smith J, Zou H, Rothstein R. Characterization of genetic interactions with RFA1: the role of RPA in DNA replication and telomere maintenance. Biochimie. 2000;82(1):71-78.

Starokadomskyy P, Gemelli T, Rios JJ, Xing C, Wang RC, Li H, Pokatayev V, Dozmorov I, Khan S, Miyata N, Fraile G, Raj P, Xu Z, Xu Z, Ma L, Lin Z, Wang H, Yang Y, Ben-Amitai D, Orenstein N, Mussaffi H, Baselga E, Tadini G, Grunebaum E, Sarajlija A, Krzewski K, Wakeland EK, Yan N, de la Morena MT, Zinn AR, Burstein E. DNA polymerase-α regulates the activation of type I interferons through cytosolic RNA:DNA synthesis. Nat Immunol. 2016 May;17(5):495-504. doi: 10.1038/ni.3409.

Stelter P, Ulrich HD. Control of spontaneous and damage-induced mutagenesis by SUMO and ubiquitin conjugation. Nature. 2003;425(6954):188-191.

Stodola JL, Burgers PM. Mechanism of lagging-strand dna replication in eukaryotes. Adv Exp Med Biol. 2017;1042:117-133.

Sugiyama T, New JH, Kowalczykowski SC. DNA annealing by RAD52 protein is stimulated by specific interaction with the complex of replication protein A and single-stranded DNA. Proc Natl Acad Sci U S A. 1998;95(11):6049-6054.

Sun, Jia & Yu, Eun Young & Yang, Yuting & Confer, Laura & Sun, Steven & Wan, ke & Lue, Neal & Lei, Ming. (2009). Stn1-Ten1 is an Rpa2-Rpa3-like complex at telomeres. Genes & development. 23. 2900-14. 10.1101/gad.1851909.

Sun J, Yang Y, Wan K, Mao N, Yu TY, Lin YC, DeZwaan DC, Freeman BC, Lin JJ, Lue NF, Lei M. Structural bases of dimerization of yeast telomere protein Cdc13 and its interaction with

the catalytic subunit of DNA polymerase α. Cell Res. 2011 Feb;21(2):258-74. doi: 10.1038/cr.2010.138.

Sun X, Thrower D, Qiu J, Wu P, Zheng L, Zhou M, Bachant J, Wilson DM 3rd, Shen B. Complementary functions of the Saccharomyces cerevisiae Rad2 family nucleases in Okazaki fragment maturation, mutation avoidance, and chromosome stability. DNA Repair (Amst). 2003 Aug 12;2(8):925-40. doi: 10.1016/s1568-7864(03)00093-4.

Suwa Y, Gu J, Baranovskiy AG, Babayeva ND, Pavlov YI, Tahirov TH. Crystal Structure of the Human Pol α B Subunit in Complex with the C-terminal Domain of the Catalytic Subunit. J Biol Chem. 2015;290(23):14328-37.

Symington LS. Role of RAD52 epistasis group genes in homologous recombination and double-strand break repair. Microbiol Mol Biol Rev. 2002;66(4):630-670, table of contents.

Teixeira MT. Saccharomyces cerevisiae as a model to study replicative senescence triggered by telomere shortening. Front Oncol. 2013;3.

Theobald DL, Mitton-Fry RM, Wuttke DS. Nucleic acid recognition by ob-fold proteins. Annu Rev Biophys Biomol Struct. 2003;32:115-133.

Tishkoff DX, Filosi N, Gaida GM, Kolodner RD. A novel mutation avoidance mechanism dependent on S. cerevisiae RAD27 is distinct from DNA mismatch repair. Cell. 1997;88(2):253-263.

Townsley DM, Dumitriu B, Young NS. Bone marrow failure and the telomeropathies. Blood. 2014;124(18):2775-2783.

Tran PT, Erdeniz N, Dudley S, Liskay RM. Characterization of nuclease-dependent functions of Exo1p in Saccharomyces cerevisiae. DNA Repair (Amst). 2002;1(11):895-912.

Umezu K, Sugawara N, Chen C, Haber JE, Kolodner RD. Genetic analysis of yeast RPA1 reveals its multiple functions in DNA metabolism. Genetics. 1998;148(3):989-1005.

Veaute X, Jeusset J, Soustelle C, Kowalczykowski SC, Le Cam E, Fabre F. The Srs2 helicase prevents recombination by disrupting Rad51 nucleoprotein filaments. Nature. 2003;423(6937):309-312.

Vaithiyalingam S, Arnett DR, Aggarwal A, Eichman BF, Fanning E, Chazin WJ. Insights into eukaryotic primer synthesis from structures of the p48 subunit of human DNA primase. J Mol Biol. 2014;426(3):558-569.

Vijayakumar S, Chapados BR, Schmidt KH, Kolodner RD, Tainer JA, Tomkinson AE. The C-terminal domain of yeast PCNA is required for physical and functional interactions with Cdc9 DNA ligase. Nucleic Acids Res. 2007;35(5):1624-1637.

Waga S, Stillman B. The DNA replication fork in eukaryotic cells. Annu Rev Biochem. 1998;67:721-751.

Watson JD, Crick FH. The structure of DNA. Cold Spring Harb Symp Quant Biol. 1953;18:123-31.

Weinert TA, Hartwell LH. The RAD9 gene controls the cell cycle response to DNA damage in Saccharomyces cerevisiae. Science. 1988;241(4863):317-22.

Wellinger RJ, Zakian VA. Everything you ever wanted to know about Saccharomyces cerevisiae telomeres: beginning to end. Genetics. 2012;191(4):1073-105.

Wu Y, Zakian VA. The telomeric Cdc13 protein interacts directly with the telomerase subunit Est1 to bring it to telomeric DNA ends in vitro. Proc Natl Acad Sci U S A. 2011;108(51):20362-20369.

Xu H, Boone C, Klein HL. Mrc1 is required for sister chromatid cohesion to aid in recombination repair of spontaneous damage. Mol Cell Biol. 2004;24(16):7082-7090.

Xu L, Petreaca RC, Gasparyan HJ, Vu S, Nugent CI. TEN1 is essential for CDC13-mediated telomere capping. Genetics. 2009;183(3):793-810.

Yang JS, Seo SW, Jang S, Jung GY, Kim S. Rational engineering of enzyme allosteric regulation through sequence evolution analysis. PLoS Comput Biol. 2012;8(7):e1002612.

Young L, Jernigan RL, Covell DG. A role for surface hydrophobicity in protein-protein recognition. Protein Sci. 1994;3(5):717-29.

Yu H, Braun P, Yildirim MA, Lemmens I, Venkatesan K, Sahalie J, Hirozane-Kishikawa T, Gebreab F, Li N, Simonis N, Hao T, Rual JF, Dricot A, Vazquez A, Murray RR, Simon C, Tardivo L, Tam S, Svrzikapa N, Fan C, de Smet AS, Motyl A, Hudson ME, Park J, Xin X,

Cusick ME, Moore T, Boone C, Snyder M, Roth FP, Barabási AL, Tavernier J, Hill DE, Vidal M. High-quality binary protein interaction map of the yeast interactome network. Science. 2008 Oct 3;322(5898):104-10. doi: 10.1126/science.1158684.

Zhang Z, Shibahara K, Stillman B. PCNA connects DNA replication to epigenetic inheritance in yeast. Nature. 2000;408(6809):221-225.

Zhao Y, Sfeir AJ, Zou Y, Buseman CM, Chow TT, Shay JW, Wright WE. Telomere extension occurs at most chromosome ends and is uncoupled from fill-in in human cancer cells. Cell. 2009 Aug 7;138(3):463-75. doi: 10.1016/j.cell.2009.05.026.

Zheng L, Jia J, Finger LD, Guo Z, Zer C, Shen B. Functional regulation of FEN1 nuclease and its link to cancer. Nucleic Acids Research. 2011;39(3):781-794.

Zhou B, Arnett DR, Yu X, Brewster A, Sowd GA, Xie CL, Vila S, Gai D, Fanning E, Chen XS. Structural basis for the interaction of a hexameric replicative helicase with the regulatory subunit of human DNA polymerase α-primase. J Biol Chem. 2012 Aug 3;287(32):26854-66. doi: 10.1074/jbc.M112.363655.

Zou H, Rothstein R. Holliday junctions accumulate in replication mutants via a RecA homolog-independent mechanism. Cell. 1997;90(1):87-96.

Zubko MK, Guillard S, Lydall D. Exo1 and rad24 differentially regulate generation of ssDNA at telomeres of saccharomyces cerevisiae cdc13-1 mutants. Genetics. 2004;168(1):103-115.